INVESTIGATIONS OF PRIMATE PLACENTATION UNDER NORMAL AND PATHOLOGICAL PREGNANCY CONDITIONS

By
Jimi L. Rosenkrantz

A DISSERTATION

The Department of Molecular and Medical Genetics at
Oregon Health & Science University
School of Medicine

In partial fulfillment of
the requirement for the degree of

Doctor of Philosophy

April 2021

CERTIFICATE OF APPROVAL

This is to certify that the PhD Dissertation thesis of

Jimi L. Rosenkrantz

has been approved

_____
Mentor, Shawn L. Chavez, Ph.D.

_____
Mentor, Lucia Carbone, Ph.D.

_____
Member and Chair, Scott Stadler, Ph.D.

_____
Member, Andrew Adey, Ph.D.

_____
Member, Jonah Sacha, Ph.D.

_____
Member, Daniel Streblow, Ph.D.

TABLE OF CONTENTS

LIST OF FIGURES AND TABLES

Figures

Supplemental Figures

Tables

LIST OF ABBREVIATIONS

ALS	Amyotrophic lateral sclerosis
CCM	Cell culture media
CDH1	E-cadherin
cDNA	complementary DNA
CNRQ	Calibrated normalized relative quantity
CNV	Copy-number variation
CTB	Cytotrophoblast
CTM	Complete trophoblast media
DE	Differential expression
DEG	Differentially expressed gene
dsRNA	Double-stranded RNA
eEVT	Endovascular EVT
EGA	Embryonic genome activation
env	Envelope
ERV	Endogenous retrovirus
ERVK	Endogenous retrovirus-K
ERVK-env	ERVK envelope
ERVs	Endogenous retroviruses
EVT	Extravillous trophoblast
FBS	Fetal bovine serum
FcRn	Fc receptor
FGR	Fetal growth restriction
FP	Fusion peptide
GA	Gestational age
gag	Group-specific antigen
HBSS	Hanks balanced salt solution
hCG	Human chorionic gonadotropin
HDAC	Histone deacetylase
HERV	Human endogenous retrovirus
hESC	Human embryonic stem cell
HPA	Human protein atlas
HPG	Human placental marker gene
hPL	Human placental lactogen
HPT	Human primary trophoblast
HSV1	Herpes simplex virus 1
iEVT	Interstitial EVT
IF	Immunofluorescence
IFN	Interferon
IHC	Immunohistochemistry
IL6	Interleukin-6
iRFb	Immortalized rhesus fibroblast
iRP	Immortalized rhesus placental
ISG	Interferon-stimulated gene
ISU	Immunosuppression
IUGR	Intrauterine growth restriction
KD	Knockdown
L2FC	Log2 fold change

LH	Luteinizing hormone
LTR	Long terminal repeat
mCG	Monkey chorionic gonadotropin
MS	Multiple sclerosis
NC1	Nontargeting universal negative control
NK	Natural killer
NTC	No template control
ORA	Over-representation analysis
ORF	Open reading frame
OVX	Ovariectomized
PAC	Puromycin resistance
padj	Adjusted p-value
PBMC	Peripheral blood mononuclear cell
PBS--	Phosphate-buffered saline without Ca2+ and Mg2+
PCA	Principle component analysis
PE	Preeclampsia
PGC	Primordial germ cell
PGF	Placental growth factor
pol	Polymerase
PPROM	Premature rupture of the membranes
pro	Protease
qRT-PCR	Quantitative reverse transcription PCR
RIA	Radioimmunoassay
RPT	Rhesus primary trophoblast
SDE	Sex-differentially expressed
SE	Standard error
SEM	Standard error of the mean
siENK	siRNA targeting the ERVK11q23.3 transcript
siHPRT1	siRNA targeting the HPRT1 gene
siNC1	siRNA targeting no known sequence in the human transcriptome
siRNA	small interfering RNA
STB	Syncytiotrophoblast
SU	Surface unit
SV40	Simian virus 40
TCF4	T-cell factor 4
TE	Trophectoderm
TERT	Telomerase reverse transcriptase
TM	Transmembrane
TPM	Transcripts per million
VIM	Vimentin
VLP	Viral-like particle
VST	Variance stabilizing transformation

ACKNOWLEDGMENTS

First and foremost, I would like to thank my advisors, Drs. Shawn Chavez and Lucia Carbone, for the tremendous amount of support and guidance they provided throughout my time at OHSU. I am incredibly appreciative of the freedom I was given during my time as their trainee, and for the opportunity to develop and pursue my own research project under their guidance. The Ruth L. Kirschstein Predoctoral National Research Service Award (NRSA) I received under their mentorship has been invaluable to my training experience and scientific career. I would also like to acknowledge and thank my dissertation committee members who aided the completion of this work by providing their countless time, wisdom, and insights; the current and former members of the Chavez and Carbone labs, especially Drs. Josh Meyer, Sweta Ravisankar, Mariam Okhovat, and Kelsey Brooks, for their support and camaraderie throughout my Ph.D.; as well as the funding I received during my time at OHSU: NICHD/NIH F31 NRSA, Glenn/AFAR Scholarship for Research in the Biology of Aging, and the Nicholas L. Tartar Research Fellowship.

I would also like to thank the members of the Haussler lab during my time as an undergraduate and research technician at UC Santa Cruz, especially Dr. Frank Jacobs for being the first person to give me a research opportunity and for helping me build the confidence to pursue a career in scientific research.

Last but not least, I would like to thank all my incredible friends and family for keeping me grounded and somewhat sane throughout this arduous process. In particular, I want to thank my parents (Vicki and Wayne), siblings (Shannon and Bryan), and cats (Jaspurr and Tchotchke) for the unconditional love and support throughout this journey. I also want to thank my best friend and classmate, Dr. Holly Corbitt, for always having my back, reminding me to have fun, and pushing me outside of my comfort zone. Finally, I want to thank my amazing partner and best friend, Patrick Dougherty, for being a constant source of positivity and encouragement, and for all of the fun, love, support, and home-cooked meals he has provided over the past four years <3.

ABSTRACT

Normal placentation is essential for the health and well-being of both the mother and fetus throughout pregnancy. In humans, defective placental development contributes to pregnancy complications such as preeclampsia, fetal growth restriction, and preterm birth. The etiology of these pregnancy disorders is poorly understood since they are thought to arise during the early stages of development which is difficult to study in humans due to ethical reasons. To overcome these limitations, the highly-translatable rhesus macaque animal model can be used in two ways: (1) as a traditional animal model studying early placentation with and without experimental manipulations, and (2) as a comparator to identify the molecular and physiological features underlying the heightened susceptibility of preeclampsia in humans compared to rhesus. Thus, in the first half of this dissertation, to enhance *in vitro* investigations of rhesus placentation, I present the generation and characterization of two telomerase-immortalized first trimester rhesus trophoblast cell lines. Further, to elucidate the molecular differences between human and rhesus placenta, I present a comprehensive list of differentially expressed genes between the two species. While a majority of genes were found to be similarly expressed between human and rhesus placenta, genes associated with preeclampsia and several other pregnancy complications were upregulated in human. These results highlight the value of using rhesus in comparative studies and suggest that rhesus is a suitable surrogate for investigating human placentation; however, notable molecular differences related to preeclampsia should be considered and further interrogated in future studies.

While investigating the molecular differences between human and rhesus placenta, I became interested in endogenous retrovirus (ERVs) since ERV-derived proteins are known to play important roles during normal placentation and the genomic distribution and placental expression of certain ERVs varies between primates. A protein derived from the youngest ERV in primates, ERVK (HML2), was recently shown to be expressed during human placentation; however, the native expression and function of placentally-expressed ERVK remain largely uncharacterized.

Thus, in the second half of this dissertation, I present a thorough characterization of locus-specific ERVK transcription from several human placental tissue samples and trophoblast cell lines. My studies highlighted the expression of ERVK11q23.3, an ERVK locus present in the human but not the rhesus genome, that is highly expressed in mononuclear trophoblasts and upregulated in human preterm compared to term placental tissue. I also provide evidence that altered placental expression of ERVK11q23.3 influences IFN antiviral response, which may contribute to preterm birth and other pregnancy complications in humans.

CHAPTER 1: Introduction and background

1.1 General overview

Normal placenta development and function are essential for the health and well-being of both the mother and fetus throughout pregnancy. The placenta is responsible for establishing the maternal-fetal interface, which is the critical site of nutrient and waste exchange between mom and baby throughout gestation. Placental abnormalities are strongly associated with pregnancy complications such as fetal growth restriction, preeclampsia, and preterm birth, which affect roughly a quarter of pregnancies [1]. Despite its importance in reproductive success, there is still a limited understanding of how the human placenta develops and functions.

During early placentation, trophoblast cells along the outside of the developing embryo invade the decidua (pregnant endometrium) and remodel maternal blood vessels to establish maternal blood flow to the placenta. This process is important to accommodate normal placental and fetal growth during pregnancy. Therefore, it is not surprising that inadequate trophoblast invasion and/or restricted artery remodeling is associated with adverse pregnancy outcomes [2]. Many pregnancy complications are thought to originate from defective trophoblast differentiation and/or invasion during the early stages of placentation. However, *early human placentation and the placental dysfunctions underlying pregnancy complications are not well understood, since several challenges have historically limited the study of developing human tissues, including limited access, tissue degradation, as well as ethical and experimental constraints.*

The use of animal models allows access to high-quality early gestational placental samples and opens up the possibility of *in vivo* functional investigations. Non-human primates, such as rhesus macaque (*Macaque mulatta*) represent an ideal animal model for studying early human development, as they are genetically and anatomically very similar to humans. However, *many of the resources available for human placental studies (i.e. immortalized cell lines, clearly defined trophoblast subtype markers, publicly available databases, and sequencing datasets) are limited*

or do not currently exist for rhesus, which impedes the use of this animal model. Additionally, while previous studies have shown that rhesus share many key features of human placentation [3-7], some differences related to trophoblast invasion and occurrence of pregnancy complications have been noted between the two species [4]. *The molecular and cellular characteristics underlying these differences are currently not well-defined, which further limits the use and translatability of the rhesus animal model for studying human placentation.*

The placenta is remarkable in its expression of endogenous retrovirus (ERV) sequences as placenta-specific genes. ERV-derived placental proteins are known to facilitate normal trophoblast specification and placental development within numerous mammalian species [8]. Thus, there is a growing body of evidence indicating the importance of ERV-derived proteins during early development and reproduction in humans [9]. Recently, a protein derived from the youngest ERV in primates, ERVK (HML2), was shown to be expressed during human placentation [10-12], but the precise function of ERVK in the placenta remains unknown. Since a number of highly similar ERVK proviral loci exist across the human genome, analysis of ERVK transcription and identification of the coding sequence expressed in the human placenta is difficult. Thus, despite its apparent activity in early human development [10,13], *the native expression and function of ERVK in the human placenta and its possible role in placental dysfunction remains largely uncharacterized.*

In order to develop novel tools for diagnosing and treating pregnancy complications, it is necessary to understand how the human placenta develops and functions under normal and pathological conditions. Therefore, my research focuses on establishing first trimester non-human primate trophoblast cell lines capable of bridging *in vitro* and *in vivo* placental investigations, identifying molecular differences between human and rhesus placenta to improve translational studies, and elucidating the expression and function of ERVK during human placentation. In this chapter, I will provide an overview of *human placental development and structure*, *placental pathologies associated with pregnancy complications*, *models for studying human placentation*,

and *the role of endogenous retroviruses during early development and placentation*. Of note, the background section on endogenous retroviruses is largely derived from a review article I co-authored with Dr. Joshua Meyer and my advisors entitled "Endogenous Retroviruses: With Us and against Us" [9]. At the end of this chapter, I will discuss the significance of previous findings and outline my specific project objectives. The results of my studies will be presented in Chapters 2-3 as follows:

- Transcriptomic analysis of primate placentas and novel rhesus trophoblast cell lines informs investigations of human placentation (Chapter 2)
- Investigation of ERVK expression and function in placentation (Chapter 3)

In chapter 4, I will discuss the overall conclusions of my findings, future directions, as well as the clinical relevance of my studies.

1.2 Development and structure of the human placenta

The human placenta is derived from the trophectoderm (TE), the layer along the outside of the developing blastocyst. While the early stages of implantation are difficult to study in human, observations from early pregnancy hysterectomies and non-human primate animal models suggest that after the embryo attaches to the surface of the maternal uterine wall (endometrium), the cells of the TE fuse to form the initial multinucleated syncytiotrophoblast (STB) or primary syncytium [14] (**Figure 1.1A**). The primary syncytium invades into the underlying endometrium, which is transformed during pregnancy into a tissue known as decidua [15]. During this process, the syncytium develops a number of fluid-filled spaces, called lacunae, that eventually give rise to the intervillous space where maternal blood flows. The mononuclear trophoblast cells beneath the primary syncytium, called cytotrophoblasts (CTBs), proliferate into columns that protrude into the multinucleated STB to form primary villi (a CTB core with an outer STB layer). CTBs at the tips of villi eventually penetrate through the primary syncytium and form a continuous

cytotrophoblastic shell between the villi and the decidua (**Figure 1.1B**). At this stage, approximately two weeks after fertilization, the placenta consists of three layers: The CTB layer surrounding the developing embryo (inner chorionic plate), the villi separated by the intervillous space, and the cytotrophoblastic shell that is in contact with the decidua (**Figure 1.1B**).

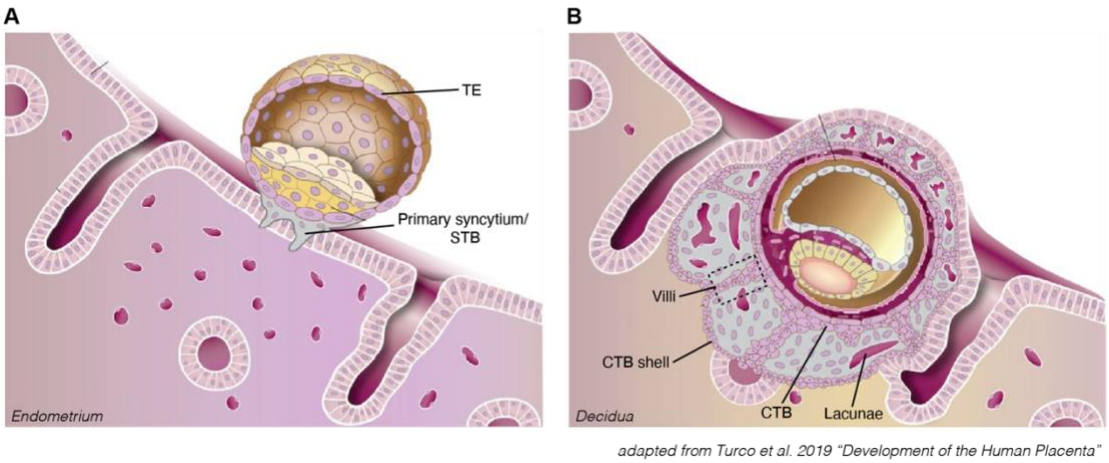

Figure 1.1 The early stages of human placental development

As placentation progresses, secondary and tertiary villi are established once extraembryonic mesenchymal cells invade through the villous core and fetal capillaries appear, respectively. Eventually, CTB cells located at the tips of villi and in the cytotrophoblastic shell differentiate and invade the decidua as extravillous trophoblasts (EVT). In a similar manner to cancer metastasis, these EVTs cells go on to remodel maternal spiral arteries; thus, by the end of the first trimester, maternal blood flow through the intervillous space (hemochorial circulation) is fully established. In human, this requires deep EVT invasion and remodeling of both decidual and myometrial segments of spiral arteries. To maximize the maternal-fetal exchange surface area, the villi and underlying fetal vascular system continue to grow and branch throughout the remainder of gestation. As the villous tree expands, the STB barrier separating the maternal and fetal circulations thin, further enhancing maternal-fetal exchange. By term, the mean maternal-fetal diffusion distance between maternal and fetal circulation is less than 5 μm and the surface area of

the villous tree is estimated to be around 12.5 m^2 (~330 times larger than if the exchange surface was flat) [16].

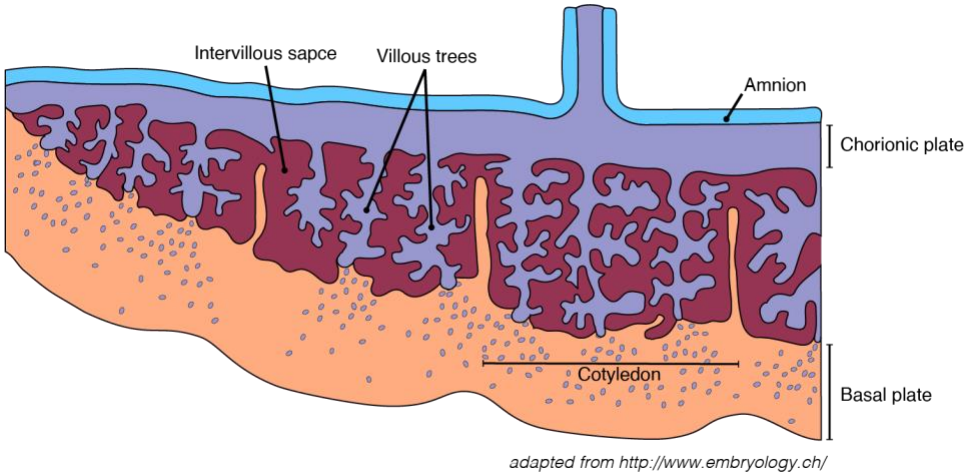

Figure 1.2 Structure of the mature human placenta

Around 12 weeks' gestation, the placenta has fully formed and is ready to take over the requirements of maintaining the pregnancy as both the fetus and placenta continue to grow. The name "placenta" is derived from the Greek *plakuos*, meaning flat cake, which is an accurate description of the gross anatomical appearance of this organ at term. It is disk-like in shape (flat and round to oval), and consists of the fetal chorionic plate, villous trees with underlying fetal vasculature system, maternal blood-filled intervillous space, and the basal plate which is a mixture of trophoblastic (fetal) and endometrium-derived (maternal) cells. At birth, the fetal surface (chorionic plate) has a glossy appearance due to the intact amnion covering, and the maternal surface (basal plate) is wrinkled and contains numerous slightly elevated areas called maternal lobes or cotyledons that correspond to clusters of underlying villous trees [14] (**Figure 1.2**). While the placenta as a whole is a mix of both fetal and maternal cells, fetal-derived trophoblast cells are inarguably the most important cell type of the placenta. Human trophoblast cells are classified into several different subtypes, including mononuclear villous CTBs, multinucleated STB/syncytia, and several subtypes of invasive EVTs. Each trophoblast subtype has a number of unique characteristics

and important functions that they serve during human placentation, which are discussed in more detail below.

1.2.1 The cytotrophoblast (CTB)

Villous CTB cells reside below the syncytial layer on a basement membrane that separates trophoblasts from the underlying mesenchymal villous core and fetal vascular system. In early pregnancy (**Figure 1.1**), CTBs are abundant and form a continuous layer where they rapidly divide and fuse with the STB to maintain this layer throughout gestation. However, as the placenta grows, villous CTBs become discontinuous and by term, CTBs cover less than a quarter of the villous surface [17]. Consequently, at term only a thin layer of STB separates most of the villous core from the maternal blood [17]. In addition to STB differentiation, the CTBs located at the tips of villi and/or in the cytotrophoblastic shell differentiate and give rise to EVTs that invade the maternal decidua [18-21]. Since villous CTBs have the ability to self-renew and differentiate into STB and EVT trophoblast subtypes [22], they are considered stem or progenitor cells of the placenta. Thus, CTB dysfunction can impair the formation and function of both STB and EVT trophoblast cell types.

1.2.2 The syncytiotrophoblast (STB)

The STB, also referred to as the syncytial layer or syncytia, is a continuous multinucleated layer that covers the surface of the villous trees and is estimated to have a surface area of 12–14 m^2 at term in human [23]. As mentioned above, fusion of the underlying mononuclear CTB cells with the STB maintains this layer throughout gestation [24,25]. However, if the STB is severely stressed or damaged *in vivo*, fusion can take place between neighboring CTBs to generate a new syncytium, and the original syncytial layer is then shed into maternal circulation [26,27]. This process has also been observed *in vitro* in both first trimester and term villous explants [28,29]. The apical or maternal facing membrane of the STB is in direct contact with maternal blood and is densely

covered with microvilli, which is estimated to increase the maternal-fetal interface surface area five- to seven-fold [30]. In contrast, the basal surface of the STB is either in direct contact with the underlying CTBs or the basement membrane [31]. Endogenous retroviral particles have been reported budding from the basal surface of the STB in human and several primate species, and are thought to be associated with the expression of fusogenic retroviral proteins during CTB cell fusion [32,33].

The STB acts as an endothelium to the intervillous space and is the main site of nutrient and gas transport between the maternal and fetal circulation, which is critical for fetal/placental development and growth throughout pregnancy. It also represents the major endocrine unit of the placenta and secretes numerous pregnancy-maintaining hormones, including human chorionic gonadotropin (hCG), human placental lactogen (hPL), estrogen and progesterone into the maternal circulation [34]. Further, the SCT expresses the neonatal Fc receptor (FcRn) that allows transport of maternal IgG antibodies to the fetal circulation [35]. This receptor preferentially binds and transports IgG1 antibodies that are effective at activating fetal natural killer (NK) cells to protect the neonate before birth [36].

Since the syncytial layer expresses paternal alleles and is in direct contact with circulating maternal immune cells, from a transplantation perspective, it should be recognized as foreign and targeted by the maternal immune system. However, this is not the case during pregnancy and the semi-allogeneic placenta and fetus are able to evade maternal immune rejection. The syncytia and villous CTBs do not express any class I or class II MHC molecules [37-39], suggesting that STB cannot present antigens to activate circulating maternal immune cells. This is thought to contribute to the normal immune evasion and/or suppression that occurs during pregnancy, however, the molecular mechanisms underlying the regulation of this ability are currently not well understood. *Uncovering these regulatory factors is key to elucidating immunological tolerance and developing interventions to treat pregnancy complications as well as cancer, HIV, and other diseases influencing the immune response.*

1.2.3 The extravillous trophoblast (EVT)

While the term "EVT" is most commonly used to describe invasive EVTs located within maternal decidua or spiral arteries, it can also be used to describe any trophoblast located outside of the villous tree. In human, EVT cells invade the decidua as well as part of the myometrium, which is critical for remodeling spiral arteries and establishing maternal blood flow into the intervillous space during pregnancy [40]. These EVTs originate from CTBs adjacent to the maternal decidua, including the CTBs within the cytotrophoblastic shell and/or at the tips of anchoring villi (CTB cell columns), which are thought to differentiate and become truly invasive EVTs once they contact the endometrial stroma and/or decidua [18-21]. Differentiation from a villous CTB stem cell to an invasive EVT involves a coordinated series of expression changes in adhesion molecules, metalloproteinases and cytokines, and immune-modulatory molecules. This switch in human is characterized by the upregulation of EVT-specific marker genes, including *HLA-G* [41], integrin α (*ITGA1* and *ITGA5*) [42], T-cell factor 4 (*TCF4*) [43], and *ADAM-12* [44,45].

There are two major subtypes of human invasive EVTs, which are identifiable by their localization: interstitial EVTs (iEVTs) that invade the decidual stroma, and endovascular EVTs (eEVTs) that colonize the spiral arteries [46]. Both iEVTs and eEVTs are derived from CTB cells, however, eEVTs represent a terminal stage of iEVT differentiation. [42,47,48]. iEVTs are numerous within the decidua surrounding the maternal spiral arteries during the first and second trimesters of pregnancy and are also present in the term placenta but to a much lesser extent. By the end of the first trimester, eEVTs appear and migrate along the inside of the arteries, where they facilitate spiral artery remodeling and the establishment of the full maternal arterial blood flow to the placenta [49].

Similar to the syncytia, EVT cells are in direct contact with maternal immune cells, including decidual natural killer (NK) cells, macrophages, and T cells [50]. Thus, the semi-allogeneic EVTs must also evade and/or suppress maternal immune rejection throughout pregnancy. To facilitate this, invasive EVTs express the nonclassical class I HLA-G molecule,

which protects EVTs from uterine NK lysis by activating an NK inhibitory receptor [51-55]. In addition to HLA-G, EVTs express HLA-C and -E that also act as ligands for inhibitory receptors to downregulate the cytotoxicity of NK cells [56-58]. Despite this negative regulation by EVTs, the complete absence of maternal immune cells is detrimental to placentation and can lead to pregnancy loss [59]. For instance, the specific deletion of decidual NK cells results in poor endometrial vascularization and impedes EVT trophoblast invasion [60]. This suggests that despite the risk of maternal immune rejection, maternal immune cell infiltrates are crucial for proper angiogenesis, EVT invasion, and ultimately a successful pregnancy.

1.3 Defective deep placentation

It is well-established that human placentation is associated with unique deep EVT invasion and vascular remodeling. This deep placentation involves an almost full transformation of the decidual and myometrial segments of approximately 30 to 40 spiral arteries [61,62], and defective deep placentation is thought to underlie a number of major pregnancy complications. Since the physiologic transformation of the spiral arteries is not an “all or none” phenomenon, defective deep placentation is characterized by the absent or incomplete remodeling of the myometrial segment of the spiral arteries [63]. Preeclampsia and fetal growth restriction were the first pregnancy complications shown to be associated with defective deep placentation [64,65], and in recent years it has also been described in spontaneous abortion [66,67], and preterm birth [68,69]. Thus, defective deep placentation is associated with a spectrum of clinical outcomes and pregnancy complications.

In addition to defective deep EVT invasion, abnormalities in the uterus and its vascular supply may also lead to inadequate spiral artery remodeling [70]. The maternal factors preventing normal vascular remodeling are not fully understood but may include underlying vascular disease leading to local tissue hypoxia (diabetes, hypertension), genetic polymorphisms associated with

abnormal vascular function, autoantibodies directed against maternal endothelium, and dysfunction of uterine NK cells. While more than one mechanism may lead to defective deep placentation, the common pathophysiologic consequence is placental ischemia due to maternal under perfusion of the intervillous space. The clinical outcome and complications associated with placental ischemia may be influenced by several factors, including the extent, onset, and duration of ischemia, as well as genetic and environmental factors. For instance, it has been suggested that the placental defects in preeclampsia are more severe and may begin earlier in gestation than those associated with spontaneous preterm birth. The pregnancy complications associated with defective deep placentation including fetal growth restriction, preeclampsia, preterm birth, and pregnancy loss are discussed in more detail below.

1.3.1 Fetal growth restriction

Fetal growth restriction, also called 'intrauterine growth restriction' and 'small for gestational age', refers to a fetus with an estimated weight below the 10th percentile for gestational age with evidence of adverse perinatal outcomes [71]. It can occur in up to 10% of pregnancies, and fetuses that suffer from fetal growth restriction are at risk for adverse neonatal outcomes, including stillbirth or preterm birth, and long-term health consequences such as neurodevelopmental delay [72,73]. Risk factors for fetal growth restriction can be divided into three broad categories: fetal, maternal, and placental. Fetal risk factors include chromosomal disorders, confined placental mosaicism, viral infections, and congenital malformations. When the fetus is devoid of structural and genetic defects, preeclampsia is the most common maternal condition associated with fetal growth restriction. Additional maternal risk factors include chronic or pregnancy-induced hypertension, vascular diseases, thrombophilia, poor nutrition, smoking, and drug or alcohol abuse.

The underlying cause of fetal growth restriction, when not attributable to structural or genetic defects of the fetus, is considered 'placental insufficiency' [74,75]. This is a universal term that encompasses the failure of the fetus to acquire adequate nutrients and oxygen. Several reports

have shown that placentas from pregnancies complicated by fetal growth restriction have incomplete remodeling of the myometrial segment of the spiral arteries [66,76,77], as well as reduced levels of endovascular EVT invasion [78-80]. These studies suggest that inadequate EVT invasion and spiral artery remodeling likely lead to maternal under perfusion in fetal growth restriction. Since the placenta consumes a large proportion of nutrients transferred during pregnancy, even a mild reduction in maternal blood perfusion can lead to inadequate nutrient transfer and fetal growth restriction [81,82].

1.3.2 Preeclampsia

Preeclampsia, also referred to as toxemia or pregnancy-induced hypertension, is a pregnancy-specific syndrome, and is defined as *de novo* hypertension present after 20 weeks of gestation combined with proteinuria (>300 mg/day) [83]. It affects 3-5% of pregnancies, and is one of the main causes of maternal, fetal, and neonatal mortality, especially in low- and middle-income countries [84,85]. Pregnancies complicated by preeclampsia are also often complicated by fetal growth restriction and placental abruption and are at a higher risk for adverse outcomes, such as stillbirth, neonatal death, and prematurity-associated problems from early delivery. Further, the risk of maternal morbidity is significantly elevated when preeclampsia develops before 32 weeks' gestation [86]. Severe preeclampsia can also manifest as a pregnancy complication characterized by hemolysis, elevated liver enzymes, and a low platelet count (HELLP syndrome). Risk factors for developing preeclampsia include chronic maternal hypertension, diabetes, renal disease, advanced maternal age, first pregnancy, and previous/family history of pre-eclampsia [87,88].

While the exact pathogenesis of preeclampsia remains unclear, placental dysfunction is thought to be the underlying cause since several clinical symptoms are placenta-derived and the only cure for preeclampsia is delivery of the placenta [89,90]. Further, the placental bed of patients with preeclampsia is characterized by a large number of non-transformed myometrial spiral arteries and the presence of obstructive lesions, such as acute atherosis and thrombosis [64,69,91]. These

findings highlight the potential role of defective deep placentation and ischemic insult in preeclampsia. An association between preeclampsia and gene variants involved in thrombophilia, inflammation, oxidative stress, and the renin angiotensin system have also been identified [92-97]. Interactions between maternal thrombophilic gene variants and genes encoding fetal HLA-C (expressed by EVTs) have also been shown to predispose women to preeclampsia in several populations, suggesting a role of an impaired immune tolerance in the pathogenesis of preeclampsia [98-100].

1.3.3 Preterm birth

Preterm birth is defined as delivery before 37 weeks' gestation and the major unifying factor impacting both fetal and neonatal mortality and morbidity [101]. In 2014, preterm birth occurs in ~10.6% of pregnancies globally, ~13.4% of pregnancies in North Africa, ~11.2% of pregnancies in North America, and 8.7% of pregnancies in Europe [102]. Besides an increased likelihood of perinatal mortality, prematurely born infants are also at greater risk for having subsequent serious chronic health problems, including neurological, cardiovascular, respiratory, gastrointestinal, hematological, and immunological complications. Preterm birth can arise via several different obstetric scenarios, including (1) delivery for the benefit of maternal or fetal health, in which labor is either induced or the infant is delivered by pre-labor cesarean section (30-35% of preterm births); (2) spontaneous preterm labor with intact membranes (40-45% of preterm births); and (3) preterm premature rupture of the membranes (PPROM), irrespective of whether delivery is vaginal or by cesarean section (25-30% of preterm births) [103]. Severe preeclampsia, fetal growth restriction, and placental abruption are all common reasons for the induction of preterm birth. Risk factors for spontaneous preterm births include: previous preterm birth, black race, and low maternal body-mass index [104].

Several features are commonly observed in preterm birth, including infection or inflammation, uteroplacental ischemia or hemorrhage, uterine overdistension, stress, and other

immunologically mediated processes [105]. Since many of these features can be directly or indirectly attributed to defective spiral artery remodeling and ischemic insult, defective deep placentation is thought to be one of the main underlying mechanisms of preterm birth. This is further supported by several studies showing that placentas from preterm birth had a greater degree of failed spiral artery remodeling in both the myometrial and decidual segments [68,69]. It has also been noted that the extent of this defect was much greater in patients with preeclampsia than in women with preterm birth alone [69]. These observations suggest that the defective placentation in preeclampsia, which consistently involves the decidual and myometrial segments, is more severe and likely begins earlier in gestation than in most cases of preterm birth.

1.3.4 Miscarriage, stillbirth, and pregnancy loss

Miscarriage, also called spontaneous abortion, is defined as fetal death before 20 weeks gestational age; while stillbirth, or intrauterine fetal demise, is defined as fetal death after 20 weeks gestational age. 'Pregnancy loss' serves as an umbrella term for fetal death regardless of the gestational age. An estimated 50% of all conceptions are lost at preclinical stages due to biochemical or implantation errors [106,107], and a further 9-20% of clinically recognized pregnancies are miscarried, largely within the first 5 to 12 weeks of gestation [108,109]. Maternal risk factors of pregnancy loss include: autoimmune disorders, bacterial and viral infections, induction from medical procedures, alcohol and drug use, poor nutrition, advanced maternal age, environmental exposures, diabetes, preeclampsia, and physical trauma. Further, fetal risk factors for pregnancy loss include: birth defects, chromosomal aberrations, fetal growth restriction, and placental abruptions.

Pregnancy loss may occur for many reasons, not all of which are known. However, placental malformation and/or dysfunction is commonly described in both early miscarriages and stillbirths [110-113], suggesting that placental pathologies play a substantial role in pregnancy loss. Indeed, compared with normal pregnancies, placentas from miscarriages have significantly

decreased levels of endovascular EVT invasion in the deeper myometrial segments of the spiral arteries, but increased levels in the lower decidual segments [67]. This suggests that endovascular EVT invasion may become arrested at the decidual level and fail to progress into the deeper myometrial segment of the spiral artery in patients with miscarriage. Further, Khong et al. described that the failure of physiologic transformation of the spiral arteries was observed in the placental bed of a late-stage spontaneous abortion [114]. In another study, the predominant defect in placental samples from early miscarriages was described as a poorly developed cytotrophoblastic shell and scant cell columns [115], which are important precursors for normal EVT invasion. These observations support the idea that placental defects contributing to miscarriage occur much earlier and are more severe compared to those contributing to fetal growth restriction and preeclampsia.

1.4 Models for studying human placentation

1.4.1 Animal models

A wide variety of different placentation strategies exist across mammals. This is especially apparent when comparing the maternal-fetal interface and the cellular barrier(s) that exist between the maternal and fetal circulations [116]. Humans, as well as many non-human primates and rodents have a *hemochorial* placenta, where the invasive trophoblast cells infiltrate the uterine arterial walls and come into direct contact with maternal blood [117]. Cats, dogs, and most other carnivores have an *endotheliochorial* placenta, where the placental trophoblast cells contact the maternal endothelial cells. Whales, horses, and most ruminants have an *epitheliochorial* placenta, where the placental trophoblast cells contact the maternal uterine epithelium [118].

Even though both human and mouse have hemochorial placentas, there are considerable structural and developmental differences that exist between the placentas of these two species. For instance, initial human placental invasion occurs via the multinucleated primary syncytium at the beginning of gestation, while initial mouse placental invasion occurs via mononuclear trophoblasts

almost halfway through gestation [117]. Further, the deep interstitial EVT invasion observed during human placentation is not recapitulated in mouse. Unlike the human villous placenta, the site maternal-fetal exchange in the mouse is a labyrinth that has a complex tightly packed arrangement of maternal and vascular channels. Lastly, transcriptomic comparison of mouse and human placental samples across gestation has identified several clusters of genes with very different expression patterns between the two species [119]. These substantial differences in placentation make it difficult to translate findings across human and mouse. Despite these caveats, valuable insights have been attained using genetic knockout mouse models to study placentation [120]. For example, placental defects are highly prevalent in embryonic lethal mouse mutants, and several genes involved in epithelial-mesenchymal transition in cancer play a critical role during normal mouse placental development [121]. These findings are relevant to all placental mammals that experience pregnancy loss, including humans.

While most mammalian species poorly recapitulate human placentation, non-human primate animal models, particularly rhesus macaques (*Macaque mulatta*), share many key features of human placentation. Besides being comparable in placental morphogenesis, the overall structure and nature of both the STB interface layer and intervillous space, as well as endocrine functions and extracellular matrix changes are similar between rhesus and human placenta [3-5,7]. Further, there is a strong resemblance between human and rhesus placental endovascular EVT invasion and spiral artery transformation [6], processes known to play a central role in the pathogenesis of several pregnancy complications in humans [61]. Thus, unlike mouse, the rhesus monkey represents a suitable animal model for studying arterial transformation in the context of normal and abnormal human placentation.

Even though the structural and developmental characteristics of the rhesus placenta are highly similar to human, previous studies have revealed some notable differences in the expression level and/or protein-coding potential of well-known human placental markers in rhesus, including CGA, HLA-G, ERVW-1, and SIGLEC6 [122-125]. Differences in placental invasion have also

been noted, as the extent and depth of interstitial EVT invasion is greater in human compared to rhesus placentation [4]. Further, while a few cases of preeclampsia have been documented in rhesus and other non-human primates, this disease is often associated with defective deep interstitial EVT invasion that is unique to humans and great apes [126-130]. Therefore, further comparison of these two closely related species will not only help elucidate the translatability between human and rhesus placental studies but may also provide valuable insight into the molecular origin of human-specific placental features and pregnancy-related diseases, like preeclampsia.

1.4.2 In vitro cell models

1.4.2.1 Human primary trophoblast and placental explant cultures

Primary cell cultures of villous CTBs have been a valuable *in vitro* model for studying human trophoblast differentiation since they spontaneously differentiate and fuse after ~24 h in culture and form a syncytium that secretes hCG and hPL [24]. Villous CTBs can be isolated from placentas of any gestational age but they are most commonly from first trimester placentas obtained following termination of pregnancies, or from human term placentas that are readily available following delivery [131,132]. Placentas from early gestation may be more challenging to obtain in some countries due to ethical and/or legal issues, while access to mid-gestation human placental samples is extremely rare. Late gestation placentas have the additional advantage of being much larger than first trimester placentas, they often allow higher yield of isolated villous CTBs. However, preparations from term tissue may contain an abundance of other cell types since the tissue contains a large fraction of cells from the villous core (i.e. fetal fibroblast, endothelial, and immune cells), as well as decidual and maternal/fetal blood. A purer population of villous CTB cells is possible using first trimester placental tissue since very little maternal/fetal blood is present, the decidua is easily removed, and the villous core is less developed at this gestational age. Regardless of the gestational age of the placenta, the methods used for CTB isolation are broadly similar and are based on enzymatic digestion of mechanically minced villous tissue, from which contaminating

maternal blood has been removed. An initial digestion is frequently performed to remove the overlaying STB and EVTs, and a discontinuous Percoll density gradient is typically used to purify the CTB cells before culture [24].

Since invasion and transformation of the spiral arteries is mostly complete by mid-gestation, trophoblasts isolated from late gestation placentas are largely non-invasive. Thus, it is more common to study EVTs from first trimester placentas since they retain their invasive phenotype *in vitro* [133]. To study EVT invasion, first trimester villous explants are often cultured on top of a layer of Matrigel. Culturing the explants on a deep layer of Matrigel allows the depth of EVT invasion to be quantified [134] while culturing them on a thin layer of Matrigel facilitates EVT two-dimensional outgrowth, which allows for easy isolation and quantification [135]. In addition to EVT invasion, placental explant cultures have been useful for studying other characteristics of the human placenta. For instance, some of the earliest studies using placental explants were used to measure oxygen consumption [136-138]. In 1970, Fox et al., cultured placental explants at varying oxygen concentrations and revealed that low oxygen conditions increased CTB proliferation [139]. Overall, placental explants and primary trophoblast cultures represent valuable *in vitro* models for studying many different features of human placentation, including cellular uptake, production and release of secretory components, cell interactions, proliferation, growth and differentiation, gene delivery, pharmacology, toxicology, and disease processes. However, there are several limiting factors associated with these *in vitro* models that should be considered before use, including a lack of access to researchers not located at a medical center, restricted experimental use due to ethical regulations and/or patient consent constraints, and issues relating to sample variability and experimental reproducibility.

1.4.2.2 Immortalized and choriocarcinoma-derived human trophoblast cell lines

Since primary trophoblasts have a limited life span, fresh cell preparations are needed for each new experiment. This requires continuous access to viable placental tissues, which can be difficult,

particularly for early gestation tissues. For this reason, researchers have turned to established human trophoblast cell lines, which have been generated using a range of immortalization techniques. Two of the most widely used human trophoblast cell lines, HTR8/SVneo and Swan 71, were both derived from first trimester trophoblasts and exhibit features of primary invasive EVT cells. The HTR8/SVneo trophoblast cell line was immortalized via electroporation of the pSV3-neo plasmid containing simian virus 40 large T antigen and was classified as a trophoblast cell line based on the following characteristics: cytokeratin-positive, expresses hCG, secretes type IV collagenase, and exhibits invasive abilities *in vitro* [140]. In contrast, the Swan 71 trophoblast cell line was immortalized by exogenous expression of hTERT and classified as a trophoblast cell line based on the following characteristics: expresses cytokeratin-7, vimentin, and HLA-G, secretes fetal fibronectin and low-levels of hCG and exhibits a cytokine and growth factor profile that is similar to primary trophoblast cells [141]. Spontaneously immortalized trophoblast cell lines also exist, including the source of the HTR8/SVneo cell line, HTR-8 [140]. Unlike primary trophoblasts, these immortalized cell lines can be cultured indefinitely and easily frozen down and thawed for new experiments.

Other widely used cell lines for studying trophoblast functions include BeWo, JEG3, and JAR [142]. Both BeWo and JAR were derived from metastatic deposits of gestational choriocarcinoma [143,144]. The JEG-3 line was sub-cloned from BeWo and both are hypertriploid with approximately 70 chromosomes [145]. BeWo cells are the most extensively used *in vitro* model to study trophoblast fusion and STB formation, as this cell line exhibits small amounts of spontaneous fusion that can be enhanced by treatment with cAMP, its analog 8-bromo-cAMP, or forskolin [146]. The JEG-3 cell line is widely used to study the molecular mechanisms underlying trophoblast invasion, however, it has also been proposed as a model for STB endocrine function since it retains the ability to produce progesterone, hCG [147], several steroids, and other placental hormones and enzymes [148-150]. While these cells are easy to culture and manipulate, providing a much-needed starting point for evaluation of trophoblast gene regulation and signaling pathways,

they have abnormally expanded and/or aneuploid genomes [151]. A recent study also revealed how poorly the expression profiles of freshly-isolated CTBs and EVTs matched those of JAR and JEG-3 cell lines, which are commonly used as models of the two cell types, respectively [152,153]. These differences highlight the importance of confirming findings using primary cultures and ultimately bring into question whether or not these cell lines are representative of bona fide trophoblasts *in vivo.*

1.4.2.3 Human embryonic stem cell derived trophoblasts

Since immortalized and choriocarcinoma-derived trophoblast cell lines can only mimic specific phenotypes of either EVTs or STBs and are unable to differentiate from a progenitor to a terminally differentiated phenotype, they are suboptimal for studying trophoblast differentiation. Thus, researchers have turned to pluripotent stem cells for a consistent, widely accessible model to study human trophoblast differentiation. By culturing them in the presence of BMP4 and inhibitors of FGF2 and TGFβ signaling, human embryonic stem cells (hESCs) have successfully been differentiated into trophoblast cells by several groups [154-156]. These hESC-derived trophoblast cells exhibit several characteristics similar to primary trophoblast cells, including the downregulation of C19MC microRNAs, hypomethylation of the ELF5 promoter, formation of STB that secretes hCG and expresses the EVT marker, HLA-G, as well as expression of other well-documented trophoblast genes (KRT7, GATA2/3, and TCFAP2A/C) [155-158]. However, the comparative transcriptomic analysis revealed that hESC-derived trophoblasts represent a trophoblast subtype unlike those of primary term trophoblasts [159]. While this approach is able to promote hESC differentiation towards the trophoblast lineage, the identity of hESC-derived trophoblasts and the cells they most closely resemble *in vivo* remains unclear.

1.5 Endogenous retrovirus activity during early development and placentation

As mentioned above, endogenous retrovirus (ERV) derived proteins appear to play an important role in placentation and other reproductive processes in mammals. ERVs are derived from exogenous retroviruses, which exist in different forms throughout their life cycle. A viral particle, or virion, protects the RNA genome of the retrovirus outside of the host cell during infection of new cells. A virion that enters a new host cell deploys its genomic payload, using its reverse transcriptase to convert the two copies of single stranded RNA viral genome into a double stranded DNA copy that is then integrated into the host genome and referred to as a provirus (**Figure** 1.3). Subsequently, a provirus can be transcribed into RNA again, and either translated by the host's ribosomal machinery to produce more virions or reverse transcribed to create new insertions in the host genome. Ancient retroviral infections have occasionally resulted in proviral integrations into the germline of the host, becoming so-called endogenous retroviruses (ERVs). While some ERVs have been shown to produce infectious particles [160], most ERV copies suffer mutations over evolutionary time. This prevents not only the normal assembly of viral particles but also the horizontal transmission of infections between individuals. However, even though ERVs are trapped within the host genome, some provirus copies are still transcribed and can encode some if not all of the original viral proteins. Therefore, ERVs are classified as a family of autonomous retrotransposons. Vertical transmission of ERVs is possible since offspring can inherit germline ERV insertions from their parents (**Figure** 1.4). As much as 8% of the human genome consists of ERV sequences acquired through repeated endogenization events and subsequent expansion of captured viral subfamilies [8].

While there are no known replication-competent ERV proviral insertions within the human genome, the presence of several polymorphic ERV insertions indicates that some ERVs were active and infectious up until at least 5-6 million years ago [337,338]. A consequence of this recent activity is that many ERV loci are highly-similar, which makes it difficult to analyze locus-specific ERV

expression using traditional short-read RNA-seq data. Due to these challenges, alternative long-read RNA-sequencing strategies (e.g. PacBio, Oxford Nanopore), as well as specialized bioinformatic tools and strategies designed for short-read RNA-seq data (e.g. TE toolkit, filtering of non-uniquely mapping reads) are commonly used to study ERV locus specific attributes, including regulation and expression.

These ancient genomic prisoners represent a potent source of genomic and regulatory variability. The high degree of homology between the long terminal repeats (LTRs) at either end ERV proviruses (**Figure** 1.3) provides an opportunity for non-allelic homologous recombination. This can result in the excision of a given insertion, leaving behind only a single LTR copy. Recombination events between the different insertions of the same or similar ERV subfamilies can produce deletions, duplications, and other rearrangements of intervening genomic sequences. Additionally, the ERV sequences themselves can contain motifs that can disrupt or modulate nearby genes and regulatory regions. Thus, it is not surprising that ERV activity is associated with a number of human diseases and the target of epigenetic repression by the host genome. However, the consequences of ERV activity are not solely deleterious, as there is evidence that ERVs have been co-opted into important developmental roles as well.

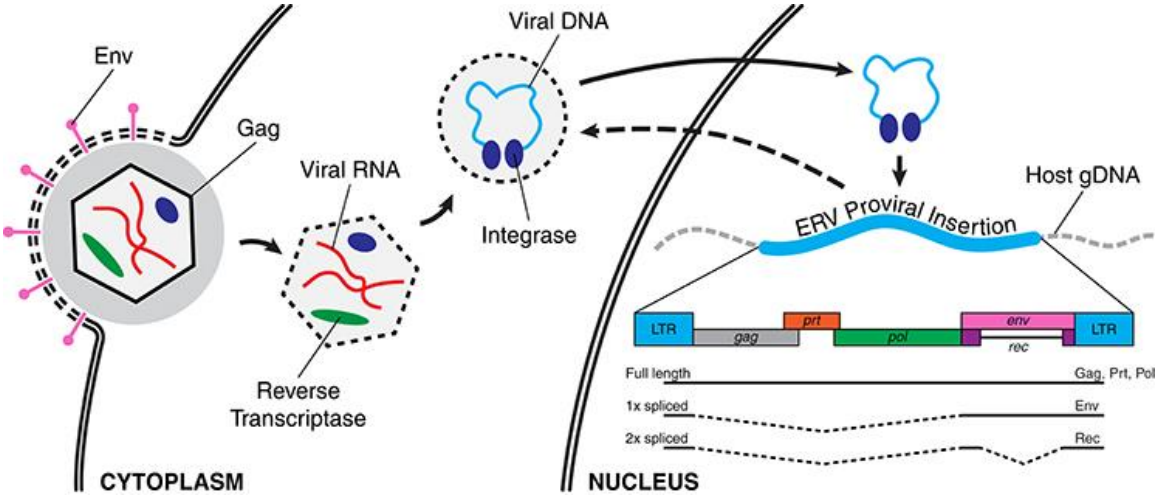

Figure 1.3 Retroviral infection and integration into the host genome

Left to right: An infecting viral particle enters the host cell after its envelope, containing Env proteins (pink), fuses with the cell membrane. The viral capsid (hexagon), consisting largely of Gag proteins, contains the RNA form of the retroviral genome (red) as well as a reverse transcriptase (green). The viral genome is subsequently reverse transcribed into its DNA complement (light blue) and this viral genome then enters the nucleus with its associated integrase proteins (dark blue). A new viral integration is then inserted into the host genome, becoming a provirus. Lower right: A schematic of a retroviral genome with components indicated as colored boxes (gag, group-specific antigen; prt, protease; pol, polymerase; env, envelope protein; rec, accessory protein; LTR, long terminal repeat). Three splice variant transcripts are shown and their translated products are given.

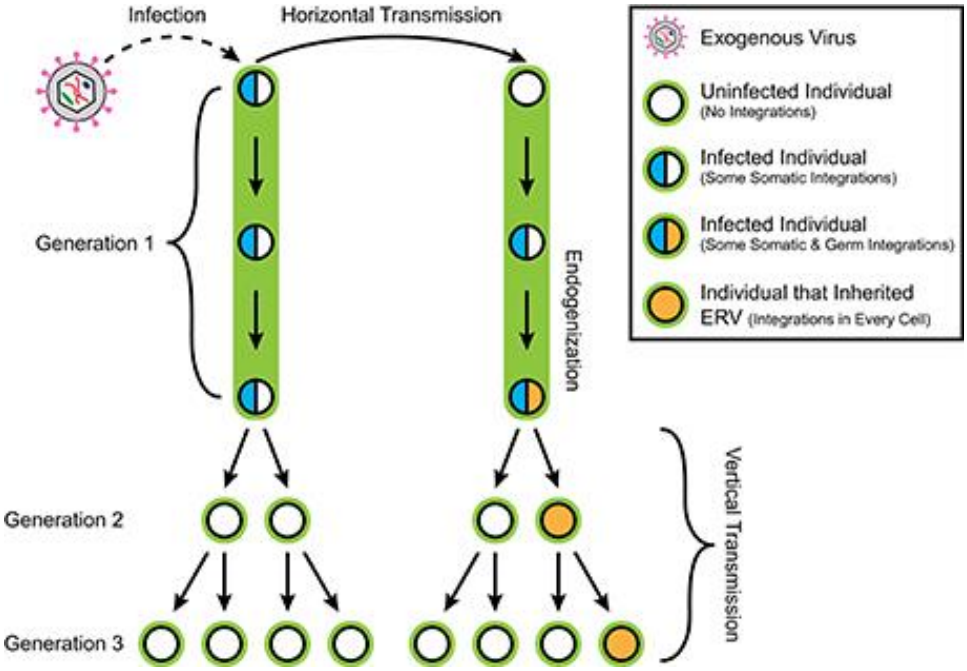

Figure 1.4 Retroviral infection, horizontal transmission, endogenization, and vertical transmission

An exogenous retrovirus infects an individual in generation 1, resulting in their accruing provirus integrations in some somatic cells. Horizontal transmission of the virus from the first individual to the second results in the second accruing somatic integrations as well. However, the second individual subsequently receives germline integrations. The descendants of the first individual do not inherit any retroviral integrations, while any germline integrations in the second individual are transmitted vertically to half of its descendants as endogenous retrovirus insertions present in every cell. Only half of the descendants of this second individual in Generation 2 inherit any given germline integration locus because any cell receiving a new integration does so on only one copy of the affected chromosome. This results in a heterozygous pattern of inheritance.

1.5.1 ERVs in germ cells and pre-implantation embryos

Certain stages in mammalian pre-implantation embryo and germ cell development pose a unique challenge for the control of endogenous retroviral activity, as multiple waves of epigenetic reprogramming during this period cause major regulatory and expression changes across the genome. During the two waves of epigenetic reprogramming that occur in primordial germ cells (PGCs) and fertilized oocytes, a considerable amount of DNA demethylation occurs. Examination of global DNA methylation at these stages has shown that levels within human and mouse pre-implantation embryos decrease beginning at the 1- to 2-cell stage, depending on the species, and up to or soon after reaching the blastocyst stage [161-165]. Since DNA methylation is largely responsible for the repression of many transposable elements, including ERVs in somatic cells [166], the activity of ERVs and the alternative mechanisms repressing ERV activation during these periods of global hypomethylation have been the focus of a number of recent investigations.

Given that some ERV families have substantially expanded their number of proviral genomic insertions in animals [167,168], it has been hypothesized that widespread reactivation of ERVs during the waves of global reprogramming within germ cell and pre-implantation development is largely responsible for this expansion. On the other hand, it is also known that additional ERV repressive mechanisms must be in place to maintain genomic stability throughout epigenetic reprogramming and the highly choreographed molecular processes required for normal germ cell development, fertilization, and embryonic development. These ideas are not mutually exclusive, as there is substantial evidence supporting both reactivation [13,169,170] and alternative repression [171-177] of ERVs within the genome during germ cell development and embryogenesis.

Despite the existence of elaborate mechanisms that mediate ERV inactivation, there is also extensive evidence that some ERVs are still active and play essential roles during gametogenesis and pre-implantation development. Upregulation of ERV proviral transcription and protein expression has been well-documented in hESCs and early human embryos. For example, elevated

expression of the ERVH family has been observed within both naïve-like and primed hESC sub-populations [170,178]. Additional transcripts from the ERVK (HML-2) family are also observed at high levels within hESCs and rapidly decrease upon differentiation [169]. Expression of ERVK begins at the 8-cell stage, concurrent with embryonic genome activation (EGA), and continues throughout pre-implantation development into the blastocyst stage. A majority of actively transcribed ERVK loci during this time are associated with LTR5HS, a specific subclass of LTR, which is confined to human and chimpanzee and contains an OCT4 binding motif. The LTR5HS subclass requires both hypomethylation and OCT4 binding for transcriptional activation, which synergistically facilitate ERVK expression [13]. Based on the elevated activity of these ERVs within hESCs and pre-implantation embryos, as well as their known interactions with other factors during this time, it is thought that these ERVs have been functionally incorporated into roles important for defining and maintaining pluripotent specific states.

The role of LTRs as regulatory regions for proviral DNA represents an additional function that can be utilized by or incorporated into host genomes. In particular, LTRs are known to be co-opted as promoters or enhancer elements of nearby genes important during embryonic development and maintenance of pluripotency [179]. Nearly, ~33% of all transcripts in human embryonic tissues are associated with repetitive elements, suggesting a clear pattern of embryonic cell specificity for viral promoters [180]. Many transcripts detected in the totipotent blastomeres of mouse 2-cell embryos are initiated from LTRs upon EGA as well, indicating that these repeat sequences may help drive cell-fate regulation in mammals [181]. Certain LTRs have also been shown to provide important regulatory functions not only in embryonic cells but also within germ cells during gametogenesis. For example, germline-specific transactivating p63 (GTAp63), a member of the p53 family important for maintaining genetic fidelity in the human male germline, is under the transcriptional control of ERV9 LTR [182-184]. Transcriptionally active GTAp63 suppresses proliferation and induces apoptosis upon DNA damage in the germ cells of normal testes and is frequently lost in human testicular cancers. Restoration of GTAp63 expression levels in cancer

cells was observed upon treatment with a histone deacetylase (HDAC) inhibitor, indicating possible epigenetic control of ERV9-mediated GTAp63 expression via activating histone acetylation marks. Thus, the ability of ERV9 regulatory regions to contribute to the maintenance of male germline stability is yet another example of how ERVs have evolved to serve an important function in their human hosts [184].

1.5.2 ERVs in the placenta

It is well established that the DNA in both mouse and human placentas are hypomethylated compared to other somatic cells derived from either *in vivo* or *in vitro* sources [185-189]. As such, the DNA methylation levels of LTRs within human placentas more closely resemble those observed in oocytes than in somatic tissues such as the brain, averaging ~60% methylation across the genome [190]. Given the hypomethylation of LTRs in the placenta, it is not surprising that numerous sub-families of ERV proviruses are expressed within human placental tissues. More specifically, there is evidence of proviral transcription from ERVE [191], ERV3 [192], ERVK [10], ERVfb1 [193], ERVV1/2 [124], ERVW [194] and ERVFRD [195].

The most notable ERV families producing functional proteins during placentation are ERVW and ERVFRD, corresponding to Syncytin-1 and Syncytin-2, respectively, which are critical for the cellular fusion underlying human placental syncytia formation and maintenance [194-198]. Cell fusion is a relatively unique function in normal healthy tissues, with muscle, bone, and placenta being the major exceptions. Since regulation of this highly specified function is of much interest, the precise mechanisms underlying the transcriptional control of the Syncytin genes have been the topic of several investigations. Both DNA and histone H3K9 methylation have been reported to be important for inactivating ERVW and repressing Syncytin-1 expression, resulting in pathological conditions such as exogenous viral infections and preeclampsia when repression does not occur [199-202]. It has also been shown that transcriptional activation of the ERVW locus and promotion of cell fusion also requires the synergism of LTR promoter hypomethylation, along with the binding

of several transcription factors such as GCM1, SP1, and GATA family members [203-207]. Recently, another ERV-derived protein called Suppressyn was identified to alternatively regulate Syncytin-1, but not Syncytin-2-based cell fusion by inhibiting its interaction with the Syncytin-1 associated receptor, ASCT2 [193]. Suppressyn is a truncation product of the proviral env gene from the ERVfb1 element and is transcribed within the placenta. Within normal human placentas, Suppressyn is co-expressed with Syncytin-1 in the syncytiotrophoblast layer [193], further supporting that these two factors are involved in cell-cell fusion regulation at the maternal-fetal interface *in utero*.

Notably, integration of ERVW and ERVFRD into the genome occurred before the segregation of Old World monkeys (Catarrhini) [208] and New World (Platyrrhini) monkeys [195] respectively. Thus, Syncytin-1 and Syncytin-2 are only present in higher-order primate species [209]. Interestingly, functionally similar yet distinct ERV proviral proteins have been discovered throughout most mammalian genomes, representing a spectacular example of convergent evolution (reviewed in detail [209]). The ERVV *env* gene present within Old World monkeys has also been implicated in trophoblast fusion activity, possibly alleviating the lack of functional Syncytin-1 within these species, while the ERVV proviruses in the human genome are not functional in this capacity [124]. Syncytin-A and Syncytin-B appear to function like human Syncytin proteins within the mouse placenta and are known to have entered the murine lineages approximately 20 million years ago [210]. Similarly, Syncytin-Ory1 has been discovered in rabbits and hares (Leporidae; [211]), Syncytin-Car1 within 26 different species of carnivorans (Carnivora; [212]), Syncytin-Mar1 within the squirrel-related clade (either Scuridae or Marmotini; [213]), Syncytin-Ten1 within tenrec (Tenrecidae; [214]), Syncytin-Rum1 in ruminants (Ruminantia; [215]), and Syncytin-Opo1 within the short-lived placenta of opossum and kangaroo marsupials (Marsupialia; [216]).

Several ERV-captured *env* genes have been proposed to have an immunosuppressive role that is important for preventing maternal rejection of the semi-allogenic fetus during pregnancy. In addition to fusogenic properties derived from the ERVFRD *env* gene, Syncytin-2 contains a

classical env retroviral immunosuppressive (ISU) domain that has been shown to have immunosuppressive activity via an *in vitro* tumor-rejection assay [217]. Given observed protein expression within the cytotrophoblasts cells of the human placenta, Syncytin-2 has been suggested to facilitate fetal tolerance by suppressing the maternal immune system. Other ERV-derived env proteins from ERVV and ERVK have also been proposed to possess an immunosuppressive role in controlling the maternal immune system during pregnancy. This is based on findings that both families have one or more proviral loci in the genome with intact env open reading frames and a corresponding immunosuppressive domain. Additionally, both ERVV and ERVK expression has been observed within placental trophoblast cells at the maternal-fetal interface, although corresponding *in vitro* functional assays have not yet been completed to directly support this finding *in vivo* [10,218]. Until these studies are undertaken, the exact function of ERVV and ERVK and whether env protein expression from these ERVs induce maternal immunosuppression within the placenta will remain unknown.

1.5.3 ERVs and human disease

Through insertional mutagenesis, recombination between homologous copies, and the regulatory disruption that epigenetic suppression of ERV insertions can cause to nearby gene loci, there are many mechanisms by which these elements might cause disease. In particular, their association with various cancers has been well demonstrated, as reviewed in [219]. For instance, ERV activity has been strongly associated with many breast cancers [220-222]. While in melanoma tissues, ERVK expression of both RNA and protein has been shown [223], and one recent study identified 24 ERVK (HML-2) loci transcribed [224]. In another study of Hodgkin's lymphoma, all cancer patient samples were found to have alternative transcripts of the CSF1R, that initiated at the LTR of an ERV located ~6.2 kb upstream of the normal promoter [225].

Besides multiple types of cancers, ERVs have also been demonstrated to be associated with a variety of neurologic diseases, as reviewed in [226]. In cases of amyotrophic lateral sclerosis

(ALS), elevated ERVK (HML-2) activity was detected in the brain tissue of ALS patients [227]. Moreover, transgenic animals expressing the ERVK env gene in cortical and spinal neurons were shown to develop motor dysfunction, suggesting that these elements may contribute to neurodegeneration [228]. Lastly, the expression of ERVW env and gag has been observed in muscle samples from ALS patients [229], which may be due to the inflammatory response from the disease itself [230]. Nonetheless, the support for the involvement of at least ERVK in ALS is mounting, though causality has yet to be demonstrated.

Multiple sclerosis (MS) is another neurological disease in which ERVs have been strongly implicated. MSRV (multiple sclerosis-associated retrovirus), a subtype of ERVW, as well as ERVW1/W2 and ERVH/F, have all been linked to MS (reviewed in [231]). In particular, one study showed significantly elevated env antigen in the serum of MS patients relative to controls, and qPCR of peripheral blood mononuclear cells (PBMC) revealed an association between ERVW and MS [232]. This same study demonstrated elevated Env expression in eight well-characterized MS brains that had lesions throughout the parenchyma and in both perivascular infiltrates and the rim of chronic active lesions. Other studies have reported ERV expression associated with schizophrenia and bipolar disorder through the detection of ERVK and ERVW in blood, cerebrospinal fluid, and the pre-frontal cortex [233-236]. In one study of schizophrenia, hypermethylation of a specific ERVW LTR insertion located in the regulatory region of the *GABBR1* gene was associated with increased risk of schizophrenia [237]. A nearly full-length ERVK insertion near the *PRODH* gene, which is known to be associated with schizophrenia and other neuropsychiatric disorders, has been shown to work in concert with the internal *PRODH* CpG island to activate the gene. Thus, it is thought that aberrant DNA methylation of this locus may contribute to the development of schizophrenia [238].

1.5.4 ERVs may play a role in the innate immune response

While the majority of ERV proviruses have acquired mutations, thereby preventing translation into protein, certain families have been especially well preserved and contain functional ORFs for one or more of the classical proviral genes. Within primates, ERVK (HML-2) represents the best-preserved and most recently active ERV, containing a substantial number of loci that have predicted coding potential throughout different primate genomes. It has also been observed that ERVK encodes a small accessory protein, Rec, in naïve ES cells and human blastocysts. Overexpression of Rec protein within human pluripotent cells increases the innate antiviral response and can inhibit exogenous viral infections, suggesting an immunoprotective role of the ERVK Rec protein during early embryonic development [13]. An additional ERVK proviral protein, Gag, which makes up the core of viral particles in exogenous retroviruses, is also expressed within human blastocysts and pluripotent cells. Immunolabeling of ERVK gag protein followed by confocal and transmission electron microscopy revealed ERVK gag protein within structures of blastocysts resembling viral-like particles (VLPs). This suggested that some ERV proviral sequences in the human genome still retain the ability to code for viral proteins and form VLPs during normal human embryogenesis. Similarly, proteins produced from ERV env genes have also been demonstrated to function as restriction factors against exogenous retroviral infection [239].

Even though some ERV proviruses do not contain functional ORFs, they can still harbor sequence motifs that serve to modulate the activity of nearby genes. For instance, interferon (IFN)-inducible enhancers have been dispersed by ERV insertions adjacent to IFN-inducible genes over mammalian evolution. This has resulted in gene regulatory networks being able to work in concert due to the presence of these ERV sequences. Further, CRISPR-Cas9 deletion of a MER41 insertion upstream of AIM2 in HeLa cells was shown to disrupt the endogenous IFNG-inducible regulation of this locus, demonstrating that host genomes can harness ERV sequences over time [240]. In another example of ERV involvement in innate immunity, Chiappinelli et al. demonstrated that induction of ERV expression, especially bidirectional transcription of ERVs, activated a double-

stranded RNA sensing pathway that triggered a type I interferon response and apoptosis [241]. Determining exactly how ERVs influence interferon expression and function to regulate innate immunity should be the focus of future studies.

1.5.5 Conclusions

The relationship between ERVs and the human genome is a diverse and complicated one, resulting from millions of years of co-evolution. ERVs are known to be involved in disease through insertional mutagenesis, as targets of epigenetic repression, and via recombination of sequences between the homologous copies of these elements scattered across the genome. Throughout mammalian evolution, the deleterious effects of ERVs seem to be balanced by the benefits gained from the innovative co-option of their sequences and proteins by host genomes. These innovations include the intimate relationship between ERV activity with embryonic and placental development, as well as a number of ERV-associated regulatory networks that have become important components of our genome. An innate immune response to exogenous retroviral infection is likely only one of several roles that ERVs serve. Once thought to have been quiescent, non-functional residents of the human genome, we are only beginning to uncover the scope of how actively intertwined our biology is with these long-time genomic partners.

1.6 Summary

Altogether, these studies clearly demonstrate the importance of normal placentation for the health and well-being of both the mother and fetus throughout pregnancy. However, despite its importance in reproductive success, there is still a limited understanding of how the human placenta develops and functions. Additionally, even though ERV expression is known to play important roles during early development and reproduction, the native expression and function of ERVK in the human placenta remains largely uncharacterized. In the following section, I will discuss the importance of primate placental research as well as the specific objectives of my studies.

1.7 Significance and Project Aims

1.7.1 Significance

The human placenta is a remarkable organ that depends on normal trophoblast differentiation and invasion to transport nutrients and protect the fetus throughout pregnancy. *Since trophoblast invasion and spiral artery remodeling predominantly occurs during the first trimester in humans [49], and defective deep placentation is thought to give rise to a number of major pregnancy complications [2], it is important to understand the early stages of human placentation during normal and pathological pregnancy conditions*. Because several challenges have historically limited the study of human and non-human primate tissues, relatively little is still known about the molecular mechanisms underlying the characteristic deep placentation observed in humans and great apes [126-130]. **My central hypothesis is that human-specific and/or human-elaborated features of placental development, including deep placentation and expression of human restricted ERVs, not only maximize the nourishing and protective capabilities of the placenta but also increase the susceptibility of humans to preeclampsia and other pregnancy complications.** The resources and findings presented here should enhance our understanding of

human placentation during normal and pathological pregnancy conditions, and may ultimately provide new diagnostic approaches and treatments for major pregnancy-related diseases in human.

1.7.2 Project Aims

Specific Aim I: To identify the transcriptional differences between the human and rhesus placenta. Although the human and rhesus placenta appear to be morphologically and functionally similar, previous studies have revealed some notable differences between the two species, including: (1) an increased extent and depth of interstitial EVT invasion in human compared to rhesus [4], (2) fewer cases of preeclampsia in rhesus and other non-human primates compared to humans [126-130], and (3) differences in the expression level and/or protein-coding potential of well-known human placental markers in rhesus [122-125]. Given these differences, *I hypothesize that many of the genes differentially expressed between human and rhesus placenta contribute to the molecular and cellular processes underlying EVT invasion and preeclampsia differences between these two species*. Ultimately, the identification of both shared and different molecular aspects of human and rhesus placentation will not only help elucidate the translatability of the rhesus animal model it may also provide valuable insight into the molecular origin of human-specific placental features and pregnancy-related diseases.

Specific Aim II: To elucidate the expression and function of ERVK (HML-2) during placentation. A recent expansion of ERVK insertions specifically within the human lineage has resulted in a number of largely intact human-specific proviral insertions with the ability to encode viral-like proteins when transcribed [242-245]. While the ERVK envelope-derived viral-like protein is known to be expressed during normal human placentation [10], the proviral locus/loci it is derived from and its potential functional role remains unknown. Previous studies have highlighted the fusogenic role of other ERV-derived envelope proteins (Syncytins) in mammalian placentation [194-198], as well as the fusogenic and immunomodulatory functions of exogenous

retroviral envelope proteins [246,247] and recombinantly expressed ancestral-predicted ERVK envelope proteins [248-251]. Given these previous findings, *I hypothesize that placentally-expressed ERVK envelope protein plays an important role in the trophoblast fusion and/or maternal immunomodulation required during normal human placentation, and that abnormal placental ERVK expression may contribute to pregnancy complications associated with placental dysfunction*. Therefore, my second aim was to elucidate the expression and function of ERVK in human placental tissues and/or trophoblast cells under normal conditions and in cases of preterm birth.

CHAPTER 2: Transcriptomic Analysis of Primate Placentas and Novel Rhesus Trophoblast Cell Lines Informs Investigations of Human Placentation

The work described throughout this chapter has been released as a preprint [252] and is currently under revision for publication in BMC Biology. For access to full supplemental data please refer to published material.

Jimi L. Rosenkrantz (rosenkrj@ohsu.edu)[1,2], Jessica E. Gaffney (jessgaffney@gmail.com)[2], Victoria HJ. Roberts (robertsv@ohsu.edu)[2], Lucia Carbone (carbone@ohsu.edu)[1,3-5*] and Shawn L. Chavez (chavesh@ohsu.edu)[1,2,6,7*]

[1]Department of Molecular and Medical Genetics, Oregon Health and Science University, Portland, OR 97239; [2]Division of Reproductive and Developmental Sciences, Oregon National Primate Research Center, Beaverton, OR 97006; [3]Division of Genetics, Oregon National Primate Research Center, Beaverton, OR 97006; [4]Department of Medicine, Knight Cardiovascular Institute, Oregon Health and Science University, Portland, OR 97239; [5]Department of Medical Informatics and Clinical Epidemiology, Oregon Health and Science University, Portland, OR 97239; [6]Department of Obstetrics and Gynecology, Oregon Health and Science University School of Medicine, Portland, OR 97239; [7]Department of Biomedical Engineering, Oregon Health and Science University School of Medicine, Portland, OR 97239

*To whom correspondence should be addressed:

Shawn L. Chavez, Ph.D.
505 NW 185th Avenue
Beaverton, OR 97006
email: chavesh@ohsu.edu
phone: 503-346-5423

Lucia Carbone, Ph.D.
3303 SW Bond Avenue
Portland, OR 97239
email: carbone@ohsu.edu
phone: 503-494-7342

2.1 Abstract

Background: Proper placentation, including trophoblast differentiation and function, is essential for the health and well-being of both the mother and baby throughout pregnancy. Placental abnormalities that occur during the early stages of development are thought to contribute to preeclampsia and other placenta-related pregnancy complications. However, relatively little is known about these stages in humans due to obvious ethical and technical limitations. Rhesus macaques are considered an ideal surrogate for studying human placentation, but the unclear translatability of known human placental markers and lack of accessible rhesus trophoblast cell lines can impede the use of this animal model.

Results: Here, we performed a cross-species transcriptomic comparison of human and rhesus placenta and determined that while the majority of human placental marker genes (HPGs) were similarly expressed, 952 differentially expressed genes (DEGs) were identified between the two species. Functional enrichment analysis of the 447 human-upregulated DEGs, including *ADAM12*, *ERVW-1*, *KISS1*, *LGALS13*, *PAPPA2*, *PGF*, and *SIGLEC6*, revealed an over-representation of genes implicated in preeclampsia and other pregnancy disorders. Additionally, to enable *in vitro* functional studies of early placentation, we generated and thoroughly characterized two highly-pure first trimester telomerase (TERT) immortalized rhesus trophoblast cell lines (iRP-D26 and iRP-D28A) that retained crucial features of isolated primary trophoblasts.

Conclusions: Overall, our findings help elucidate the molecular translatability between human and rhesus placenta and reveal notable expression differences in several HPGs and genes implicated in pregnancy complications that should be considered when using the rhesus animal model to study normal and pathological human placentation.

2.2 Background

The placenta is the physical link between the mother and fetus as well as a critical site for nutrient and waste exchange during pregnancy. Trophoblasts are the major functional cell type of the placenta, and can be divided into three subtypes: (1) proliferative cytotrophoblasts (CTBs), which can differentiate into (2) invasive extravillous trophoblasts (EVTs), or fuse to form (3) multinucleated syncytiotrophoblasts (STBs). Proper trophoblast differentiation and function are essential for normal placentation and fetal development throughout gestation. In humans, abnormal placentation is the primary defect associated with major pregnancy complications, such as preeclampsia, fetal growth restriction, recurrent miscarriage, and still-birth [2]. Investigation of early placentation is particularly important for combating these diseases since many of the associated defects are thought to arise early to mid-gestation. However, the ethical and technical limitations of studying early human development have confined many human placentation investigations to late gestational stages closer to term. Thus, early human placental development, including the origin and cause(s) of the placental abnormalities underlying major pregnancy complications, is poorly understood.

To overcome the limitations of studying early human placentation, numerous human first trimester trophoblast cell lines have been isolated and immortalized using various methods for *in vitro* investigations [140,141,143]. Unlike primary trophoblasts, immortalized trophoblast cell lines are readily available, can be grown in culture indefinitely, and are relatively easy to transfect for functional studies. However, recent studies suggest that these cell lines are not necessarily a pure population of trophoblasts and/or have acquired karyotypic and phenotypic aberrations with continued passaging [253-255]. The human choriocarcinoma cell lines, BeWo, JEG-3, and JAR, have also been used to study trophoblast differentiation and syncytialization [145], but these cells are highly malignant and exhibit considerably different transcriptomic profiles than primary trophoblasts [253], questioning whether these lines are truly representative of trophoblast cells *in vivo*.

While some of the limitations of performing human *in vitro* and *in vivo* placental studies are overcome using animal models, most mammalian species poorly recapitulate human placentation. This is due, in large part, to inherent genetic differences and variations in the placental structure, steroidogenic synthesis, and the intracellular signaling pathways mediating lineage-specific trophoblast differentiation amongst mammals [256,257]. However, non-human primate animal models, particularly rhesus macaques (*Macaque mulatta*), are genetically similar to humans and share many key features of human placentation. Besides being comparable in placental morphogenesis, the overall structure and nature of both the STB interface layer and intervillous space, as well as endocrine functions and extracellular matrix changes are similar between rhesus and human placenta [3-5,7]. Further, there is a strong resemblance between human and rhesus placental endovascular EVT invasion and spiral artery transformation [6], processes known to play a central role in the pathogenesis of several pregnancy complications in humans [61]. Unlike studies relying on human samples, access to high-quality early gestational placental samples and *in vivo* functional investigations are possible under approved rhesus animal studies. However, rhesus first trimester trophoblast cell lines are still not readily available, which limits rhesus-based placental studies and requires the laborious isolation and use of primary term rhesus trophoblasts for *in vitro* investigations.

Although the human and rhesus placenta appear to be morphologically and functionally similar, previous studies have revealed some notable differences in the expression level and/or protein-coding potential of well-known human placental markers, including CGA, HLA-G, ERVW-1, and SIGLEC6 [122-125]. Differences in placental invasion have also been noted, as the extent and depth of interstitial EVT invasion is greater in human compared to rhesus placentation [4]. Further, while a few cases of preeclampsia have been documented in rhesus and other non-human primates, this disease predominantly occurs in humans [126-130]. Thus, the identification of the molecular differences between human and rhesus placenta will not only help elucidate the

translatability between primate placental studies but may also provide valuable insight into the molecular origin of human-specific placental features and pregnancy-related diseases.

Here, we performed a cross-species transcriptomic comparison of human and rhesus placenta to identify differentially expressed genes (DEGs) and determined that even though the majority of human placental marker genes (HPGs) are similarly expressed across the two species, there are gene expression differences that likely underlie the distinct features of human placentation. Additionally, we generated and thoroughly characterized two highly pure TERT-immortalized rhesus trophoblast cell lines for *in vitro* functional studies that retained features of primary rhesus trophoblasts. Overall, this work provides a comprehensive list of genes differentially expressed between human and rhesus placenta that enhances the translatability of primate placental investigations, helps delineate the molecular differences underlying human susceptibility to preeclampsia and other pregnancy-related diseases, and provides previously unavailable first trimester immortalized rhesus trophoblast cell lines for further functional investigation and understanding of early primate placentation.

2.3 Results

2.3.1 Identification of genes differentially expressed between human and rhesus placenta

Despite the structural and functional similarities between human and rhesus placentas, differences in the level and route of invasion, as well as the increased propensity to develop pregnancy-related diseases in humans, suggests that molecular differences exist across primate species. To characterize such differences, we compared gene expression levels between human and rhesus macaque (*Macaque mulatta*) placentas using a combination of newly-generated and publicly-available RNA-seq data from bulk third trimester placenta samples [258] (**Table** 2.1). The presence of EVTs in rhesus placental samples at this gestational time was confirmed via immunohistochemical (IHC) staining of the pan-trophoblast marker, KRT7 (**Supplemental Figure**

2.1). In order to make RNA-seq gene expression data comparable across species, we limited our comparison to human protein-coding genes with ENSEMBL-defined "high-confidence" "one2one" rhesus orthologs and DEGs were identified by intersecting the results of two complementary differential expression (DE) analyses (**Supplemental Figure** 2.2**A**). First, RNA-seq data from both species were mapped to the human reference genome (GRCh38) (**Figure** 2.1**A**) and DEGs were identified based on the human gene annotations (DE-GRCh38). Second, RNA-seq data from both species were mapped to the rhesus reference genome (Mmul10) and DEGs were identified based on the rhesus gene annotations (DE-Mmul10) (**Figure** 2.1**B**). A gene was considered differentially expressed only if it was identified as significantly (padj<0.05) upregulated or downregulated (|L2FC|>2) by both analyses (**Figure** 2.1**C**). Thus, DEGs called due to mappability issues instead of true expression difference would not be called in the reciprocal analysis and excluded from the final set of DEGs. To avoid potential batch effects, we repeated the DE analysis using three independent human placenta RNA-seq datasets [259,260] (**Supplemental Figure** 2.2**A-C**). This final set of DEGs consisted only of genes determined to be significantly upregulated or downregulated by all three DE analyses and resulted in a total of 952 DEGs, including 447 human-upregulated and 505 rhesus-upregulated genes (**Figure** 2.1**D, Table 2.2-2.3**). Quantitative reverse transcription PCR (qRT-PCR) was used to validate eight of the DEGs (

Supplemental Figure 2.3**A,B**). The 25 most significant human and rhesus upregulated DEGs are shown in **Figure** 2.1**E** and highlights the upregulation of several well-known placental markers in human including, *ADAM12*, *SERPINB2*, *BPGM*, *CYP19A1*, *SVEP1*, *GPC3*, *PGF*, *FBN2*, and *PAPPA2*. Collectively, these results provide a comprehensive list of gene expression differences between human and rhesus placenta and show that not all established human placental markers are expressed equivalently in the two species.

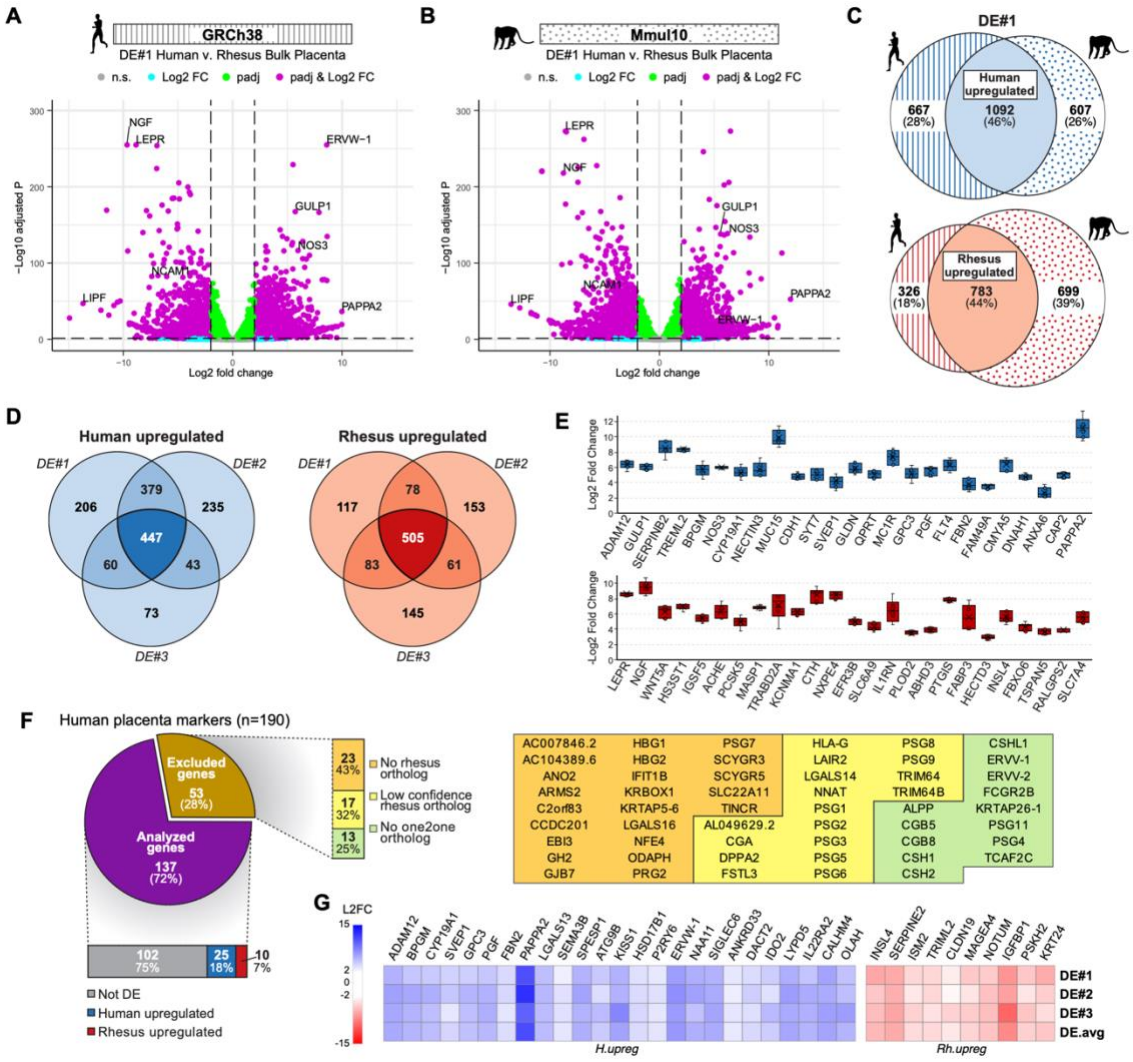

Figure 2.1 Cross-species DE analysis of human and rhesus bulk placental tissue

Volcano plots showing gene expression fold differences between human and rhesus term placental tissue from DE#1, using data mapped to (A) the human genome and (B) the rhesus genome. Dashed lines denote DE significance (padj<0.05) and fold change (|L2FC|>2) thresholds; genes passing padj threshold (green), passing L2FC threshold (cyan), passing both (magenta), or none (grey). (C) Venn-diagram depicting intersection of DEGs identified using data mapped to human genome (stripes) and rhesus genome (spotted) to identify intermediate human-upregulated (light blue) and rhesus-upregulated (light red) genes sets. (D) Venn-diagram depicting the intersection of the results from the three DE analyses to identify final set of 447 human-upregulated genes (blue), and 505 rhesus-upregulated genes (red). (E) Top 25 most significant differentially expressed (ranked by mean padj) human-upregulated (blue) and rhesus-upregulated genes (red); box plots depict average Log2 fold change of each gene from the three DE analyses. (F) Differential expression results of HPGs. (Left) Proportion of placental marker genes analyzed (purple) or

excluded from (brown) DE analysis. Analyzed genes are further classified as either not differentially expressed (not DE) (grey), human-upregulated (blue), or rhesus-upregulated (red). (Right) ENSEMBL-classification of HPGs excluded from DE analysis; “no rhesus ortholog” (orange), “low confidence rhesus ortholog” (yellow), or “no one2one rhesus ortholog” (green). (G) Heatmap of differentially expressed HPGs; human-upregulated genes (L2FC>2) are shown in blue and rhesus-upregulated genes (L2FC<2) are shown in red.

2.3.2 Comparison of human, rhesus, and mouse placenta confirms the overall molecular similarity between primate placentas

To validate the primary DE analysis and provide an unbiased assessment of the molecular similarity between human, rhesus, and mouse placenta, an orthologous cross-species transcriptomic comparison was performed that relied exclusively on RNA-seq data mapped to respective species genome. We used an approach similar to the one recently described by Sun et al. [261] in which Transcripts Per Million (TPM) normalized gene expression values were calculated for each sample (**Table 2.4-2.6**), then filtered to include only genes with one-to-one orthologues across all three species (human, rhesus, and mouse) for cross-species comparison. Consistent with Sun et. al, hierarchical clustering of TPM-normalized expression data showed that rhesus placental samples were more closely related to human than mouse (**Supplemental Figure** 2.4**A,B, Table 2.7**). A total of 1787 DEGs, including 879 human-upregulated and 814 rhesus-upregulated DEGs, were identified between human and rhesus placenta using TPM-normalized expression data (**Table 2.8**). Of the 952 DEGs identified in our primary DE analysis, 58% (n=554) were also identified by the TPM-based analysis (**Supplemental Figure** 2.4**C**). It should be noted that ~8% (73/952) of DEGs in our primary analysis were excluded from the novel TPM-based approach due to lack of ENSEMBL-defined one-to-one human-to-mouse ortholog, including preeclampsia associated genes (*ERVW-1, KISS1, LGALS13, SIGLEC6*) and HPGs (*GPC3, INSL4, MAGEA4, NAA11, OLAH, PSKH2)* (**Supplemental Figure** 2.4**D,E**). Thus, while the inclusion of mouse in the TPM-based transcriptomic comparison allowed for an unbiased assessment of molecular similarities between human and rhesus, it also minimized the number of orthologous genes that could reliably be compared, thereby excluding several key DEGs identified by our primary analysis. Nonetheless, the results of the TPM-based comparative analysis confirm the overall molecular similarity between human and rhesus placenta, as well as the stringency and confidence of our primary DE approach and the final DEG set reported.

2.3.3 Genes implicated in human pregnancy complications are upregulated in human compared to rhesus placenta

To elucidate the translatability of human placental markers between human and rhesus, a set of previously defined HPGs [262] was examined for differential expression between the two species. Out of the 190 HPGs, ~72% (n=137/190) were included in the primary DE analysis, while 28% (n=53/190) were excluded due to nonexistent (43%), low confidence (32%), or a lack of "one2one" (25%) ENSEMBL-defined rhesus ortholog (**Figure** 2.1**F**). In certain cases, ENSEMBL-defined orthology conflicts with orthologous genes described by previous studies. For instance, the *GH2* gene is defined as having no ENSEMBL rhesus ortholog despite the well-described placentally expressed *GH/CS* locus in the rhesus genome that is highly similar to human [263-265]. Further, both *HLA-G* and *CGA* are defined as having only "low-confidence" rhesus orthologs, opposed to previous studies describing highly similar orthologous genes in the rhesus genome [122,123]. Of the 137 HPGs included in the analysis, the vast majority (~75%; n=102/137) showed similar expression levels between human and rhesus placenta. The remaining ~25% of HPGs (n=35/137) were identified as differentially expressed between the two species, with ~18% (n=25/137) upregulated in human and ~7% (n=10/137) upregulated in rhesus placenta (**Figure** 2.1**F**). Notably, several HPGs associated with invasive EVTs (*ADAM12*, *PAPPA2*, *PGF*) [266-268], and pregnancy complications such as preterm birth and preeclampsia (*ADAM12, HSD17B1, KISS1, LGALS13, PAPPA2, SIGLEC6, ERVW-1*) [269-275], were found to be upregulated in human compared to rhesus placenta (**Figure** 2.1**G**). Over-representation analysis (ORA) demonstrated that genes associated with pregnancy disorders including, "preeclampsia" (padj=6.73E-04), "HELLP syndrome" (padj=1.48E-01), "Gestational trophoblastic tumor" (padj=1.52E-01), and "Eclampsia" (padj=4.43E-01) were indeed upregulated in human compared to rhesus placenta (**Supplemental Figure** 2.5). Overall, these results provide a comprehensive list of differentially expressed HPGs between human and rhesus placenta that should be considered when studying certain aspects of

placentation in rhesus, particularly those that are associated with EVT invasion, preeclampsia, or other placenta-related diseases.

2.3.4 DEGs detected between human and rhesus placenta largely reflect species-specific changes

While both the human and rhesus RNA-seq data used for our DE analysis were isolated from placenta samples collected from third trimester cesarean sections without labor, we note that the publicly available rhesus data was generated from a slightly earlier (~80%) gestational age (GA) than the term human placental samples. Therefore, some of the gene expression differences observed between the human and rhesus samples may be the result of GA rather than species-specific changes. However, examination of a set of previously defined "GA-specific" genes expressed in primate placentas [276] revealed that only a single GA-specific gene (*BAALC*) was identified as differentially expressed in our analysis. In addition, closer examination of the rhesus placenta RNA-seq data showed little to no expression of Y-linked genes in any of the samples, suggesting an unequal distribution of male and female samples may have influenced the cross-species comparison. To determine whether any of the DEGs identified were due to sex-specific rather than species-specific differences, we compiled a set of sex-differentially expressed (SDE) genes via DE analysis of known male (n=6) and female (n=5) human placentas. A total of 11 significant SDE genes were identified (**Table 2.9**), five of which overlapped with our human-upregulated DEGs (*ZFY, RPS4Y1, KDM5D, DDX3Y, CCK*). Therefore, sex-specific changes accounted for only ~0.53% (5/952) of the DEGs in the cross-species analysis of human and rhesus placentas. These results indicate that the DEGs identified in our study largely reflect species-specific changes rather than GA-related or sex-specific differences.

2.3.5 Establishment of TERT-immortalized rhesus cell lines from placenta and skin fibroblasts

Because the placenta is a heterogeneous organ comprised of many cell types in addition to trophoblasts, such as immune, stromal and vascular cells [277], we next sought to isolate primary trophoblasts from bulk rhesus placentas for immortalization and characterization, including a comparison of gene expression. While previous studies have successfully isolated and cultured primary trophoblasts from first and third trimester rhesus placenta [278-281], no rhesus immortalized trophoblast cell lines currently exist for *in vitro* investigations. Using the strategy described in **Figure** 2.2**A**, we isolated primary trophoblast cells from rhesus placental tissues collected at gestational day 26 (~6 wks human pregnancy), day 28 (~7 wks human pregnancy), day 50 (~12 wks human pregnancy), day 141 (~34 wks human pregnancy), and day 149 (~35 wks human pregnancy). After depletion of contaminating immune cells using immunopurification, the cells were cultured for 24 h before transduction with lentivirus containing *TERT* and puromycin resistance (*PAC*) genes for antibiotic selection. First and third trimester primary cell isolation methods resulted in ~98% and ~69% Cytokeratin (KRT7) positive trophoblast cells, respectively (**Supplemental Figure** 2.6). A total of six immortalized rhesus placental (iRP) cell lines were generated, including four from first trimester (iRP-D26, iRP-D28A, iRP-D28B, iRP-D50) and two from third trimester (iRP-D140, iRP-D141) rhesus placentas. Male and female rhesus primary skin fibroblasts were also used to establish two immortalized rhesus fibroblast (iRFb) cell lines, iRFb-XY and iRFb-XX, as controls. Cultures of iRP-D26 and iRP-D28A contained purely polygonal epithelial-like cells, while the other cell lines appeared heterogeneous with a mix of large flattened and elongated fibroblast-like cells (**Figure** 2.2**B**). Expression of the lentiviral-transduced genes, *TERT* and *PAC*, was confirmed in each of the cell lines via RT-PCR (**Figure** 2.2**C**). These results suggested that the lentiviral-based TERT-transduction strategy was quite robust, with 100% (n=8/8) of attempts resulting in the generation of a cell line with stable *TERT* expression. Moreover,

both the iRP-D26 and iRP-D28A have been cultured beyond 30 passages, further supporting successful TERT-immortalization of these cell lines.

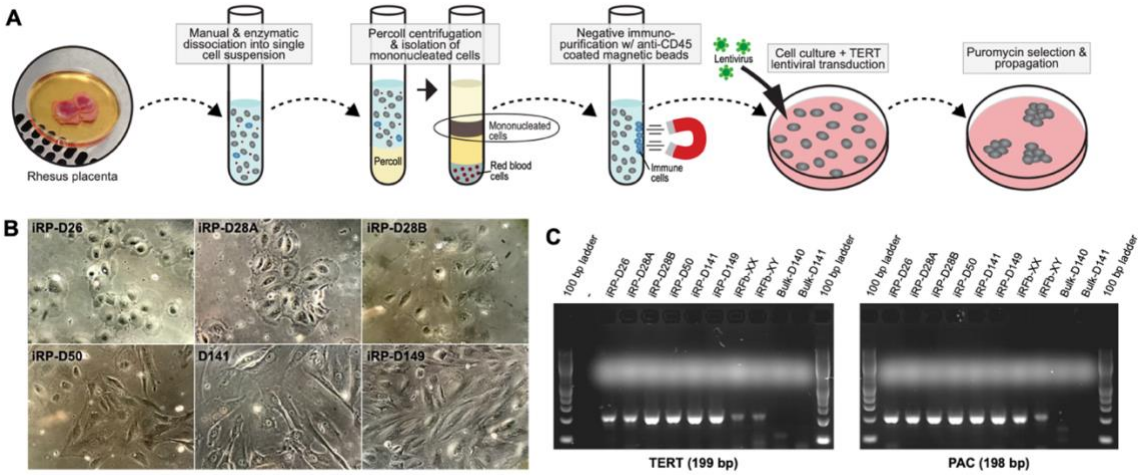

Figure 2.2 Establishment of TERT immortalized rhesus cell lines

(A) Schematic of primary trophoblast cell isolation from rhesus placental tissue and TERT immortalization. (B) Phase contrast microphotographs of immortalized placental cell lines. (C) Confirmation of TERT immortalization via RT-PCR detection of TERT and PAC gene expression.

2.3.6 Assessment of genomic integrity in TERT-immortalized rhesus cell lines

Cell lines are known to develop genetic abnormalities during immortalization and/or prolonged cell culture, such as aneuploidies, copy number variations (CNVs), and chromosomal fusions. This is particularly true for cell lines derived by Simian Virus 40 (SV40) or a similar transformation approach as has been shown for first trimester human trophoblast cell lines [282,283], but it can also occur in TERT-immortalized human trophoblasts over time [255]. In addition, primary trophoblasts normally undergo cell fusion (syncytialization), which can complicate nuclear assessment. Here, CNVs and whole chromosome counts were determined using low-input DNA-seq and metaphase spreads, respectively. Approximately ten cells from each TERT-immortalized cell line were manually transferred into a single tube and prepared for DNA-seq as previously described [284]. Normal diploid copy-numbers were observed for all autosomes in iRP-D26, iRP-D28A, and iRP-D141, although sub-chromosomal losses of Chr1 and Chr7 were observed in iRP-D26, sub-chromosomal gains of Chr11 and Chr16 in iRP-D28A, and a small sub-chromosomal loss of Chr1 in iRP-D141 (**Figure** 2.3**A**). In contrast, numerous whole and sub-chromosomal CNVs were identified in the other iRP cell lines, iRP-D28B, iRP-D50, and iRP-D149 (**Figure** 2.3**A**). As expected, CNV analysis of the female rhesus fibroblasts (iRFb-XX) showed normal diploid copy numbers for all 21 rhesus chromosomes, while the male fibroblasts (iRFb-XY) exhibited the expected ChrX "loss" and detection of ChrY (**Figure** 2.3**A,B**). Comparison to the male iRFb-XY control revealed a single copy of ChrX without the detection of ChrY in iRP-D26, highlighting the loss of a whole sex chromosome (**Figure** 2.3**A,B**). Metaphase spreads of iRP-D26 cells confirmed the loss of one to two whole chromosomes, supporting the DNA-seq results, and suggesting the existence of chromosome fusion in cells with only 40 chromosomes (**Figure** 2.3**C,D**). Examination of metaphase spreads from iRP-D28B, iRP-D50, and iRP-D149 further demonstrated a heterogenous mix of predominantly polyploid cells, containing between three (triploid) and four (tetraploid) sets of chromosomes (**Figure** 2.3**C,D**). Overall, these results suggest that TERT-immortalization can be used to establish normal diploid rhesus placental cell lines, but we expect

that these cells cell could accumulate chromosomal abnormalities with continued passaging as has been shown for human TERT-immortalized trophoblast cell lines [255,285].

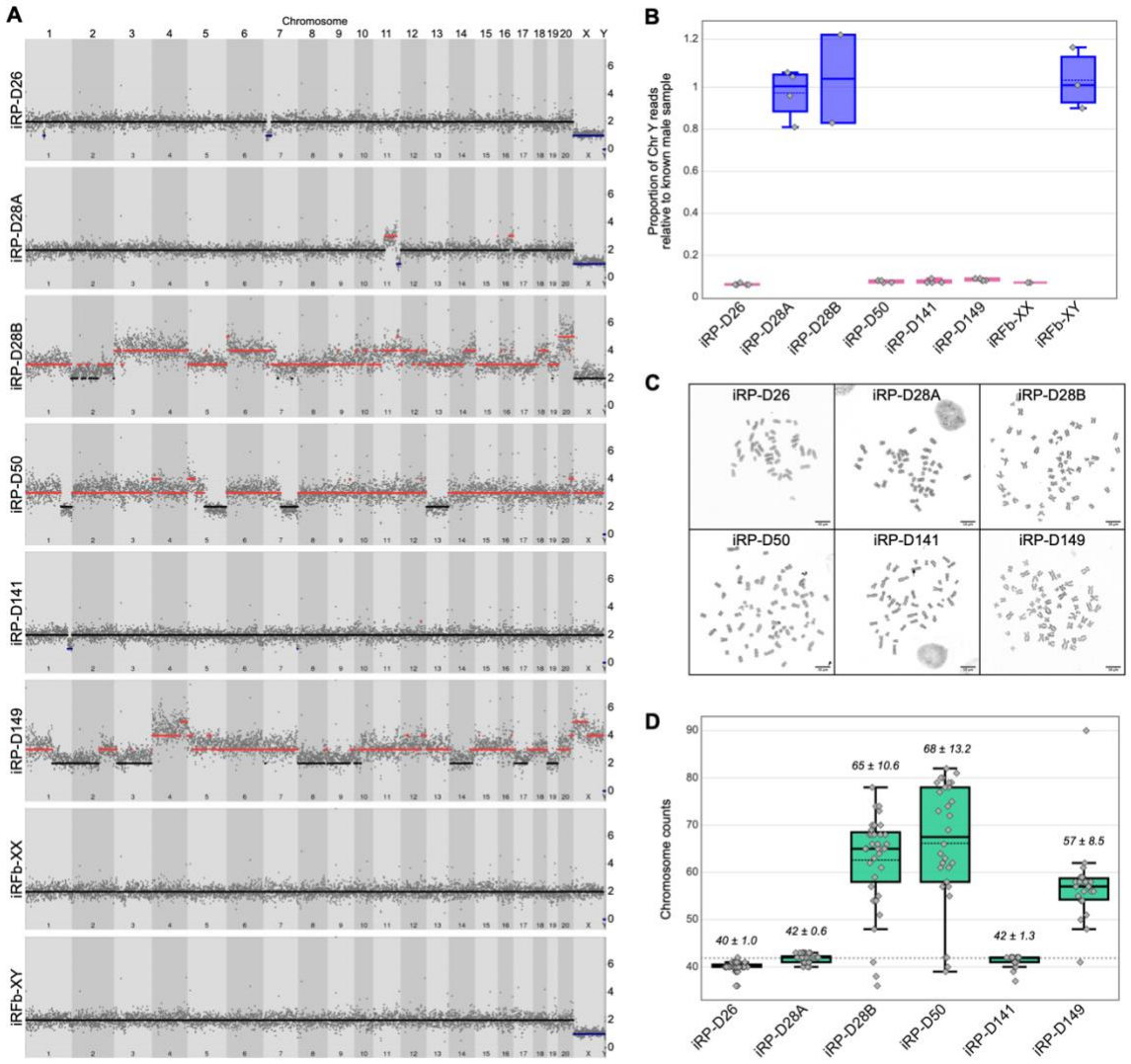

Figure 2.3 Assessment of genomic integrity in immortalized placental cell lines

(A) Manhattan plots of whole genome CNVs organized by chromosome; copy number gains (red), copy number losses (blue) show the presence of CNV in most of the placental cell lines but not in the fibroblast used for comparison. (B) Box plots depicting proportion of Chr Y mapped reads normalized to known male sample, iRFb-XY; cell lines were identified as male if mean > 0.5 (blue), or as female if mean < 0.5 (pink). (C) Representative metaphase spreads; 10uM scale bar. (D) Box plots of chromosome count results; median ± standard deviation values included above each plot.

2.3.7 iRP-D26 and iRP-D28A represent two highly pure TERT-immortalized rhesus trophoblast cell lines

In order to identify the placental cell lines containing a pure population of trophoblast cells, we analyzed each line for expression of highly conserved trophoblast and non-trophoblast cell markers [157], including, KRT7, a pan-trophoblast cell marker; CDH1, a mononuclear trophoblast cell marker; VIM, non-trophoblast stromal marker; and PTPRC (CD45), a pan-leukocyte marker. Antibodies for these markers were first validated in rhesus placental tissues using IHC staining and the observed expression patterns were consistent with known patterns in the human placenta (**Figure** 2.4**A**). Immunofluorescent (IF) staining using the same antibodies showed robust staining of KRT7 and CDH1 trophoblast markers, and the absence of VIM and CD45 staining in both iRP-D26 and iRP-D28A, indicating the enrichment of trophoblasts and the absence of mesenchymal and immune cells within these cell lines, respectively. In contrast, the remaining iRP cell lines (iRP-D28B, iRP-D50, iRP-D141, and iRP-D149) were largely contaminated with VIM positive mesenchymal cells (**Figure** 2.4**B**). These findings were consistent with qRT-PCR expression analysis, which showed significant enrichment of KRT7 and CDH1 expression in iRP-D26 and iRP-D28A compared to the other cell lines or bulk rhesus placental tissue (**Figure** 2.4**C**). Additionally, VIM and PTPRC (CD45) expression was not detected by qRT-PCR in iRP-D26 and iRP-D28A but were highly expressed in all other cell lines analyzed (**Figure** 2.4**C**). Thus, despite careful trophoblast isolation procedures, only 50% (n=2/4) of the attempts with first trimester placentas and 0% (n=2/2) with third trimester placentas resulted in highly pure immortalized trophoblast cell lines. This indicated that contamination of non-trophoblast stromal cells occurred in ~67% (n=4/6) of the primary trophoblast isolations and that only the iRP-D26 and iRP-D28A cell lines should be carried forward for further characterization.

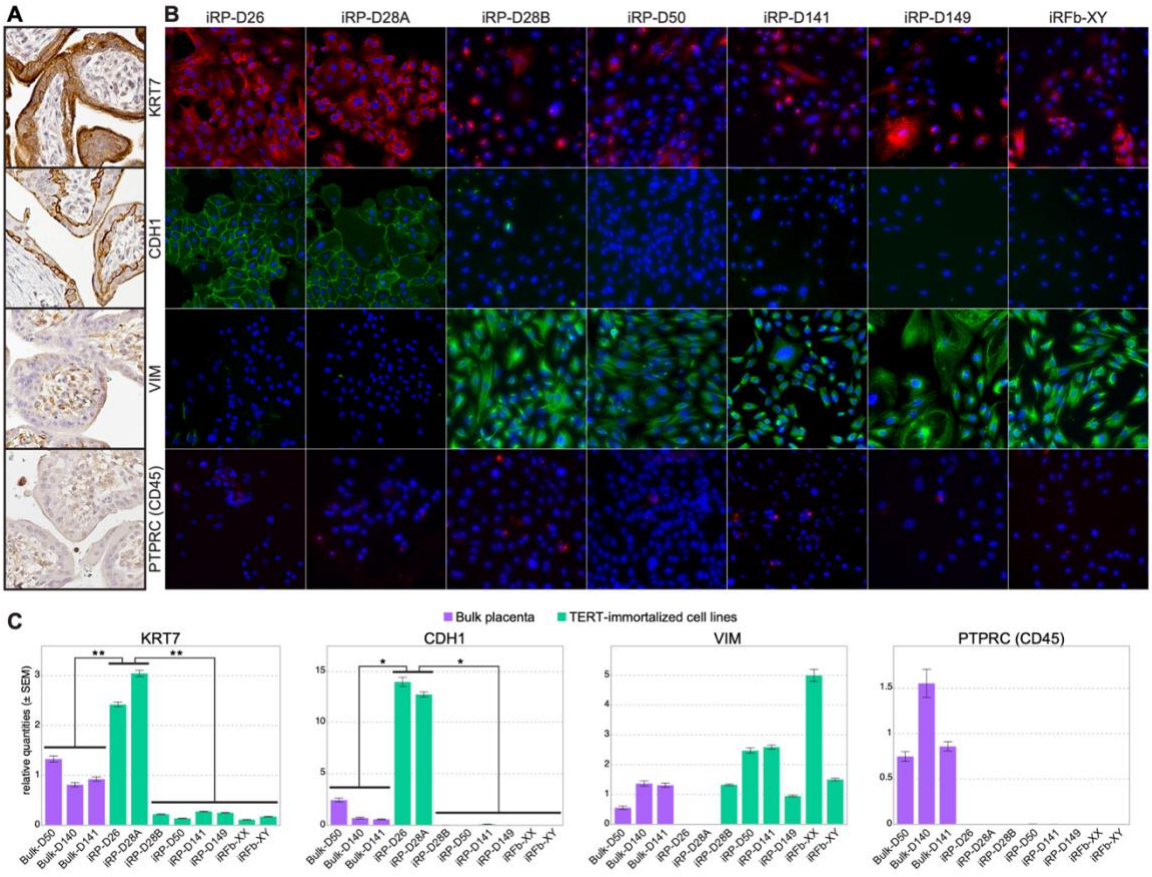

Figure 2.4 iRP-D26 and iRP-D28A represent two highly pure rhesus immortalized trophoblast cell lines

(A) IHC staining of gestational day 50 rhesus placental tissue for mononuclear trophoblast (KRT7 and CDH1), stromal (VIM), and immune cell (PTPRC) markers (DAB, brown); hematoxylin nuclear counter stain (blue). (B) IF staining of immortalized cell lines for KRT7 (red), CDH1 (green), VIM (green), and PTPRC (red); DAPI nuclear counterstain (blue); results show that iRP-D26 and iRP-D28A cells express known mononuclear trophoblast markers, KRT7 and CDH1. (C) Bar graphs of qRT-PCR expression results; bulk rhesus placental samples (purple), iRP cell lines (green). Statistical significance was determined using two-sided unpaired t-test with alpha of 0.05 (*p<0.05, **p<0.01).

2.3.8 Transcriptomic comparison of immortalized and primary rhesus trophoblast cells

To characterize gene expression levels in the immortalized trophoblast cell lines and compare them to first trimester rhesus primary trophoblast (RPT) cells, RNA-seq was performed on two replicates each of iRP-D26, iRP-D28A, and freshly isolated first trimester RPTs. RPT trophoblast purity was confirmed via KRT7 staining and showed ~98% KRT7+ trophoblast cells (**Supplemental Figure** 2.6). For reference, publicly available human and rhesus peripheral blood mononuclear cells (PBMC) [286,287], human primary trophoblasts (HPT) [288,289], BeWo [289,290], and rhesus bulk placenta [258] RNA-seq datasets were also included in the assessment. Principle component analysis (PCA) based on the expression of all analyzed genes (n=15,787) revealed that a majority of the sample variance was due to tissue-type differences, separating the PBMC samples from the placental/trophoblast samples (**Figure** 2.5**A**). Bulk human and rhesus placenta samples clustered closely together, further supporting the overall molecular similarity between these two closely related species. Both iRP-D26 and iRP-D28A clustered with the primary trophoblast samples, indicating that our newly generated immortalized trophoblast cell lines were most similar to freshly isolated RPT cells. In contrast, the BeWo samples formed a distinct cluster away from the other trophoblast samples, confirming the major transcriptomic differences between primary trophoblasts and this widely-used choriocarcinoma model. (**Figure** 2.5**A**). Despite broad transcriptomic similarities across the human and rhesus placenta/trophoblast samples, distinct HPG expression was observed between the two species. Hierarchical clustering of the samples based on this expression showed clustering of placenta/trophoblasts by species, with iRP-D26, iRP-D28A, RPT, and bulk rhesus placenta samples forming a distinct branch and HPT and bulk human placenta forming another (**Figure** 2.5**B**). Thus, except for HPGs, transcriptomic profiles were largely shared between our newly generated immortalized trophoblast cell lines and freshly isolated RPT cells, demonstrating the suitability of these lines for *in vitro* primate placental studies.

To identify DEGs and specific pathways in immortalized trophoblasts versus RPTs, DE analysis was performed between (1) iRP-D26 vs. RPT and (2) iRP-D28A vs. RPT. Out of the total

21,575 protein-coding rhesus genes examined, 5884 DEGs (padj<0.05 & |L2FC|>|1|) were found between iRP-D26 and RPT, with ~39% (n=2,290) upregulated and ~61% (n=3,594) downregulated in iRP-D26 (**Figure** 2.5**C, Table 2.10**). Further, a total of 6,017 DEGs were identified between iRP-D28A and RPT, with ~43% (n=2,592) upregulated and ~57% (n=3,425) downregulated in iRP-D28A (**Figure** 2.5**C**, **Table 2.11**). Over-representation analysis demonstrated that genes associated with herpes simplex virus 1 (HSV1) infection were upregulated in both iRP-D26 and iRP-D28A compared to RPTs. Since HSV1 infection is known to upregulate TERT activity [291], upregulation of HSV1-associated genes in both immortalized trophoblast cell lines is likely a result of TERT-immortalization induced expression changes. In addition, genes associated with human EVTs and extracellular matrix organization were upregulated in both iRP-D26 and iRP-D28A, while genes associated with human STBs, CTBs, and the immune system were downregulated in both immortalized trophoblast cell lines relative to RPTs (**Supplemental Figure** 2.5). These results suggest that the RPT samples may have contained a more heterogeneous population of trophoblast subtypes than the immortalized trophoblast cell lines. Thus, downregulation of immune system/response related genes may be due to the absence of specific trophoblast subtypes (CTB and/or STB) in the cell lines, or the presence of cytokine-stimulated trophoblasts within the freshly isolated RPT samples analyzed.

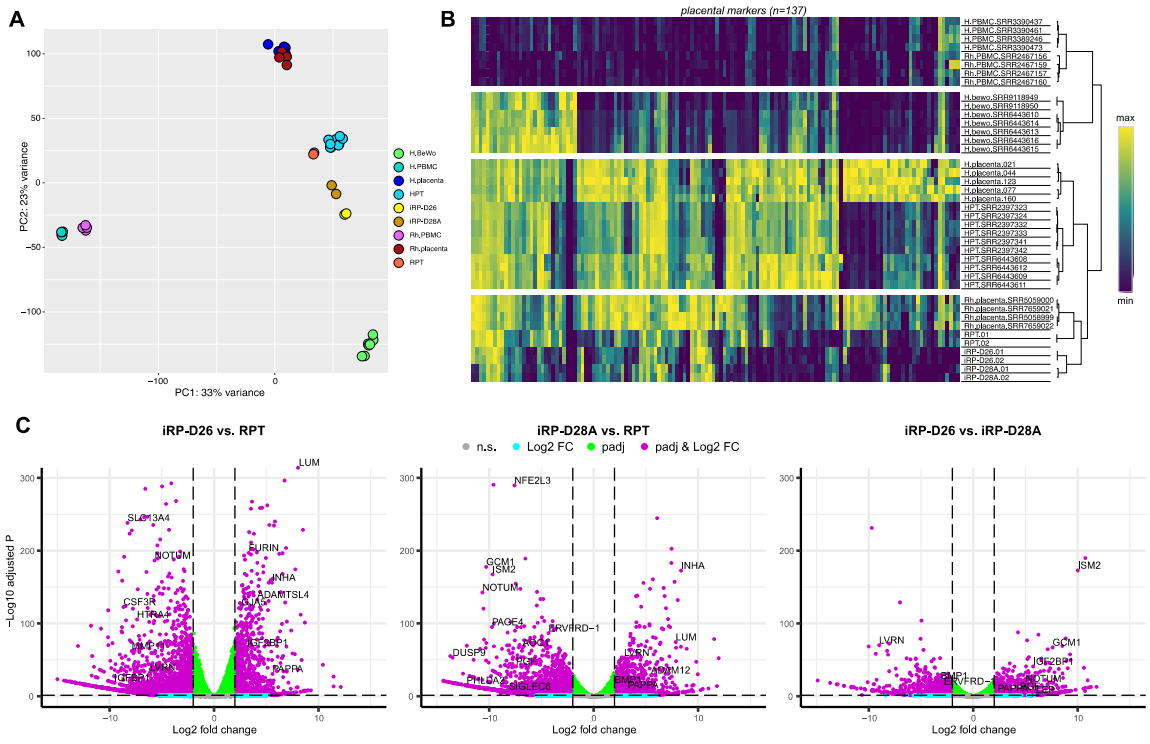

Figure 2.5 Transcriptomic comparison of immortalized and primary rhesus trophoblast cells

(A) PCA plot of RNA-seq gene expression from human and rhesus bulk placentas, PBMCs, primary trophoblasts, BeWo, iRP-D26 and iRP-D28A cell lines. (B) Heatmap of HPG expression results. Color scale depicts minimum (purple) and maximum (yellow) one plus log2 normalized expression values compared across all human and rhesus samples. (C) Volcano plots of DE analysis results; positive L2FC values represent genes upregulated in iRP-D26 compared to RPT (left), iRP-D28A compared to RPT (middle), iRP-D26 compared to iRP-D28A (right).

2.3.9 Functional characterization of immortalized trophoblast cell lines

In order to test whether iRP-D26 and iRP-D28A behaved more like CTBs or EVTs, the fusogenic potential of the cell lines was assessed by treating them with forskolin, an activator of adenylate cyclase and known inducer of fusion and STB formation in BeWo human choriocarcinoma [146] and trophoblast stem cells [292]. Unlike RPTs and/or forskolin treatment of BeWo cells, neither iRP-D26 nor iRP-D28A showed upregulation of key fusogenic/STB genes (ERVFRD-1 and ERVW-1) or obvious changes in syncytialization when treated with forskolin (**Supplemental Figure** 2.7**A-D**). Additionally, monkey chorionic gonadotropin (mCG) secretion could not be detected in either the iRP-D26 or iRP-D28A cell line (**Supplemental Figure** 2.7**F**). Since mCG is primarily secreted by the syncytiotrophoblast, this indicated that the cell lines might be more EVT-like in origin. Indeed, both iRP-D26 and iRP-D28A showed upregulation of several genes known to facilitate human EVT and/or tumor cell invasion (**Table 2.10-2.11**), including *SDC2*, *TIMP3*, *MMP14*, and *ADAM12* [293-296]. Thus, to evaluate whether the immortalized trophoblast cell lines were capable of invasion, trans-well migration and Matrigel extracellular matrix invasion assays were performed. When grown on uncoated transmembrane inserts (n=3) for 48 h, both the iRP-D26 and iRP-D28A cell lines exhibited migration to the bottom side of the insert, indicating that the cell lines possessed migratory capabilities (**Figure** 2.6**A,B**). Additionally, 22% of the iRP-D26 and 30% of the iRP-D28A migratory cells were also able to invade through Matrigel-coated inserts (n=3) after 48 h of culture (**Figure** 2.6**C**). However, despite previous studies showing an increased level of EVT invasion under hypoxic conditions [297,298], no significant differences in invasion were identified when the assays were performed under hypoxic (1% O_2) compared to normoxic conditions (**Figure** 2.6**C**). This further supports the idea that even though they are prevalent throughout pregnancy (**Supplemental Figure** 2.1), EVTs in rhesus placentas appear to be less invasive than their human counterparts. Nonetheless, using qRT-PCR the EVT-like characteristics of both iRP-D26 and iRP-D28A were confirmed by high expression levels of *IGF2* (**Figure** 2.6**D**), which is most abundantly expressed by EVTs in both human and rhesus [299,300]. Despite high

levels of *IGF2* mRNA, the iRP-D26 and iRP-D28A cell lines did not exhibit substantial IGF2 protein secretion (**Figure** 2.6**E**) known to promote EVT migration [301,302]. Thus, cultures of these cell lines with IGF2 supplemented media and/or co-culture with IGF2 secreting cells may enhance their migration and invasion abilities in subsequent studies.

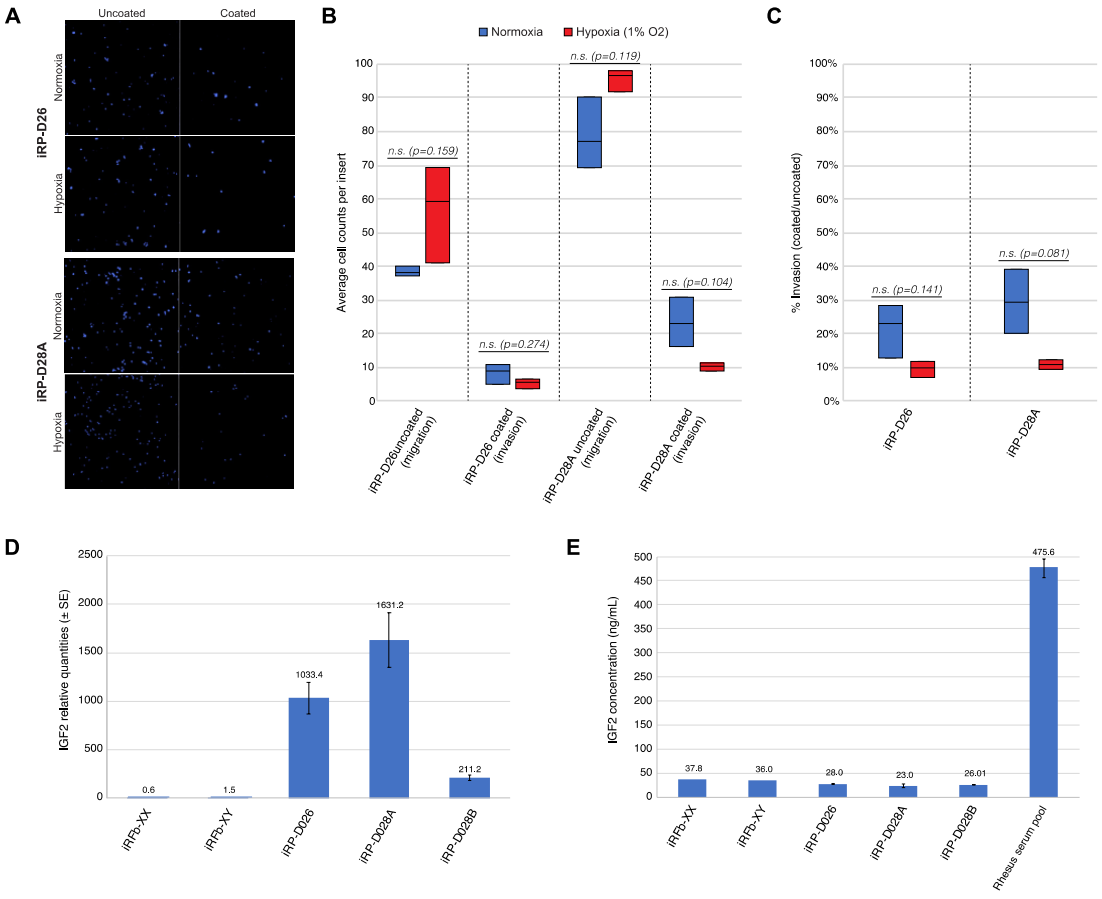

Figure 2.6 Functional characterization of iRP-D26 and iRP-D28A

(A) Representative micrographs of iRP-D26 and iRP-D28A trans-well inserts after migration and Matrigel invasion assays. Nuclei were counterstained with DAPI (blue). (B) Box plot of average cell counts (n=5) from uncoated (migration, n=3) and Matrigel-coated (invasion, n=3) inserts under normoxia (blue) and hypoxia (red) conditions. A two-sided unpaired t-test with alpha of 0.05 was used to determine significance. (C) Box plot of percent invasion (ratio of invasive cells relative to migratory cells) determined for each of the cell lines under normoxic (blue) and hypoxic (red) conditions. (D) Bar chart of IGF2 qRT-PCR expression levels (n=2 for iRFb; n=4 for iRP samples) and (E) Bar chart of IGF2 protein secretion levels; error bars depict standard error (SE).

2.4 Discussion

The wide variety of placental morphologies and physiologies that exist among mammals makes it difficult to adequately model human placentation and placental pathologies in other species [303-305]. However, many distinctive features of human placentation are reportedly conserved in rhesus monkeys [3-7]. Despite this conservation, no study has been conducted to comprehensively assess the molecular similarities and potential differences between human and rhesus placental tissues. Comparative analyses of human and closely related species are beginning to identify specific genetic and molecular changes that seem to account, in part, for specific aspects of human evolution, including human diseases [306]. Thus, identification of the molecular differences between human and rhesus placenta is not only needed to elucidate the translatability between human and rhesus placental studies, but it may also provide valuable insight into the molecular origin of human placental diseases, such as preeclampsia. Here, we performed a cross-species transcriptomic comparison of human and rhesus placental tissue in order to identify molecular differences and ultimately elucidate the translatability between human and rhesus placental investigations. Further, to increase the accessibility of rhesus *in vitro* placental studies, we generated and thoroughly characterized two highly pure TERT-immortalized rhesus trophoblast cell lines that retained features of primary rhesus trophoblasts cells.

Our DE analysis of human and rhesus placental tissue revealed that while a majority of HPGs were similarly represented, certain genes were differentially expressed between the two species. Specifically, genes associated with preeclampsia and several well-known invasive EVT markers were upregulated in human compared to rhesus placenta. These results are consistent with previously reported differences between human and rhesus placentation, such as the increased extent and depth of interstitial EVT invasion [3,4,307] and heightened risk of preeclampsia in humans [308]. Even though preeclampsia is thought to originate in the first trimester, many of the molecular and/or cellular processes that occur during first trimester can also occur at lower levels or in a smaller number of cells in third trimester placentas, including EVT differentiation and

invasion. Additionally, third trimester placental abnormalities are well-documented in cases of preeclampsia [309] and thus, examination of third trimester placental tissues may still provide insight into the genes associated with preeclampsia as shown here. While this study was not designed to provide mechanistic insight into preeclampsia, our findings are not surprising considering that preeclampsia occurs frequently in humans and rarely in rhesus and other primates. Comparison of first trimester human and rhesus placental transcriptomes would likely identify more significant differences and/or numerous additional human-upregulated genes related to preeclampsia. However, it is difficult to simultaneously analyze first trimester placentas and allow the pregnancy to continue unless chorionic villous samples are collected as part of prenatal screening. Nonetheless, our results provide novel insight into the molecular differences underlying human and rhesus placentation and an evolutionary perspective of how preeclampsia and other pregnancy-related diseases may have arisen during human development.

Despite the existence of several previous cross-species placental transcriptomic comparisons [310,311], a majority of the DEGs identified here have not been previously reported. Unlike prior studies that compared placental gene expression across numerous distantly-related species and examined only highly-conserved orthologous genes [310,311], our study was able to compare and identify differential expression of recently-evolved primate placental genes such as *LGALS13* [312]. In particular, we show that *LGALS13* is significantly upregulated in human compared to rhesus placenta. This gene encodes galectin-13, which interacts with glycoproteins and glycolipids to facilitate the expansion of uterine arteries and veins during pregnancy in an endothelial cell-dependent manner via the eNOS and prostaglandin signaling pathways [313]. While downregulation of *LGALS13* in preeclampsia and other pregnancy disorders is thought to contribute to aberrant uteroplacental blood flow [272,314], lower expression in rhesus placenta may underlie differences in the extent and depth of EVT invasion or represent an alternative mechanism for uterine vessel expansion. Thus, our results suggest that recently-evolved highly-expressed human placental genes may contribute to the increased risk of aberrant placentation and

preeclampsia [2]; however, further investigation of the evolutionary and functional requirements of these genes is required to confirm this notion.

Ideally, equivalent gestational ages should be used to compare DE in placentas between primates, but access to early third trimester samples (~80% gestation) from healthy human pregnancies was not possible due to obvious ethical constraints. Further, since rhesus monkeys are known to consume the placenta immediately after birth, both in captivity and in the wild, placentas from time-mated breeding pregnancies are typically collected before term to prevent the risk of losing precious third trimester rhesus placental samples. Due to these limitations, and the samples used for DE analysis it was possible that some of the gene expression differences we detected between the human and rhesus were due to GA rather than species-specific differences. However, examination of a set of previously defined "GA-specific" placentally-expressed genes [276] demonstrated that only a single GA-specific gene (*BAALC*) was differentially expressed in our analysis. Further, the seemingly unequal distribution of male and female samples within the rhesus RNA-seq data used suggested that some of the gene expression differences we detected might have been sex-specific rather than species-specific differences. However, only five SDE (*ZFY, RPS4Y1, KDM5D, DDX3Y, CCK*) overlapped with DEGs identified from our cross-species analysis. Taken together, this suggests that GA- and sex-related changes accounted for a small percentage of the DEGs in our cross-species analysis, substantiating that the DE differences detected between human and rhesus placenta were largely species-specific.

Although there are previous reports of primary rhesus first and third trimester trophoblast collections [278-280], the procedure for their isolation is laborious and the cells have a finite lifespan once in culture. Immortalization of isolated primary rhesus trophoblast cells could help overcome these limitations, but such a cell line does not currently exist. In this study, we generated several TERT-immortalized cell lines from freshly isolated primary rhesus placental cells and demonstrated the robustness of the lentiviral-based TERT-immortalization approach. However, contamination with non-trophoblast stromal cells occurred in the majority of primary trophoblast

isolations. Thus, additional efforts to reduce contaminating non-trophoblast cells during primary cell isolation, such as additional immunopurification steps or FACS sorting, should be implemented to increase the success rate of future attempts. In total, six TERT-immortalized rhesus placental cell lines were generated; however, only two of the lines (iRP-D26 and iRP-D28A) consisted of highly pure mononuclear trophoblast cells devoid of large-scale CNVs. These results are consistent with previous studies that revealed few karyotypic differences in TERT-immortalized cells compared to SV40-immortalized cells [315]. Nevertheless, genome duplication may still occur in TERT-immortalized trophoblast cells over time with continued passaging [255], suggesting that the genome integrity of the cell lines be routinely monitored.

Despite broad transcriptomic similarities across human and rhesus placenta/trophoblast samples, distinct HPG expression was observed between the two species, indicating that not all human placental markers are conserved in rhesus. Transcriptomic differences between immortalized and primary rhesus trophoblasts likely reflect TERT-induced gene expression differences, changes acquired with extended culture, enrichment of specific rhesus trophoblast cell subtypes, or the stage of differentiation captured in the immortalized cell lines. We suspect that the increase of HSV1 associated genes in iRP-D26 and iRP-D28A compared to RPTs was the result of TERT-immortalization since HSV1 infection upregulates TERT activity [291]. However, the upregulation of EVT markers and extracellular matrix organization-related genes is likely due to an enrichment of EVT-like cells in the immortalized cell lines compared to primary trophoblast samples. Thus, even though we intended to isolate and immortalize CTBs, it is possible that residual cell column EVTs were still attached to the villous tissue and carried over during primary trophoblast isolation, or that TERT-immortalization drove the cells towards a more EVT-like phenotype during culture. We note that the same isolation procedure used here resulted in the generation of other immortalized human first trimester EVT cell lines that retained characteristics of their *in vivo* counterparts [141,313,314]. Single-cell RNA-seq studies of human first trimester placenta recently identified the presence of several different EVT and CTB subtypes [277] as well

as cells at different stages of EVT/STB differentiation within primary trophoblast isolates [316]. Thus, the differences we detected within and between the immortalized trophoblasts and RPTs may reflect two distinct subtypes or unique stages of EVT differentiation (e.g. interstitial, endovascular, cell column, etc.) normally present in first trimester rhesus placenta. Integration of rhesus placenta single-cell RNA-seq data would help elucidate whether these transcriptomic differences represent natural variation among rhesus trophoblast populations or are simply a byproduct of immortalization and continued culture; however, no such dataset currently exists. Nonetheless, iRP-D26 and iRP-D28A showed overall transcriptomic similarity to primary rhesus trophoblasts and retained expression and functional characteristics of invasive EVTs, highlighting the suitability of these lines for future *in vitro* functional investigations. Specifically, these cell lines could be used for overexpression and/or knockdown studies of the genes identified as differentially expressed in human placentas here or other reports since primary cells, trophoblast or otherwise, are notoriously difficult to transfect. In particular, we envision assessing the function of genes shown to be upregulated in human placentas that are associated with preeclampsia to determine the effects on trophoblast invasion and signaling as well as provide insight into the mechanisms underlying the disproportionate incidence of pregnancy-related disease between humans and non-human primates.

In conclusion, our comparative analysis between human and rhesus bulk placenta showed that while a majority of HPGs are similarly expressed between the two species, certain genes are differentially expressed between human and rhesus placenta. These results suggest that rhesus is a suitable surrogate for most investigations of human placentation; however, notable molecular differences related to EVT function and preeclampsia should be considered and further interrogated in future investigations. Moreover, we generated immortalized rhesus trophoblast cell lines that represent a useful tool for primate placental investigations, especially for *in vitro* experiments that interrogate the putative function of genes identified in this study. Transcriptomic comparison and functional assessment of these cell lines suggest that they retain attributes of primary first trimester

rhesus EVTs. Collectively, the results of this study: (1) provide a comprehensive list of genes differentially expressed between human and rhesus placenta that informs the translatability of primate placental investigations; (2) help delineate the underlying molecular basis of increased EVT invasion and heightened susceptibility to preeclampsia and other pregnancy-related diseases in human; and (3) offer a reliable source of first trimester rhesus trophoblasts for current and future *in vitro* studies of early primate placentation.

2.5 Methods

2.5.1 Tissues and cell lines

Deidentified human term placental samples were collected by and acquired through the Labor and Delivery Unit at the Oregon Health and Science University Hospital and deposited into a repository under a protocol approved by the Institutional Review Board with informed consent from the patients. A total of five different human placentas from healthy cesarean section term births, ranging from 38.9 to 41.3 weeks gestation, were used for RNA-seq library generation (**Table 2.1**). All rhesus monkey (*Macaque mulatta*) tissues were collected in compliance with the guidelines established by the Animal Welfare Act for housing and care of laboratory animals and conducted per the Institutional Animal Care and Use Committee (IACUC protocols #0514 and #0580) at the Oregon National Primate Research Center (ONPRC). All rhesus placentas were collected from time mated breeding pregnancies delivered via cesarean section. Two frozen rhesus third trimester placental samples, collected at 140 and 141 gestational days, were used for RNA isolation and qRT-PCR validation of DE analysis results. Six fresh rhesus placentas were used for primary rhesus trophoblast TERT-immortalization, including two placentas from term (D141, D149) and four placentas from the first trimester (D26, D28A, D28B, D50). An additional first trimester rhesus placenta (D50) was used for primary trophoblast culture and RNA-seq analysis; these cells were not included in TERT-immortalization experiments. For all samples, the placentas were separated

from the fetus and amniotic sac, collected in cold sterile saline, and immediately processed for isolation of primary trophoblasts. The primary female and male rhesus macaque skin fibroblasts cell lines, Fb.XX (AG08312) and Fb.XY (AG08305), were acquired through Coriell Institute. Frozen stocks of the highly pure rhesus first trimester trophoblast cell lines, iRP-D26 and iRP-D28A, were generated at various passage numbers and can be made available to researchers upon request. While earlier passages were used for the initial characterization (passage 8-26), later passages were subjected to functional analyses, including Matrigel invasion, forskolin treatment, and hormone/growth factor secretion (passage 19-32) (**Table 2.12**).

2.5.2 RNA isolation and purification

Frozen placental samples were ground into a powder using liquid nitrogen-cooled mortar and pestle then directly added to TRIzol reagent (Thermo Fisher #15596026); for cell lines media was removed and TRIzol reagent was added directly to the tissue culture dish. RNA was isolated from TRIzol reagent, treated with Turbo DNAse (Thermo Fisher #AM1907), and purified using RNA Clean and Concentrator-5 spin columns (Zymo #R1013) according to manufactures instructions.

2.5.3 RNA-seq library preparation and sequencing

NEBNext® Ultra II Directional RNA Library Prep Kit for Illumina and NEBNext rRNA Depletion Kit (NEB, Ipswich, MA) was used to generate RNA-seq libraries from purified RNA following the manufacturer's instructions. Libraries were quantified with the Qubit High Sensitivity dsDNA Assay (Invitrogen, Carlsbad, CA) and size distribution was assessed with a 2100 Bioanalyzer High Sensitivity DNA Analysis Kit (Agilent). Multiplexed bulk human placental libraries were sequenced on the NextSeq500 platform using 150 cycle single-end protocol generating a total of 36.9 to 70.9 million 101bp reads per sample. Multiplexed rhesus trophoblast cell lines were sequenced on the NextSeq500 platform using a 100-cycle single-end protocol generating a total of 57.8 to 68.5 million 75bp reads per sample.

2.5.4 Human and rhesus orthologous gene annotations

Human protein-coding gene annotations (GRCh38.99) including associated rhesus orthologous gene annotations (Mmul10.99) were downloaded from ENSEMBL BioMart [317,318]. Gene annotations used for DE analysis were filtered to include only human protein-coding genes with "high-confidence" "one2one" rhesus orthologous genes, producing a final set of 15,787 human gene annotations and associated 15,787 rhesus orthologs. A total of 13,471 orthologues genes passed the minimum DEseq2 default expression threshold for differential expression statistical analysis.

2.5.5 Differential expression analysis

For human and rhesus cross-species DE analysis, raw fastq files were trimmed of low-quality and adapter sequences using Trimmomatic [319] and mapped to both the human (GCh38) and rhesus (Mmul10) reference genomes using Bowtie2 [320] with --very-sensitive parameter. The resulting BAM files were filtered to remove low-quality and multi-mapped reads (MAPQ ≥10) using samtools [321] view -q 10. Raw read counts for GRCh38.99 human gene annotations were generated from GRCh38 mapped data, while raw read counts for Mmul10.99 rhesus gene annotation were generated from Mmul10 mapped data, using featureCounts [322] –primary and filtered to include gene annotations described above. Gene counts were normalized and DEGs (padj<0.05 & Log2FC>|2|) were identified using default setting of DEseq2 [323]. DE analysis was performed with human mapped data (DE-GRCh38) and with rhesus mapped data (DE-Mmul10). A gene was considered differentially expressed only if it was identified as significantly (padj<0.05) upregulated or downregulated (|L2FC|>2) by both DE-GRCh38 and DE-Mmul10 analyses. The DE analysis was repeated a total of three times, with three independent sets of human placental RNA-seq data (**Supplemental Figure** 2.2**A-C**). The first DE analysis included the five human placental RNA-seq samples generated by our group (DE#1), the second DE analysis included six publicly available human placental RNA-seq datasets (DE#2), and the third DE analysis included two

publicly available human placental RNA-seq datasets (DE#3); all three DE analyses included the same four publicly available rhesus placental RNA-seq datasets. The final set of DEGs consisted only of genes determined to be significantly upregulated or downregulated by all three DE analyses.

The DE analysis between male and female human placental samples was performed as described above with the exception that trimmed reads were mapped exclusively to human reference genome. Additionally, the DE analysis between immortalized trophoblast and RPT cells was performed as described above with the following exceptions: (1) trimmed reads were mapped exclusively to rhesus reference genome, (2) differential expression was analyzed for all 21,575 protein-coding rhesus gene annotations (ENSEMBL v98), and (3) a gene was identified as significantly differentially expressed if padj<0.05 and Log2FC>|1|.

PCA and heatmap visualizations were generated using DEseq2 variance stabilizing transformation (VST) normalized human gene count data. PCA analysis was performed with VST-normalized expression data from all genes included in DE analysis. Morpheus web tool (https://software.broadinstitute.org/morpheus) was used to generated heatmap and perform hierarchical clustering (metric: one minus Pearson correlation, linkage method: complete). Statistical over-representation analysis of the human and rhesus upregulated gene lists was performed using g:Profiler webtool [324]. Custom background gene lists containing the final 15,787 orthologs described earlier and 21,575 rhesus protein-coding genes were used for human/rhesus upregulated and iRP over-representation tests, respectively. Query DEG lists were tested for over-representation of several functional genes sets, including the default g:Profiler biological pathway (KEGG, Reactome, and WikiPathways) gene sets; Human Protein Atlas (HPA) trophoblast subtypes gene sets (https://www.proteinatlas.org/humanproteome/celltype); “Rare_Diseases_GeneRIF_Gene_Lists” and “Jensen_DISEASES” human disease gene sets extracted from Enrichr webtool [325,326] (https://maayanlab.cloud/Enrichr/).

2.5.6 qRT-PCR

Primers were carefully designed to amplify both human and rhesus sequences of all genes examined, with noted exceptions (**Table 2.13**). Purified RNA was reverse transcribed into complementary DNA (cDNA) using SuperScript VILO cDNA Synthesis Kit (Thermo Fisher #11754050). Samples were prepared for high-throughput qRT-PCR using 96.96 gene expression dynamic array (Fluidigm BioMark) following manufactures protocol "Fast gene expression analysis using Evagreen". Briefly, preamplification of cDNA was performed using 500nM pooled primer mix, unincorporated primers were removed with exonuclease I treatment, and diluted 5-fold before samples and detectors were loaded and run on a 96.96 array with the following thermocycler settings: 70°C for 40 min, 60°C for 30 s, 95°C for 1 min, 40 cycles of 95°C 15 s, 59.5°C for 15 s, 72°C for 15 s. Two no template control (NTC) samples and four technical replicates of each reaction were included. The analysis was performed using qbase+ software, with GAPDH, HPRT1, and TBP serving as the reference genes used for normalization. Statistical significance was determined using a two-sided unpaired t-test with an alpha of 0.05. Mean calibrated normalized relative quantities (CNRQ) were exported from qbase+, Log2 transformed, then used as input for heatmap generation with Morpheus web tool.

2.5.7 Human placental marker gene set analysis

HPGs were defined by combining previously identified placenta "tissue enriched" and "group enriched" genes from The Human Protein Atlas [262]. A total of 190 human placental markers were extracted from this database, including 91 "placenta enriched" genes having at least four-fold higher mRNA level in the placenta compared to any other tissue, and 99 "placenta group enriched" genes having at least four-fold higher average mRNA level in a group of 2-5 tissues compared to any other tissue [262]. Human placental marker genes lacking an ENSEMBL-defined "one2one" or "high-confidence" rhesus orthologous gene could not reliably be compared and were excluded from our DE analysis.

2.5.8 Rhesus primary trophoblast cell isolations

Primary trophoblast cells were isolated from rhesus placentas using protocols adapted from previously described methods for human first trimester tissue [141,327,328] and human term tissue [24]. All rhesus placentas were obtained immediately after cesarean section delivery, and procedures were performed in a biosafety cabinet using ice-cold and sterile solutions unless otherwise noted. Placental tissue was transferred to a petri dish and covered with sterile saline, and the villous tissue was dissected from the decidua and chorionic plate using scissors and forceps; decidua and fetal membranes were discarded. To remove any contaminating blood, the villous tissue was washed until clear with several changes of sterile saline then crudely minced using scissors.

For first trimester placentas, villous tissue was transferred to a 50 mL tube containing warmed 0.25% trypsin solution and incubated at 37 °C for 10 min, inverting mixing every 2-3 min. The tissue was allowed to settle at bottom of the tube for 5 min before the supernatant was discarded and the tissue was washed with three changes of 1X phosphate-buffered saline without Ca2+ and Mg2+ (PBS--) (Caisson Labs #PBL05). To release the CTB, the tissue was transferred to a fresh petri dish containing warmed 0.25% trypsin 0.2mg/mL DNAse I solution, and a scalpel or glass slide was used to thoroughly scrape the villi. The surrounding trypsin solution containing desired CTBs was collected through a 70µm cell strainers into 50 mL tubes containing 5 mL fetal bovine serum (FBS) (Fisher #16-140-063). Cells were centrifuged at 300 g for 10 min and resuspended in Hanks Balanced Salt Solution (HBSS). This suspension was carefully layered over an equal volume of Lymphocyte Separation Media (Corning #25-072-CI) in a 15 mL conical tube, and centrifuging the gradient at 400g for 15min with the break off. While the red blood cells collect as a pellet at the bottom of the tube, the interface between the HBSS and LSM, containing the trophoblast cells, was carefully removed using a transfer pipet. The cells were pelleted then resuspended in cell culture media (CCM): DMEM high-glucose glutaMAX (Fisher, #10566-016), 10% FBS, 100 U/mL Pen-Strep (Fisher #15-140-148).

For term placentas, villous tissue was digested for 30 min shaking at 37°C with 0.25% trypsin and 0.2mg/mL DNAse I. Supernatant was reserved and the digest was repeated two additional times. The three digests were combined and centrifuged through Normal Calf Serum. Pellets were resuspended in DMEM and re-pelleted. Cells were carefully layered over a preformed Percoll gradient layered at 60, 55, 50, 45, 35, 30 and 25%, prior to centrifugation at 2800 rpm for 30 min without brake. The CTB cells between 35% and 55% were collected, counted, and resuspended in CCM. For both first trimester and term placentas, cells were centrifuged at 300g for 10 min, and the cell pellet was resuspended to 108 cells/mL in 1X Nanobead buffer (BioLegend #480017). Contaminating immune cells were depleted using anti-CD45 Magnetic Nanobeads (BioLegend #488028) following the manufactures instructions. Purified trophoblast cells were resuspended in complete trophoblast media (CTM): MEM – Earle's with D-Val (Caisson Labs #MEL12), 10% Normal Human Serum (Gemini Bio #100-110), 100 U/mL Pen-Strep, 1mM Sodium Pyruvate (Fisher #11-360-070), and 0.1M HEPES (Fisher #15-630-106); and grown on enhanced tissue culture dishes (Corning Primaria, #C353802) in a humidified 37°C environment with 5% CO_2. Primary rhesus trophoblasts included in RNA-seq (D50B) were harvested after nanobead immuno-purification and additional CTM wash step.

2.5.9 TERT-immortalization

Primary rhesus trophoblasts and rhesus skin fibroblast cells were immortalized using Alstem's TERT-immortalization kit (Alstem #CILV02) following manufactures instructions. In brief, following isolation of primary cells or 24 h after thawing of skin fibroblasts, the cells were plated at a density of 1.5 x 10^5 cells/well in a 6-well plate and transduced the following day. Each well received 1 mL of media containing 4 µL recombinant TERT lentivirus and 500x TransPlus reagent (Alstem # V020). After 16 h, the media was replaced with fresh culture media, and the cells were allowed to recover for 48 h before beginning puromycin selection (Santa Cruz Biotechnology #SC-108071). Cells were treated with 800ng/mL puromycin for a total of 72 h. The surviving cells were

propagated and represent the TERT-immortalized cell lines established and characterized throughout these studies. Mock transductions using the same transduction conditions without lentivirus added to media were included throughout puromycin selection to ensure depletion of non-transduced cells.

2.5.10 Cell culture

All cell lines were grown in a humidified 37 °C environment with 5% CO2. Cell culture media was changed every 2 days, and cells were enzymatically passaged using TrypLE (Gibco). Primary and TERT-immortalized trophoblast cell lines were cultured in CTM, while fibroblast samples were cultured in CCM. iRP-D26 and iRP-D28A cell lines were passaged at a density of 30,000 cells/cm^2, while all other lines were passaged at a density of 15,000 cells/cm^2.

2.5.11 DNA sequencing and chromosome copy number calling

Cells were dissociated using TryplE, pelleted, and resuspended in PBS^{--} containing 0.05% trypsin-EDTA (Thermo Fisher Scientific). A stereomicroscope was used to isolate, wash, and collect cells into individual sterile PCR tubes. Immediately after collection, PCR tubes containing single-cells (n=4), five-cells (n=1), and ten-cells (n=1) were flash-frozen on dry ice, and stored at -80C until library preparation. Individual samples underwent DNA extraction and whole-genome amplification, library pooling, DNA sequencing were performed as previously described [284]. Multiplexed libraries were loaded at 1.6pM and sequenced on the NextSeq 500 platform using 75 cycle single-end protocol. The resulting sequencing data was filtered, trimmed and mapped to the rhesus reference genome (Mmul8) as previously described [284]. Chromosome copy number calling and plots were generated using Ginkgo [329]. The proportion of Chr Y reads was determined for each sample using by dividing the number of reads mapped to Chr Y by the total number of mapped reads. The relative proportion of Chr Y reads was identified by normalizing

samples to the known male sample (iRFb-XY), and samples with a mean relative proportion ≥ 0.50 were identified as male.

2.5.12 Metaphase spread chromosome counts

Cells were treated with 0.015ug/mL colcemid overnight (~12 h) to induce metaphase arrest. Cells were dissociated using TryplE, pelleted, and resuspended in a warm hypotonic solution (0.06 M KCl, 5% FBS) for 15 min before being fixed with 3:1 methanol:acetic acid. Slides were made and baked at 95C for 20 min, cooled, trypsinized for 45 s and stained with Wright's stain. At least 20 metaphase spreads brightfield images were captured using 100X objective on Nikon microscope and counted using FIJI software.

2.5.13 IHC staining

Paraffin sections were deparaffinized and rehydrated through xylene and graded alcohol series, then washed for 5 min in running tap water. Antigen unmasking was performed using sodium citrate (pH 6.0) buffer in a pressure cooker for 20 min, washed in three changes of PBS. An endogenous enzyme block was performed by incubating sections in 0.3% hydrogen peroxide for 10 min, washed in three changes of PBS. Nonspecific proteins were blocked by incubating sections in 5% horse serum for 30 min Primary antibodies were diluted as described for IF staining, and tissue was incubated in primary antibody dilutions for 2 h at room temperature. Mouse IgG H+L (Vector Labs, BA-2000) and rabbit IgG H+L (Vector Labs, BA-1100) biotinylated secondary antibody dilutions were prepared at 1:250 in PBS + 1% BSA. The tissue sections were incubated in secondary antibody dilution for 1 h at room temperature, then washed in three changes of PBS. VECTASTAIN Elite ABC HRP Kit (Vector Laboratories, PK-6100) and ImmPACT DAB Peroxidase HRP substrate (Vector Labs, SK-4105) were used according to manufacturer's instructions. Nuclei were counterstained with hematoxylin (Electron Microscopy Sciences, 26043-05), and imaged using a brightfield microscope.

2.5.14 IF staining

The cell culture media was removed from cells, fixed with ice-cold methanol for 15 min at -20C, then washed in three changes of PBS. Nonspecific proteins were blocked by incubating cells in 5% donkey serum for 30 min anti-KRT7 (mouse monoclonal, Dako, M7018), anti-CDH1 rabbit monoclonal (Cell Signaling, 3195S), anti-VIM rabbit monoclonal (Cell Signaling, 5741T), and anti-PTPRC rabbit monoclonal (Cell Signaling, 13917S) antibodies were diluted in PBS + 1% BSA (KRT7 1:250, CDH1 1:250, VIM 1:250, CD45 1:250), and incubated for 2 h at room temperature. The cells were then washed in three changes of PBS, before incubating in secondary antibody dilutions for 1 h. at room temperature. Alexa Fluor 488 and 594 (Life Technologies) secondary antibody dilutions were prepared at 1:1000 in PBS + 1% BSA. Cells were counterstained with DAPI and washed with three changes of PBS before imaging. Images of cells were captured using 20X objective on epifluorescence microscope and processed using FIJI software.

2.5.15 Trans-well migration and Matrigel invasion assay

24-well trans-well inserts with 8uM pores (Falcon #353097) were coated with 1.2mg/mL Matrigel (Corning #354234), following the manufacturer's instructions. Migration and invasion assays were performed by culturing cells at 37°C for 48 h on uncoated (n=3) and Matrigel-coated (n=3) trans-well inserts, respectively. Assays were carried out under both normoxia and hypoxia (~1% O_2) conditions. A total of 25,000 cells in 250 µL serum-free media was added to each insert and 650 µL of complete trophoblast media was added to each surrounding insert. At 48 h, the cells remaining on the topside of the insert were wiped away with sterile cotton swap before the insert was fixed with 4% paraformaldehyde and the nuclei were stained with DAPI. The 10X objective of a Nikon Eclipse epifluorescence microscope was used to capture five micrographs of the bottom side of each insert, and the number of cells/nuclei were counted automatically using FIJI software with default threshold and measure functions. For each insert, the mean average cell counts across the five micrographs were used to calculate the "average cell counts per insert" reported. For each

cell line, the mean average cell counts across all three uncoated inserts was used as the denominator for calculating the percent invasion (coated/uncoated) represented. A two-sided t-test with an alpha of 0.05 was used to determine the significance between conditions.

2.5.16 IGF2 secretion assay

Culture media samples were collected from cell lines cultured for 48 h (n=2 for: iRFb, iRP-D26, iRP-D28A, iRP-D28B; n=4 for rhesus serum pool), then centrifuged for 5min at 300g to remove cellular debris before IGF-2 secretion analysis. Secreted IGF-2 concentrations were determined by ELISA following the manufacturer's instructions (R&D Systems DG-100, Minneapolis, MN) in the Endocrine Technologies Core (ETC) at ONPRC. The assay range was 12.5 – 800 pg/mL. Intra-assay variation for an in-house monkey serum pool was 4.0%. All samples were quantified in a single assay and no inter-assay variation was determined. The assay was validated for use in monkey samples by the ETC prior to the analysis of samples. This validation included analysis of a dilution series to test for assay specificity as well as a spike and dilution analysis to test for analyte recovery and matrix effects.

2.5.17 Transcriptomic comparison of human, rhesus, and mouse placenta

Human gene annotations (GRCh38.101) including associated rhesus (Mmul10.101) and mouse (GRCm38.101) orthologous gene annotations were downloaded from Ensembl BioMart [317,318]. Gene annotations were filtered to include only human protein-coding genes with "one2one" rhesus and mouse orthologous genes. The orthologues were further filtered to exclude ribosomal genes and genes from chromosomes X, Y and MT, producing a final set of 14,054 orthologous human, rhesus and mouse 1:1:1 gene annotations. The method used for transcriptomic comparison of three species is largely based off a previously described approach [261]. For this, we used RNA-seq data generated in-house from human (n=5) and publicly available rhesus (n=4) and mouse (n=4) placenta RNA-seq data (**Table 2.1**). Raw fastq files were trimmed of low-quality and adapter

sequences as described in main manuscript. Transcripts per Million (TPM) gene expression values were calculated using RSEM v1.3.1 [330] with reference genome and gene annotation downloaded from Ensembl (version 101) [317,318]. For this, trimmed data were mapped to respective genomes/gene annotations (RSEM index) using Bowtie2 [320] with the following parameters --sensitive --dpad 0 --gbar 99999999 --mp 1,1 --np 1 --score-min L,0,-0.1. DEseq2 was used for normalization and differential expression calling, with TPM values as inputs. One plus Log2 normalized TPM values were used for heatmap generation and hierarchical clustering using Morpheus webtool. DE results were filtered to include only genes with |L2FC|>2 and padj<0.05.

2.5.18 Forskolin fusion assay

The cell lines were passaged onto 6-well plates and treated the following day with either media containing 25uM forskolin or DMSO. After 48 h, two wells from each condition were processed for RNA isolation and a single well was processed for IF staining as described in the Methods Section. Four technical replicates were included in subsequent qRT-PCR analysis, and five micrographs of immunostained cells were captured per condition.

2.5.19 mCG secretion levels

mCG radioimmunoassay (RIA) was performed on media collected after two days in culture from both iRP-D26 (n=2) and iRP-D28A (n=2) cell lines. Highly purified hCG for radioiodination and reference standard was obtained from Dr. Leo Reichert, Tucker Endocrine Research Institute (P.O. Box 0811, Tucker, GA 30085-0811; *Endoc* 1973; 92: 411-6). Each ampule of hCG contained 50 micrograms. An ampule of hCG was re-dissolved in 50 ml of phosphate-buffered saline (PBS) so that the concentration of hCG was 1 mg/ml. After being completely dissolved, the hCG was separated into aliquots of 5 mg/5 ml for radioiodination. For reference standards, 24.95 ml of 1% BSA-PBS was added to one hCG ampoule, resulting in a concentration of 200 ng/ml which was divided into 0.5 ml per aliquot and stored at -80C. Ovine antiserum H-26 has been established in

RIA and used extensively for measuring monkey CG concentrations in blood, urine and cells (Hodgen G, *J Clin Endocrinol Metab* 39: 457, 1974). While the antiserum was generated against ovine luteinizing hormone (LH), it was targeted toward monkey CG, and, for a very long time, has been the only antibody available to a few laboratories for measuring monkey CG. H-26 antiserum was diluted to 1:2000 for use as the primary antibody in our laboratory. For precipitation, the anti-rabbit gamma globulin, NIH #1, was diluted to 1:50 for use in the mCG RIA. Assay tubes were centrifuged at 3000 rpm for 30 min in a Beckman J-6 refrigerated centrifuge. Before the assay, hCG was radioiodinated with Iodine-125 (I-125) (Perkin-Elmer, Billerica, MA) for use as a trace. Briefly, 1.0 mCi of fresh I-125 was mixed with 5 μg of hCG for 1 minute under oxidative conditions. The reaction was stopped by adding reductive solution, and the I-125-labeled hCG was separated from free I-125 by column chromatography (using Bio-Gel P60, 200-300 wet mesh, from Bio-Rad, Hercules, CA). The fractions containing proteins were tested with antibody within 24 h and the specific and non-specific bindings were assessed. All samples for mCG determinations were assayed at the original concentration. Overall, the characteristics of the standard curves indicated that the assays were well executed. Of the 12 standard points in serial dilutions of hCG from 10 ng/ml to 0.0049 ng/ml, 10 maintained dose-response between 5-95% binding. The highest point (10 ng/ml) and the lowest point (0.0049 ng/ml) were outside the 5% confidence limit at the upper and lower end of the standard curve, respectively. However, these standard points did not affect the calculation of samples as the sample values were based on their specific bindings. The sensitivity of the assay was estimated to be 0.1 ng/ml (at about 90% binding).

2.6 Supplemental Figures

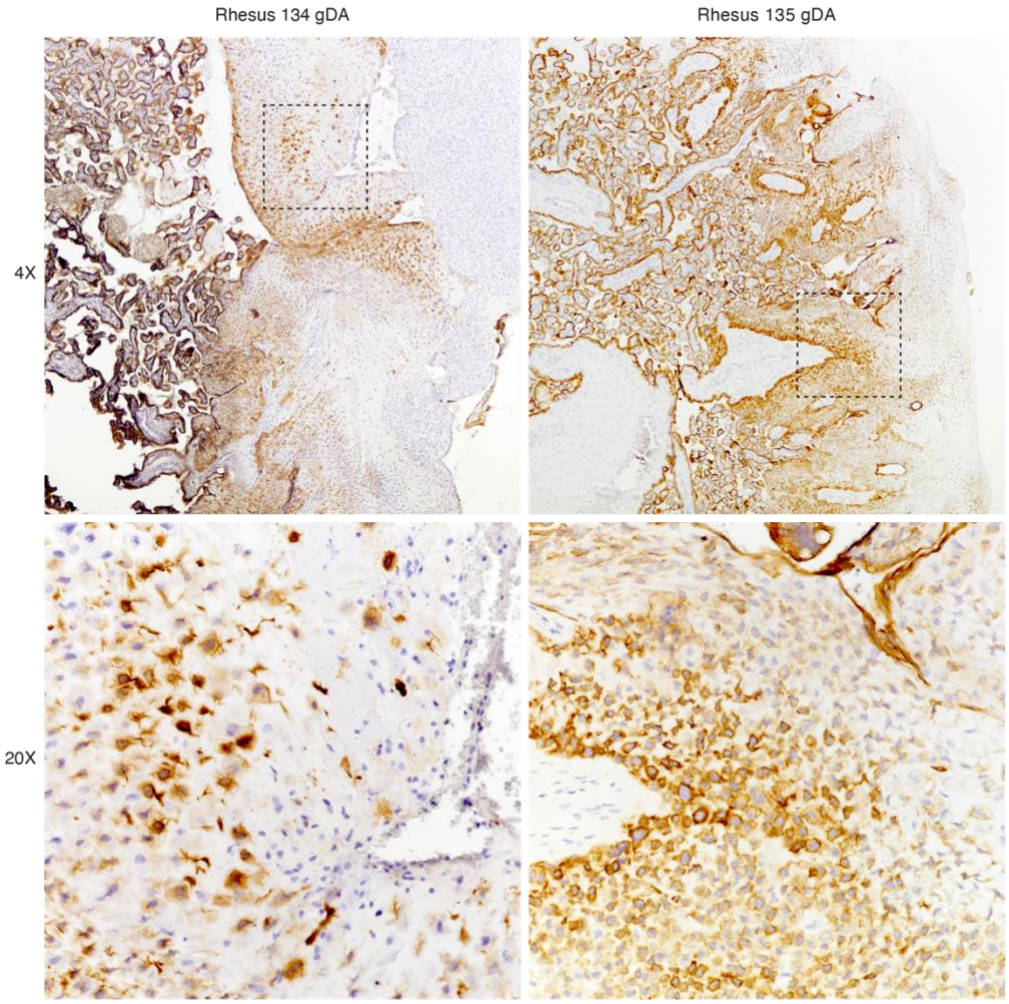

Supplemental Figure 2.1 Rhesus placenta IHC

Rhesus placental tissue at ~80% gestation stained for KRT7 (DAPI/brown). Tissue from gestational day 134 (left) and 135 (right), imaged using 4X (top) and 20X objective (bottom). Dashed boxes denote regions examined at higher magnification.

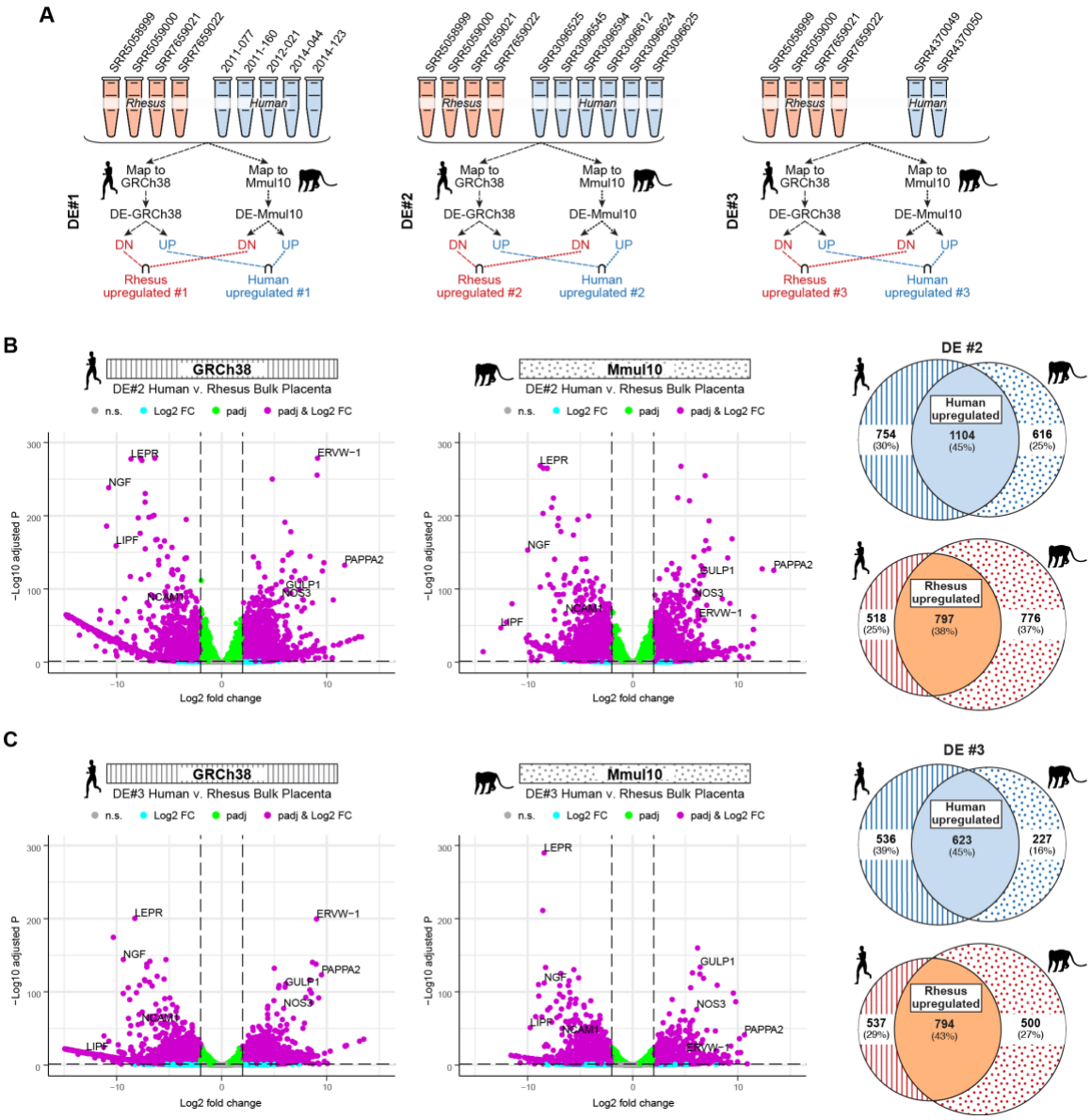

Supplemental Figure 2.2 Human versus rhesus placenta differential expression

(A-C) Schematic of DE analysis (A) DE#1 (B) DE#2 (C) DE#3. (D,E,G,H) Volcano plots showing gene expression fold differences between human and rhesus term placental tissue from (D,E) DE#2 and (G,H) DE#3 using data mapped to (D,G) human genome and gene annotations (DE-GRCh38), and data mapped to (E,H) rhesus genome and gene annotations (DE-Mmul10). Dashed lines denote DE significance (padj<0.05) and fold change (|L2FC|>2) thresholds; genes passing significance threshold (green), passing L2FC threshold (cyan), passing both (magenta), or none (grey). (F,I) Venn-diagram depicting intersection of DE-GRCh38 (stripes) and DE-Mmul10 (spotted) results to identify intermediate human upregulated (light blue) and rhesus upregulated (light red) genes sets from (F) DE#2 and (I) DE#3.

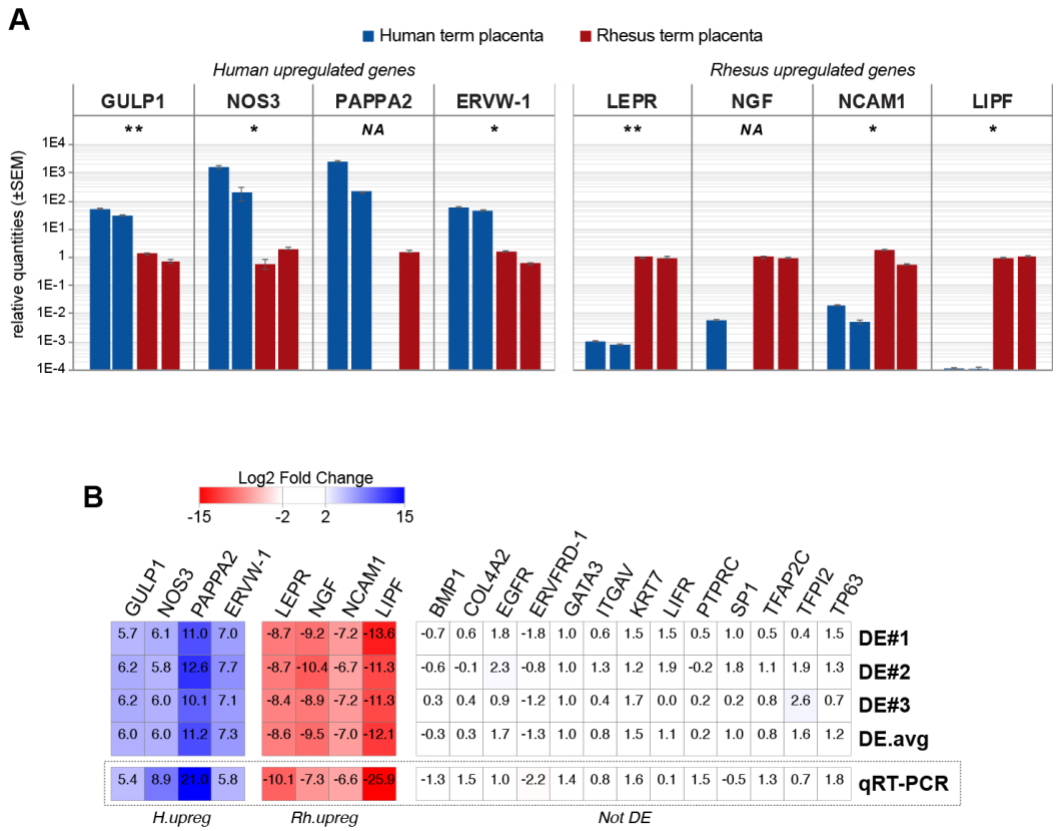

Supplemental Figure 2.3 qRT-PCR validation of DEGs identified from DE analysis

(A) qRT-PCR relative gene expression quantities (mean ± SEM) of human (blue) and rhesus (red) bulk placental samples; all samples were normalized to GAPDH, HPRT1, and TBP, and scaled to rhesus bulk placental samples. Four technical replicates for PCR reaction, and two biological replicates for each group species were included. Statistically significant differences between human and rhesus groups were identified using two-sided unpaired t-test with alpha of 0.05 (*p<0.05, **p<0.01). (B) Heatmap depicting human versus rhesus log2 fold-change values determined via qRT-PCR and the RNA-seq based DE analyses.

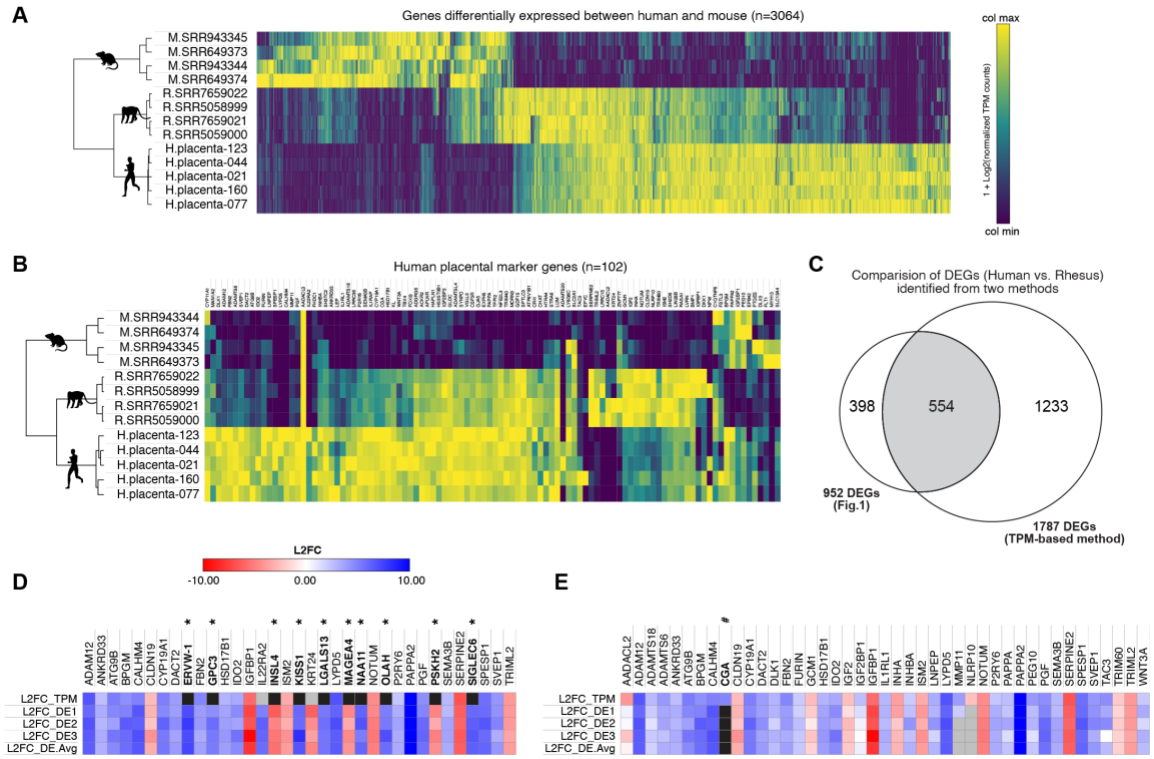

Supplemental Figure 2.4 TPM-based transcriptomic comparison of human, rhesus and mouse placenta

(A) Heatmap depicting expression levels (Log2(1+ TPM)) of genes differentially expressed between human and mouse placenta, and (B) HPGs. Hierarchal clustering shows rhesus samples cluster more closely to human than mouse samples for both gene sets, highlighting molecular similarities between human and rhesus placental samples. (C) Venn-diagram depicting the intersection of DEGs (Human vs. Rhesus) identified from our primary DE approach (left) and TPM-based DE strategy (right). (D) Heatmap comparing Log2 fold change of differentially expressed HPGs identified from the primary DE approach between human and rhesus, and (E) TPM-based DE strategy; grey boxes denote NA values; black boxes denote excluded genes; *=genes excluded from TPM-based analysis due to lack of mouse orthologue; #=genes excluded from primary DE analysis due to low-confidence rhesus orthologue.

Human vs. Rhesus bulk placenta

source	term name	Human upreg. (padj)	Rhesus upreg. (padj)
JD	pre-eclampsia	6.73E-04	1
JD	Intestinal obstruction	1	3.46E-03
JD	Hypertension	1	2.60E-02
JD	Nephrogenic adenoma	1	2.86E-02
JD	Burning mouth syndrome	3.58E-02	1
RDGR	Cystic fibrosis	1	7.27E-02
JD	Thrombocytopenia	1	1.30E-01
RDGR	HELLP syndrome	1.48E-01	1
RDGR	Gestational trophoblastic tumor	1.52E-01	1
RDGR	Basilar migraine	1	1.71E-01
RDGR	Cardiac rupture	1	2.10E-01
RDGR	Pyridoxine deficiency	1	2.41E-01
JD	Short bowel syndrome	1	2.54E-01
RDGR	Glycine N-methyltransferase deficiency	1	2.84E-01
JD	Xanthinuria	2.93E-01	1
JD	Liver cancer	3.14E-01	1
JD	Male infertility	3.23E-01	1
RDGR	Eclampsia	4.43E-01	1

iRP-D26 vs. RPT

source	term name	iRP-D26 upreg. (padj)	iRP-D26 downreg. (padj)
HPA	Extravillous-enhanced	1.20E-11	1
HPA	Syncytiotrophoblast-group-enriched	1	2.56E-08
HPA	Cytotrophoblast-group-enriched	1	6.65E-05
HPA	Syncytiotrophoblast-enhanced	1	6.64E-04
HPA	Syncytiotrophoblast-enriched	1	5.33E-03
HPA	Extravillous-enriched	7.29E-03	1
HPA	Extravillous-group-enriched	1.59E-02	1
HPA	Cytotrophoblast-enhanced	1	9.25E-02

source	term name	iRP-D26 upreg. (padj)	iRP-D26 downreg. (padj)
KEGG	Herpes simplex virus 1 infection	5.11E-11	1
KEGG	Cell adhesion molecules	1	1.13E-03
KEGG	Proteoglycans in cancer	2.86E-02	1
KEGG	ECM-receptor interaction	5.54E-02	1
REAC	Immune System	1	9.73E-08
REAC	Immunoregulatory interactions between a Lymphoid and a non-Lymphoid cell	1	1.29E-06
REAC	Generic Transcription Pathway	5.24E-03	1
REAC	Extracellular matrix organization	2.36E-02	1
REAC	Phosphorylation of CD3 and TCR zeta chains	1	3.07E-02
REAC	Signaling by Rho GTPases	3.25E-02	1
REAC	Generation of second messenger molecules	1	4.92E-02
WP	Genotoxicity pathway	1.27E-03	1

iRP-D28A vs. RPT

source	term name	iRP-D28A upreg. (padj)	iRP-D28A downreg.
HPA	Syncytiotrophoblast-group-enriched	1	3.33E-07
HPA	Cytotrophoblast-group-enriched	1	4.24E-05
HPA	Syncytiotrophoblast-enriched	1	3.76E-02
HPA	Extravillous-enhanced	8.87E-02	1

source	term name	iRP-D28A upreg. (padj)	iRP-D28A downreg.
KEGG	Herpes simplex virus 1 infection	1.22E-18	1
KEGG	Axon guidance	1.35E-04	1
REAC	TCR signaling	1	5.15E-05
REAC	Generic Transcription Pathway	7.60E-05	1
REAC	Immune System	1	1.47E-04
REAC	Generation of second messenger molecules	1	8.04E-04
REAC	Non-integrin membrane-ECM interactions	1.54E-03	1
REAC	Extracellular matrix organization	4.93E-03	1
REAC	Immunoregulatory interactions between a Lymphoid and a non-Lymphoid cell	1	1.64E-02
REAC	RNA Polymerase II Transcription	2.63E-02	1
REAC	DNA Replication Pre-Initiation	1	2.75E-02
REAC	G1/S Transition	1	3.97E-02
REAC	Fatty acid metabolism	1	7.18E-02
REAC	Laminin interactions	9.82E-02	1
WP	Mitochondrial LC-Fatty Acid Beta-Oxidation	1	2.21E-03

Supplemental Figure 2.5 Functional over-representation analysis

Over-representation analysis of human-upregulated and rhesus-upregulated DEG sets (top), iRP-D26 upregulated and downregulated DEG sets (middle), and iRP-D28A upregulated and downregulated DEG sets (bottom); functional terms with padj<0.1 (green), padj<0.5 (yellow); JD=Jensen_DISEASES, RDGR=Rare_Diseases_GeneRIF_Gene_Lists, HPA=Human Protein Atlas, REAC=Reactome, WP=WikiPathways.

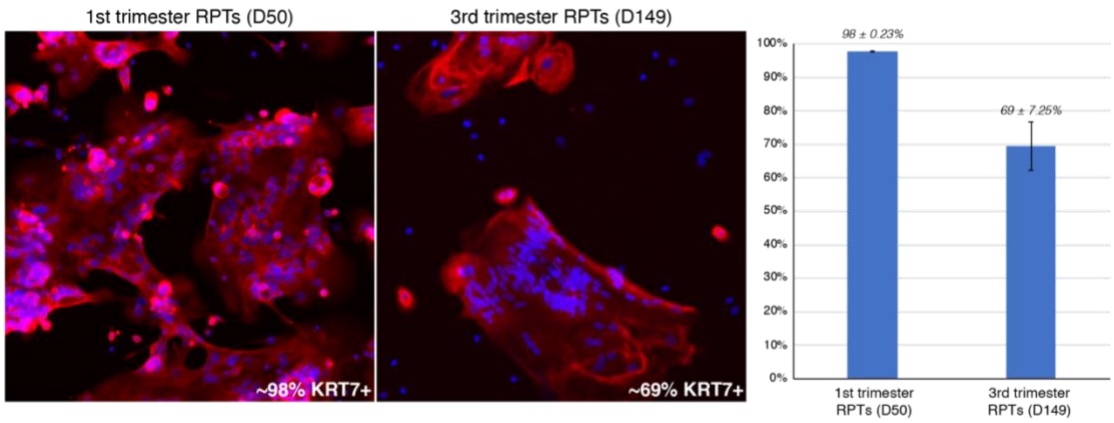

Supplemental Figure 2.6 Purity of primary rhesus trophoblast cell isolations

KRT7 IF staining of primary rhesus trophoblast cells isolated from D50 first trimester (left) and D149 third trimester (middle) rhesus placenta. Bar graph depicts average percent KRT7 positive cells calculated across five immunostained micrographs from 1st (n=1) and 3rd (n=1) trimester primary cell cultures.

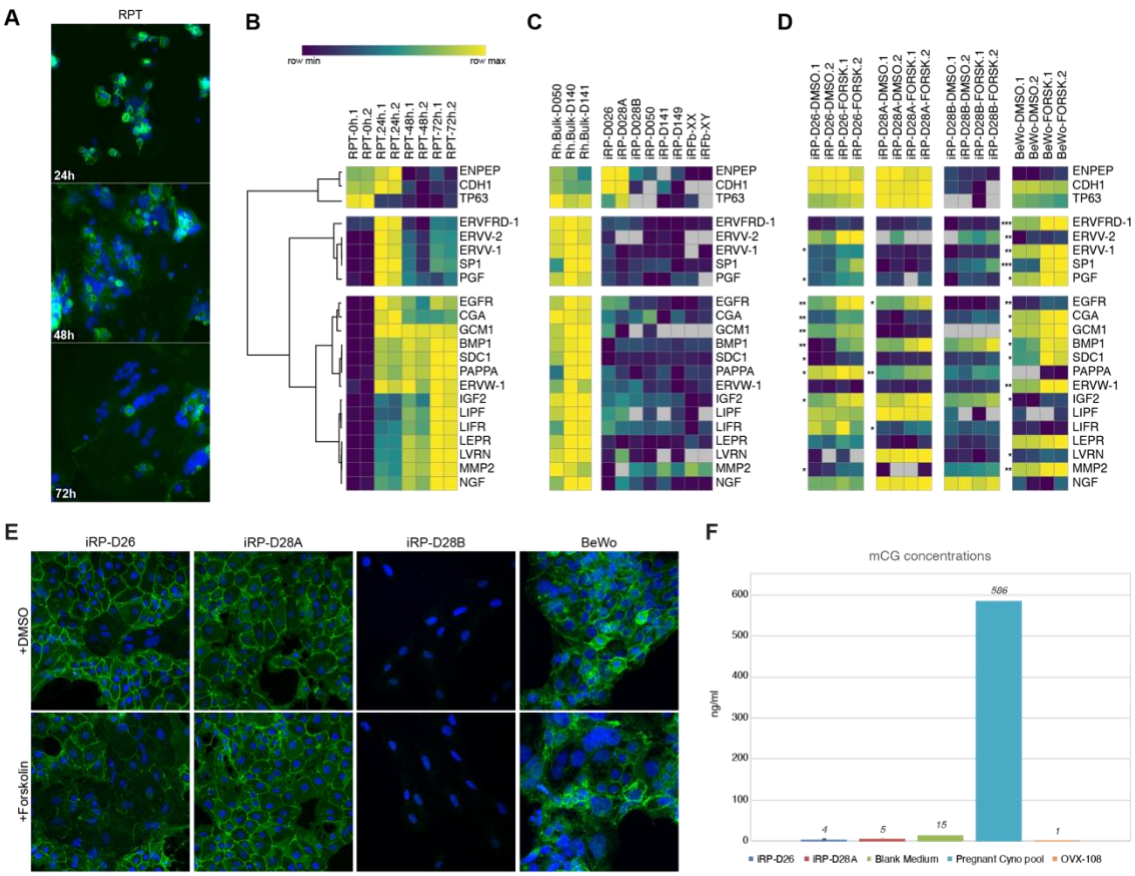

Supplemental Figure 2.7 Functional characterization of primary and immortalized rhesus trophoblast cells.

(A) CDH1 IF staining of RPT cells after 24 h, 48 h, and 72 h in culture, showing spontaneous fusion/syncytialization of RPTs (B-D) Heatmaps of qRT-PCR RNA expression levels. Color scale depicts minimum (purple) and maximum (yellow) Log2 relative gene expression values compared across (B) RPT cells after 24 h, 48 h, and 72 h in culture (C) bulk rhesus placenta, iRP, and iRFb cell lines; (D) iRP and BeWo cell lines treated with DMSO (n=2) or Forskolin (n=2) for 48 h. Statistically significant differences between DMSO and forskolin treatment groups were identified using two-sided unpaired t-test with alpha of 0.05 (*p<0.05, **p<0.01, ***p <0.001). (E) CDH1 IF staining of iRP and BeWo cell lines treated with DMSO or Forskolin for 48 h (F) Bar graph of mCG secretion concentrations detected via radioimmunoassay (RIA) in cell culture media from iRP-D26 (blue), iRP-D28A (pink), blank media (green); and in serum from pregnant (light blue) and ovariectomized (OVX) cynomolgus macaques (orange).

2.7 Tables

Table 2.1 Sample details

Sample name	Sample type	Sample subtype	species	ID
H-placenta-021	bulk placenta	H.placenta (DE#1)	Human	SRR12363247
H-placenta-044	bulk placenta	H.placenta (DE#1)	Human	SRR12363246
H-placenta-077	bulk placenta	H.placenta (DE#1)	Human	SRR12363245
H-placenta-123	bulk placenta	H.placenta (DE#1)	Human	SRR12363244
H-placenta-160	bulk placenta	H.placenta (DE#1)	Human	SRR12363248
H.placenta.SRR3096525	bulk placenta	H.placenta (DE#2)	Human	SRR3096525
H.placenta.SRR3096545	bulk placenta	H.placenta (DE#2)	Human	SRR3096545
H.placenta.SRR3096594	bulk placenta	H.placenta (DE#2)	Human	SRR3096594
H.placenta.SRR3096612	bulk placenta	H.placenta (DE#2)	Human	SRR3096612
H.placenta.SRR3096624	bulk placenta	H.placenta (DE#2)	Human	SRR3096624
H.placenta.SRR3096625	bulk placenta	H.placenta (DE#2)	Human	SRR3096625
H.placenta.SRR4370049	bulk placenta	H.placenta (DE#3)	Human	SRR4370049
H.placenta.SRR4370050	bulk placenta	H.placenta (DE#3)	Human	SRR4370050
M.placenta.SRR649373	bulk placenta	M.placenta	Mouse	SRR649373
M.placenta.SRR649374	bulk placenta	M.placenta	Mouse	SRR649374
M.placenta.SRR943344	bulk placenta	M.placenta	Mouse	SRR943344
M.placenta.SRR943345	bulk placenta	M.placenta	Mouse	SRR943345
Rh.placenta.SRR5058999	bulk placenta	Rh.placenta	Rhesus	SRR5058999
Rh.placenta.SRR5059000	bulk placenta	Rh.placenta	Rhesus	SRR5059000
Rh.placenta.SRR7659021	bulk placenta	Rh.placenta	Rhesus	SRR7659021
Rh.placenta.SRR7659022	bulk placenta	Rh.placenta	Rhesus	SRR7659022
H.PBMC.SRR3389246	PBMC	H.PBMC	Human	SRR3389246
H.PBMC.SRR3390437	PBMC	H.PBMC	Human	SRR3390437
H.PBMC.SRR3390461	PBMC	H.PBMC	Human	SRR3390461
H.PBMC.SRR3390473	PBMC	H.PBMC	Human	SRR3390473
Rh.PBMC.SRR2467156	PBMC	Rh.PBMC	Rhesus	SRR2467156
Rh.PBMC.SRR2467157	PBMC	Rh.PBMC	Rhesus	SRR2467157
Rh.PBMC.SRR2467159	PBMC	Rh.PBMC	Rhesus	SRR2467159
Rh.PBMC.SRR2467160	PBMC	Rh.PBMC	Rhesus	SRR2467160
BeWo.SRR6443610	trophoblast	BeWo	Human	SRR6443610
BeWo.SRR6443613	trophoblast	BeWo	Human	SRR6443613
BeWo.SRR6443614	trophoblast	BeWo	Human	SRR6443614
BeWo.SRR6443615	trophoblast	BeWo	Human	SRR6443615
BeWo.SRR6443616	trophoblast	BeWo	Human	SRR6443616
BeWo.SRR9118949	trophoblast	BeWo	Human	SRR9118949
BeWo.SRR9118950	trophoblast	BeWo	Human	SRR9118950
HPT.SRR2397323	trophoblast	HPT	Human	SRR2397323
HPT.SRR2397324	trophoblast	HPT	Human	SRR2397324
HPT.SRR2397332	trophoblast	HPT	Human	SRR2397332
HPT.SRR2397333	trophoblast	HPT	Human	SRR2397333
HPT.SRR2397341	trophoblast	HPT	Human	SRR2397341
HPT.SRR2397342	trophoblast	HPT	Human	SRR2397342
HPT.SRR6443608	trophoblast	HPT	Human	SRR6443608
HPT.SRR6443609	trophoblast	HPT	Human	SRR6443609
HPT.SRR6443611	trophoblast	HPT	Human	SRR6443611
HPT.SRR6443612	trophoblast	HPT	Human	SRR6443612
iRP-D26-01	trophoblast	iRP	Rhesus	SRR12363173
iRP-D26-02	trophoblast	iRP	Rhesus	SRR12363172
iRP-D28A-01	trophoblast	iRP	Rhesus	SRR12363171
iRP-D28A-02	trophoblast	iRP	Rhesus	SRR12363170
RPT-D50-01	trophoblast	RPT	Rhesus	SRR12363169
RPT-D50-02	trophoblast	RPT	Rhesus	SRR12363168

Table 2.2 Human-upregulated DEGs (top 50 out of 448)

H.GeneID	H.Gene.name	Rh.GeneID	Mean L2FC	Mean padj
ENSG00000148848	ADAM12	ENSMMUG00000009661	6.36	1.87E-114
ENSG00000144366	GULP1	ENSMMUG00000008265	6.04	1.63E-100
ENSG00000197632	SERPINB2	ENSMMUG00000016617	8.55	1.70E-87
ENSG00000112195	TREML2	ENSMMUG00000049500	8.36	3.31E-80
ENSG00000172331	BPGM	ENSMMUG00000004598	5.72	1.75E-77
ENSG00000164867	NOS3	ENSMMUG00000020437	5.96	5.61E-77
ENSG00000137869	CYP19A1	ENSMMUG00000002553	5.38	3.90E-74
ENSG00000177707	NECTIN3	ENSMMUG00000009998	5.79	1.14E-71
ENSG00000169550	MUC15	ENSMMUG00000012926	9.85	1.28E-63
ENSG00000039068	CDH1	ENSMMUG00000011850	4.81	5.60E-63
ENSG00000011347	SYT7	ENSMMUG00000005122	5.07	2.42E-59
ENSG00000165124	SVEP1	ENSMMUG00000047960	4.13	1.13E-54
ENSG00000186417	GLDN	ENSMMUG00000005976	5.89	8.25E-49
ENSG00000103485	QPRT	ENSMMUG00000042891	5.10	1.80E-46
ENSG00000258839	MC1R	ENSMMUG00000053514	7.36	2.45E-42
ENSG00000147257	GPC3	ENSMMUG00000009622	5.16	1.44E-41
ENSG00000119630	PGF	ENSMMUG00000002909	5.59	8.22E-41
ENSG00000037280	FLT4	ENSMMUG00000018693	6.24	8.27E-41
ENSG00000138829	FBN2	ENSMMUG00000010682	3.73	5.82E-40
ENSG00000197872	FAM49A	ENSMMUG00000020385	3.52	9.22E-40
ENSG00000164309	CMYA5	ENSMMUG00000020733	6.41	8.37E-39
ENSG00000114841	DNAH1	ENSMMUG00000016974	4.81	1.23E-38
ENSG00000197043	ANXA6	ENSMMUG00000021053	2.73	4.25E-38
ENSG00000112186	CAP2	ENSMMUG00000001990	5.05	4.37E-38
ENSG00000116183	PAPPA2	ENSMMUG00000023214	11.21	5.10E-38
ENSG00000105198	LGALS13	ENSMMUG00000004245	5.45	6.53E-36
ENSG00000182492	BGN	ENSMMUG00000012743	2.89	2.96E-35
ENSG00000154265	ABCA5	ENSMMUG00000018608	3.15	1.62E-34
ENSG00000178338	ZNF354B	ENSMMUG00000008976	3.97	6.76E-34
ENSG00000070182	SPTB	ENSMMUG00000019172	3.96	9.36E-34
ENSG00000147113	DIPK2B	ENSMMUG00000041157	4.61	1.30E-33
ENSG00000035499	DEPDC1B	ENSMMUG00000018379	3.80	1.63E-33
ENSG00000167232	ZNF91	ENSMMUG00000003688	7.05	1.70E-31
ENSG00000063660	GPC1	ENSMMUG00000056083	4.21	3.08E-31
ENSG00000148218	ALAD	ENSMMUG00000031965	3.78	1.13E-30
ENSG00000026559	KCNG1	ENSMMUG00000000683	5.70	5.98E-30
ENSG00000163293	NIPAL1	ENSMMUG00000018625	5.77	6.98E-30
ENSG00000159450	TCHH	ENSMMUG00000056263	6.61	9.18E-30
ENSG00000054277	OPN3	ENSMMUG00000005669	3.62	9.21E-30
ENSG00000012171	SEMA3B	ENSMMUG00000020117	3.29	1.37E-29
ENSG00000196411	EPHB4	ENSMMUG00000007375	3.09	4.29E-29
ENSG00000173269	MMRN2	ENSMMUG00000011851	2.75	8.30E-28
ENSG00000109062	SLC9A3R1	ENSMMUG00000005737	2.50	1.80E-27
ENSG00000005108	THSD7A	ENSMMUG00000012694	4.26	3.40E-27
ENSG00000204323	SMIM5	ENSMMUG00000063604	4.63	5.29E-26
ENSG00000025772	TOMM34	ENSMMUG00000013211	3.22	3.65E-25
ENSG00000174652	ZNF266	ENSMMUG00000061661	3.52	4.03E-25
ENSG00000138166	DUSP5	ENSMMUG00000057793	3.17	2.05E-24
ENSG00000152583	SPARCL1	ENSMMUG00000019047	3.58	2.11E-24
ENSG00000165895	ARHGAP42	ENSMMUG00000022603	3.55	1.18E-23

Table 2.3 Rhesus-upregulated DEGs (top 50 out of 505)

H.GeneID	H.Gene.name	Rh.GeneID	mean L2FC	mean padj
ENSG00000116678	LEPR	ENSMMUG00000003265	-8.60	1.36E-278
ENSG00000134259	NGF	ENSMMUG00000062180	-9.50	3.05E-114
ENSG00000114251	WNT5A	ENSMMUG00000061281	-6.33	1.27E-103
ENSG00000002587	HS3ST1	ENSMMUG00000001341	-6.95	4.79E-98
ENSG00000183067	IGSF5	ENSMMUG00000003427	-5.41	2.42E-93
ENSG00000087085	ACHE	ENSMMUG00000058568	-6.31	1.80E-86
ENSG00000099139	PCSK5	ENSMMUG00000022023	-4.98	1.14E-84
ENSG00000127241	MASP1	ENSMMUG00000013004	-6.89	7.75E-79
ENSG00000186854	TRABD2A	ENSMMUG00000008855	-7.15	3.05E-75
ENSG00000156113	KCNMA1	ENSMMUG00000018390	-6.27	1.28E-68
ENSG00000116761	CTH	ENSMMUG00000019326	-8.47	1.49E-66
ENSG00000137634	NXPE4	ENSMMUG00000012268	-8.47	2.28E-65
ENSG00000084710	EFR3B	ENSMMUG00000016461	-5.03	5.80E-64
ENSG00000196517	SLC6A9	ENSMMUG00000015158	-4.31	1.73E-60
ENSG00000136689	IL1RN	ENSMMUG00000013014	-6.39	1.40E-58
ENSG00000152952	PLOD2	ENSMMUG00000011577	-3.57	2.59E-50
ENSG00000158201	ABHD3	ENSMMUG00000004382	-3.91	1.63E-49
ENSG00000124212	PTGIS	ENSMMUG00000021692	-7.84	1.23E-48
ENSG00000121769	FABP3	ENSMMUG00000064353	-5.63	2.03E-48
ENSG00000126107	HECTD3	ENSMMUG00000012993	-2.98	5.40E-48
ENSG00000120211	INSL4	ENSMMUG00000058221	-5.55	9.60E-48
ENSG00000116663	FBXO6	ENSMMUG00000023668	-4.30	1.75E-47
ENSG00000168785	TSPAN5	ENSMMUG00000011702	-3.70	2.15E-47
ENSG00000116191	RALGPS2	ENSMMUG00000017551	-3.93	2.67E-47
ENSG00000099960	SLC7A4	ENSMMUG00000063154	-5.54	1.63E-44
ENSG00000254535	PABPC4L	ENSMMUG00000007193	-5.39	2.72E-44
ENSG00000113578	FGF1	ENSMMUG00000057828	-4.61	3.60E-44
ENSG00000149294	NCAM1	ENSMMUG00000004688	-7.02	8.42E-43
ENSG00000163710	PCOLCE2	ENSMMUG00000012406	-4.96	1.67E-41
ENSG00000183196	CHST6	ENSMMUG00000001563	-6.11	2.38E-41
ENSG00000166578	IQCD	ENSMMUG00000001128	-5.28	3.23E-41
ENSG00000131171	SH3BGRL	ENSMMUG00000001689	-3.64	9.85E-41
ENSG00000006210	CX3CL1	ENSMMUG00000059578	-6.23	4.02E-39
ENSG00000167641	PPP1R14A	ENSMMUG00000028772	-4.66	4.47E-39
ENSG00000173567	ADGRF3	ENSMMUG00000004383	-3.98	2.32E-38
ENSG00000125089	SH3TC1	ENSMMUG00000030400	-4.58	2.86E-37
ENSG00000102575	ACP5	ENSMMUG00000002974	-4.13	8.53E-37
ENSG00000023330	ALAS1	ENSMMUG00000005596	-3.17	1.17E-36
ENSG00000123496	IL13RA2	ENSMMUG00000022224	-10.71	1.27E-36
ENSG00000041880	PARP3	ENSMMUG00000022203	-3.76	1.50E-36
ENSG00000141540	TTYH2	ENSMMUG00000003981	-3.93	3.00E-36
ENSG00000135919	SERPINE2	ENSMMUG00000006161	-6.30	2.18E-35
ENSG00000139405	RITA1	ENSMMUG00000056457	-2.91	7.72E-35
ENSG00000103034	NDRG4	ENSMMUG00000014618	-4.62	2.12E-34
ENSG00000065183	WDR3	ENSMMUG00000008513	-3.68	7.90E-32
ENSG00000125753	VASP	ENSMMUG00000022938	-2.89	1.90E-31
ENSG00000187957	DNER	ENSMMUG00000002103	-5.30	3.42E-31
ENSG00000149260	CAPN5	ENSMMUG00000018174	-4.07	4.05E-31
ENSG00000101844	ATG4A	ENSMMUG00000007190	-3.63	4.25E-31
ENSG00000140853	NLRC5	ENSMMUG00000000769	-4.30	5.60E-31

Table 2.4 Mean TPM of human bulk placenta (Top 50)

H.Gene.name	H.Gene.ID	Avg.TPM
RN7SL1	ENSG00000276168	174327.0
RN7SL2	ENSG00000274012	72330.3
AL162581.1	ENSG00000202198	34732.7
RN7SK	ENSG00000283293	34564.3
CSH1	ENSG00000136488	28774.5
AL627171.2	ENSG00000282885	22635.1
CSH2	ENSG00000213218	16903.2
RN7SL5P	ENSG00000265735	16567.3
RN7SL4P	ENSG00000263740	10175.5
RMRP	ENSG00000277027	9163.5
RMRP	ENSG00000269900	9136.7
RPPH1	ENSG00000277209	7826.6
RN7SKP71	ENSG00000201428	5207.4
MALAT1	ENSG00000251562	4995.8
RN7SKP80	ENSG00000202058	4892.6
H19	ENSG00000130600	4460.9
RNU4-2	ENSG00000202538	4434.5
MIR663B	ENSG00000221288	3840.4
TFPI2	ENSG00000105825	3803.8
FP236383.4	ENSG00000280614	3699.7
FP671120.6	ENSG00000280800	3691.9
FP236383.5	ENSG00000281181	3687.0
AL355075.4	ENSG00000259001	3571.3
RN7SL3	ENSG00000278771	3474.8
AD000090.1	ENSG00000283907	3330.6
RNU2-2P	ENSG00000222328	3067.3
KISS1	ENSG00000170498	2989.8
CGA	ENSG00000135346	2934.3
FP671120.7	ENSG00000281383	2727.8
MT-CO1	ENSG00000198804	2460.1
RN7SKP203	ENSG00000200488	2386.8
CYP19A1	ENSG00000137869	2357.0
PSG4	ENSG00000243137	2217.6
HBA2	ENSG00000188536	2128.7
PSG1	ENSG00000231924	2025.3
FBLN1	ENSG00000077942	2016.4
HBA1	ENSG00000206172	2000.0
ADAM12	ENSG00000148848	1974.7
SNORA73B	ENSG00000200087	1828.3
MT-ATP6	ENSG00000198899	1797.9
MT-ND4	ENSG00000198886	1688.7
RNU1-4	ENSG00000207389	1649.0
RNU1-28P	ENSG00000206588	1636.0
RNU1-1	ENSG00000206652	1630.0
RNU1-2	ENSG00000207005	1619.7
RNVU1-18	ENSG00000206737	1614.5
MT-CO3	ENSG00000198938	1610.2
U1	ENSG00000275405	1605.5
PAPPA	ENSG00000182752	1597.7
RNU1-3	ENSG00000207513	1593.8

Table 2.5 Mean TPM of rhesus bulk placenta (Top 50)

Rh.Gene.name	Rh.Gene.ID	Avg.TPM
GHV	ENSMMUG00000039847	116039.7
CSH2	ENSMMUG00000023707	44172.7
	ENSMMUG00000011358	41919.9
	ENSMMUG00000000578	41390.4
CSH4	ENSMMUG00000023706	32589.8
	ENSMMUG00000064479	21498.8
	ENSMMUG00000059128	21009.3
SERPINE2	ENSMMUG00000006161	20541.8
	ENSMMUG00000049459	20155.4
	ENSMMUG00000061777	18211.5
WFDC2	ENSMMUG00000002751	15085.1
	ENSMMUG00000028689	8368.3
IGF2	ENSMMUG00000047449	8152.9
	ENSMMUG00000039210	6822.0
INSL4	ENSMMUG00000058221	6172.5
	ENSMMUG00000056194	5102.4
	ENSMMUG00000028699	5014.2
	ENSMMUG00000061010	4736.5
FBLN1	ENSMMUG00000002424	4603.7
	ENSMMUG00000049833	4496.2
	ENSMMUG00000047533	3941.4
	ENSMMUG00000055813	3827.1
	ENSMMUG00000055687	3636.6
	ENSMMUG00000050799	3203.3
	ENSMMUG00000058532	3176.8
SLC43A3	ENSMMUG00000010601	2641.1
B2M	ENSMMUG00000060797	2639.3
mml-mir-675	ENSMMUG00000032643	2424.5
SAT1	ENSMMUG00000060580	2327.2
IGFBP1	ENSMMUG00000059330	2322.1
NOTUM	ENSMMUG00000049343	2145.3
TFPI2	ENSMMUG00000020581	2145.2
FN1	ENSMMUG00000012321	2080.6
	ENSMMUG00000054416	2041.0
	ENSMMUG00000054167	2040.7
	ENSMMUG00000062077	2002.3
TPT1	ENSMMUG00000022979	1989.3
EEF1A1	ENSMMUG00000004852	1911.4
	ENSMMUG00000061125	1877.2
DEFB1	ENSMMUG00000053229	1744.3
	ENSMMUG00000063316	1723.7
	ENSMMUG00000028701	1718.2
IL13RA2	ENSMMUG00000022224	1717.3
ISM2	ENSMMUG00000013555	1656.3
	ENSMMUG00000052127	1637.2
S100A6	ENSMMUG00000008917	1606.6
	ENSMMUG00000058325	1518.8
LEPR	ENSMMUG00000003265	1504.8
	ENSMMUG00000002320	1456.1
GDF15	ENSMMUG00000050122	1417.7

Table 2.6 Mean TPM of mouse bulk placenta (Top 50)

M.Gene.name	M.Gene.ID	Avg.TPM
Tpbpa	ENSMUSG00000033834	20515.2
Prl3b1	ENSMUSG00000038891	17450.7
Tpbpb	ENSMUSG00000062705	17094.2
H19	ENSMUSG00000000031	11119.2
Ctsj	ENSMUSG00000055298	9538.3
Hbb-bs	ENSMUSG00000052305	8280.7
Prl2c3	ENSMUSG00000056457	7461.7
mt-Atp8	ENSMUSG00000064356	6977.5
CT010467.1	ENSMUSG00000106106	6892.4
Hba-a1	ENSMUSG00000069919	6594.8
Prl8a9	ENSMUSG00000006490	6499.7
Gm27786	ENSMUSG00000098816	6424.5
mt-Co1	ENSMUSG00000064351	5945.6
Ctsq	ENSMUSG00000021439	5929.0
Eef1a1	ENSMUSG00000037742	5926.6
Prl2c2	ENSMUSG00000079092	4930.8
Gm29216	ENSMUSG00000101249	4791.1
Hba-a2	ENSMUSG00000069917	4754.4
Psg21	ENSMUSG00000070796	4701.5
Gm28661	ENSMUSG00000102070	4652.2
mt-Co2	ENSMUSG00000064354	4619.0
mt-Nd1	ENSMUSG00000064341	3963.1
Prl2b1	ENSMUSG00000069258	3944.4
Gm10925	ENSMUSG00000100862	3757.7
mt-Atp6	ENSMUSG00000064357	3754.4
Hsp90aa1	ENSMUSG00000021270	3659.4
mt-Cytb	ENSMUSG00000064370	3417.7
Cts3	ENSMUSG00000074870	3119.1
Calr	ENSMUSG00000003814	3116.3
Hsp90ab1	ENSMUSG00000023944	3069.0
Psg16	ENSMUSG00000066760	3061.8
Cts6	ENSMUSG00000021441	2797.3
Tfpi	ENSMUSG00000027082	2669.0
Creg1	ENSMUSG00000040713	2591.9
Ceacam11	ENSMUSG00000030368	2589.3
Prl2c5	ENSMUSG00000055360	2585.8
Cdkn1c	ENSMUSG00000037664	2537.7
Hspa8	ENSMUSG00000015656	2525.5
Prl7a1	ENSMUSG00000006488	2525.5
mt-Co3	ENSMUSG00000064358	2453.8
Gm28437	ENSMUSG00000101111	2452.8
Gm24270	ENSMUSG00000076281	2306.7
mt-Nd2	ENSMUSG00000064345	2305.5
Npm1	ENSMUSG00000057113	2289.6
Actg1	ENSMUSG00000062825	2262.7
Hsp90b1	ENSMUSG00000020048	2200.9
Psg23	ENSMUSG00000074359	2182.5
Peg10	ENSMUSG00000092035	2174.1
Hbb-bt	ENSMUSG00000073940	2119.7
Actb	ENSMUSG00000029580	1966.4

Table 2.7 human/mouse bulk placenta TPM DE analysis (Top 50)

H.Gene.ID	Gene.name	baseMean	log2FoldChange	padj
ENSG00000148848	ADAM12	1333.8	8.74	3.69E-100
ENSG00000138829	FBN2	256.6	7.16	1.09E-57
ENSG00000165124	SVEP1	353.5	7.54	1.09E-57
ENSG00000172493	AFF1	229.4	7.08	1.09E-57
ENSG00000166147	FBN1	150.2	5.72	9.40E-56
ENSG00000164292	RHOBTB3	397.4	8.80	3.33E-53
ENSG00000072778	ACADVL	309.1	3.64	1.45E-52
ENSG00000124491	F13A1	210.1	6.87	1.86E-51
ENSG00000167703	SLC43A2	230.1	4.45	4.13E-49
ENSG00000070031	SCT	429.2	-8.99	1.45E-48
ENSG00000263001	GTF2I	112.4	3.80	8.60E-48
ENSG00000105825	TFPI2	2604.4	7.82	3.86E-46
ENSG00000133316	WDR74	557.8	5.15	5.29E-46
ENSG00000012171	SEMA3B	426.1	6.94	4.26E-45
ENSG00000130382	MLLT1	169.6	3.72	5.49E-44
ENSG00000151014	NOCT	133.0	-4.42	6.06E-44
ENSG00000167434	CA4	310.5	-8.19	1.54E-41
ENSG00000132386	SERPINF1	120.2	6.47	2.03E-40
ENSG00000137203	TFAP2A	94.7	4.34	5.86E-40
ENSG00000119630	PGF	200.8	4.48	6.70E-40
ENSG00000173757	STAT5B	100.6	5.79	5.94E-39
ENSG00000067606	PRKCZ	162.0	3.26	6.76E-39
ENSG00000066827	ZFAT	80.9	4.65	7.79E-39
ENSG00000135048	CEMIP2	133.0	5.01	1.87E-38
ENSG00000153071	DAB2	370.0	4.36	4.19E-38
ENSG00000074181	NOTCH3	90.4	5.54	6.66E-38
ENSG00000145715	RASA1	174.7	2.80	1.43E-37
ENSG00000137869	CYP19A1	1594.3	14.23	1.51E-37
ENSG00000183955	KMT5A	133.4	-3.86	1.91E-37
ENSG00000119535	CSF3R	247.6	8.53	1.95E-37
ENSG00000135346	CGA	1988.0	14.55	2.35E-37
ENSG00000082438	COBLL1	255.5	3.24	5.16E-37
ENSG00000132470	ITGB4	86.1	3.91	1.55E-36
ENSG00000157557	ETS2	122.6	-3.30	7.93E-35
ENSG00000115461	IGFBP5	86.3	5.03	1.28E-34
ENSG00000143382	ADAMTSL4	136.4	5.94	1.45E-34
ENSG00000135111	TBX3	93.9	4.11	2.18E-34
ENSG00000206538	VGLL3	196.0	4.05	4.27E-34
ENSG00000065882	TBC1D1	76.5	4.11	5.89E-34
ENSG00000123243	ITIH5	84.3	3.81	9.36E-34
ENSG00000148926	ADM	179.1	3.34	2.74E-33
ENSG00000049249	TNFRSF9	185.7	-8.46	2.85E-33
ENSG00000108821	COL1A1	613.1	3.87	3.54E-33
ENSG00000107175	CREB3	103.8	-3.82	3.58E-33
ENSG00000182752	PAPPA	1082.6	13.67	1.14E-32
ENSG00000019582	CD74	117.0	5.57	1.56E-32
ENSG00000141736	ERBB2	88.5	6.15	2.35E-32
ENSG00000170458	CD14	80.4	5.90	5.41E-32
ENSG00000054654	SYNE2	94.4	3.06	5.43E-32
ENSG00000188994	ZNF292	61.2	4.59	5.43E-32

Table 2.8 human/rhesus bulk placenta TPM DE analysis (Top 50)

H.Gene.ID	Gene.name	baseMean	log2FoldChange	padj
ENSG00000114251	WNT5A	335.4	-6.02	7.05E-113
ENSG00000134802	SLC43A3	1170.5	-9.06	2.70E-107
ENSG00000163710	PCOLCE2	309.5	-4.77	4.60E-104
ENSG00000116678	LEPR	667.9	-8.89	8.81E-101
ENSG00000148848	ADAM12	1117.2	6.62	8.81E-101
ENSG00000145287	PLAC8	190.6	-5.18	3.20E-99
ENSG00000167552	TUBA1A	230.1	-2.99	7.02E-91
ENSG00000167641	PPP1R14A	223.3	-4.15	4.45E-89
ENSG00000099960	SLC7A4	564.5	-6.73	2.52E-87
ENSG00000023330	ALAS1	155.6	-3.56	3.85E-86
ENSG00000167703	SLC43A2	194.8	3.90	8.78E-82
ENSG00000111341	MGP	166.9	-3.54	2.86E-78
ENSG00000011007	ELOA	100.3	-4.40	1.29E-76
ENSG00000213366	GSTM2	118.2	-4.75	1.08E-74
ENSG00000138829	FBN2	218.7	4.77	2.97E-74
ENSG00000125868	DSTN	184.5	-2.87	3.35E-71
ENSG00000136160	EDNRB	145.1	-3.12	9.56E-70
ENSG00000152952	PLOD2	100.1	-3.36	3.46E-69
ENSG00000011052	NME1-NME2	96.8	-4.20	6.42E-67
ENSG00000117245	KIF17	154.7	-6.86	1.45E-66
ENSG00000119630	PGF	167.6	4.43	3.73E-65
ENSG00000112715	VEGFA	104.3	-5.31	1.33E-64
ENSG00000102760	RGCC	242.8	-2.37	3.79E-64
ENSG00000137869	CYP19A1	1359.1	5.06	7.61E-64
ENSG00000130164	LDLR	119.6	-3.28	8.21E-64
ENSG00000133316	WDR74	461.5	5.72	1.73E-63
ENSG00000100345	MYH9	316.3	2.31	1.57E-61
ENSG00000158201	ABHD3	87.7	-4.14	2.38E-59
ENSG00000119632	IFI27L2	127.3	-6.58	3.24E-59
ENSG00000151150	ANK3	121.8	4.60	7.19E-59
ENSG00000065717	TLE2	118.5	-3.30	2.88E-58
ENSG00000127241	MASP1	145.4	-6.87	6.09E-58
ENSG00000186480	INSIG1	221.4	-3.01	2.29E-57
ENSG00000197111	PCBP2	120.7	2.81	2.65E-56
ENSG00000140285	FGF7	81.4	-5.04	3.70E-56
ENSG00000242265	PEG10	316.8	4.09	6.16E-56
ENSG00000264364	DYNLL2	73.3	-3.39	7.98E-56
ENSG00000004399	PLXND1	121.5	3.11	2.79E-55
ENSG00000270800	RPS10-NUDT3	215.7	-4.02	9.63E-55
ENSG00000174021	GNG5	87.2	-3.06	1.01E-54
ENSG00000136888	ATP6V1G1	92.7	-2.78	1.20E-53
ENSG00000165124	SVEP1	306.8	4.12	2.54E-53
ENSG00000135919	SERPINE2	9231.6	-6.75	4.86E-53
ENSG00000099953	MMP11	189.6	3.86	6.68E-53
ENSG00000101443	WFDC2	6710.9	-15.76	8.92E-53
ENSG00000125753	VASP	152.1	-2.37	1.05E-52
ENSG00000178104	PDE4DIP	93.2	3.63	3.44E-52
ENSG00000137270	GCM1	138.1	-2.61	4.28E-52
ENSG00000148110	MFSD14B	79.2	-2.97	6.05E-51
ENSG00000135862	LAMC1	195.6	2.15	9.14E-51

Table 2.9 male/female human bulk placenta DE analysis (All DEGs)

H.Gene.name	H.GeneID	baseMean	log2FoldChange	padj
KDM5D	ENSG00000012817	363.82	9.38	1.60E-42
DDX3Y	ENSG00000067048	1073.31	8.34	3.10E-15
ZFY	ENSG00000067646	557.02	8.88	1.71E-55
EPYC	ENSG00000083782	23.62	-4.61	2.79E-02
USP9Y	ENSG00000114374	844.57	8.33	5.50E-50
RPS4Y1	ENSG00000129824	307.93	8.88	2.14E-45
NLGN4Y	ENSG00000165246	41.88	8.67	7.21E-13
UTY	ENSG00000183878	748.32	8.35	1.53E-106
SRY	ENSG00000184895	4.29	5.39	3.72E-02
CCK	ENSG00000187094	440.44	2.15	1.40E-02
EIF1AY	ENSG00000198692	81.71	7.55	1.55E-19

Table 2.10 iRP-D26/RPT DE analysis (Top 50)

Rh.Gene.name	Rh.GeneID	baseMean	log2FoldChange	padj
ERVFRD-1	ENSMMUG00000043161	4533.9	-7.18	0.00E+00
SH3BGRL2	ENSMMUG00000062749	7348.3	-5.76	0.00E+00
PEG3	ENSMMUG00000055669	39724.0	-9.13	0.00E+00
LAMB3	ENSMMUG00000016925	5388.9	6.53	0.00E+00
MMP1	ENSMMUG00000002037	22181.0	10.03	0.00E+00
SIAH1	ENSMMUG00000007400	8820.2	-4.68	0.00E+00
SDC2	ENSMMUG00000000963	4523.8	6.63	0.00E+00
HTRA1	ENSMMUG00000056637	32953.6	4.86	0.00E+00
FRMD6	ENSMMUG00000018274	6474.6	-4.91	0.00E+00
LUM	ENSMMUG00000016995	6710.0	7.08	0.00E+00
SEMA6D	ENSMMUG00000012144	4385.0	-7.69	0.00E+00
MPP1	ENSMMUG00000005772	4056.6	-5.88	0.00E+00
LEPR	ENSMMUG00000003265	5461.9	-8.11	0.00E+00
FN1	ENSMMUG00000012321	802152.0	3.79	0.00E+00
SPOCK2	ENSMMUG00000002122	4280.6	-6.66	0.00E+00
CRISPLD2	ENSMMUG00000011245	10657.9	4.28	0.00E+00
PAGE4	ENSMMUG00000003082	8482.7	-7.19	0.00E+00
LAMB1	ENSMMUG00000006567	10315.6	-6.52	0.00E+00
MBNL3	ENSMMUG00000003071	26070.9	-4.48	0.00E+00
NFE2L3	ENSMMUG00000003615	20434.8	-7.14	0.00E+00
PCDH7	ENSMMUG00000011898	3952.7	6.73	3.44E-294
CLDN1	ENSMMUG00000001915	3294.1	-6.60	1.31E-281
DAB2	ENSMMUG00000019879	3282.9	-4.99	1.35E-270
JUN	ENSMMUG00000059326	9171.3	-4.11	7.80E-266
GREB1L	ENSMMUG00000003974	5421.3	4.12	4.26E-263
FDX1	ENSMMUG00000060188	5959.4	-4.61	2.75E-257
SLC2A3	ENSMMUG00000046124	35819.2	4.58	4.35E-257
KCTD12	ENSMMUG00000060210	3199.9	-6.40	3.78E-251
MPP7	ENSMMUG00000020663	4516.7	-5.84	2.00E-247
SLC12A2	ENSMMUG00000011214	2704.3	5.08	2.35E-247
FOSB	ENSMMUG00000014430	3001.7	-7.08	1.55E-244
CDO1	ENSMMUG00000061758	2371.8	-6.71	2.06E-240
SLC13A4	ENSMMUG00000016386	3548.7	-8.30	5.02E-235
PECAM1	ENSMMUG00000011809	7464.1	-3.65	1.59E-234
REPS2	ENSMMUG00000010598	2756.6	4.39	9.40E-234
PATJ	ENSMMUG00000003113	2096.3	5.81	1.57E-231
	ENSMMUG00000011582	2410.5	-7.12	8.94E-231
FREM2	ENSMMUG00000002702	2166.6	5.72	4.67E-229
COL17A1	ENSMMUG00000015325	7802.3	3.61	1.53E-228
LAMA3	ENSMMUG00000004321	2275.0	5.28	1.73E-226
	ENSMMUG00000051498	1917.2	5.20	6.99E-226
TBC1D9	ENSMMUG00000015246	2854.1	-7.89	4.35E-224
OXGR1	ENSMMUG00000064141	3353.1	8.49	4.46E-224
LAPTM4B	ENSMMUG00000008926	12586.1	3.52	1.15E-223
COL8A1	ENSMMUG00000002935	3227.6	-8.10	1.91E-222
INTS6L	ENSMMUG00000017881	2774.8	-4.33	7.93E-215
ITGB8	ENSMMUG00000006898	1963.6	-5.18	5.00E-209
LOXL2	ENSMMUG00000050549	3756.1	6.54	1.48E-207
NOTUM	ENSMMUG00000049343	8495.5	-5.70	1.75E-204
SLC25A29	ENSMMUG00000009738	1734.2	-5.44	2.35E-201

Table 2.11 iRP-D28A/RPT DE analysis (Top 50)

Rh.Gene.name	Rh.GeneID	baseMean	log2FoldChange	padj
MBNL3	ENSMMUG00000003071	23563.1	-9.66	0.00E+00
NFE2L3	ENSMMUG00000003615	19230.9	-7.65	7.10E-242
SLC1A4	ENSMMUG00000010279	7448.2	6.01	4.17E-189
LAMB3	ENSMMUG00000016925	9154.1	7.39	1.19E-175
GCM1	ENSMMUG00000022083	8282.2	-10.36	1.18E-168
SPOCK2	ENSMMUG00000002122	4038.5	-6.61	2.24E-163
PCDH7	ENSMMUG00000011898	5805.4	7.37	1.61E-161
	ENSMMUG00000063583	6514.0	-9.77	1.09E-160
INHA	ENSMMUG00000007483	12412.8	8.30	4.74E-160
ISM2	ENSMMUG00000013555	8920.4	-9.75	1.18E-159
CGA	ENSMMUG00000000222	9077.4	-9.66	1.43E-146
FOSB	ENSMMUG00000014430	2825.1	-7.54	1.00E-144
SLC27A6	ENSMMUG00000017031	4744.7	7.67	6.55E-143
PDK4	ENSMMUG00000021389	3025.3	-7.09	1.62E-138
NOTUM	ENSMMUG00000049343	7866.6	-10.72	2.15E-138
SEMA5A	ENSMMUG00000020160	2176.5	6.63	1.89E-134
COL12A1	ENSMMUG00000019261	15009.8	5.61	7.72E-133
FRMD6	ENSMMUG00000018274	6041.0	-5.50	7.06E-131
CPE	ENSMMUG00000023400	12024.1	5.33	2.50E-126
LAMA3	ENSMMUG00000004321	5747.3	6.72	1.99E-123
PTPRD	ENSMMUG00000006952	1989.9	7.98	4.06E-123
SLC26A2	ENSMMUG00000029776	10845.5	-5.16	1.81E-122
	ENSMMUG00000011582	2274.5	-7.01	1.05E-120
CDKN1C	ENSMMUG00000037980	6484.0	-10.62	9.64E-119
UPK1B	ENSMMUG00000057343	4522.4	4.70	2.98E-116
EFEMP1	ENSMMUG00000016872	30181.7	-4.89	1.87E-111
MYO10	ENSMMUG00000012672	2845.0	-5.51	5.33E-109
SYT16	ENSMMUG00000042895	1517.0	6.85	7.30E-108
	ENSMMUG00000045497	1478.4	-6.00	8.59E-108
PAGE4	ENSMMUG00000003082	7954.9	-9.80	1.19E-106
LOXL2	ENSMMUG00000050549	5070.7	7.06	1.19E-106
LEPR	ENSMMUG00000003265	5139.0	-9.62	6.27E-103
PIK3CD	ENSMMUG00000006224	6817.3	4.12	2.32E-99
TCP11L1	ENSMMUG00000002539	3005.3	4.48	3.54E-99
MPEG1	ENSMMUG00000045775	1689.3	-8.00	4.26E-98
EPB41L3	ENSMMUG00000019418	4319.1	-4.80	6.97E-97
HTRA1	ENSMMUG00000056637	17271.7	3.98	8.15E-96
ABTB2	ENSMMUG00000058619	1682.9	-5.01	1.92E-95
VIT	ENSMMUG00000001278	10075.0	7.26	8.91E-93
CPM	ENSMMUG00000000946	1195.3	-6.71	2.51E-92
SERPINF1	ENSMMUG00000022194	4514.8	-5.43	2.52E-92
CACNA2D3	ENSMMUG00000047365	2055.1	7.13	6.11E-92
	ENSMMUG00000051498	1686.5	5.09	1.02E-91
ATP6V0A4	ENSMMUG00000006547	1386.4	-7.39	2.34E-91
CDC42EP4	ENSMMUG00000018148	1200.2	-7.04	5.38E-91
PATJ	ENSMMUG00000003113	3077.3	6.46	2.81E-89
SVEP1	ENSMMUG00000047960	2022.3	-8.31	3.10E-88
MMP2	ENSMMUG00000004475	1256.6	-5.75	4.91E-88
TRABD2A	ENSMMUG00000008855	3843.5	6.61	1.30E-87
IL4R	ENSMMUG00000004666	1230.2	-7.60	1.70E-87

Table 2.12 iRP cell culture passage details

	iRP-D26	iRP-D28A	iRP-D28B	iRP-D50	iRP-D141	iRP-D149	iRFb-XX	iRFb-XY
Phase contrast	p.14	p.15	p.11	p.8	p.8	p.9	NA	NA
TERT & PAC RT-PCR	p.16	p.17	p.13	p.11	p.11	p.12	p.8	p.8
IF staining	p.16	p.17	p.13	p.11	p.11	p.12	p.8	p.8
qRT-PCR	p.16	p.17	p.13	p.11	p.11	p.12	p.8	p.8
mCG secretion assay	p.16	p.17	NA	NA	NA	NA	NA	NA
single-cell DNA-seq	p.17	p.18	p.14	p.12	p.12	p.13	p.9	p.9
Metaphase spreads	p.19	p.20	p.16	p.14	p.14	p.15	NA	NA
RNA-seq	p.25	p.26	NA	NA	NA	NA	NA	NA
qRT-PCR (DMSO/Forskolin)	p.25	p.26	p.19	NA	NA	NA	NA	NA
IGF2 secretion assay	p.30	p.31	p.23	NA	NA	NA	p.12	p.12
Matrigel invasion assay	p.31	p.32	NA	NA	NA	NA	NA	NA

Table 2.13 Primers

Gene.name	Species	Forward_primer_seq	Reverse_primer_seq
BMP1	H & Rh	AGTCCCTGGGGGAGACCTAT	CCGTTCACCTCATACTTGGG
CDH1	H & Rh	GCCGAGAGCTACACGTTCAC	GCTGTCCTTTGTCGACCG
EGFR	H & Rh	GAGGTGGTCCTTGGGAATTT	TGAGGACATAACCAGCCACC
ENPEP	H & Rh	AGCACACAGCCGAATATGCT	TGCCAAAATCTGGAATAGCG
ERVFRD-1	H & Rh	TGGAGCAGTTGCTGAGCTTT	GCAGCTCGTTTTGTGACCAG
ERVV-1	H & Rh	TCGAGACAAGTCACCCCAAA	GTGTGCCTTGGGAAGCAAATA
ERVV-2	H & Rh	TTCCACTCCAGGTTTCGCTT	TCCCTCCTTAGAGGTGCTTT
ERVW-1	H & Rh	AGCAGAGGAGCTTCGAAACA	AGAGGTCCTAAGAAGGGGAGAA
GAPDH	H & Rh	GGAAGGTGAAGGTCGGAGTC	GTTGAGGTCAATGAAGGGGTC
GCM1	H & Rh	GCCTCTGAAGCTCATCCCTT	GGATGATCATGCTCTCCCTTT
GULP1	H & Rh	TGATGGCAACTGTATGATAGAAGC	TCATGATGAGGATCAGCCAA
HPRT1	H & Rh	GCTGAGGATTTGGAAAGGGT	CATCTCGAGCAAGACGTTCA
TERT	H	CCAAGAACGCAGGGATGTCG	AGGGCAGTCAGCGTCGTC
IGF2	H & Rh	GGACACCCTCCAGTTCGTCT	CGGAAACAGCACTCCTCAAC
KRT7	H & Rh	GGATGCCCTGAATGATGAGA	CACCACAGATGTGTCGGAGA
LEPR	H & Rh	AACCTTCAATTCCAGATTCGC	TCTGGAACTGGGAGACTGACA
LIFR	H & Rh	TGCGAGCCTATACAGATGGTG	CACTCCAACAATGACAGCCA
LIPF	H & Rh	CTATGTTGGCCATTCCCAGG	CACAGTGGCAACAGGAGCTA
LVRN	H & Rh	TCATCCAAGTTATGTGGCCC	TTGCTTCCATTCACATCTTCTTT
CGA	H & Rh	CCGGGTGCCCCAATATATCA	AGCTACACAGCAAGTGGACTC
MMP2	H & Rh	AGTACGGCTTCTGTCCCCAT	CATAGGATGTGCCCTGGAAG
NCAM1	H & Rh	GGATGGCAGTGAGTCAGAGG	ACATCACACACAATCACGGC
NGF	H & Rh	CACAGGGAATGTGGTGAGGT	GAGCTGAGCTTGGGTCCAG
NOS3	H & Rh	AGGTGGGGAGCATCACCTAT	TGTAGGTGAACATTTCCTGTGC
PAPPA	H & Rh	TGGCAGGAGTAGCAACTTGG	ACAGTGCATTCTGGCGACTT
PAPPA2	H & Rh	GACAGAACAACCCAGCCATC	CTTTCCCTTGTCCTTCCCTG
PGF	H & Rh	CTTGCTTCCTGCAGCTCCT	CTTCCACCTCTGACGAGCC
PTPRC	H & Rh	CACTCGGGCTTTTGGAGAT	ACCTCTCTTCCAGTTGCTTTTTC
PAC	NA	TGACCGAGTACAAGCCCAC	ACACCTTGCCGATGTCGAG
SDC1	H & Rh	GCCAAGCTGACCTTCACACT	TCCCCAGAGGTTTCAAAGGTG
SP1	H & Rh	AGGCCTCCAGACCATTAACC	GACCAAGCTGAGCTCCATGA
TBP	H & Rh	AACAACAGCCTGCCACCTTA	GCCATAAGGCATCATTGGAC
TP63	H & Rh	GACGTGTCCTTCCAGCAGTC	GGGTCATCACCTTGATCTGG
VIM	H & Rh	TCTGGATTCACTCCCTCTGG	TCAAGGTCATCGTGATGCTG

2.8 Availability of data and materials

All RNA-seq and DNA-seq raw sequencing data generated in this study have been submitted to the NCBI Sequencing Read Archive (SRA; https://www.ncbi.nlm.nih.gov/sra/) under BioProject accession number PRJNA649979. Additional publicly available RNA-seq data from human, rhesus, and mouse were downloaded from NCBI SRA using SRA Toolkit (http://ncbi.github.io/sra-tools/): human placenta (DE#2): SRR3096525, SRR3096545, SRR3096594, SRR3096612, SRR3096624, SRR3096625 [259]; human placenta (DE#3): SRR4370049, SRR4370050 [260]; HPT: SRR2397323, SRR2397324, SRR2397332, SRR2397333, SRR2397341, SRR2397342, SRR6443608, SRR6443609, SRR6443611, SRR6443612 [288,289]; human PBMC: SRR3389246, SRR3390437, SRR3390461, SRR3390473 [286]; human BeWo: SRR6443610, SRR6443613, SRR6443614, SRR6443615, SRR6443616, SRR9118949, SRR9118950 [289,290]; rhesus placenta: SRR5058999, SRR5059000, SRR7659021, SRR7659022 [258]; rhesus PBMC: SRR2467156, SRR2467157, SRR2467159, SRR2467160 [287]; mouse placenta: SRR649373, SRR649374, SRR943344, SRR943345 [331] (**Table 2.1**).

2.9 Authors' contributions

J.L.R, S.L.C. and L.C. designed research; J.L.R, J.G. and V.R performed research; J.L.R. analyzed data; S.L.C. and L.C. supervised progress of all research; and J.L.R, S.L.C. and L.C. wrote the paper. All authors were involved in manuscript editing.

2.10 Acknowledgements

We thank L. Myatt for help obtaining placental samples; J. Hennebold and A. Clark for access to rhesus first trimester placental samples; A. Frias for use of tissue culture facilities and access to rhesus third trimester primary trophoblast cells; A. Adey and A. Fields for the assistance and use of NextSeq500 sequencer; J. Hennebold and M. Murphy for use of tissue culture and microscope

facilities; S. Stadler, A. Adey, J. Sacha, M. Okhovat, and B. Davis for insight and advice; The Molecular Technologies Core and The Endocrine Technologies Core (ETC) at the ONPRC (supported by NIH P51 OD011092).

2.11 Authors' information

[1]Department of Molecular and Medical Genetics, Oregon Health and Science University, Portland, OR 97239; [2]Division of Reproductive and Developmental Sciences, Oregon National Primate Research Center, Beaverton, OR 97006; [3]Division of Genetics, Oregon National Primate Research Center, Beaverton, OR 97006; [4]Department of Medicine, Knight Cardiovascular Institute, Oregon Health and Science University, Portland, OR 97239; [5]Department of Medical Informatics and Clinical Epidemiology, Oregon Health and Science University, Portland, OR 97239; [6]Department of Obstetrics and Gynecology, Oregon Health and Science University School of Medicine, Portland, OR 97239; [7]Department of Biomedical Engineering, Oregon Health and Science University School of Medicine, Portland, OR 97239.

CHAPTER 3: Investigation of Human Endogenous Retrovirus-K (ERVK) Expression and Function in Placentation

Jimi L. Rosenkrantz[1,2], Michael Martinez[1], Adithi Mahankali, Lucia Carbone[1,3-5*] and Shawn L. Chavez[1,2,6,7*]

[1]Department of Molecular and Medical Genetics, Oregon Health and Science University, Portland, OR 97239; [2]Division of Reproductive and Developmental Sciences, Oregon National Primate Research Center, Beaverton, OR 97006; [3]Division of Genetics, Oregon National Primate Research Center, Beaverton, OR 97006; [4]Department of Medicine, Knight Cardiovascular Institute, Oregon Health and Science University, Portland, OR 97239; [5]Department of Medical Informatics and Clinical Epidemiology, Oregon Health and Science University, Portland, OR 97239; [6]Department of Obstetrics and Gynecology, Oregon Health and Science University School of Medicine, Portland, OR 97239; [7]Department of Biomedical Engineering, Oregon Health and Science University School of Medicine, Portland, OR 97239

3.1 Abstract

Background: There is a growing body of evidence indicating the importance of endogenous retrovirus (ERV) derived proteins during early development and reproduction in mammals. Recently, a protein derived from the youngest ERV in primates, ERVK (HML2), was shown to be expressed during human placentation. Since a number of highly similar ERVK proviral loci exist across the human genome, locus-specific analysis of ERVK transcription and identification of the coding sequence expressed in the human placenta is difficult. Thus, despite its activity in early human development, the native expression and function of ERVK in the human placenta remains largely uncharacterized.

Results: In this study, we comprehensively examined locus-specific ERVK transcription across several different human placental tissues and cell types. Through a combination of RNA-seq and siRNA knock-down analyses, we identified the expression of a single ERVK locus, ERVK11q23.3, as (1) being significantly upregulated in preterm placenta, (2) predominantly expressed by mononuclear trophoblasts, (3) capable of encoding a truncated viral-like envelope protein, and (4) contributing to the expression cytokines involved in both antiviral and anti-inflammatory innate immune responses in HPTs and BeWo cells, respectively.

Conclusions: Collectively, the results of this study: highlight the utility of studying locus-specific ERVK expression, provide a thorough characterization of locus-specific ERVK transcription from human placental tissues, and indicate that altered expression of placental ERVK11q23.3 influences IFN antiviral response, which may contribute to preterm birth and other pregnancy complications.

3.2 Background

Mammalian genomes are littered with thousands of copies of endogenous retroviruses (ERVs), mobile genetic elements that are relics of ancient retroviral infections. ERVs are abundant within the DNA of all vertebrates and specifically comprise ~8% of the human genome [332]. Despite being considered 'junk DNA' for many years, there has been a growing interest in the biological role of ERV-derived proteins in human early development and reproduction, including placentation. ERV proviral insertions within the human genome are classified into different groups based on sequence similarity [333]. Full-length ERV insertions possess similar genomic organization to exogenous retroviruses, including two flanking long terminal repeats (LTRs), an internal sequence corresponding to group-specific antigen (*gag)*, protease (*pro*), polymerase (*pol)*, and envelope (*env)* proviral genes (**Figure** 1.3). The vast majority of ERVs within the genome are truncated and/or have become highly mutated and thus, are unable to produce functional viral proteins and are non-infectious [334]. However, a few ERV insertions have remained relatively well-conserved, and contain open reading frames (ORFs) that can encode viral-like proteins. Several ERV viral-like proteins expressed during development are known to play important physiological roles. The most notable examples of this are the Syncytin proteins, which are expressed during human placentation. Syncytin-1 [335] and Syncytin-2 [195] are encoded from *env* genes of ERVW and ERVFRD groups, respectively. Similar to exogenous retroviral envelope proteins, Syncytin proteins contain fusion peptide (FP) and/or immunosuppression (ISU) domains. Exogenous retroviruses utilize the FP and ISU domain to facilitate fusion of the viral particle into the host cell and suppression of the host immune response, respectively [246,247]. However, unlike exogenous retroviruses, the Syncytin proteins, containing these domains, have been co-opted to facilitate important processes underlying normal human placentation. Specifically, Syncytin FPs are utilized by mononuclear cytotrophoblasts (CTBs) to facilitate the cell fusion underlying the formation and maintenance of the multinucleated syncytiotrophoblast (STB) layer [194-196,336],

and there is evidence suggesting that the ISU domain of Syncytin-2 aids maternal immune evasion during pregnancy [217].

Similar to Syncytins, ERVK envelope (ERVK-env) protein has been shown to be expressed during human placentation. This protein is derived from the ERVK (HML-2) group, the youngest and most recently expanded ERV in primate genomes [239-242]. Thus, unlike the ERV families encoding the Syncytin proteins, dozens of ERVK proviral insertions with intact envelope ORFs exist across the human genome. While there are no replication-competent ERVK proviral insertions, the presence of polymorphic ERVK insertions in human indicates that the family was active and infectious up until at least 5-6 million years ago [337,338]. A consequence of this recent activity is that many ERVK loci are highly-similar, which makes it difficult to analyze locus-specific ERVK expression using traditional short-read RNA-seq data. Due to these challenges, a thorough characterization ERVK placental expression, including locus-specific transcription, splicing, and putative protein-coding sequences has been lacking.

Several studies using ERVK ancestral-predicted consensus sequences, have identified a functional FP [248-250] and ISU domain [251] within the ERVK-env protein, and its ability to elicit cell fusion when ectopically expressed in cell lines or incorporated into viral particles [248-250], as well as inhibit immune cell proliferation *in vitro* [251]. These reports suggest that placental ERVK expression, and specifically ERVK-env protein expression, may facilitate trophoblast cell fusion and/or maternal immunosuppression during normal placentation. However, since it is unclear which ERVK loci are expressed in the placenta, whether ERVK-env is fusogenic and/or immunosuppressive at this site remains unknown. Here, we hypothesize that ERVK expression, and specifically ERVK-env protein, has been co-opted to facilitate trophoblast cell fusion and/or maternal immunosuppression during normal placentation. Additionally, since trophoblast dysfunction and heightened inflammation are associated with pregnancy complications [339,340], we further postulate that abnormal ERVK expression is associated with placental dysfunction in preterm birth. Thus, to test these hypotheses, we aimed to (1) thoroughly characterize placental

ERVK expression, including locus-specific transcription levels and ERVK-env protein-coding potential, (2) identify ERVK loci differentially expressed between placenta from healthy and pathological pregnancies, and (3) assess the fusogenic and/or immunomodulatory function of placentally-expressed ERVK.

3.3 Results

3.3.1 ERVK-env protein is expressed in the STB layer of term placenta, but its expression varies across preterm placentas.

ERVK-env protein expression has previously been documented in human placental tissues from healthy pregnancies [10]. Since functional FP and ISU domains were identified within the ancestral-predicted ERVK-env protein and trophoblast dysfunction and heightened inflammation are commonly associated with preeclampsia and preterm birth [339,340], aberrant placental ERVK-env protein expression may be associated with these pregnancy complications. Thus, we sought to compare placental ERVK-env protein expression and localization between normal and pathological pregnancy conditions. For this, we preformed immunohistochemical (IHC) staining on human placental tissue collected from term (n=4) and preterm (n=4) pregnancies using a well-established commercially available anti-ERVK-env monoclonal antibody [10] (**Table 3.1**). In term placenta samples, ERVK-env staining was observed at the maternal-fetal interface in multinucleated STBs. The staining pattern was diffuse throughout the cytoplasm and microvilli of the STB (**Figure** 3.1**A**), similar to the known STB secreted proteins, CGB and KISS1 [262]. In preterm placental tissue, a similar expression pattern was observed, however variable staining intensities were noted across the four different samples examined (**Figure** 3.1**A**). The absence of non-specific staining was confirmed by substituting the anti-ERVK-env antibody with an appropriate mouse igG2A isotype control (**Figure** 3.1**B**). Collectively, these results show that ERVK-env protein is expressed by placental trophoblasts, and suggest that the expression level may be affected in placenta from preterm birth pregnancies.

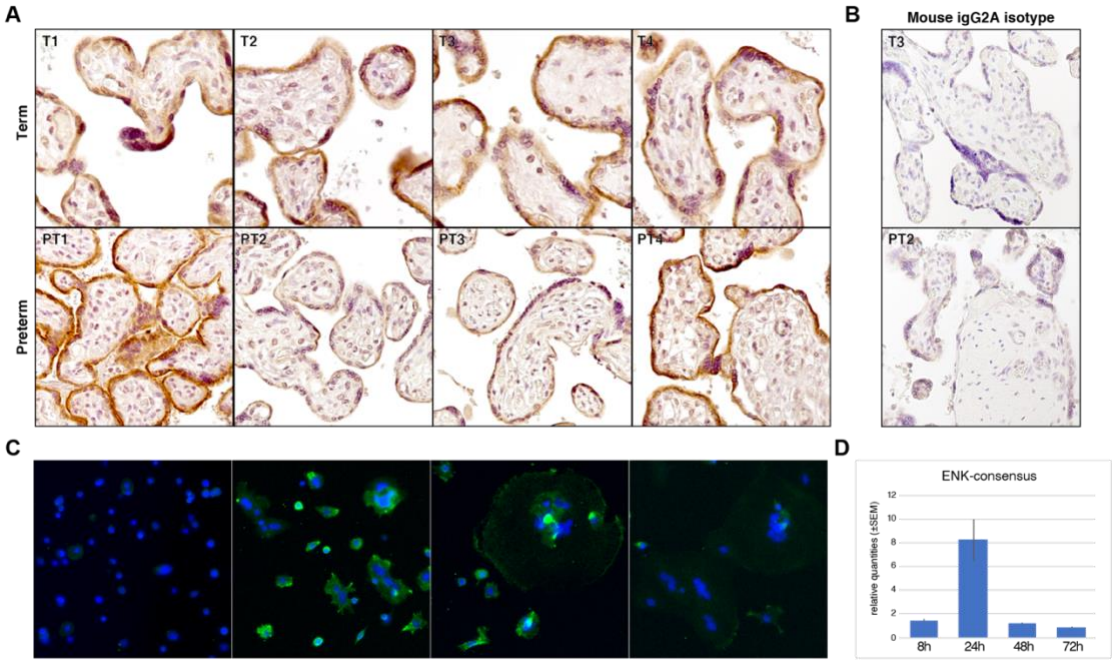

Figure 3.1 placental ERVK-env protein expression

(A) IHC staining of human term (n=4) and preterm (n=4) placental tissue sections for ERVK-env TM protein and (B) mouse igG2A isotype negative control. Positive staining (DAB, brown), nuclear counterstain (purple). (C) ERVK-env IF staining of HPTs at 8, 24, 48, 72 h (left to right); ERVK-env (green) and DAPI nuclear counterstain (blue). (D) qRT-PCR of HPTs at 8, 24, 48, 72 h (n=3 each); four technical replicates were used per sample and samples were normalized to GAPDH.

3.3.2 ERVK-env protein is predominantly expressed in unfused mononuclear CTBs in vitro.

Mononuclear CTB cell fusion is critical for the formation and maintenance of the multinucleated STB layer in the placenta [24,25]. Similar to the Syncytin proteins, the ERVK-env protein is speculated to play a role in CTB fusion and STB formation. This is largely based on the fusogenic capabilities of ancestral-predicted recombinant ERVK-env proteins [248-250], and the report that native ERVK-env protein is expressed at the cell surface of villous CTBs in the human placenta [10], which is the expected localization of a protein involved in CTB cell-cell fusion [341]. To further evaluate native ERVK-env expression and localization throughout CTB differentiation and fusion, we utilized human primary trophoblast (HPT) cell cultures, which consist highly purified CTBs that spontaneously differentiate and fuse into STBs over time [24,25]. Thus, we examined ERVK-env protein and mRNA expression in HPTs after 8, 24, 48, and 72 h in culture (**Figure** 3.1**C**-**D**). ERVK-env protein expression and localization was assessed via immunofluorescence (IF) using a well-established monoclonal antibody targeting the TM envelope protein of ERVK (anti-ENK); while, ERVK-env RNA expression was assessed via qRT-PCR using primers designed based on the ancestral-predicted ERVK-env sequence (ENK-consensus) [342]. Consistent with previous reports [10], the IF results showed that ERVK-env protein expression appeared most prominent around the membrane of mononuclear CTBs 24 h after culturing (**Figure 3.1C**). Cytoplasmic staining of multinucleated STBs was also observed in HPT cultures, supporting the results from our IHC analysis of bulk placental tissues (**Figure 3.1A,C**). The qRT-PCR results further demonstrated that the highest ERVK-env transcription levels were detected at 24 h of culture (**Figure 3.1D**). Collectively, these data indicate that ERVK-env expression peaks after 24 h in culture and that its protein is predominantly located at the plasma membrane of unfused mononuclear CTBs, which is consistent with ERVK11q23.3 being involved in trophoblast fusion.

3.3.3 Multiple ERVK loci with intact envelope ORFs are transcribed in term and preterm placental samples

A number of ERVK proviral loci exist across the human genome [218], and the transcriptional activity of each locus is dependent on the tissue/cell type [343]. To identify which specific ERVK proviral loci are expressed in the placenta, we performed locus-specific ERVK transcriptional analysis using RNA-seq data from term (n=5) and preterm (n=5) bulk placental samples (**Table 3.2**). Since a number of highly similar ERVK loci exist across the human genome, several regions across ERVK loci are non-unique and have low mappability. In order to avoid false positive ERVK locus expression, non-uniquely mapping RNA-seq reads were discarded for this analysis. Approximately 49% (61/124) of the ERVK loci (**Table 3.3**) were expressed (mean normalized read count >1) in the placental tissue examined (**Figure** 3.2). A number of the placentally expressed ERVK loci were predicted to contain envelope ORFs possessing the monoclonal antibody epitope [10]. This includes ERVK loci with a predicted full-length envelope ORFs (>588aa) (ERVK6q25.1, ERVK1q21.3a, ERVK6p21.1, ERVK1q22, ERVK1p31.1a, ERVK1p34.3) [218]; and loci with partial envelope ORFs (>300aa) (ERVK3q21.2b, ERVK1q21.3b, ERVK1q23.3, ERVK4q35.2, ERVK5q33.2, ERVKXq28b) [218]. Thus, the immunostaining results in **Figure** 3.1 likely reflect envelope protein expression from one or more of these ERVK loci. Several other ERVK loci containing partial envelope ORFs with a Furin cleavage site [344], but without the monoclonal antibody epitope were also expressed in the placentas (ERVK3q12.3, ERVK8q24.3b, ERVK11q23.3, ERVK1q32.2, ERVK10p14, ERVK3q13.2). Because the Furin cleavage site is necessary for the formation of a fusogenic TM protein [344], expression these loci may result in functional Furin-cleaved ERVK-env proteins that are undetected by the antibody used in this study.

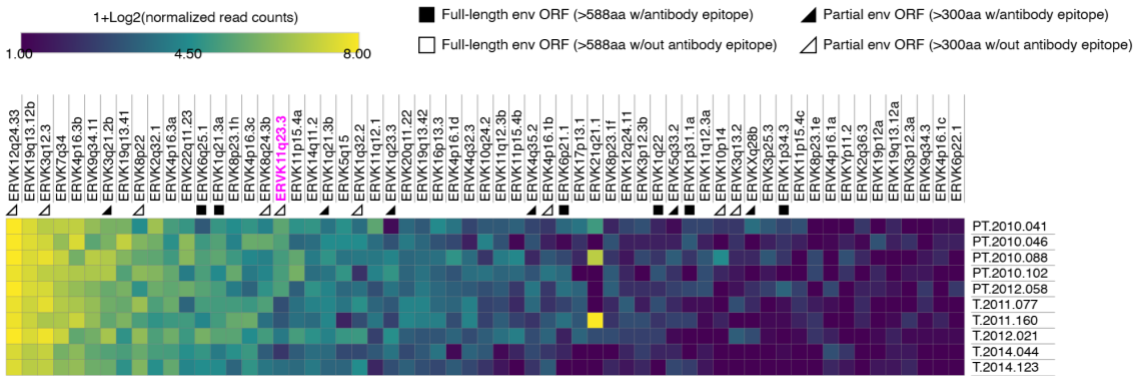

Figure 3.2 ERVK locus-specific RNA expression analysis

Heatmap depicting ERVK locus-specific RNA expression levels in human term (n=5) and preterm (n=5) placental tissue samples. Only loci with mean normalized read count >1 are shown (n=61). Loci with full-length envelope ORFs (>588aa, square), partial envelope ORF (>300aa, triangle), containing ERVK-env antibody epitope (black), or not containing ERVK-env antibody epitope (white) are shown below each locus.

3.3.4 ERVK11q23.3 RNA expression is upregulated in preterm compared to term placental tissue

To determine whether ERVK loci or other genes were differentially expressed between the human term and preterm placentas, we used the RNA-seq data generated from both conditions to perform differential expression (DE) analysis. A total of 143 differentially expressed genes (DEGs) (padj<0.05 and |L2FC|>1) were identified, including 49 upregulated and 94 downregulated genes in preterm compared to term placenta (**Table 3.4**). Consistent with previously studies of pregnancy complications, *NTRK2* and *BTNL9* were found to be upregulated [198], while *APLN* was found to be downregulated [345] (**Figure** 3.3). Of all the DEGs, the most significant was *TLR7* (padj=9.87E-08), which was downregulated 2.5-fold in preterm compared to term placenta. The *TLR7* gene encodes the toll-like receptor 7 protein that detects single-stranded RNA and plays an important role in the recognition of retroviral infections and activation of innate immunity [346]. While the majority of ERVK loci examined were similarly expressed, one of the top DEGs was the ERVK11q23.3 locus (also known as ERVK-20, c11_B, HERV-K37), which was found to be approximately four times higher in preterm compared to term placental tissue (padj=1.20E-05, L2FC=2.04) (**Figure** 3.3). Since TLR7 is considered essential for the control of ERVs [347], the decreased expression of TLR7 may contribute to the upregulation of the ERVK11q23.3 locus in preterm placenta. These results suggest that differences in antiviral innate immunity may exist between term and preterm placenta.

To determine whether there were differences associated with a specific trophoblast subtypes between preterm and term placenta we performed an over-representation analysis (ORA) using gene sets known to be enriched in multinucleated STBs, mononuclear CTBs, or invasive extravillous trophoblasts (EVTs). The analysis revealed that STB-associated genes (CGB5, CGB7, CGB8, ERVV-1, INHA, GREM2, TCL1B) were significantly over-represented in preterm-upregulated DEGs, while there was no significant enrichment of CTB or EVT associated genes found in either the upregulated or downregulated DEG sets. These results suggest that the

expression differences between term and preterm placenta are predominantly associated with STB cells rather than the other trophoblast subtypes.

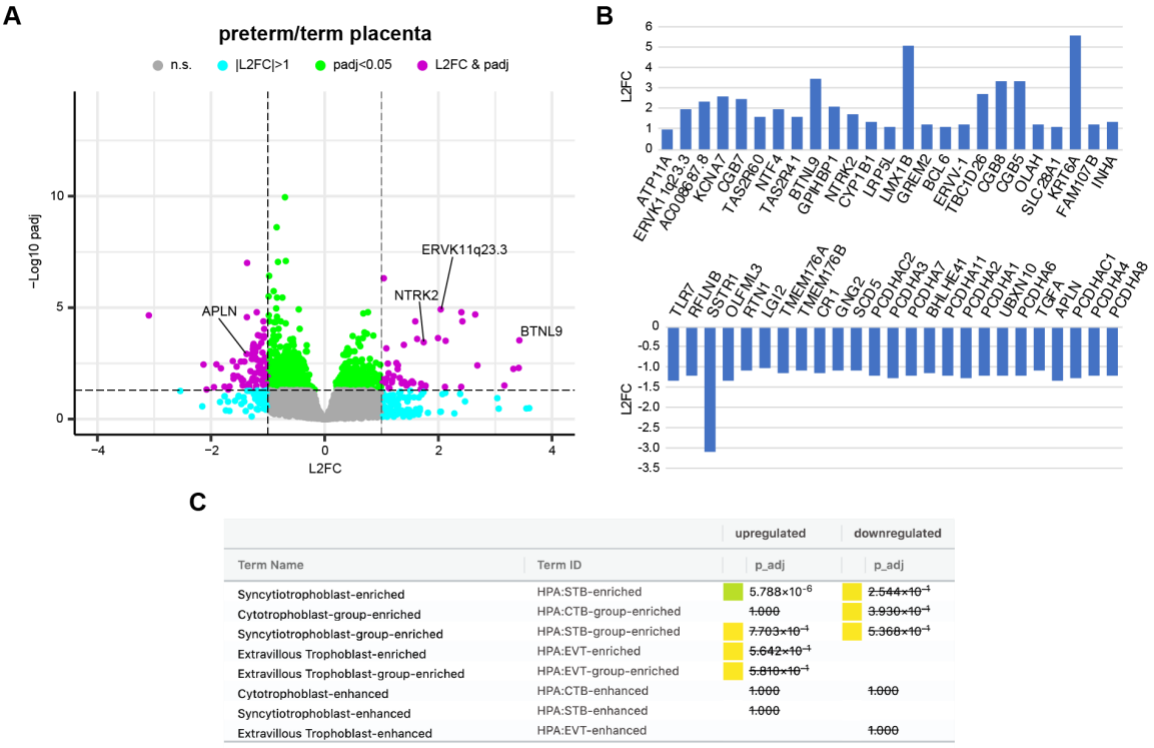

Figure 3.3 DE analysis of preterm vs. term placental tissue

(A) Volcano plot of preterm vs. term placenta DE results. DEGs (|L2FC| >1 and padj<0.05) are shown in purple. (B) Bar chart depicting L2FC values of 25 most significant upregulated (top) and downregulated (bottom) DEGs. (C) Trophoblast subtype ORA results highlighting enrichment of STB-associated genes in preterm placenta. n.s.=not significant; L2FC=Log2 fold-change; padj=adjusted p-value; STB=syncytiotrophoblast; CTB=cytotrophoblasts; EVT=extravillous trophoblasts; HPA=Human Protein Atlas.

3.3.5 ERVK11q23.3 RNA expression is enriched in undifferentiated mononuclear CTBs

The transcriptional activity of each ERVK locus is known to vary between different tissue and cell types [343], and the placenta is a heterogeneous organ comprised of many cell types [277]. To determine whether ERVK11q23.3 was predominantly transcribed from trophoblasts or some other placental cell type, we utilized publicly available RNA-seq data to preform DE analysis between HPTs (n=2) and bulk placenta tissue (n=5). The results showed that ERVK11q23.3 was significantly upregulated (padj=1.38E-33, L2FC=4.8) in HPTs compared to bulk placenta (**Figure** 3.4**A, Table 3.5**), indicating that placental ERVK11q23.3 RNA expression predominantly originates from trophoblast cells. An additional DE analysis using publicly available RNA-seq data from undifferentiated (n=6) and differentiated/fused (n=6) HPTs revealed that ERVK11q23.3 was significantly downregulated (padj=7.87E-21, L2FC=-2.5) in differentiated compared to undifferentiated HPTs (**Figure** 3.4**B, Table 3.6**). Collectively, these results suggest that ERVK11q23.3 RNA expression is enriched specifically within unfused mononuclear trophoblast cells of the placenta.

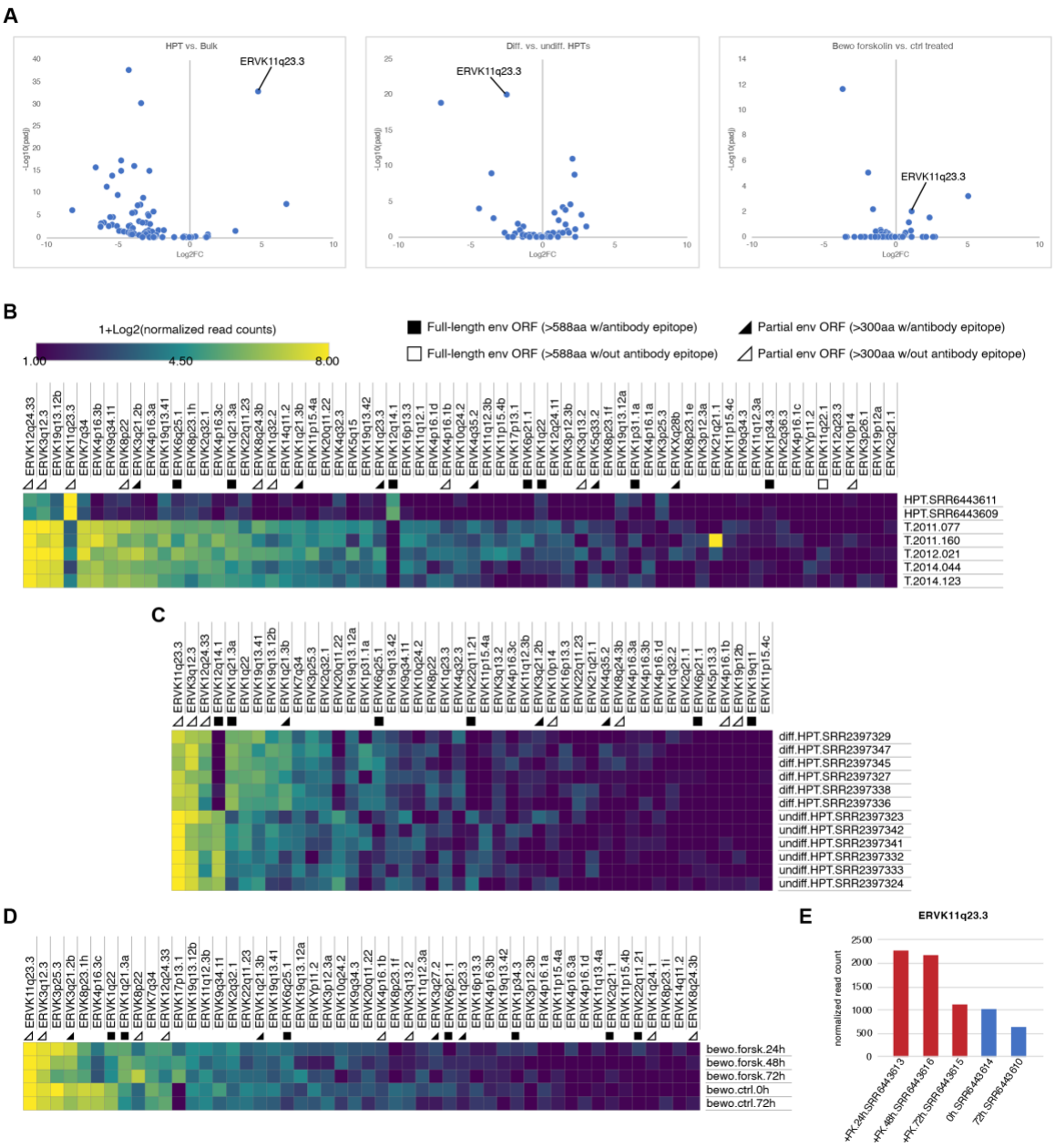

Figure 3.4 ERVK11q23.3 expression is enriched in mononuclear trophoblast cells

(A) Volcano plots of ERVK loci DE results from HPT vs. bulk placenta (left), differentiated vs. undifferentiated HPTs (middle), and forskolin-treated vs. untreated BeWo cells. ERVK11q23.3 is significantly differentially expressed in all three analyses. (B) Heatmap depicting 1+Log2(normalized read counts) for ERVK loci with mean normalized read count > 1 from comparison of (B) HPT vs. bulk placenta, (C) differentiated vs. undifferentiated HPTs, and (D) forskolin-treated vs. untreated BeWo cells. (E) Bar chart of ERVK11q23.3 normalized read counts across forskolin-treated (red) and untreated (blue) BeWo samples.

3.3.6 ERVK11q23.3 RNA expression increases in fusogenic BeWo cells

Because the BeWo choriocarcinoma cell line is a well-established model for studying trophoblast fusion *in vitro* following treatment with forskolin, we used publicly-available BeWo RNA-seq data to investigate ERVK11q23.3 expression levels between untreated (n=2) and forskolin-treated (n=3) BeWo cells [289]. The DE analysis showed significant upregulation (padj=9.69E-03, L2FC=1.2) of ERVK11q23.3 in forskolin-induced fusogenic cells compared to untreated BeWo cells (**Figure** 3.4**C, Table 3.6**). Closer examination of forskolin-treated samples, including cells treated with forskolin for 24, 48, and 72 h, showed that ERVK11q23.3 expression was highest in cells at 24h and 48h, while the expression level at 72h was similar to untreated samples (**Figure 3.4E**). Since the fusion of BeWo cells is known to occur between 48 and 72 h after the addition of forskolin [146], these data suggest that ERVK11q23.3 may be involved in the initiation of BeWo cell fusion.

3.3.7 A spliced envelope transcript is expressed from the ERVK11q23.3 locus

While full-length proviral RNA transcripts encode the *gag*, *pro*, and *pol* gene products, the envelope and accessory proteins are encoded by spliced RNA molecules [348]. Without expression of a properly spliced transcript, the envelope protein will not be produced and the resulting viruses are replication-defective [349,350]. As a first step to assess envelope protein-coding ability, we examined the uniquely-mapped RNA-seq reads for evidence of splicing at the ERVK11q23.3 locus. Unlike single-end sequencing, paired-end RNA-seq data can increase the alignment coverage of repetitive sequences, since uniquely-mapping mates can be used to correctly align multimapping reads. Because several regions across ERVK11q23.3 are non-unique and have low mappability (**Figure** 3.5), we relied strictly on the use of paired-end RNA-seq data to identify spliced ERVK11q23.3 transcripts. Therefore, to identify spliced transcripts we manually examined the unmapped mates of reads uniquely mapping to the ERVK11q23.3 locus from publicly-available BeWo paired-end RNA-seq data [290]. We identified numerous unmapped mates spanning splice sites and ultimately uncovered the presence of at least four splice sites and distinct transcripts

generated from the ERVK11q23.3 locus (**Figure** 3.5). This includes a (1) full-length transcript with a 437aa truncated *gag ORF*, (2) single-spliced transcript with a 438aa truncated *env ORF*, (3) single-spliced transcript with 44aa truncated *Np9* (accessory protein) ORF, and (4) double-spliced transcript with a 74aa full-length *Np9* ORF (**Figure** 3.5). These results suggest that the ERVK11q23.3 locus has the ability to encode a truncated envelope protein.

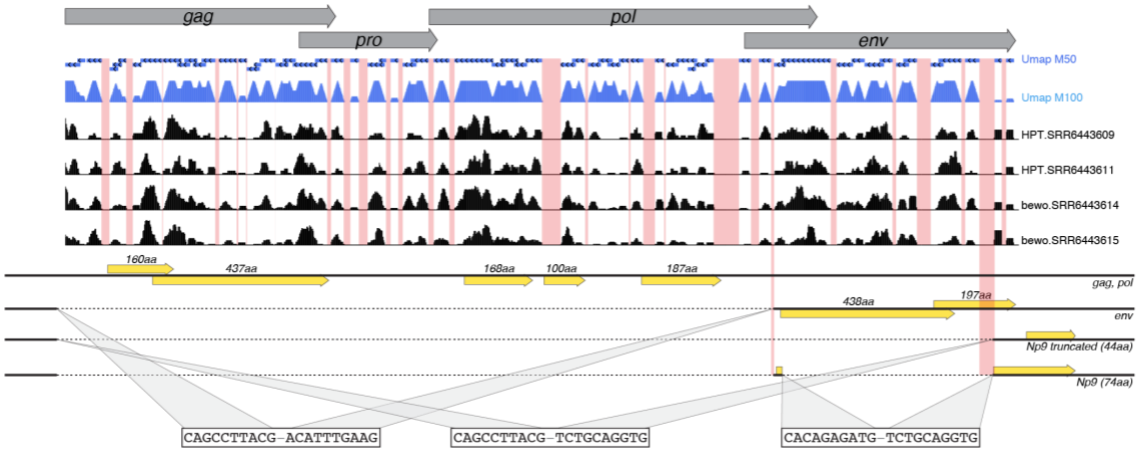

Figure 3.5 Expression of ERVK11q23.3 spliced transcripts

Schematic of the ERVK11q23.3 locus, including proviral genes (grey). Umap tracks (blue) highlight the regions with low mappability (red). Tracks of mapped RNA-seq data from human primary trophoblast (HPT) (n=2) and BeWo (n=2) samples are included (black). Unmapped mate reads from BeWo RNA-seq data were analyzed and identified the presence of at least four splice sites and three distinct spliced transcripts generated from the ERVK11q23.3 locus. Putative ORFs for each transcript are shown in yellow.

3.3.8 Predicted ERVK11q23.3 envelope protein contains fusion and immunosuppressive domains, but lacks a membrane spanning region

The retroviral envelope gene product encodes a polyprotein that is cleaved by cellular proteases to yield mature surface unit (SU) and transmembrane (TM) envelope proteins [351], with the FP and ISU domains located on the TM protein [246,247]. Similar to exogenous retroviruses, the ERVK ancestral-predicted TM protein contains functional FP and ISU domains [248-251]. Currently, the presence of these domains within the putative ERVK11q23.3 envelope protein is not known. Therefore, we examined the amino acid sequence of two overlapping ORFs identified within the ERVK11q23.3 single-spliced envelope transcript for the presence of the FP and ISU domain sequences. The first and longest ORF is predicted to encode a partial 438aa polyprotein containing the SU and part of the TM envelope protein; while the second ORF is 197aa long and corresponds to the remainder of the TM subunit. The 438aa ORF protein sequence contains a Furin cleavage site [344], FP [352], and ISU domain [251]; whereas the 197aa ORF protein sequence contains the MSR and anti-ENK epitope (**Figure** 3.6**A**). A hydrophobicity plot along the merged protein sequences confirmed the presence of both a FP and MSR, which are known to be hydrophobic [246,247] (**Figure 3.6B**). Compared to the ancestral-predicted ERVK-env sequence [342], an apparent 2bp deletion at the end of the ISU domain caused a frameshift and subsequent premature stop codon in the ERVK11q23.3 envelope protein. Notably, a +1 frameshift near the end of the first ORF could result in translation of full-length envelope protein from this locus (**Figure** 3.6**C**). However, Sanger sequencing of cDNA from HPTs (n=6 clones) showed no insertions, deletions or splicing events that would allow a full-length envelope protein to be translated (**Figure** 3.6**C**). This suggests that the single-spliced transcript from the ERVK11q23.3 locus encodes a 438aa truncated envelope protein that may be secreted due to lack of MSR, and is likely not detectable by the ERVK-env monoclonal antibody used in this study due to lack of epitope. Nonetheless, the presence of FP and ISU domain indicates that this protein may be involved in trophoblast fusion and/or immunosuppression.

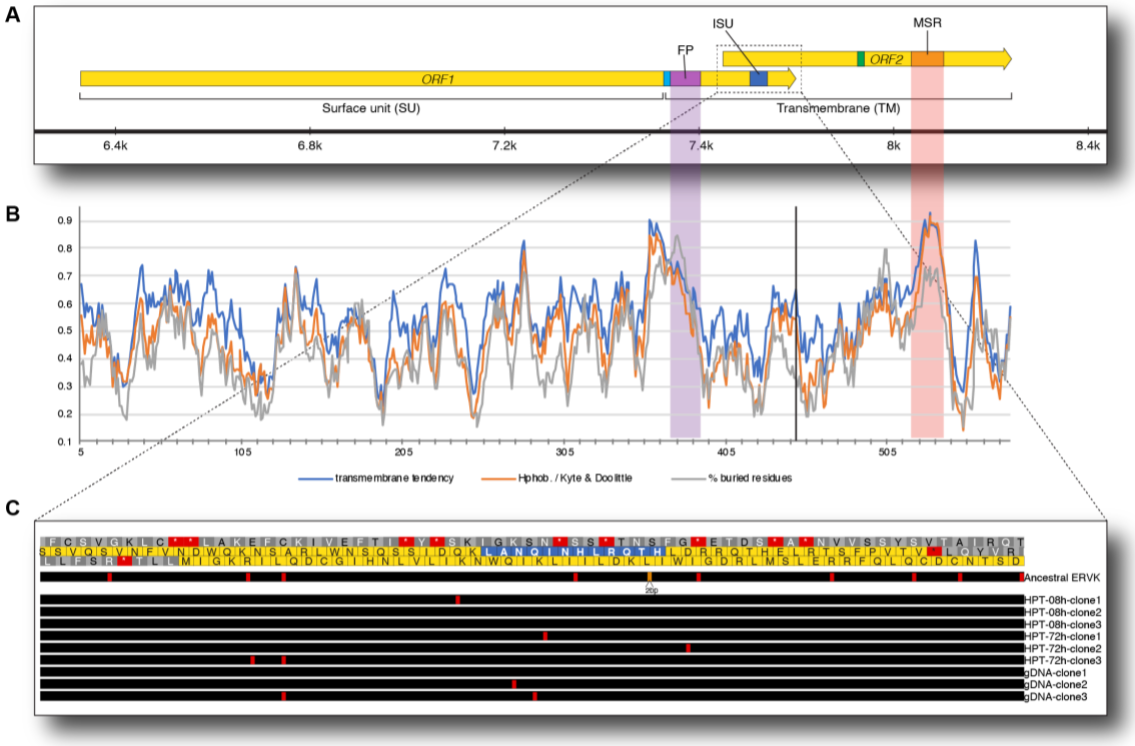

Figure 3.6 Predicted ERVK11q23.3 envelope protein contains fusion and immunosuppressive domains, but lacks a membrane spanning region

(A) Schematic of the two overlapping ORFs (yellow) in the ERVK11q23.3 envelope gene. ORF1 (left), contains a well-documented Furin cleavage site (cyan), FP (purple), and ISU domain (blue), while ORF2 (right), contains ERVK-env monoclonal antibody epitope (green), and MSR (orange). (B) Plot of hydrophobicity (orange), transmembrane tendency (blue), and % buried residues (gray), across 9aa windows of the predicted envelope protein. (C) Comparison to the ancestral predicted ERVK sequence (top track) revealed a 2bp deletion in ERVK11q23.3 envelope gene (orange). Examination of cDNA clones from HPTs showed several mismatched bases (red), but no insertions, deletions or splicing events that would result in translation of a full-length envelope protein.

3.3.9 Knockdown of ERVK11q23.3 envelope had no effect on HPT and BeWo cell fusion levels.

Since truncated ERV envelope proteins have previously been shown to influence trophoblast cell-cell fusion [193], we sought to elucidate the effect of ERVK11q23.3 expression on trophoblast cell fusion. For this, small interfering RNAs (siRNAs) targeting the envelope gene were used to knockdown (KD) ERVK11q23.3 expression in both fusogenic BeWo and HPT cells. Greater than 70% of both BeWo and HPT cells showed successful uptake of a fluorescently labeled siRNA transfection control (**Figure** 3.7**A**). An siRNA targeting no known sequence in the human transcriptome (siNC1) was included as a negative control, and an siRNA targeting the HPRT1 gene (siHPRT1) was included as positive control. When transfected with siHPRT1 both BeWo (n=4, p=3.38E-06) and HPT (n=3, p=2.25E-02) showed ~82% reduction in HPRT1 RNA level compared to siNC1 transfected cells (**Figure** 3.7**B**). Out of three different siRNAs tested (siENK13.13, siENK13.7, and siENK13.34) siENK13.34 was determined to be the most effective, reducing ERVK11q23.3 expression by ~70% (n=4, p=1.21E-04) compared to siNC1 transfected cells (**Figure** 3.7**C**). Thus, siENK13.34 was utilized in all subsequent experiments (referred to as siENK hereinafter). To assess the effect of ERVK11q23.3 silencing on cell-cell fusion, IF staining of plasma membrane marker, E-cadherin (CDH1), was used to calculate the percent fusion for both siENK (n=4) and siNC1 (n=4) transfected cells. Transfection of siENK significantly reduced ERVK11q23.3 expression by ~74% in BeWo cells (p=1.01E-04) and by ~60% in HPTs (p=2.18E-02). However, this decrease was not associated with any significant changes in cell fusion levels in either BeWo or HPT cells (**Figure** 3.8). Despite the role of other ERVs in trophoblast fusion, these results suggest that ERVK11q23.3 envelope expression is not involved in the cell-cell fusion normally observed in forskolin-treated BeWo cells or primary human trophoblast cells.

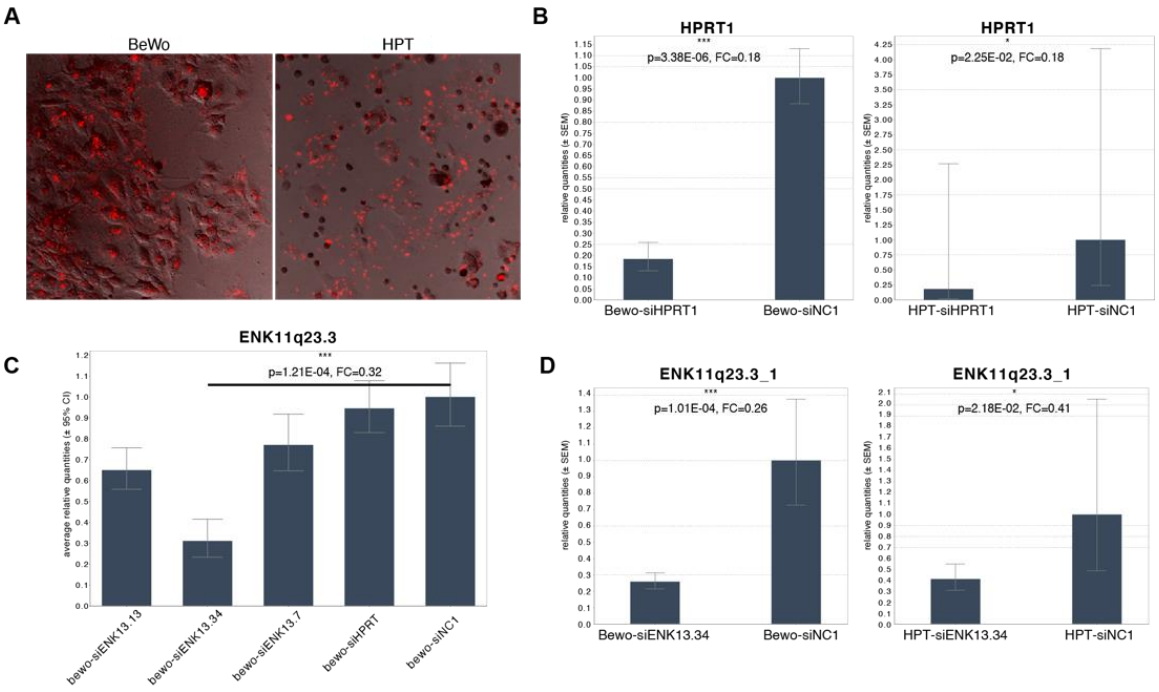

Figure 3.7 Validation and optimization of ERVK11q23.3 siRNA knockdown

(A) Microphotograph of cells transfected with fluorescently-labeled siRNA control. (B) HPRT1 relative quantities determined via qRT-PCR from cells transfected with siHPRT1 or siNC1. (C) ERVK11q23.3 envelope transcript (ENK11q23.3) relative quantities determined via qRT-PCR from BeWo cells transfected with either siENK13.13, siENK13.34, siENK13.7, siHPRT1, or siNC1. (D) ENK11q23.3 relative quantities determined via qRT-PCR from cells transfected with siENK13.34 or siNC1. Samples were normalized to GAPDH; error bars reflect SEM; a two-sided unpaired t-test was used to determine significance.

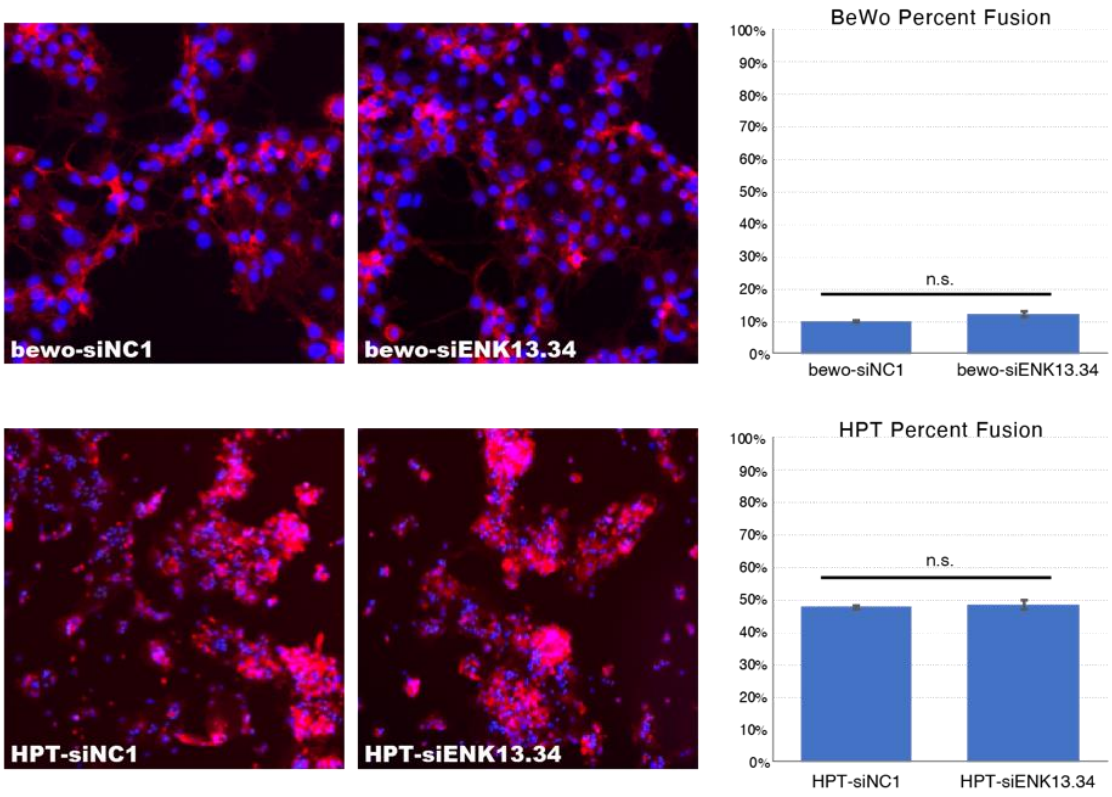

Figure 3.8 siRNA KD of ERVK11q23.3 showed no change in trophoblast fusion levels

Representative CDH1 (red) and DAPI (blue) immunostained microphotographs (n=5 per well) from BeWo (top) and HPT (bottom) cells transfected with siNC1 (n=3) (left) and siENK (n=3) (right). Bar charts depict fusion percentage (± standard deviation) calculated for each condition. A two-sided unpaired t-test was used to evaluate significance.

3.3.10 Knockdown of ERVK11q23.3 envelope decreased expression of type I interferon and antiviral immune response in trophoblast cells.

Innate immune responses can be divided into two categories: acute inflammatory responses and antiviral responses. The inflammatory response is marked by an induction of small signaling molecules called cytokines, including interleukin-6 (IL6) and tumor necrosis factor α (TNF) [353,354], while the antiviral response is characterized by the release of type I interferons (IFN), including IFNB1 [355]. To assess the putative role of ERVK11q23.3 in the innate immune response, we compared the expression level of several immune modulatory genes between siENK (n=3) and siNC1 transfected (n=3) cells via qRT-PCR. Additionally, since siRNA alone is capable of inducing double-stranded RNA (dsRNA) triggered innate immune responses [356], we also compared siNC1 (n=3) to mock (n=3) transfected cell to assess the effect of siRNA transfection on gene expression levels. Indeed, compared to mock transfected cells, HPTs transfected with siNC1 showed significant upregulation of antiviral type I IFN, IFNB1 (12-fold, p=2.62E-02) (**Figure** 3.9), suggesting that siRNA transfection likely induces a dsRNA triggered antiviral response. However, when HPTs were transfected with siENK (n=3), a 78% reduction in IFNB1 expression (0.22-fold, p=8.66E-04) was observed compared to siNC1 (n=3) (**Figure** 3.9). This suggests that the loss of ERVK11q23.3 diminishes the antiviral cytokine expression normally initiated by siRNA transfection. To a lesser extent, siRNA transfection of HPTs also induced expression of the pro-inflammatory cytokines IL6 (3.46-fold, p=4.34E-03) and TNF (3.51-fold, p=3.14E-02) (**Figure** 3.9). Unlike IFNB1, IL6 and TNF expression levels were not significantly different between siENK and siNC1 transfected HPT cells (**Figure** 3.9), suggesting that loss of ERVK11q23.3 expression has no significant effect on the pro-inflammatory response elicited by the siRNA transfection in HPTs.

In BeWo cells, IFNB1 and TNF expression levels were undetectable in all samples (**Figure** 3.9), indicating that siRNA transfection failed to induce an IFNB1-mediated antiviral and/or an TNF-associated proinflammatory response. However, there was a significant increase in IL6 (2.65-

fold, 5.03E-04) and IL10 expression levels in siNC1 (n=3) compared to mock transfected (n=3) BeWo cells (**Figure** 3.9). While IL6 is often considered a pro-inflammatory cytokine, in the absence of TNF and other stress agents, it can induce the expression of immunosuppressive factors, including IL10 [357-359]. Thus, these results suggest that siRNA transfection of BeWo cells increased the expression of anti-inflammatory cytokines which are known to promote immunosuppression. However, KD of ERVK11q23.3 in BeWo cells significantly reduced levels of IL6 (0.57-fold, p=2.44E-03) and IL10 (0.0004-fold, p=9.59E-03) compared to siNC1 transfected cells (**Figure** 3.9), indicating that ERVK11q23.3 expression facilitates upregulation of these anti-inflammatory cytokines. Collectively, these results show that ERVK11q23.3 expression mediates the upregulation of antiviral and anti-inflammatory cytokines induced via siRNA transfection of HPTs and BeWo cells, respectively. Thus, altered expression levels of ERVK11q23.3 in trophoblast cells at the maternal-fetal interface may result in aberrant antiviral and/or anti-inflammatory maternal immune responses during pregnancy.

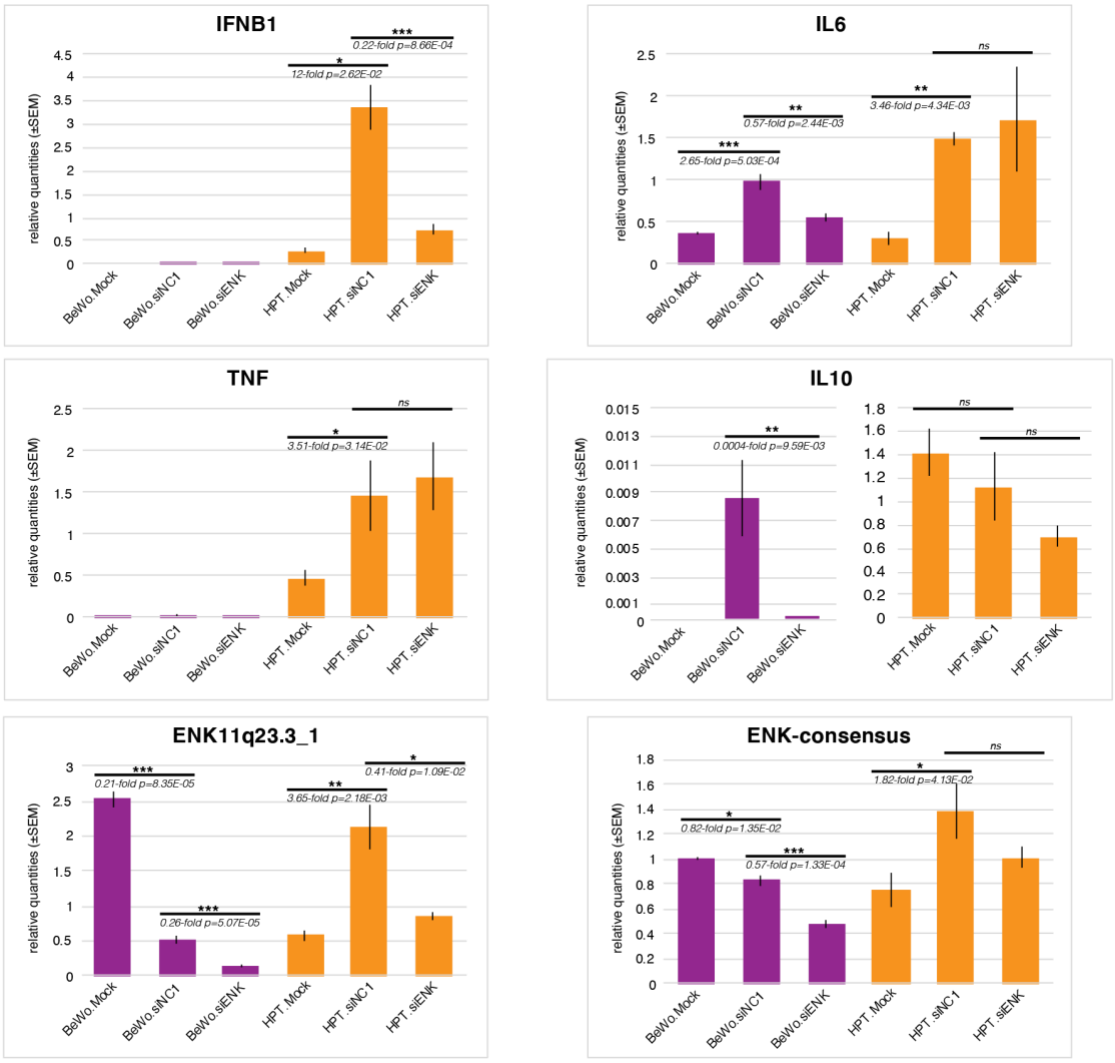

Figure 3.9 siRNA KD of ERVK11q23.3 decreased expression of several key immunomodulatory genes

Relative gene expression levels determined via qRT-PCR of several well-known immunomodulatory genes from BeWo (purple) and HPT (orange) cells transfected with siENK13.34 (light colored, n=3) and siNC1 (dark colored, n=3). Samples were normalized to GAPDH and scaled to siNC1 negative control samples. Error bars reflect SEM. A two-sided unpaired t-test was used to determine significance.

3.4 Discussion

It is well-recognized that ERV viral-like proteins can be co-opted to play important biological roles during normal human placentation. While it is currently known that ERVK-env protein is expressed in the placenta and that the ancestral-predicted envelope protein possesses fusogenic and immunosuppressive functions [10,248-251], the characteristics and putative function of natively expressed ERVK-env protein during human placentation remains unclear. To assess the putative fusogenic and/or immunosuppressive role of the ERVK-env in the placenta, a more thorough characterization of placental ERVK expression including, locus-specific transcription levels, splicing, and envelope protein-coding potential is required. In this study, we comprehensively examined locus-specific ERVK transcription across several different human placental tissues and cell types. Through a combination of RNA-seq and siRNA KD analyses, we identified the expression of a single ERVK locus, ERVK11q23.3, as (1) being significantly upregulated in preterm placenta, (2) predominantly expressed by mononuclear trophoblasts, (3) capable of encoding a truncated viral-like envelope protein, and (4) contributing to the expression cytokines involved in both antiviral and anti-inflammatory innate immune responses in HPTs and BeWo cells, respectively.

While abnormal placental ERVW and ERVFRD expression has been linked to several pregnancy complications [360-364], an association between aberrant placental ERVK expression and pathological pregnancy conditions has not yet been shown. To our knowledge, this is the first study to evaluate ERVK locus-specific expression levels in human placental samples, and specifically identify that the ERVK11q23.3 locus is significantly upregulated in preterm compared to term placental tissue. This discovery was only possible via the implementation of a locus-specific strategy that examined transcription of each ERVK proviral insertion, since numerous ERVK loci were found to be similarly expressed between term and preterm placenta. Previous reports using similar locus-specific strategies have shown that ERVK11q23.3 is transcribed within germ cell tumors [343], HIV-1 infected HeLa cells [365], as well as embryonic and induced pluripotent stem

cells [169]. Since ERVK11q23.3 is predominantly expressed by mononuclear CTBs, it is possible that this cell type is more abundant in preterm placental tissue. However, the DEGs identified between preterm and term placenta and the subsequent ORA results suggest that CTB abundance was equal across the two groups.

Previous studies have demonstrated that ERVK-derived transcripts and viral-like proteins are expressed during human placentation [10,366]. These reports are consistent with our RNA-seq and immunostaining results, which highlight placental ERVK RNA and ERVK-env protein expression, respectively. However, some notable differences were observed between our ERVK-env IHC staining results and those reported by a previous study using the same monoclonal antibody [10]. While Kammerer et al. showed ERVK-env staining predominantly localized to mononuclear CTBs within placental tissue, we observed staining majorly localized to the multinucleated STB layer. Since we followed the IHC procedure described by Kammerer et al., we speculate that the different staining patterns observed were due to lack of CTBs in the tissue sections examined or possibly variability between the antibody lots used. Nonetheless, our IF staining results showed strong ERVK-env membrane staining of mononuclear HPTs, which is consistent with the CTB expression previously described [10]. Notably, the envelope ORF of the ERVK11q23.3 locus is not predicted to contain the antibody epitope, suggesting that the protein staining detected via IHC and IF is not derived from the ERVK11q23.3 locus. A total of twelve ERVK loci expressed in bulk placenta are predicted to possess an envelope ORF containing the ERVK antibody epitope. Thus, the ERVK-env protein detected via the monoclonal antibody (HERM-1811-5) used in this study is likely derived from one or more of these loci.

Numerous studies of exogenous retroviruses have shown that full-length proviral RNA transcripts encode the *gag* and *pol* gene products, while the envelope and accessory proteins are encoded by spliced RNA molecules [348]. Very similar splicing has been documented for several ERVK proviruses [367-369]. This is consistent with our examination of BeWo paired-end RNA-seq data, which revealed the expression of several spliced transcripts from the ERVK11q23.3 locus,

including a single-spliced envelope transcript. Previous studies have shown that without expression of a properly spliced proviral transcript the envelope protein cannot be encoded [349,350]. While expression of a single-spliced envelope transcript is consistent with envelope protein expression, confirmation that a truncated envelope protein is encoded from the ERVK11q23.3 locus is still needed using an alternative ERVK-env antibody or protein-based approach. Notably, a 2bp deletion relative to ancestral-predicted ERVK introduced a premature stop codon within the envelope ORF, indicating that the putative ERVK11q23.3 envelope protein is truncated. However, the presence of a secondary overlapping ORF suggests expression of a full-length envelope protein from this locus is still possible via a ribosomal frameshift event, which are well-documented in retroviruses [370].

Placental ERVK expression has been hypothesized to aid in maternal immunomodulation [10], our study implicates its expression to immune regulation. While the mechanism remains unclear, expression of ERVK11q23.3 viral-like RNA and/or protein sequences is able to modulate cytokine gene expression levels associated with both antiviral and immunosuppressive immune responses. Similar to exogenous retroviral infections, previous studies have shown that ERVs can induce innate antiviral immune responses when expressed in certain tissues and cell lines [13,371,372]. These reports are consistent with our finding that loss of ERVK11q23.3 in HPTs significantly reduces expression of *IFN1B*, a type I IFN involved in antiviral immune response. Activation of type I IFN response has been shown to exacerbate systemic and uterine proinflammatory cytokine production, and increase susceptibility to inflammation-induced preterm birth in mice [373]. Since loss of ERVK11q23.3 expression significantly reduced *IFNB1* expression in HPTs, upregulation of placental ERVK11q23.3 expression may enhance type I IFN response and reduce the inflammatory challenge required for induction of preterm birth. This is further supported by our DE results showing that ERVK11q23.3 is upregulated in preterm placental tissue.

In addition to eliciting antiviral immune response, retroviral infections are frequently accompanied by immunosuppression which allows retroviruses to escape host immunologic

defenses. This immunosuppression is largely attributed to the retroviral TM envelope protein, which contains peptide sequences that functionally suppress immune effector cells [247]. Several ERV-derived envelope proteins sequences, including the ancestral-predicted ERVK-env sequence, are known to impair immune responsiveness in a similar manner to retroviral TM envelope proteins [197,217,251,374,375]. Thus, placental ERVK expression may also facilitate maternal immunosuppression required throughout normal pregnancy. This is consistent with our finding that siRNA KD of ERVK11q23.3 in BeWo cells significantly reduced immunosuppressive cytokines, IL10 and IL6. However, these same results were not observed with siRNA KD of ERVK11q23.3 expression in HPTs, which predominantly affected antiviral cytokine expression. These different cytokine responses suggest that BeWo choriocarcinoma cells might not accurately recapitulate ERVK11q23.3 function in normal trophoblast cells. However, it also suggests that ERVK11q23.3 expression may have multiple functions and/or its function is context-dependent. For instance, ERVK11q23.3 RNA expression could elicit an antiviral immune response, while ERVK11q23.3 envelope protein elicits an immunosuppressive response. Another possibility is that ERVK11q23.3 only elicits an antiviral immune response in the presence of adequate IFNB1 and TNF, which are expressed at much higher levels in HPTs compared to BeWo cells. To help clarify this, examination of additional cytokines and the quantification of both ERVK11q23.3 RNA and protein from HPTs and BeWo cells should be performed.

Besides ERVK11q23.3, our locus-specific ERVK analysis revealed high expression levels of a number of other loci within placental tissues and cells. Notably, two of the most highly expressed loci in bulk placenta, ERVK12q24.33 and ERVK19q13.12b, are located antisense within the introns of placentally expressed ZNF genes, *ZNF140* and *ZNF420*, respectively. Thus, expression of ERVK12q24.33 and ERVK19q13.12b can produce antisense transcripts to unspliced ZNF transcripts, which may inhibit translation of associated ZNF proteins through complementary binding and induction of the RNA interference pathway [376]. Several ERVK loci highly expressed in HPTs were not detected within bulk placental samples, including ERVK12q14.1, which was

shown to be significantly upregulated in HPTs compared to bulk placenta and in undifferentiated compared to differentiated HPTs. Unlike ERVK11q23.3, ERVK12q14.1 contains a full-length envelope ORF and is predicted to encode an ERVK-env protein possessing MSR and antibody epitope. Based on these characteristics, we suspect that the ERVK-env IF staining observed along the membrane of mononuclear HPTs is likely derived from this locus and may facilitate trophoblast fusion. Since ERVK12q14.1 expression is not detected within any of the BeWo samples examined, its putative role is likely enhanced or specific to HPTs. This is the case for cell fusion, which we show occurs much more in HPTs compared to forskolin treated BeWo cells. In order to assess its putative fusogenic role, a similar siRNA KD approach specifically targeting the ERVK12q14.1 locus within HPT cells and/or a transgene overexpression approach in BeWo cells should be used.

In conclusion, we showed that ERVK11q23.3 transcription is upregulated in preterm placenta and facilitates antiviral cytokine gene expression in trophoblast cells, suggesting that expression of this element helps activate an antiviral immune response in the placenta. Thus, aberrant ERVK11q23.3 expression levels may contribute to pregnancy complications and/or diseases affecting innate antiviral immune response and should be further investigated. Moreover, our analysis revealed that ERVK11q23.3 has the ability to encode a partial envelope protein, however it is still unclear whether this protein is generated and if it is involved in the innate immune response we observed in siRNA transfected trophoblast cells. Thus, the specific mechanism underlying ERVK11q23.3-mediated antiviral cytokine expression, including the role of ERVK11q23.3 RNA and proteins, should be further interrogated in future investigation. Collectively, the results of this study: (1) highlight the utility of studying locus-specific ERVK expression, (2) provide a thorough characterization of locus-specific ERVK transcription from human placental tissues, and (3) help delineate the molecular and functional differences between term and preterm placenta, as well as mononuclear and multinucleated trophoblast cells. Additional studies focused on identifying other factors mediating trophoblast fusion and/or maternal immune suppression will not only enhance our understanding of the basic molecular biology underlying

human placentation, but will also facilitate the development of novel diagnostic tools and therapeutics for alleviating pregnancy complications with underlying placental defects.

3.5 Methods

3.5.1 Placental tissues and cells

Deidentified human placental samples were collected by and acquired through the Labor and Delivery Unit at the Oregon Health and Science University Hospital and deposited into a repository under a protocol approved by the Institutional Review Board with informed consent from the patients. A total of five different term placenta samples collected from healthy cesarean section term births (ranging from 38.9 to 41.3 gestational wks), and five preterm placental samples (ranging from 33.3 to 36.4 gestational wks) were used for RNA isolation and RNA-seq based analyses. Further, banked formalin-fixed paraffin-embedded tissues (FFPE) tissues collected from human term (n=4) and preterm (n=4) placentas were used for IHC staining. All FFPE samples were deidentified and collected from cesarean section deliveries without labor. Frozen vials of HPTs used for IF and siRNA KD experiments were obtained from Amy Valent's lab. The HPTs samples, consisting of highly purified CTB cells, were isolated from human term placental tissue using a Percoll gradient as previously described [24].

3.5.2 IHC staining

Paraffin sections were deparaffinized and rehydrated through xylene and graded alcohol series, then washed for 5 min in running tap water. Antigen unmasking was performed using sodium citrate (pH 6.0) buffer in a pressure cooker for 20 min, washed in three changes of PBS. An endogenous enzyme block was performed by incubating sections in 0.3% hydrogen peroxide for 10 min, washed in three changes of PBS. Nonspecific proteins were blocked by incubating sections in 5% horse serum for 30 min. The mouse monoclonal antibody specific for the ERVK-env TM

protein (Austral Biologicals, HERM-1811-5) was diluted 1:250, and the mouse igG2A isotype was diluted to an equivalent concentration. The tissue sections were incubated in primary antibody dilutions for 2 h at room temperature. Mouse IgG H+L (Vector Labs, BA-2000) and biotinylated secondary antibody dilutions were prepared at 1:250 in PBS + 1% BSA. The sections were incubated in secondary antibody dilution for 1 h at room temperature, then washed in three changes of PBS. VECTASTAIN Elite ABC HRP Kit (Vector Laboratories, PK-6100) and ImmPACT DAB Peroxidase HRP substrate (Vector Labs, SK-4105) were used according to manufactures instructions. Notably, all tissue sections were stained in a single batch using the same incubation times. Nuclei were counterstained with hematoxylin (Electron Microscopy Sciences, 26043-05), and imaged using a brightfield microscope.

3.5.3 Transcriptional analysis of human ERVK loci

UCSC table browser RepeatMasker track was used to extract bed file of all genomic regions identified as HERVK-int, LTR5A, LTR5B, or LTR5_Hs (filter by repNames: HERVK-int* OR LTR5A* OR LTR5B* OR LTR5_Hs*). Nearby regions (within 2000bp) were merged into single loci using Bedtools merge (options: -s -d 2000 -c 4,5,6 -o collapse,sum,distinct -delim ";"). Solo LTR elements were discarded, and only loci containing at least one "HERVK-int" annotation were examined within the subsequent analysis. RNA-seq raw fastq files were trimmed of low-quality and adapter sequences using Trimmomatic [319] and mapped to the human (GRCh38) reference genome using Bowtie2 [320] with --very-sensitive parameter. Resulting BAM files were filtered to remove low quality and multi-mapped reads (MAPQ ≥10) using samtools [321] view -q 10. A custom gtf file including the 124 ERVK loci and ENSEMBL human genome protein-coding gene annotations (Homo_sapian.GRCh38.98.protein_coding) was used to generate raw read count tables (n=20128 genes) using featureCounts [322] (–primary). DEseq2 [323] was used to generate VST-normalized read counts for transcriptomic comparison. The default settings of DEseq2 were used for DE analyses and genes with padj<0.05 & Log2FC>|1| were identified as DEGs. A total of four

separate DE analyses were carried out, including (1) preterm (n=5) vs. term (n=5) human placenta samples, (2) HPTs (n=2) vs. bulk term placenta (n=5), (3) differentiated (n=6) vs. undifferentiated (n=6) HPTs, and (4) untreated (n=2) vs. forskolin-treated (n=3) BeWo cells. The human term and preterm RNA-seq data was generated in-house while all other RNA-seq data was publicly available and downloaded NCBI SRA using SRA Toolkit (http://ncbi.github.io/sra-tools/). The following RNA-seq data was used in DE analyses described above: Bulk preterm placenta (SRR13632931, SRR13632932, SRR13632933, SRR13632934, SRR13632935); Bulk term placenta (SRR12363244, SRR12363245, SRR12363246, SRR12363247, SRR12363248); HPTs (SRR6443609, SRR6443611); Undiff. HPTs (SRR2397323, SRR2397324, SRR2397332, SRR2397333, SRR2397341, SRR2397342); Diff. HPTs (SRR2397327, SRR2397329, SRR2397336, SRR2397338, SRR2397345, SRR2397347); BeWo (SRR6443614, SRR6443610); Forskolin-treated BeWo (SRR6443613, SRR6443615, SRR6443616); paired-end BeWo (SRR9118949, SRR9118950).

3.5.4 Splicing and ORF analysis

Paired-end BeWo RNA-seq data was used. The unmapped mates of reads uniquely mapping to ERVK11q23.3 locus were extracted from BAM files using samtools. The unmapped sequences were manually aligned to ERVK11q23.3 DNA sequence using UGENE. The protscale expasy webtool (https://web.expasy.org/protscale/) with a window size of 9 was used to examine the "Hydrophobicity (Kyte & Doolittle)", "Transmembrane tendency", and "% buried residues" across the predicted ERVK11q23.3 envelope protein. The ERVK11q23.3 envelope protein sequence containing ORF1 + ORF2 (partial) was used as input;
ORF1:MVTPVTWMDNPIEVYVNDSVRVPGPTDDRCPIKPEEEGIMINISTGYRYPICLGRA
PGCLIHAVQNWLVEVPTVSPNGRFTYHMVSGMSLRPRVNYLQDFSYQRSLKFRPKGKPC
PKEIPKESKNTEVLVWEECVANSAVILQNNEFGTIIDWAPRGQFDHNCSGQTQLCPSAQV
SPAVDSDLTESLDKHKHKKLQSLYPWEWGEKGISTPRPKIISPVSGPEHPELWRLIVASHH

IRIWSGNQTSETRDRKPFYTIDLNSSLTVPLQSCVKPPYMLVVGNIVIKPDSQTITCENCRL
FTCIDSTFNWQQRILLVRAREGVWIPVSMDRPWEASPSIHILTEVLKGILNRSKRFIFTLIA
VIMGLIAVTATAAVAGVALHSSVQSVNFVNDWQKNSARLWNSQSSIDQKLANQINHLR
QTHLDRRQTHELRTSFPVTV;
ORF2(partial):CNTSDFCITPQIYNESEHHWDMVRHHLQGREDNLTLDISKLKEKIFEASKA
HLNLVPGTEAIAGVADGLANLNPVTWVKTIGSTTIINLILILVCLFCLLLVCRCTQQLRRD
SDHREWAMMTMAVLSKRKGGNVGKSKRDQIVTVSV.

3.5.5 Cell culture

BeWo cells were cultured at 37C 5% CO_2 in Ham's F-12 (Kaighn's Modification) media (Caisson Labs, HFL06-500ML) supplemented with 10% FBS (Sigma, 12106C-100ML) and Pen/Strep (Fisher, 15-140-148). Media was changed every other day, and cells were passaged approximately every 4 days or at ~80% confluency. For fusion induction, BeWo cells were seeded at 20,000 cells/cm2, treated with 25uM Forskolin (EMD Millipore, 344282-5MG) one day after passaging, and analyzed 72 h after start of treatment. DMSO treated cells were included alongside forskolin treated cells as negative/vehicle controls.

3.5.6 siRNA transfection

Custom duplex siRNAs targeting ERVK envelope (siENK) transcripts were designed with IDT's online siRNA design tool (https://www.idtdna.com/site/order/designtool/index/DSIRNA_CUSTOM), using ERVK11q23.3 sequence as input. In total, three siRNA's targeting ERVK with no predicted cross-reacting transcripts were used: siENK13.7, siENK13.13, and siENK13.34 (Design IDs: CD.Ri.218416.13.7, CD.Ri.218416.13.13, CD.Ri.218416.13.34, respectively); siENK13.13 was predicted to uniquely target ERVK11q23.3 transcripts, while siENK13.7 and siENK13.34 were predicted to target putative ERVK transcripts from 29 and 33 ERVK genomic loci, respectively. For BeWo cells,

transfections were performed 24 h after start of forskolin treatment according to Lipofectamine RNAiMAX reagent protocol optimized for efficiency, viability and reproducibility. Briefly, for each well of 24-well plate 1.5ul of RNAiMAX solution (Thermo Fisher, 13778030) and siRNA were diluted in 50ul Opti-MEM media (Thermo Fisher, 31985062), incubated for 5min at room temperature, and added to cells containing 500ul culture media (from previous day/containing forskolin). All siRNAs, including HPRT1 positive control (IDT, 51-01-08-02), nontargeting universal negative control (NC1) (IDT, 51-01-14-03), and ERVK-targeting siRNAs were transfected at a final concentration of 25nM and analyzed 48 h post-transfection (72 h post-forskolin treatment). Initial fluorescent TYE 563 transfection control used to calculate transfection efficiency was used at a final concentration of 10nM and analyzed 24 h post-transfection in unstimulated BeWo cells. For HPTs, RNAiMAX reverse transfection protocol was used. For this, siRNA + RNAiMAX complexes were prepared inside the wells, after which the freshly thawed HPT cells and medium were added. All siRNAs, including HPRT1 positive control, NC1, and ERVK-targeting siRNAs were transfected at a final concentration of 25nM and analyzed 72 h post-transfection.

3.5.7 RNA isolation and purification

Frozen placental samples were ground into a powder using liquid nitrogen-cooled mortar and pestle then directly added to TRIzol reagent (Thermo Fisher #15596026); for cell lines media was removed and TRIzol reagent was added directly to the tissue culture dish. RNA was isolated from TRIzol reagent, treated with Turbo DNAse (Thermo Fisher #AM1907), and purified using RNA Clean and Concentrator-5 spin columns (Zymo #R1013) according to manufactures instructions.

3.5.8 qRT-PCR

qRT-PCR analysis was preformed using qbase+ software, with GAPDH as reference gene and unpaired t-tests (two-sided) were used to determine significance. two sets of gene expression

primers, ENK11q23.3_1 and ENK11q23.3_2, were designed to uniquely amplify the ERVK11q23.3 envelope transcript; the first, ENK11q23.3_1, targeting the region of the transcript encoding the surface unit (SU), and ENK11q23.3_2 targeting the region encoding the transmembrane (TM) portion of the envelope protein. An additional primer set, ENK-consensus, was designed to amplify putative ERVK envelope transcript sequences from 17 different genomic loci, including ERVK11q23.3 (chr1:155627693-155627856, chr1:160698826+160698989, chr1:75382268+75382431, chr11:118722041-118722204, chr12:58328486-58328649, chr19:27638644-27638807, chr19:35572497-35572660, chr2:129962985-129963148, chr22:18946662+18946825, chr3:101699824+101699987, chr3:113025296-113025459, chr3:125898575+125898733, chr5:156658733-156658896, chr6:77717964-77718127, chr7:4583453-4583616, chr7:4591957-4592120, chr8:139460933-139461096, chr8:7498902-7499065).

3.5.9 IF staining

Cell culture media was removed from cells, fixed with ice-cold methanol for 15 min at -20C, then washed in three changes of PBS. Nonspecific proteins were blocked by incubating cells in 5% donkey serum for 30 min. Both Anti-ERVK-env mouse monoclonal (HERM-1811-5, Austral Biologicals, San Ramon, CA, USA) and anti-CDH1 rabbit monoclonal (Cell Signaling, 3195S) antibody were diluted 1:250 in PBS + 1% BSA, and incubated overnight at 4C. Donkey anti-mouse Alexa Fluor 488 (A-21202, Invitrogen) and Donkey anti-rabbit Alexa Fluor 594 (A-21207, Invitrogen) secondary antibodies were diluted 1:1000 in PBS + 1% BSA. The cells were washed in three changes of PBS, before incubating in secondary antibody dilutions for 1 h at room temperature. Nuclei were counterstained with DAPI and washed with three changes of PBS before imaging.

3.5.10 Trophoblast cell fusion quantification

A total of five E-cadherin (CDH1) immunostained micrographs were captured from each well using 20X objective on Nikon epifluorescence microscope. The CDH1-immunostained micrographs were deidentified and nuclei were quantified by a blind reviewer using the "cell counter" tools from the FIJI software package. DAPI staining was used to count the total number of nuclei per micrograph (n_t). An overlay of CDH1 and DAPI was used to quantify the total number of nuclei within multinucleated cells (n_m). A multinucleated cell was identified by the presence of two or more nuclei bound by a single CDH1-positive membrane staining. The fusion percentage was calculated for each micrograph using the following formula.

$$Fusion\ percentage = \left(\frac{n_m}{n_t}\right) * 100$$

The mean average fusion percentage was calculated for each well, and these values were used to compare fusion levels between siNC1 (n=3) and siENK (n=3) transfected cells using a two-sided unpaired t-test.

3.6 Tables

Table 3.1 IHC tissue details

ID	Category	Fetus sex	Gest Age (wks.)	Labor	C-section	Mat Age (yr.)	Mat Race
PT1	Preterm	Female	35	No	Yes	24	White Hispanic
PT2	Preterm	Female	35	No	Yes	23	White Non-Hispanic
PT3	Preterm	Female	35	No	Yes	19	White Non-Hispanic
PT4	Preterm	Male	35	No	Yes	22	White Hispanic
T1	Term	Female	39	No	Yes	28	White Non-Hispanic
T2	Term	Male	39	No	Yes	32	White Non-Hispanic
T3	Term	Male	39	No	Yes	24	White Non-Hispanic
T4	Term	Male	39	No	Yes	29	White Non-Hispanic

Table 3.2 RNA-seq sample details

ID	Category	Fetus sex	Gest Age (wks.)	Labor	C-section
PT.2010-041	Preterm	Female	33.29	No	Yes
PT.2010-102	Preterm	Male	33.29	No	Yes
PT.2010-046	Preterm	Male	36.43	No	Yes
PT.2012-058	Preterm	Female	36.43	No	Yes
PT.2010-088	Preterm	Male	34.00	No	Yes
T.2014-123	Term	Male	39.29	No	Yes
T.2014-044	Term	Male	39.00	No	Yes
T.2012-021	Term	Female	41.29	No	Yes
T.2011-160	Term	Female	39.00	No	Yes
T.2011-077	Term	Female	38.86	No	Yes

Table 3.3 Details of ERVK loci (n=124)

ID	chr	start	stop	strand	Longest env ORF (aa)	Antibody epitope	ENK-consensus primer
ERVK1p36.21a	chr1	12780114	12785935	-			
ERVK1p36.21b	chr1	13012446	13021988	-	131		
ERVK1p36.21c	chr1	13206971	13216513	+	296		
ERVK1p36.21d	chr1	13352735	13362257	+	162	yes	
ERVK1p35.1	chr1	33063515	33065110	+			
ERVK1p34.3	chr1	36488983	36491127	-	588	yes	
ERVK1p31.1a	chr1	75377085	75383458	+	588	yes	yes
ERVK1p31.1b	chr1	82223389	82223522	-			
ERVK1q21.3a	chr1	150632807	150635885	+	588	yes	
ERVK1q21.3b	chr1	150632885	150634662	-	542	yes	
ERVK1q22	chr1	155626665	155635845	-	1375	yes	yes
ERVK1q23.3	chr1	160691753	160698953	+	542	yes	yes
ERVK1q24.1	chr1	166605365	166611021	-	309		
ERVK1q32.2	chr1	207635111	207639291	-	309		
ERVK1q43	chr1	238762294	238764473	-	588	yes	
ERVK2q21.1	chr2	129961964	129965044	-	687	yes	yes
ERVK2q32.1	chr2	186520906	186522372	+	170		
ERVK2q36.3	chr2	229180638	229180771	-			
ERVK3p26.1	chr3	7061961	7062102	+			
ERVK3p25.3	chr3	9847661	9854552	-	113		
ERVK3p12.3a	chr3	75536829	75538747	+			
ERVK3p12.3b	chr3	75551313	75559999	+	245		
ERVK3q12.3	chr3	101691892	101701015	+	416		yes
ERVK3q13.2	chr3	113024276	113033435	-	597 (pol/env)		yes
ERVK3q21.2a	chr3	125799250	125801161	-			
ERVK3q21.2b	chr3	125890458	125899596	+	312	yes	yes
ERVK3q22.1	chr3	130211771	130212782	+			
ERVK3q24	chr3	148563689	148567609	-			
ERVK3q27.2	chr3	185562547	185571727	-	312	yes	
ERVK4p16.3a	chr4	241199	245565	+			
ERVK4p16.3b	chr4	3977323	3986912	-	234		
ERVK4p16.3c	chr4	4073396	4075313	+			
ERVK4p16.1a	chr4	9034416	9036346	-			
ERVK4p16.1b	chr4	9121785	9131367	+	342		
ERVK4p16.1c	chr4	9567313	9569224	-			
ERVK4p16.1d	chr4	9657955	9667550	+	234		
ERVK4q13.2	chr4	68597990	68603505	+	113	yes	
ERVK4q32.1	chr4	160658785	160661208	+			
ERVK4q32.3	chr4	164995687	165002916	+	192		
ERVK4q35.2	chr4	190106258	190113546	-	312	yes	
ERVK5p13.3	chr5	30486652	30496098	-	312	yes	
ERVK5p12	chr5	46000056	46009900	-	140		
ERVK5q15	chr5	93456673	93458206	-			
ERVK5q31.1	chr5	136413959	136414650	-			
ERVK5q33.2	chr5	154635952	154644655	-	312	yes	
ERVK5q33.3	chr5	156657705	156666885	-	312	yes	yes
ERVK6p25.2	chr6	3054799	3055508	+			
ERVK6p22.1	chr6	28682590	28692958	+	134		
ERVK6p21.1	chr6	42893670	42903629	-	698	yes	
ERVK6q11.1	chr6	60654986	60660975	+			
ERVK6q13	chr6	73333257	73333407	-	162	yes	
ERVK6q14.1	chr6	77716944	77726366	-	698	yes	yes
ERVK6q25.1	chr6	150859612	150862438	+	699	yes	
ERVK7p22.1	chr7	4582425	4600400	-	699	yes	yes
ERVK7p14.3	chr7	30718255	30719589	-			
ERVK7q11.21	chr7	66004683	66007803	-	150		
ERVK7q22.2	chr7	104748901	104752819	-			
ERVK7q34	chr7	141752118	141756120	-			
ERVK8p23.1a	chr8	7126986	7128897	-			
ERVK8p23.1b	chr8	7185490	7187404	+			
ERVK8p23.1c	chr8	7497874	7507337	-	699	yes	yes
ERVK8p23.1d	chr8	8100097	8102011	-			
ERVK8p23.1e	chr8	8197177	8206699	+	264		
ERVK8p23.1f	chr8	12216460	12225988	-	126		
ERVK8p23.1g	chr8	12458982	12468498	-	261	yes	

ERVK8p23.1h	chr8	12565086	12567003	+			
ERVK8p23.1i	chr8	12623205	12625104	+			
ERVK8p22	chr8	17908095	17916431	-	379		
ERVK8q11.1	chr8	46264027	46272039	-	264		
ERVK8q24.3a	chr8	139459905	139462993	-	699	yes	yes
ERVK8q24.3b	chr8	145021243	145028834	-	309		
ERVK9q34.11	chr9	128850235	128857457	+	60		
ERVK9q34.3	chr9	136780313	136789776	-	79	yes	
ERVK10p14	chr10	6824178	6833641	-	322		
ERVK10q22.3	chr10	80108250	80108670	+			
ERVK10q24.2	chr10	99820811	99827959	-	214		
ERVK11p15.4a	chr11	3447425	3456979	-	164		
ERVK11p15.4b	chr11	3544465	3546375	+			
ERVK11p15.4c	chr11	4459434	4461473	-			
ERVK11q12.1	chr11	59000008	59005723	+	189		
ERVK11q12.3a	chr11	62368490	62370999	-	230		
ERVK11q12.3b	chr11	62375544	62383091	-			
ERVK11q13.2	chr11	67920365	67922280	+			
ERVK11q13.4a	chr11	71673667	71675588	-			
ERVK11q13.4b	chr11	71764073	71764819	+	162		
ERVK11q22.1	chr11	101695062	101704528	+	661		
ERVK11q23.3	chr11	118721014	118730174	-	438		yes
ERVK12p11.1	chr12	34619619	34629282	-	215		
ERVK12q14.1	chr12	58327458	58336915	-	698	yes	yes
ERVK12q23.3	chr12	107826195	107827421	-			
ERVK12q24.11	chr12	110570037	110571520	+			
ERVK12q24.33	chr12	133090535	133096478	-	358		
ERVK13q12.13	chr13	26509516	26510128	+			
ERVK14q11.2	chr14	24009695	24015776	-			
ERVK14q32.33	chr14	105673312	105676203	+			
ERVK15q25.2	chr15	84160267	84163612	+			
ERVK16p13.3	chr16	2926158	2927660	+			
ERVK16p11.2a	chr16	34412056	34414804	-	550	yes	
ERVK16p11.2b	chr16	34997025	34999771	+	550	yes	
ERVK16q23.3	chr16	83702132	83702178	-			
ERVK17p13.1	chr17	8056336	8063901	+			
ERVK18q21.33	chr18	63851825	63852338	-			
ERVK19p13.3	chr19	385094	387637	+	114		
ERVK19p12a	chr19	20276590	20286703	+	285	yes	
ERVK19p12b	chr19	22575021	22581759	+	312		
ERVK19q11	chr19	27637589	27646453	-	699	yes	yes
ERVK19q13.12a	chr19	35572526	35576532	-	268		yes
ERVK19q13.12b	chr19	37106646	37116164	-	206		
ERVK19q13.41	chr19	52745022	52750454	-	159		
ERVK19q13.42	chr19	53359094	53364791	+	215		
ERVK20p11.21a	chr20	23693938	23695327	-			
ERVK20p11.21b	chr20	23755866	23757247	-			
ERVK20q11.22	chr20	34126943	34136578	+	139		
ERVK21q21.1	chr21	18561340	18569644	-	55	yes	
ERVK22q11.21	chr22	18938673	18947848	+	1171	yes	yes
ERVK22q11.23	chr22	23536061	23548428	+	141		
ERVK22q13.2	chr22	40696388	40696742	-			
ERVKXq11.1	chrX	62740078	62742584	+			
ERVKXq12	chrX	66464289	66466342	-			
ERVKXq28a	chrX	154588661	154591282	+			
ERVKXq28b	chrX	154608422	154615762	-	336	yes	
ERVKYp11.2	chrY	6958399	6965343	-	225		
ERVKYq11.23a	chrY	24251689	24254888	-			
ERVKYq11.23b	chrY	25415254	25418454	+			

Table 3.4 DEGs preterm/term placenta (All DEGs)

Gene.name	GeneID	PT_avg	T_avg	L2FC	padj
TLR7	ENSG00000196664	148.9	383.1	-1.37	9.87E-08
ATP11A	ENSG00000068650	2693.0	1309.4	1.04	4.81E-07
ERVK11q23.3	NA	36.0	9.1	2.04	1.20E-05
RFLNB	ENSG00000183688	457.6	1046.9	-1.20	1.61E-05
AC008687.8	ENSG00000283663	428.8	80.9	2.41	1.61E-05
KCNA7	ENSG00000104848	396.9	63.3	2.65	2.03E-05
SSTR1	ENSG00000139874	14.3	120.6	-3.09	2.22E-05
OLFML3	ENSG00000116774	290.6	748.3	-1.37	2.68E-05
RTN1	ENSG00000139970	61.6	130.7	-1.08	4.13E-05
CGB7	ENSG00000196337	570.2	106.3	2.42	4.13E-05
TAS2R60	ENSG00000185899	72.6	24.3	1.59	4.13E-05
LGI2	ENSG00000153012	88.0	184.4	-1.06	9.03E-05
TMEM176A	ENSG00000002933	128.0	288.8	-1.17	1.71E-04
TMEM176B	ENSG00000106565	264.8	554.4	-1.07	1.88E-04
CR1	ENSG00000203710	220.5	483.2	-1.13	1.88E-04
GNG2	ENSG00000186469	224.0	470.6	-1.07	2.25E-04
NTF4	ENSG00000225950	412.8	103.7	1.99	2.32E-04
TAS2R41	ENSG00000221855	47.6	15.9	1.63	2.55E-04
BTNL9	ENSG00000165810	618.8	57.5	3.42	2.93E-04
GPIHBP1	ENSG00000277494	150.4	34.2	2.13	3.09E-04
NTRK2	ENSG00000148053	163.4	48.9	1.74	3.57E-04
SCD5	ENSG00000145284	105.8	228.1	-1.11	3.84E-04
PCDHAC2	ENSG00000243232	57.7	137.4	-1.25	4.25E-04
CYP1B1	ENSG00000138061	474.1	181.0	1.39	4.69E-04
PCDHA3	ENSG00000255408	28.8	69.3	-1.26	5.34E-04
PCDHA7	ENSG00000204963	29.1	68.3	-1.23	5.46E-04
BHLHE41	ENSG00000123095	234.7	526.1	-1.17	5.78E-04
LRP5L	ENSG00000100068	97.6	45.8	1.09	6.70E-04
PCDHA11	ENSG00000249158	28.3	66.8	-1.24	7.28E-04
PCDHA2	ENSG00000204969	27.7	66.5	-1.26	7.28E-04
PCDHA1	ENSG00000204970	27.9	66.5	-1.25	9.26E-04
UBXN10	ENSG00000162543	25.4	58.6	-1.22	9.79E-04
PCDHA6	ENSG00000081842	28.4	66.8	-1.24	9.86E-04
TGFA	ENSG00000163235	29.9	64.1	-1.09	1.05E-03
APLN	ENSG00000171388	923.6	2392.6	-1.37	1.20E-03
PCDHAC1	ENSG00000248383	28.4	69.2	-1.29	1.23E-03
PCDHA4	ENSG00000204967	29.4	69.8	-1.25	1.25E-03
PCDHA8	ENSG00000204962	28.7	67.0	-1.22	1.72E-03
CD28	ENSG00000178562	238.5	493.7	-1.05	1.76E-03
PCDHA12	ENSG00000251664	28.5	66.8	-1.23	1.99E-03
PCDHA5	ENSG00000204965	28.7	66.6	-1.21	2.01E-03
CD209	ENSG00000090659	353.9	860.4	-1.28	2.01E-03
PCDHA9	ENSG00000204961	29.3	66.6	-1.18	2.21E-03
GPR34	ENSG00000171659	242.6	505.7	-1.06	2.38E-03
FGF7	ENSG00000140285	71.8	156.8	-1.13	2.42E-03
TTPA	ENSG00000137561	32.1	98.5	-1.62	2.50E-03
FOXS1	ENSG00000179772	53.9	117.5	-1.12	2.63E-03
IGSF21	ENSG00000117154	15.2	41.0	-1.41	2.63E-03
CADM3	ENSG00000162706	377.8	1048.6	-1.48	2.63E-03
LMX1B	ENSG00000136944	62.6	1.7	5.15	2.96E-03
FCER1G	ENSG00000158869	114.9	249.6	-1.12	3.05E-03
GREM2	ENSG00000180875	741.9	309.2	1.26	3.05E-03
BCL6	ENSG00000113916	1145.5	529.9	1.11	3.23E-03
F13A1	ENSG00000124491	5341.2	10705.9	-1.00	3.43E-03
CX3CR1	ENSG00000168329	59.8	224.5	-1.90	3.52E-03
SPX	ENSG00000134548	33.4	146.2	-2.13	3.59E-03
ERVV-1	ENSG00000269526	1294.3	529.8	1.29	3.88E-03
TBC1D26	ENSG00000214946	54.9	8.5	2.69	3.91E-03
LINGO1	ENSG00000169783	98.4	288.2	-1.55	4.44E-03
PCDHA13	ENSG00000239389	30.0	67.4	-1.17	4.46E-03
MEX3B	ENSG00000183496	85.6	171.9	-1.00	4.87E-03
VCAM1	ENSG00000162692	297.7	651.4	-1.13	4.91E-03
CGB8	ENSG00000213030	831.9	78.2	3.41	5.08E-03
CYTL1	ENSG00000170891	44.0	155.9	-1.83	5.29E-03
CGB5	ENSG00000189052	1473.5	147.6	3.32	5.62E-03
COL21A1	ENSG00000124749	226.5	498.8	-1.14	5.66E-03

OLAH	ENSG00000152463	1392.0	571.6	1.28	5.73E-03
PCDHA10	ENSG00000250120	32.7	68.2	-1.07	5.97E-03
C9orf129	ENSG00000204352	24.4	53.1	-1.08	6.17E-03
SEMA5B	ENSG00000082684	41.0	88.2	-1.11	6.48E-03
CYP2S1	ENSG00000167600	18.9	45.9	-1.31	7.10E-03
GPR85	ENSG00000164604	39.8	79.4	-1.01	7.28E-03
TRIL	ENSG00000255690	47.7	107.4	-1.16	7.28E-03
LZTS1	ENSG00000061337	339.1	742.6	-1.13	8.77E-03
SLC28A1	ENSG00000156222	164.4	75.0	1.12	8.77E-03
MMP16	ENSG00000156103	65.6	153.0	-1.23	8.95E-03
CALHM4	ENSG00000164451	61.0	131.4	-1.11	9.25E-03
SELENBP1	ENSG00000143416	83.3	169.8	-1.03	9.62E-03
LRATD1	ENSG00000162981	442.5	918.1	-1.05	1.01E-02
CCL2	ENSG00000108691	89.4	272.4	-1.60	1.12E-02
PGM5	ENSG00000154330	58.8	123.8	-1.07	1.16E-02
KRT6A	ENSG00000205420	71.9	1.5	5.60	1.17E-02
FAM107B	ENSG00000065809	2905.7	1252.4	1.21	1.18E-02
EGR2	ENSG00000122877	36.4	104.4	-1.53	1.19E-02
C3orf70	ENSG00000187068	160.5	333.6	-1.05	1.25E-02
DNAH6	ENSG00000115423	23.3	46.2	-1.00	1.30E-02
ITGB6	ENSG00000115221	158.8	317.2	-1.00	1.40E-02
INHA	ENSG00000123999	974.6	390.2	1.32	1.43E-02
NUTM2G	ENSG00000188152	32.6	15.1	1.09	1.49E-02
CYSLTR1	ENSG00000173198	34.5	82.2	-1.27	1.49E-02
SCYGR4	ENSG00000284631	27.4	76.5	-1.47	1.49E-02
MEGF10	ENSG00000145794	14.5	44.1	-1.60	1.55E-02
GSAP	ENSG00000186088	397.0	195.0	1.03	1.67E-02
RARRES2	ENSG00000106538	63.2	144.4	-1.20	1.71E-02
LAMB4	ENSG00000091128	144.3	308.1	-1.09	1.75E-02
HSD3B2	ENSG00000203859	11.6	30.4	-1.44	1.83E-02
PLIN2	ENSG00000147872	6100.8	2681.7	1.19	1.87E-02
NEK11	ENSG00000114670	306.1	146.0	1.06	1.89E-02
SLC4A1	ENSG00000004939	101.0	276.0	-1.45	1.89E-02
ERC2	ENSG00000187672	21.6	50.4	-1.22	1.90E-02
CXCL2	ENSG00000081041	12.7	31.2	-1.28	1.90E-02
PAGE4	ENSG00000101951	412.7	887.3	-1.11	1.92E-02
RNF150	ENSG00000170153	96.6	196.3	-1.02	1.96E-02
KL	ENSG00000133116	944.0	1919.0	-1.02	1.98E-02
NPFFR2	ENSG00000056291	166.3	57.8	1.54	2.03E-02
NUDT19	ENSG00000213965	160.9	335.4	-1.06	2.13E-02
PHYHIP	ENSG00000168490	247.3	93.5	1.40	2.15E-02
STAB2	ENSG00000136011	68.4	30.3	1.18	2.25E-02
MYBPH	ENSG00000133055	174.7	86.4	1.02	2.31E-02
ARNT2	ENSG00000172379	224.5	78.9	1.51	2.33E-02
EBI3	ENSG00000105246	14920.1	7127.3	1.07	2.36E-02
SRRM3	ENSG00000177679	101.7	34.2	1.56	2.42E-02
QPCT	ENSG00000115828	70.7	28.0	1.36	2.48E-02
ATP13A4	ENSG00000127249	38.6	12.2	1.70	2.58E-02
PTGFR	ENSG00000122420	105.3	265.8	-1.34	2.65E-02
TCL1B	ENSG00000213231	63.6	23.1	1.46	2.72E-02
TM4SF1	ENSG00000169908	675.3	1365.1	-1.02	2.76E-02
KIAA1211	ENSG00000109265	149.9	319.6	-1.09	2.86E-02
ALAS2	ENSG00000158578	123.9	335.8	-1.44	3.12E-02
SLC7A10	ENSG00000130876	72.4	8.2	3.16	3.13E-02
OR51E1	ENSG00000180785	75.6	174.3	-1.20	3.15E-02
ALPG	ENSG00000163286	124.2	45.7	1.44	3.15E-02
CYP2A7	ENSG00000198077	46.9	13.6	1.77	3.18E-02
NA	ENSG00000276410	30.3	77.8	-1.36	3.26E-02
HEMGN	ENSG00000136929	31.7	100.6	-1.67	3.46E-02
TMEM200A	ENSG00000164484	17.3	42.9	-1.32	3.49E-02
FCGBP	ENSG00000275395	1561.9	5303.7	-1.76	3.52E-02
HTRA4	ENSG00000169495	4428.1	837.7	2.40	3.59E-02
SYNPR	ENSG00000163630	87.5	20.1	2.12	3.59E-02
RNF180	ENSG00000164197	13.9	28.8	-1.05	3.60E-02
IL1RN	ENSG00000136689	22.9	46.9	-1.01	3.61E-02
PI16	ENSG00000164530	17.5	67.0	-1.95	3.70E-02
AC008687.4	ENSG00000268655	38.2	11.1	1.76	3.75E-02
HAS2	ENSG00000170961	47.5	119.7	-1.33	3.90E-02
CBLC	ENSG00000142273	72.5	33.5	1.13	3.99E-02
MUC1	ENSG00000185499	468.5	140.9	1.74	4.02E-02

KRT86	ENSG00000170442	213.5	96.9	1.14	4.12E-02
OLFML1	ENSG00000183801	61.5	127.2	-1.04	4.46E-02
TMEM132B	ENSG00000139364	39.7	12.6	1.69	4.54E-02
AC098850.3	ENSG00000266302	12.8	53.9	-2.08	4.73E-02
FRZB	ENSG00000162998	919.1	2982.7	-1.70	4.73E-02
NA	ENSG00000276903	69.4	160.7	-1.21	4.77E-02
TNFRSF19	ENSG00000127863	106.1	217.3	-1.03	4.92E-02

Table 3.5 DEGs HPTs/Bulk placenta (Top 50)

Gene.name	GeneID	HPT_avg	Bulk_avg	L2FC	padj
CD93	ENSG00000125810	65.7	17555.8	-8.06	0.00E+00
MYLK	ENSG00000065534	82.9	5710.5	-6.10	1.73E-294
DLK1	ENSG00000185559	61.3	29232.0	-8.90	2.22E-289
PECAM1	ENSG00000261371	292.7	17711.8	-5.92	5.07E-286
CD34	ENSG00000174059	56.9	7131.5	-6.97	1.12E-283
TNS1	ENSG00000079308	356.1	9879.3	-4.79	6.89E-275
EGFL7	ENSG00000172889	36.8	3034.1	-6.37	1.05E-272
LRP6	ENSG00000070018	205.2	3265.2	-3.99	1.21E-250
MMRN2	ENSG00000173269	86.5	4465.1	-5.69	8.52E-247
KDR	ENSG00000128052	44.7	4674.5	-6.71	8.71E-230
LAMC3	ENSG00000050555	38.3	4887.3	-7.00	1.35E-217
XAGE2	ENSG00000155622	16253.1	621.4	4.71	2.64E-209
FAT4	ENSG00000196159	16.4	2324.1	-7.15	3.30E-207
GNG11	ENSG00000127920	25.7	3310.6	-7.01	5.43E-204
TCF4	ENSG00000196628	107.7	3831.0	-5.15	4.95E-202
TBX2	ENSG00000121068	139.3	4910.7	-5.14	8.45E-201
GJC1	ENSG00000182963	45.7	2965.0	-6.02	1.06E-200
CSHL1	ENSG00000204414	36.6	13196.4	-8.50	3.18E-191
A2M	ENSG00000175899	489.0	8750.4	-4.16	5.59E-191
LAMA2	ENSG00000196569	99.6	7990.6	-6.33	9.07E-190
GUCY1A2	ENSG00000152402	6.4	7344.7	-10.17	1.23E-187
TNFRSF1B	ENSG00000028137	19941.6	1876.8	3.41	1.08E-183
AFF2	ENSG00000155966	23.0	1916.4	-6.38	7.64E-180
DCHS1	ENSG00000166341	32.6	3111.3	-6.57	2.07E-179
EHD2	ENSG00000024422	30.6	2553.7	-6.39	1.36E-178
AGTR1	ENSG00000144891	22.9	2347.8	-6.69	1.39E-174
FLI1	ENSG00000151702	44.5	1296.9	-4.87	4.54E-174
FCGR2B	ENSG00000072694	11.2	2399.7	-7.75	1.94E-173
PTPRB	ENSG00000127329	35.2	3661.0	-6.70	2.24E-173
AC117378.1	ENSG00000285625	2063.7	28.0	6.21	2.42E-170
APLN	ENSG00000171388	18.8	3283.1	-7.46	5.06E-167
SHE	ENSG00000169291	15.1	1484.3	-6.62	3.06E-166
TTC28	ENSG00000100154	168.8	2101.8	-3.64	8.86E-163
ARHGAP26	ENSG00000145819	132.4	5507.5	-5.38	1.26E-162
TGIF1	ENSG00000177426	7950.0	990.4	3.01	4.26E-161
S1PR1	ENSG00000170989	20.1	1236.6	-5.94	1.47E-155
MEF2C	ENSG00000081189	35.7	1888.9	-5.72	3.84E-154
TSHZ1	ENSG00000179981	108.3	2023.6	-4.22	5.32E-150
SPARCL1	ENSG00000152583	106.7	4023.5	-5.24	4.50E-148
EEF1A1	ENSG00000156508	9809.2	1057.2	3.22	1.63E-146
NR2F1	ENSG00000175745	19.0	2841.0	-7.22	2.01E-146
CCNDBP1	ENSG00000166946	21429.3	1461.2	3.87	2.43E-146
ZBTB20	ENSG00000181722	200.4	3389.0	-4.08	4.38E-146
MARS	ENSG00000166986	8929.8	904.3	3.30	1.83E-144
PDE5A	ENSG00000138735	99.8	1425.5	-3.84	1.01E-143
C7	ENSG00000112936	34.5	6472.1	-7.55	1.14E-143
ITPKB	ENSG00000143772	113.5	1859.4	-4.03	6.25E-143
ADGRA2	ENSG00000020181	348.8	5379.4	-3.95	9.70E-143
F13A1	ENSG00000124491	2.9	14707.1	-12.30	6.82E-142
SYNM	ENSG00000182253	22.8	835.2	-5.19	3.16E-139

Table 3.6 DEGs Diff./Undiff. HPTs (Top 50)

Gene.name	GeneID	Diff_avg	Undiff_avg	L2FC	padj
ZFAT	ENSG00000066827	13542.5	3884.6	1.80	0.00E+00
TGFBR3	ENSG00000069702	14691.3	5028.2	1.55	0.00E+00
CDC6	ENSG00000094804	98.7	2046.3	-4.38	0.00E+00
SUMF2	ENSG00000129103	2905.2	695.5	2.06	0.00E+00
TBC1D5	ENSG00000131374	1662.4	216.8	2.94	0.00E+00
SLC30A2	ENSG00000158014	6043.9	42.4	7.16	0.00E+00
DEPP1	ENSG00000165507	16767.4	1964.2	3.09	0.00E+00
MCM7	ENSG00000166508	973.4	4807.6	-2.30	0.00E+00
DHCR7	ENSG00000172893	4274.8	184.2	4.54	0.00E+00
SFN	ENSG00000175793	45.0	2899.9	-6.02	0.00E+00
TCL1B	ENSG00000213231	4919.2	47.3	6.70	0.00E+00
LBH	ENSG00000213626	407.8	3795.1	-3.22	0.00E+00
LGALS13	ENSG00000105198	3981.3	60.4	6.04	4.69E-298
CDCA5	ENSG00000146670	47.0	857.0	-4.19	3.90E-293
FHDC1	ENSG00000137460	10601.9	2506.2	2.08	6.82E-293
ANLN	ENSG00000011426	168.2	2003.0	-3.57	1.87E-287
PCNA	ENSG00000132646	619.4	3000.1	-2.28	8.37E-287
HSPB1	ENSG00000106211	10068.8	2106.5	2.26	4.64E-280
SDC1	ENSG00000115884	33192.9	1471.7	4.50	5.77E-280
CCNDBP1	ENSG00000166946	11935.7	2956.6	2.01	3.16E-273
DPEP2	ENSG00000167261	1152.6	34.9	5.04	4.46E-270
TTC7B	ENSG00000165914	2163.5	253.5	3.10	1.92E-263
ADAMTS6	ENSG00000049192	1728.9	155.9	3.47	5.05E-263
CTSA	ENSG00000064601	6436.3	1958.8	1.72	5.73E-242
SMC4	ENSG00000113810	538.3	2024.2	-1.91	1.41E-228
CTNNAL1	ENSG00000119326	571.6	2867.3	-2.32	1.60E-226
INHA	ENSG00000123999	2925.9	250.9	3.54	3.00E-226
GCLM	ENSG00000023909	733.8	7405.7	-3.34	2.75E-225
ANO6	ENSG00000177119	5397.0	17931.8	-1.73	8.90E-224
ARL6IP1	ENSG00000170540	2479.0	9627.7	-1.96	1.37E-220
SPRR3	ENSG00000163209	18.6	1574.5	-6.40	2.39E-219
PLS1	ENSG00000120756	896.5	69.7	3.69	4.35E-218
DTL	ENSG00000143476	28.3	932.6	-5.03	2.24E-211
WLS	ENSG00000116729	1376.8	4075.5	-1.57	2.68E-210
LIMA1	ENSG00000050405	5421.2	22635.1	-2.06	3.10E-210
CDC25A	ENSG00000164045	23.9	725.4	-4.90	4.84E-209
CDT1	ENSG00000167513	30.3	513.8	-4.07	3.13E-205
PSMD11	ENSG00000108671	2585.1	5832.9	-1.17	4.74E-202
NDFIP2	ENSG00000102471	2440.0	6486.5	-1.41	6.81E-196
CLIC3	ENSG00000169583	5446.2	396.9	3.78	1.25E-195
ENG	ENSG00000106991	9423.0	885.0	3.41	4.80E-195
NAGK	ENSG00000124357	3637.0	987.8	1.88	1.13E-194
NA	ENSG00000187837	3805.8	331.3	3.52	1.17E-194
HOPX	ENSG00000171476	5546.9	228.6	4.60	5.99E-192
SLC9A7	ENSG00000065923	618.4	1990.4	-1.68	3.19E-191
ELMO1	ENSG00000155849	756.1	26.4	4.84	3.16E-186
NHLRC3	ENSG00000188811	2404.6	270.3	3.15	1.00E-185
C1orf115	ENSG00000162817	19614.1	4048.0	2.28	3.59E-185
SIDT2	ENSG00000149577	5690.7	1022.0	2.48	8.20E-184
JADE2	ENSG00000043143	4314.1	757.3	2.51	6.11E-183

Table 3.7. DEGs Forskolin/Control BeWo cells (Top 50)

Gene.name	GeneID	FSK.24h	FSK.48h	FSK.72h	FSK.avg	Ctrl.avg	L2FC	padj
WNT3A	ENSG00000154342	19861.9	23783.4	22143.8	21929.7	454.5	5.59	1.66E-170
OAF	ENSG00000184232	7563.0	8040.9	9505.9	8370.0	237.1	5.15	1.30E-68
PLS1	ENSG00000120756	748.5	628.2	585.9	654.2	6879.8	-3.39	1.73E-64
ST3GAL2	ENSG00000157350	386.4	363.9	349.2	366.5	2237.5	-2.61	9.03E-55
COL9A2	ENSG00000049089	151.7	125.3	127.8	134.9	1189.4	-3.14	1.59E-51
FIGNL2	ENSG00000261308	310.5	230.8	208.3	249.9	2932.2	-3.55	2.08E-48
CCL28	ENSG00000151882	118.3	113.4	94.7	108.8	950.4	-3.12	1.65E-46
FAM102B	ENSG00000162636	4597.3	5436.2	5794.0	5275.8	779.4	2.76	2.22E-44
GPRC5A	ENSG00000013588	368.2	273.2	221.3	287.6	4747.0	-4.04	3.64E-44
AKR1B10	ENSG00000198074	37.4	23.7	21.3	27.5	546.1	-4.31	5.59E-42
SLC15A2	ENSG00000163406	55.6	50.3	41.4	49.1	736.0	-3.90	6.27E-41
JPH2	ENSG00000149596	511.8	461.6	378.8	450.7	3073.6	-2.77	8.04E-40
GSDME	ENSG00000105928	165.9	150.9	118.4	145.0	1154.4	-2.99	3.38E-39
CD59	ENSG00000085063	14649.6	15348.0	16166.4	15388.0	4132.1	1.90	8.99E-38
PRR9	ENSG00000203783	2715.9	7702.6	5388.0	5268.8	118.4	5.48	1.56E-37
PRSS22	ENSG00000005001	253.9	267.3	253.3	258.2	1683.0	-2.70	6.95E-36
COLEC12	ENSG00000158270	5474.3	6161.1	6080.4	5905.3	1543.7	1.94	1.49E-35
OVOL1	ENSG00000172818	42941.4	55852.3	44166.9	47653.5	8023.2	2.57	2.05E-35
ACHE	ENSG00000087085	160.8	109.5	110.1	126.8	1317.1	-3.37	5.62E-35
TCF7L1	ENSG00000152284	56.6	38.5	33.1	42.8	800.0	-4.22	1.41E-33
KRT86	ENSG00000170442	1760.0	1893.6	1319.8	1657.8	173.3	3.25	3.17E-33
AL049629.2	ENSG00000284969	7003.7	7682.9	8321.1	7669.2	1828.1	2.07	1.43E-32
PLA2G15	ENSG00000103066	7607.5	6321.9	6416.6	6782.0	1575.5	2.11	5.74E-32
LIF	ENSG00000128342	112.3	89.7	86.4	96.1	683.9	-2.83	5.76E-31
NTN4	ENSG00000074527	167.9	137.1	129.0	144.7	905.2	-2.64	2.05E-30
FAM110A	ENSG00000125898	662.5	598.7	570.5	610.6	2411.9	-1.98	3.43E-30
RHOV	ENSG00000104140	1542.5	1032.6	1239.3	1271.5	142.7	3.16	1.28E-29
AC244197.3	ENSG00000241489	5219.4	5747.9	6636.8	5868.0	1359.1	2.11	3.25E-29
CRYBA2	ENSG00000163499	551.3	508.9	454.5	504.9	2063.0	-2.03	5.61E-29
IDS	ENSG00000010404	6680.0	7561.6	8685.7	7642.4	1714.6	2.16	5.61E-29
CABLES1	ENSG00000134508	497.7	432.0	404.8	444.8	1945.6	-2.13	6.90E-28
MTMR11	ENSG00000014914	251.9	259.4	224.9	245.4	1024.5	-2.06	9.77E-28
KCTD15	ENSG00000153885	208.4	141.0	125.5	158.3	1369.1	-3.11	2.83E-27
SYNE3	ENSG00000176438	1352.4	1307.8	1201.4	1287.2	5001.1	-1.96	9.79E-27
ATP8B2	ENSG00000143515	821.3	1241.7	661.7	908.2	68.0	3.74	1.15E-26
FGF18	ENSG00000156427	398.5	1037.5	616.7	684.3	10.0	6.06	2.20E-26
TP63	ENSG00000073282	424.8	537.5	452.2	471.5	2002.5	-2.09	3.94E-26
NR4A3	ENSG00000119508	1007.5	1402.4	2123.5	1511.1	103.5	3.87	5.89E-26
VTN	ENSG00000109072	665.6	765.3	699.5	710.1	167.3	2.09	2.05E-25
S100A16	ENSG00000188643	242.8	376.7	325.5	315.0	1995.9	-2.66	3.97E-25
VLDLR	ENSG00000147852	1634.6	1455.7	1474.8	1521.7	5170.9	-1.76	4.02E-25
GPR37	ENSG00000170775	638.3	715.0	642.7	665.3	2590.8	-1.96	1.13E-24
AL445423.3	ENSG00000286231	17719.6	14902.2	13591.9	15404.6	3882.2	1.99	1.62E-24
INSL4	ENSG00000120211	992.3	1586.9	1558.9	1379.3	135.5	3.34	2.34E-24
FAM222A	ENSG00000139438	1614.4	2083.9	1950.7	1883.0	440.5	2.10	2.44E-24
SP6	ENSG00000189120	89054.0	102984.1	70229.8	87422.6	17369.0	2.33	3.03E-24
ITGB6	ENSG00000115221	263.0	272.2	264.0	266.4	1109.3	-2.06	3.09E-24
SLC25A18	ENSG00000182902	110.3	101.6	72.2	94.7	735.6	-2.95	3.79E-24
HSD11B2	ENSG00000176387	5262.9	11219.6	5495.7	7326.0	501.2	3.87	3.79E-24
THEMIS2	ENSG00000130775	522.9	485.2	510.2	506.1	109.1	2.22	4.86E-24

Table 3.8. Primers

Primer Set ID	Forward	Reverse	Description	Reference
ENK-consensus	CTGAGGCAATTGCAGGAGTT	GCTGTCTCTTCGGAGCTGTT	Amplifies transcripts derived from several ERVK loci within the region encoding the TM envelope protein	Li et al [228]
ENK11q23.3	AGACGATCGCTGCCCTATCA	TGCTCTCCCTAGGCAAATAGGA	Amplifies transcripts derived specifically from ERVK11q23.3 within the region encoding the SU envelope protein	This study
HPRT1	GCTGAGGATTTGGAAAGGGT	CATCTCGAGCAAGACGTTCA	*HPRT1* gene	This study
IFNB1	CATCTATGAGATGCTCCAG	TTTTCCCCTGGTGAAATCTT	*IFNB1* gene	This study
IL6	GAAGATTCCAAAGATGTAGC	TTCTGCCAGTGCCTCTTTGC	*IL6* gene	This study
TNF	GGCCTGTACCTCATCTACT	TGATGGCAGAGAGGAGGT	*TNF* gene (TNFα)	This study
IL10	GCAGAGTGAAGACTTTCTTT	GGCATCACCTCCTCCAGGTA	*IL10* gene	This study

3.7 Authors' contributions

J.L.R, S.L.C. and L.C. designed research; J.L.R performed research; J.L.R., M.M, A.M. analyzed data; S.L.C. and L.C. supervised progress of research; and J.L.R wrote the chapter. S.L.C. and L.C. provided edits/comments to revise the chapter.

3.8 Acknowledgements

We thank T. Morgan for providing FFPE placental samples used for IHC; L. Myatt for help obtaining frozen human placental samples used for RNA-seq; A. Valent for providing frozen vials of HPTs; A. Frias for use of tissue culture facilities; A. Adey and A. Fields for the assistance and use of NextSeq500 sequencer; J. Hennebold and M. Murphy for use of their microscope facilities; S. Stadler, A. Adey, J. Sacha for insight and advice.

CHAPTER 4: Conclusions, Future Directions, and Clinical Applications

4.1 General Conclusions

Given the importance of the placenta to reproductive success and the shared characteristics of normal placentation to cancer metastasis and immunological diseases, the number of studies evaluating the molecular underpinnings of human placentation has significantly increased in recent years. These studies not only emphasize how crucial the early stages of placental development are for a successful pregnancy but also highlight the importance of viral-like ERV proteins during human placentation. In this dissertation, I have developed several resources to enable studies of early human placental development using the highly translatable rhesus animal model and investigated the expression and function of ERVK during human placentation. I believe that my work has made several contributions to not only placental research but also to the fields of comparative genomics and mobile DNA. First, I have generated the telomerase-immortalized rhesus first trimester trophoblast cell lines, iRP-D26 and iRP-D28A, which retain characteristics of both human and rhesus primary trophoblasts and should prove valuable for studying the early stages of primate placental development and fostering future rhesus *in vitro* and *in vivo* placental investigations. Since placental dysfunction is associated with major pregnancy-related diseases and many placental abnormalities are thought to arise during early pregnancy [2], these cell lines can be used to help elucidate the molecular and cellular processes underlying the early stages of placentation and the origin of these diseases. Secondly, our cross-species transcriptomic comparison between human and rhesus bulk placenta showed that while a majority of genes are similarly expressed between the two species, certain genes are differentially expressed between human and rhesus placenta. These results suggest that rhesus is a suitable surrogate for most investigations of human placentation; however, notable molecular differences related to EVT function and preeclampsia are present and should be further investigated in future cross-species

placental studies. Additionally, the comprehensive list of differentially expressed genes identified between human and rhesus placenta will aid future rhesus-based translational investigations as well as evolutionary studies of primate placentation. Finally, the finding that ERVK11q23.3 is upregulated in human preterm placenta and modulates expression of type I interferon genes when knocked down in trophoblast cells is pivotal considering that activation of the antiviral type I IFN response can increase susceptibility to inflammation-induced preterm birth [373]. In the future, I think that ERVK11q23.3 will prove to be an important player in the antiviral immune response during normal and abnormal human placentation. Overall, investigation of ERV activity and integration of the highly-translatable rhesus macaque animal model into human placental studies, similar to the work presented here, should enhance our understanding of human placentation and may provide novel therapeutic and diagnostic approaches for pregnancy-related diseases.

4.2 Future Directions

I believe the work presented in this dissertation provides a strong foundation for several future experiments and studies, which I have outlined below.

4.2.1 Chapter 2: Transcriptomic analysis of primate placentas and novel rhesus trophoblast cell lines informs investigations of human placentation

1. Since our cross-species comparison of human and rhesus bulk placental tissue revealed significant expression differences of several well-known human trophoblast subtype markers, *it would be important to identify whether these gene expression differences reflect expression level differences between specific human and rhesus trophoblasts subtypes (eg. human EVTs express higher levels of ADAM12 compared to rhesus EVTs), or trophoblast subtype quantity differences between the two species (eg. the human placenta contains a greater number of EVTs compared to the rhesus placenta)*. This could be accomplished via a comparison of human and rhesus placenta single-cell RNA-seq data. This type of analysis

could also be used to address the following unanswered questions that are emphasized by our work: *Are all human trophoblast subtypes also present in rhesus placenta? Are there trophoblast subtypes unique to human and/or rhesus? Are trophoblast subtypes present in equal numbers across human and rhesus placenta tissue? What are the inherent molecular differences between human and rhesus EVTs, CTBs, and STBs?*

2. While evolutionary changes likely account for some of the gene expression differences identified between human and rhesus placenta, examination of additional non-human primate placental samples is required before such conclusions can be made and the following questions can be addressed: *What aspects of human placentation are truly unique to human? Do these human-specific aspects contribute to increased susceptibility of pregnancy complications in human? Can rhesus trophoblasts be humanized to recapitulate these unique aspects?*
3. Since several well-known human EVT markers were significantly downregulated in rhesus compared to human placenta and our novel EVT-like immortalized rhesus trophoblast cell lines exhibited only low levels of invasion, this suggests that rhesus EVTs are less invasive than human EVTs. This is further supported by examination of *ADAM12* expression between human and rhesus trophoblast cells, which is known to promote trophoblast cell invasion when spliced into a short secreted (*ADAM12S*) isoform [45]. While abundant expression of the *ADAM12S* isoform was observed from human trophoblast samples, negligible expression of this isoform was observed within rhesus primary and/or immortalized trophoblast cell cultures (**Figure 4.1**). Closer examination of non-human primate mRNA sequences and gene annotations (NCBI RefSeq) suggests that the *ADAM12S* isoform is unique to human, chimp, bonobo, and gorilla, and is not expressed by orangutan, gibbon, or rhesus. However, in these species, the splice donor and acceptor sequences do not appear to be missing or altered; thus, it is currently unclear what recent molecular-evolutionary changes caused the expression of the *ADAM12S* isoform (data not

shown). *To determine whether human trophoblasts are truly more invasive than rhesus, future investigations directly comparing the invasion levels of human and rhesus primary EVTs should be performed*. Additionally, *rhesus trophoblast invasion levels with and without ADAM12S expression should be investigated, to specifically address the role of ADAM12 expression on rhesus trophoblast invasion*.

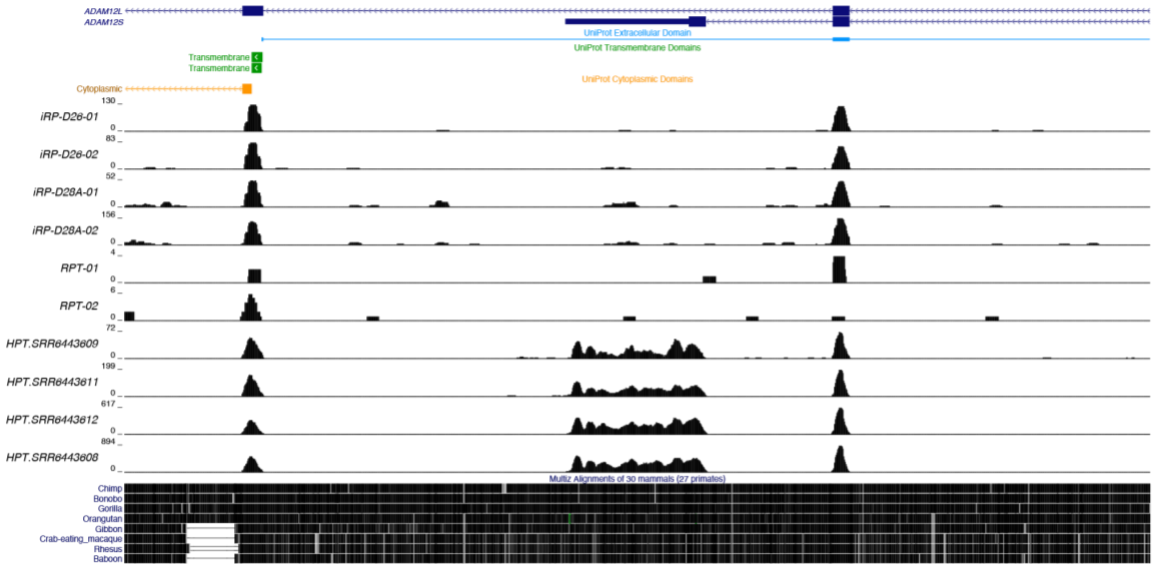

Figure 4.1 ADAM12 gene expression across human and rhesus trophoblast cells.

UCSC genome browser of ADAM12 gene. The top track depicts two alternatively spliced isoforms, ADAM12L (top) and ADAM12S (bottom). The short secreted (ADAM12S) alternatively spliced isoform of ADAM12 promotes trophoblast cell invasion, while the long transmembrane isoform (ADAM12L) does not. Human primary trophoblast (HPT) cell samples (bottom four tracks) show abundant expression of the ADAM12S isoform, while rhesus primary trophoblast (RPT) and immortalized rhesus trophoblast (iRP-D26 and iRP-D28A) samples appear to only express the ADAM12L isoform. All human and rhesus RNA-seq samples were mapped to hg38 using bowtie2 and visualized using the UCSC genome browser.

4.2.2 Chapter 3: Investigation of ERVK expression and function in placentation

1. Because the ERVK11q23.3 envelope ORF lacks the epitope of the monoclonal antibody used throughout the study, we were unable to determine whether this locus encodes an envelope protein. Thus, in future investigations, it would be important *to determine whether this locus encodes an envelope protein and if the antiviral immune response observed in HPTs is driven by the presence of RNA and/or protein from this particular locus.* This could be accomplished using an alternative antibody that specifically recognizes the predicted ERVK11q23.3 protein sequence, or via transfection of an expression construct that would encode a tagged or fluorescently-labeled ERVK11q23.3 envelope protein. Alternatively, CRISPR could be used to edit the native ERVK11q23.3 locus to encode a tagged or fluorescently labeled envelope protein. Further, if ERVK11q23.3 is found to encode an envelope protein, an antibody or fluorescently-tagged protein should be used to examine the envelope protein distribution before and after siRNA knockdown. Not only would this type of analysis validate the knockdown experiments, closer examination of its protein distribution would provide further insight into its putative function.
2. Our locus-specific ERVK expression analysis revealed numerous placentally transcribed ERVK loci. Since ERV viral-like proteins are known to play important functional roles during mammalian placentation, it would be important *to identify whether any of these transcribed loci also encoded viral-like proteins and to further characterize those potential proteins*. Thus, these results should be used as the foundation for future investigations aimed at addressing the following questions: *Which placentally-transcribed ERVK loci express an envelope protein? For each ERVK envelope protein expressed, where is it located (cell type and subcellular localization)? Does it contain functional FP and/or ISU domains? Which placentally-transcribed ERVK loci express other viral-like proteins (gag, pro, pol)?* Many of these questions could be addressed via the expression of tagged/labeled

ERVK envelope proteins using the same techniques discussed in the previous point. Additionally, since several placentally-expressed ERVK loci were found to contain partial or full-length envelope ORFs possessing the epitope of the monoclonal antibody used in this study, it would be valuable *to identify the precise ERVK loci and coding sequence contributing to the ERVK envelope protein expression observed via IHC and IF staining.*

3. Several ERVK loci highly expressed in HPTs were not detected within bulk placental samples, including ERVK12q14.1, which was shown to be significantly upregulated in HPTs compared to bulk placenta and in undifferentiated compared to differentiated HPTs. Unlike ERVK11q23.3, ERVK12q14.1 contains a full-length envelope ORF and is predicted to encode an ERVK protein possessing a membrane spanning region and antibody epitope. Based on these characteristics, I suspect that the ERVK IF staining observed along the membrane of mononuclear HPTs is likely derived from this locus and may facilitate trophoblast fusion. Since ERVK12q14.1 expression was not detected within any of the BeWo samples examined, its putative role is likely enhanced or specific to HPTs. This was the case for cell fusion, which we show occurs much more in HPTs compared to forskolin-treated BeWo cells. *In order to assess its putative fusogenic role, a similar siRNA KD approach specifically targeting the ERVK12q14.1 locus within HPTs cells and/or an overexpression approach in BeWo cells should be used*.
4. *It is unclear whether downregulation of TLR7 expression in the preterm placenta contributes to the upregulation of ERVK11q23.3 or vice versa*. Thus, in future studies, it would be important to examine *TLR7* gene expression levels within ERVK11q23.3 knockdown vs. control HPT samples, as well as ERVK11q23.3 expression levels in *TLR7* knockdown vs. control HPTs.
5. *To confirm that knockdown of ERVK11q23.3 decreases the antiviral interferon response in HPTs,* additional markers of type I IFN signaling should be examined. Thus, in addition to *IFNB1*, the expression level of *STAT1*, *IRF9*, and other interferon-stimulated genes

(ISGs) should be analyzed. Further, since ERVK11q23.3 expression is upregulated in preterm placentas and heightened type I IFN immune response can contribute to preterm birth, *the effect of ERVK11q23.3 overexpression on the antiviral interferon response should be examined in vitro using trophoblast cells, as well as in vivo using the rhesus animal model.* In order *to determine whether the immunomodulatory effects are specific to the ERVK11q23.3 locus or shared among other ERVK loci*, it would be important to target additional placentally-expressed ERVK loci and assess immunoregulatory function following knockdown or overexpression experiments.

4.3 Clinical Applications

Besides providing a firm basis for future research and experiments, the findings presented in this dissertation may also help develop new approaches for the diagnosis and treatment of pregnancy-related diseases. Previous studies have shown that compared to rhesus, the human placenta shows a notable increase in the extent and depth of EVT trophoblast invasion [4]. In humans, defective deep placentation or inadequate trophoblast invasion is highly associated with a number of obstetrical syndromes, including intrauterine growth restriction (IUGR), preeclampsia, preterm birth, and spontaneous abortions [2]. Since many of these pregnancy complications occur much less frequently or not at all in rhesus and other non-human primates [126-130], this suggests that molecular differences underlying increased EVT invasion in humans may also increase susceptibility to pregnancy-related disease. This is further supported by the results from our cross-species transcriptomic comparison, which showed that a significant number of preeclampsia-associated genes were upregulated in human compared to rhesus placenta. For instance, we show that *LGALS13* is significantly upregulated in human compared to rhesus placenta. This gene encodes galectin-13 (PP13), which interacts with glycoproteins and glycolipids to facilitate the expansion of uterine arteries and veins during pregnancy in an endothelial cell-dependent manner

via the eNOS and prostaglandin signaling pathways [313]. While the lower expression of *LGALS13* in rhesus placenta may underlie differences in the extent and depth of EVT invasion or represent an alternative mechanism for uterine vessel expansion other than spiral artery remodeling, downregulation of *LGALS13* in preeclampsia and other pregnancy disorders is thought to contribute to aberrant uteroplacental blood flow [272,314]. The PP13 protein is uniquely expressed by the placenta and can be detected in maternal blood [377]. Therefore, the detection of PP13 in maternal serum might also be a reliable predictive/diagnostic marker for pathological conditions such as preeclampsia. In addition to PP13, we suspect that there are other markers within our human-upregulated DEG set that may prove valuable for the detection and treatment of preeclampsia and other pregnancy complications.

Our finding that ERVK11q23.3 is upregulated in the preterm placenta and modulates expression of type I interferon genes when knocked down in trophoblast cells has clinical implications considering that activation of the antiviral type I IFN response can increase susceptibility to inflammation-induced preterm birth [373]. Studies directed to determine if placental ERVK11q23.3 protein expression can be detected in maternal blood could help develop a novel diagnostic marker for an increased risk of preterm birth and potentially other pregnancy complications. Additionally, since ERVK11q23.3 expression appears to be an important modulator of the antiviral immune response, therapeutics targeting ERVK11q23.3 expression may provide relief from pregnancy complications and other diseases associated with an overactive antiviral type I IFN response. However, thorough interrogation of the ERVK11q23.3 locus is necessary before its use in clinical applications can be assessed.

REFERENCES

1. Scott CL, Chavez GF, Atrash HK, Taylor DJ, Shah RS, Rowley D. Hospitalizations for severe complications of pregnancy, 1987-1992. *Obstet Gynecol*. 90(2), 225–229 (1997).
2. Brosens I, Pijnenborg R, Vercruysse L, Romero R. The "Great Obstetrical Syndromes" are associated with disorders of deep placentation. *Am J Obstet Gynecol*. 204(3), 193–201 (2011).
3. Ramsey EM, Harris JW. Comparison of uteroplacental vasculature and circulation in the rhesus monkey and man. *Carnegie Contrib Embryol*. 38, 59–70 (1966).
4. Ramsey EM, Houston ML, Harris JW. Interactions of the trophoblast and maternal tissues in three closely related primate species. *Am J Obstet Gynecol*. 124(6), 647–652 (1976).
5. Ellinwood WE, Stanczyk FZ, Lazur JJ, Novy MJ. Dynamics of steroid biosynthesis during the luteal placental shift in rhesus monkeys. *J Clin Endocrinol Metab*. 69(2), 348–355 (1989).
6. Blankenship TN, Enders AC. Modification of uterine vasculature during pregnancy in macaques. *Microsc. Res. Tech.* 60(4), 390–401 (2003).
7. King BF, Blankenship TN. Differentiation of the chorionic plate of the placenta: cellular and extracellular matrix changes during development in the macaque. *Anat. Rec.* 240(2), 267–276 (1994).
8. Mager DL, Stoye JP. Mammalian Endogenous Retroviruses. *Microbiology Spectrum*. 3(1), MDNA3–0009–2014 (2015).
9. Meyer TJ, Rosenkrantz JL, Carbone L, Chavez SL. Endogenous Retroviruses: With Us and against Us. *Frontiers in Chemistry*. 5, 23 (2017).
10. Kämmerer U, Germeyer A, Stengel S, Kapp M, Denner J. Human endogenous retrovirus K (HERV-K) is expressed in villous and extravillous cytotrophoblast cells of the human placenta. *J. Reprod. Immunol.* 91(1-2), 1–8 (2011).
11. Simpson GR, Patience C, Löwer R, *et al.* Endogenous D-type (HERV-K) related sequences are packaged into retroviral particles in the placenta and possess open reading frames for reverse transcriptase. *Virology*. 222(2), 451–456 (1996).
12. Andersson A-C, Venables PJW, Tönjes RR, Scherer J, Eriksson L, Larsson E. Developmental Expression of HERV-R (ERV3) and HERV-K in Human Tissue. *Virology*. 297(2), 220–225 (2002).
13. Grow EJ, Flynn RA, Chavez SL, *et al.* Intrinsic retroviral reactivation in human preimplantation embryos and pluripotent cells. *Nature*. 522(7555), 221–225 (2015).
14. Boyd JD, Hamilton WJ. The Human Placenta. Heffer & Sons Ltd.
15. Schlafke S, Enders AC. Cellular basis of interaction between trophoblast and uterus at implantation. *Biol Reprod*. 12(1), 41–65 (1975).
16. CLAVERO JA, BOTELLALLUSIA J. Measurement of the villus surface in normal and pathologic placentas. *Am J Obstet Gynecol*. 86, 234–240 (1963).
17. Benirschke K, Burton GJ, Baergen RN. Pathology of the human placenta. 6 ed.
18. Bulmer JN, Johnson PM, Sasagawa M, Takeuchi S. Immunohistochemical studies of fetal trophoblast and maternal decidua in hydatidiform mole and choriocarcinoma. *Placenta*. 9(2), 183–200 (1988).
19. Mühlhauser J, Crescimanno C, Kaufmann P, Höfler H, Zaccheo D, Castellucci M. Differentiation and proliferation patterns in human trophoblast revealed by c-erbB-2 oncogene product and EGF-R. *The Journal of Histochemistry \& Cytochemistry*. 41(2), 165–173 (1993).
20. Blankenship TN, King BF. Developmental expression of Ki-67 antigen and proliferating cell nuclear antigen in macaque placentas. *Dev. Dyn.* 201(4), 324–333 (1994).
21. Kaufmann P, Castellucci M. Extravillous trophoblast in the human placenta: A review. *Trophoblast Research*. 18, 21–65 (1997).

22. Simpson RA, Mayhew TM, Barnes PR. From 13 weeks to term, the trophoblast of human placenta grows by the continuous recruitment of new proliferative units: a study of nuclear number using the disector. *Placenta*. 13(5), 501–512 (1992).
23. Burton GJ, Jauniaux E. Sonographic, stereological and Doppler flow velocimetric assessments of placental maturity. *Br J Obstet Gynaecol*. 102(10), 818–825 (1995).
24. Kliman HJ, Strauss JF, Nestler JE, Sermasi E, Sanger JM. Purification, characterization, and in vitro differentiation of cytotrophoblasts from human term placentae. *Endocrinology*. 118(4), 1567–1582 (1986).
25. Wang R, Dang Y-L, Zheng R, *et al.* Live cell imaging of in vitro human trophoblast syncytialization. *Biol Reprod*. 90(6), 117 (2014).
26. Knight M, Redman CW, Linton EA, Sargent IL. Shedding of syncytiotrophoblast microvilli into the maternal circulation in pre-eclamptic pregnancies. *Br J Obstet Gynaecol*. 105(6), 632–640 (1998).
27. Oudejans CBM, Tjoa ML, Westerman BA, Mulders MAM, Van Wijk IJ, Van Vugt JMG. Circulating trophoblast in maternal blood. *Prenat. Diagn.* 23(2), 111–116 (2003).
28. Palmer ME, Watson AL, Burton GJ. Morphological analysis of degeneration and regeneration of syncytiotrophoblast in first trimester placental villi during organ culture. *Human Reproduction*. 12(2), 379–382 (1997).
29. Simán CM, Sibley CP, Jones CJ, Turner MA, Greenwood SL. The functional regeneration of syncytiotrophoblast in cultured explants of term placenta. *Am. J. Physiol. Regul. Integr. Comp. Physiol.* 280(4), R1116–22 (2001).
30. Teasdale F, Jean-Jacques G. Morphometric evaluation of the microvillous surface enlargement factor in the human placenta from mid-gestation to term. *Placenta*. 6(5), 375–381 (1985).
31. Jones CJP, Harris LK, Whittingham J, Aplin JD, Mayhew TM. A re-appraisal of the morphophenotype and basal lamina coverage of cytotrophoblasts in human term placenta. *Placenta*. 29(2), 215–219 (2008).
32. Kalter SS, Helmke RJ, Heberling RL, *et al.* Brief communication: C-type particles in normal human placentas. *J Natl Cancer Inst*. 50(4), 1081–1084 (1973).
33. Lyden TW, Johnson PM, Mwenda JM, Rote NS. Ultrastructural characterization of endogenous retroviral particles isolated from normal human placentas. *Biol Reprod*. 51(1), 152–157 (1994).
34. Murphy VE, Smith R, Giles WB, Clifton VL. Endocrine regulation of human fetal growth: the role of the mother, placenta, and fetus. *Endocr. Rev.* 27(2), 141–169 (2006).
35. Roopenian DC, Akilesh S. FcRn: the neonatal Fc receptor comes of age. *Nat. Rev. Immunol.* 7(9), 715–725 (2007).
36. Jennewein MF, Goldfarb I, Dolatshahi S, *et al.* Fc Glycan-Mediated Regulation of Placental Antibody Transfer. *Cell*. 178(1), 202–215.e14 (2019).
37. Hunt JS, Fishback JL, Chumbley G, Loke YW. Identification of class I MHC mRNA in human first trimester trophoblast cells by in situ hybridization. *J Immunol*. 144(11), 4420–4425 (1990).
38. Hunt JS, Hsi BL, King CR, Fishback JL. Detection of class I MHC mRNA in subpopulations of first trimester cytotrophoblast cells by in situ hybridization. *J. Reprod. Immunol.* 19(3), 315–323 (1991).
39. Hammer A, Hutter H, Dohr G. HLA class I expression on the materno-fetal interface. *American journal of reproductive immunology (New York, N.Y.)*. 38(3), 150–157 (1997).
40. Whitley GSJ, Cartwright JE. Cellular and molecular regulation of spiral artery remodelling: lessons from the cardiovascular field. *Placenta*. 31(6), 465–474 (2010).
41. Ellis SA, Palmer MS, McMichael AJ. Human trophoblast and the choriocarcinoma cell line BeWo express a truncated HLA Class I molecule. *J Immunol*. 144(2), 731–735 (1990).

42. Damsky CH, Fitzgerald ML, Fisher SJ. Distribution patterns of extracellular matrix components and adhesion receptors are intricately modulated during first trimester cytotrophoblast differentiation along the invasive pathway, in vivo. *J Clin Invest*. 89(1), 210–222 (1992).
43. Pollheimer J, Loregger T, Sonderegger S, *et al.* Activation of the canonical wingless/T-cell factor signaling pathway promotes invasive differentiation of human trophoblast. *The American journal of pathology*. 168(4), 1134–1147 (2006).
44. Biadasiewicz K, Fock V, Dekan S, *et al.* Extravillous trophoblast-associated ADAM12 exerts pro-invasive properties, including induction of integrin beta 1-mediated cellular spreading. *Biol Reprod*. 90(5), 101 (2014).
45. Aghababaei M, Perdu S, Irvine K, Beristain AG. A disintegrin and metalloproteinase 12 (ADAM12) localizes to invasive trophoblast, promotes cell invasion and directs column outgrowth in early placental development. *Mol. Hum. Reprod.* 20(3), 235–249 (2014).
46. Pijnenborg R, Dixon G, Robertson WB, Brosens I. Trophoblastic invasion of human decidua from 8 to 18 weeks of pregnancy. *Placenta*. 1(1), 3–19 (1980).
47. Pijnenborg R, Bland JM, Robertson WB, Brosens I. Uteroplacental arterial changes related to interstitial trophoblast migration in early human pregnancy. *Placenta*. 4(4), 397–413 (1983).
48. Fisher SJ, Damsky CH. Human cytotrophoblast invasion. *Semin Cell Biol*. 4(3), 183–188 (1993).
49. Pijnenborg R, Vercruysse L, Hanssens M. The uterine spiral arteries in human pregnancy: facts and controversies. *Placenta*. 27(9-10), 939–958 (2006).
50. Mor G, Aldo P, Alvero AB. The unique immunological and microbial aspects of pregnancy. *Nat. Rev. Immunol.* 17(8), 469–482 (2017).
51. Kovats S, Main EK, Librach C, Stubblebine M, Fisher SJ, DeMars R. A class I antigen, HLA-G, expressed in human trophoblasts. *Science*. 248(4952), 220–223 (1990).
52. McMaster MT, Librach CL, Zhou Y, *et al.* Human placental HLA-G expression is restricted to differentiated cytotrophoblasts. *J Immunol*. 154(8), 3771–3778 (1995).
53. Rouas-Freiss N, Gonçalves RM, Menier C, Dausset J, Carosella ED. Direct evidence to support the role of HLA-G in protecting the fetus from maternal uterine natural killer cytolysis. *Proc Natl Acad Sci USA*. 94(21), 11520–11525 (1997).
54. Münz C, Holmes N, King A, *et al.* Human histocompatibility leukocyte antigen (HLA)-G molecules inhibit NKAT3 expressing natural killer cells. *J Exp Med*. 185(3), 385–391 (1997).
55. Ponte M, Cantoni C, Biassoni R, *et al.* Inhibitory receptors sensing HLA-G1 molecules in pregnancy: decidua-associated natural killer cells express LIR-1 and CD94/NKG2A and acquire p49, an HLA-G1-specific receptor. *Proc Natl Acad Sci USA*. 96(10), 5674–5679 (1999).
56. Borrego F, Ulbrecht M, Weiss EH, Coligan JE, Brooks AG. Recognition of human histocompatibility leukocyte antigen (HLA)-E complexed with HLA class I signal sequence-derived peptides by CD94/NKG2 confers protection from natural killer cell-mediated lysis. *J Exp Med*. 187(5), 813–818 (1998).
57. King A, Boocock C, Sharkey AM, *et al.* Evidence for the expression of HLAA-C class I mRNA and protein by human first trimester trophoblast. *J Immunol*. 156(6), 2068–2076 (1996).
58. King A, Allan DS, Bowen M, *et al.* HLA-E is expressed on trophoblast and interacts with CD94/NKG2 receptors on decidual NK cells. *European journal of immunology*. 30(6), 1623–1631 (2000).
59. Hanna J, Bechtel P, Zhai Y, Youssef F, McLachlan K, Mandelboim O. Novel insights on human NK cells' immunological modalities revealed by gene expression profiling. *J Immunol*. 173(11), 6547–6563 (2004).

60. Hanna J, Goldman-Wohl D, Hamani Y, *et al.* Decidual NK cells regulate key developmental processes at the human fetal-maternal interface. *Nat Med*. 12(9), 1065–1074 (2006).
61. Burton GJ, Woods AW, Jauniaux E, Kingdom JCP. Rheological and Physiological Consequences of Conversion of the Maternal Spiral Arteries for Uteroplacental Blood Flow during Human Pregnancy. *Placenta*. 30(6), 473–482 (2009).
62. Collins SL, Birks JS, Stevenson GN, Papageorghiou AT, Noble JA, Impey L. Measurement of spiral artery jets: General principles and differences observed in small-for-gestational-age pregnancies. *Ultrasound in Obstetrics and Gynecology*. 40(2), 171–178 (2012).
63. Espinoza J, Romero R, Mee Kim Y, *et al.* Normal and abnormal transformation of the spiral arteries during pregnancy. *J Perinat Med*. 34(6), 447–458 (2006).
64. Brosens IA, Robertson WB, Dixon HG. The role of the spiral arteries in the pathogenesis of preeclampsia. *Obstet Gynecol Annu*. 1, 177–191 (1972).
65. Brosens I, Dixon HG, Robertson WB. Fetal growth retardation and the arteries of the placental bed. *Br J Obstet Gynaecol*. 84(9), 656–663 (1977).
66. Khong TY, De Wolf F, Robertson WB, Brosens I. Inadequate maternal vascular response to placentation in pregnancies complicated by pre-eclampsia and by small-for-gestational age infants. *Br J Obstet Gynaecol*. 93(10), 1049–1059 (1986).
67. Ball E, Bulmer JN, Ayis S, Lyall F, Robson SC. Late sporadic miscarriage is associated with abnormalities in spiral artery transformation and trophoblast invasion. *J. Pathol.* 208(4), 535–542 (2006).
68. Kim YM, Chaiworapongsa T, Gomez R, *et al.* Failure of physiologic transformation of the spiral arteries in the placental bed in preterm premature rupture of membranes. *Am J Obstet Gynecol*. 187(5), 1137–1142 (2002).
69. Kim YM, Bujold E, Chaiworapongsa T, *et al.* Failure of physiologic transformation of the spiral arteries in patients with preterm labor and intact membranes. *Am J Obstet Gynecol*. 189(4), 1063–1069 (2003).
70. Gruenwald P. Fetal deprivation and placental pathology: concepts and relationships. *Perspect Pediatr Pathol*. 2, 101–149 (1975).
71. Easter SR, Eckert LO, Boghossian N, *et al.* Fetal growth restriction: Case definition & guidelines for data collection, analysis, and presentation of immunization safety data. Vaccine. 35(48 Pt A), 6546–6554 (2017).
72. Pilliod RA, Cheng YW, Snowden JM, Doss AE, Caughey AB. The risk of intrauterine fetal death in the small-for-gestational-age fetus. *Am J Obstet Gynecol*. 207(4), 318.e1–6 (2012).
73. Beckerath von A-K, Kollmann M, Rotky-Fast C, Karpf E, Lang U, Klaritsch P. Perinatal complications and long-term neurodevelopmental outcome of infants with intrauterine growth restriction. *Am J Obstet Gynecol*. 208(2), 130.e1–6 (2013).
74. Swanson AM, David AL. Animal models of fetal growth restriction: Considerations for translational medicine. *Placenta*. 36(6), 623–630 (2015).
75. Bamfo JEAK, Odibo AO. Diagnosis and management of fetal growth restriction. *J Pregnancy*. 2011, 640715 (2011).
76. Gerretsen G, Huisjes HJ, Elema JD. Morphological changes of the spiral arteries in the placental bed in relation to pre-eclampsia and fetal growth retardation. *Br J Obstet Gynaecol*. 88(9), 876–881 (1981).
77. Hanssens M, Pijnenborg R, Keirse MJ, Vercruysse L, Verbist L, van Assche FA. Renin-like immunoreactivity in uterus and placenta from normotensive and hypertensive pregnancies. *Eur. J. Obstet. Gynecol. Reprod. Biol.* 81(2), 177–184 (1998).
78. Kadyrov M, Kingdom JCP, Huppertz B. Divergent trophoblast invasion and apoptosis in placental bed spiral arteries from pregnancies complicated by maternal anemia and early-

onset preeclampsia/intrauterine growth restriction. *Am J Obstet Gynecol*. 194(2), 557–563 (2006).
79. Lyall F, Robson SC, Bulmer JN. Spiral artery remodeling and trophoblast invasion in preeclampsia and fetal growth restriction: relationship to clinical outcome. *Hypertension*. 62(6), 1046–1054 (2013).
80. Zuckerwise L, Li J, Lu L, *et al.* H19 long noncoding RNA alters trophoblast cell migration and invasion by regulating TβR3 in placentae with fetal growth restriction. *Oncotarget*. 7(25), 38398–38407 (2016).
81. Rigano S, Bozzo M, Ferrazzi E, Bellotti M, Battaglia FC, Galan HL. Early and persistent reduction in umbilical vein blood flow in the growth-restricted fetus: a longitudinal study. *Am J Obstet Gynecol*. 185(4), 834–838 (2001).
82. Baschat AA. Fetal responses to placental insufficiency: an update. *BJOG*. 111(10), 1031–1041 (2004).
83. Tranquilli AL, Dekker G, Magee L, *et al.* The classification, diagnosis and management of the hypertensive disorders of pregnancy: A revised statement from the ISSHP. *Pregnancy Hypertens*. 4(2), 97–104 (2014).
84. Ananth CV, Keyes KM, Wapner RJ. Pre-eclampsia rates in the United States, 1980-2010: age-period-cohort analysis. *BMJ*. 347, f6564 (2013).
85. Saleem S, McClure EM, Goudar SS, *et al.* A prospective study of maternal, fetal and neonatal deaths in low- and middle-income countries. *Bull World Health Organ*. 92(8), 605–612 (2014).
86. MacKay AP, Berg CJ, Atrash HK. Pregnancy-related mortality from preeclampsia and eclampsia. *Obstet Gynecol*. 97(4), 533–538 (2001).
87. Milne F, Redman C, Walker J, *et al.* The pre-eclampsia community guideline (PRECOG): how to screen for and detect onset of pre-eclampsia in the community. BMJ. 330(7491), 576–580 (2005).
88. Arulkumaran N, Lightstone L. Severe pre-eclampsia and hypertensive crises. *Best Pract Res Clin Obstet Gynaecol*. 27(6), 877–884 (2013).
89. Venkatesha S, Toporsian M, Lam C, *et al.* Soluble endoglin contributes to the pathogenesis of preeclampsia. *Nat Med*. 12(6), 642–649 (2006).
90. Everett TR, Wilkinson IB, Lees CC. Drug development in preeclampsia: a “no go” area? *J Matern Fetal Neonatal Med*. 25(1), 50–52 (2012).
91. Guzin K, Tomruk S, Tuncay YA, *et al.* The relation of increased uterine artery blood flow resistance and impaired trophoblast invasion in pre-eclamptic pregnancies. *Arch. Gynecol. Obstet.* 272(4), 283–288 (2005).
92. Williams PJ, Broughton Pipkin F. The genetics of pre-eclampsia and other hypertensive disorders of pregnancy. *Best Pract Res Clin Obstet Gynaecol*. 25(4), 405–417 (2011).
93. Jebbink J, Wolters A, Fernando F, Afink G, van der Post J, Ris-Stalpers C. Molecular genetics of preeclampsia and HELLP syndrome - a review. *Biochimica et biophysica acta*. 1822(12), 1960–1969 (2012).
94. Staines-Urias E, Paez MC, Doyle P, *et al.* Genetic association studies in pre-eclampsia: systematic meta-analyses and field synopsis. *Int J Epidemiol*. 41(6), 1764–1775 (2012).
95. Buurma AJ, Turner RJ, Driessen JHM, *et al.* Genetic variants in pre-eclampsia: a meta-analysis. *Hum. Reprod. Update*. 19(3), 289–303 (2013).
96. Rana S, Karumanchi SA, Lindheimer MD. Angiogenic factors in diagnosis, management, and research in preeclampsia. *Hypertension*. 63(2), 198–202 (2014).
97. Fong FM, Sahemey MK, Hamedi G, *et al.* Maternal genotype and severe preeclampsia: a HuGE review. *Am J Epidemiol*. 180(4), 335–345 (2014).
98. Hiby SE, Walker JJ, O'shaughnessy KM, *et al.* Combinations of maternal KIR and fetal HLA-C genes influence the risk of preeclampsia and reproductive success. *J Exp Med*. 200(8), 957–965 (2004).

99. Nakimuli A, Chazara O, Hiby SE, *et al.* A KIR B centromeric region present in Africans but not Europeans protects pregnant women from pre-eclampsia. *Proc. Natl. Acad. Sci. U.S.A.* 112(3), 845–850 (2015).
100. Long W, Shi Z, Fan S, *et al.* Association of maternal KIR and fetal HLA-C genes with the risk of preeclampsia in the Chinese Han population. *Placenta*. 36(4), 433–437 (2015).
101. Black RE, Cousens S, Johnson HL, *et al.* Global, regional, and national causes of child mortality in 2008: a systematic analysis. *The Lancet*. 375(9730), 1969–1987 (2010).
102. Chawanpaiboon S, Vogel JP, Moller A-B, *et al.* Global, regional, and national estimates of levels of preterm birth in 2014: a systematic review and modelling analysis. *Lancet Glob Health*. 7(1), e37–e46 (2019).
103. Tucker JM, Goldenberg RL, Davis RO, Copper RL, Winkler CL, Hauth JC. Etiologies of preterm birth in an indigent population: is prevention a logical expectation? *Obstet Gynecol*. 77(3), 343–347 (1991).
104. Goldenberg RL, Culhane JF, Iams JD, Romero R. Epidemiology and causes of preterm birth. *Lancet (London, England)*. 371(9606), 75–84 (2008).
105. Romero R, Espinoza J, Kusanovic JP, *et al.* The preterm parturition syndrome. *BJOG*. 113 Suppl 3, 17–42 (2006).
106. Chard T. Frequency of implantation and early pregnancy loss in natural cycles. *Baillieres Clin Obstet Gynaecol*. 5(1), 179–189 (1991).
107. Wilcox AJ, Weinberg CR, O'Connor JF, *et al.* Incidence of early loss of pregnancy. *N Engl J Med*. 319(4), 189–194 (1988).
108. Ammon Avalos L, Galindo C, Li D-K. A systematic review to calculate background miscarriage rates using life table analysis. *Birth Defects Res A Clin Mol Teratol*. 94(6), 417–423 (2012).
109. Dimitriadis E, Menkhorst E, Saito S, Kutteh WH, Brosens JJ. Recurrent pregnancy loss. *Nat Rev Dis Primers*. 6(1), 98–19 (2020).
110. Jauniaux E, Burton GJ. Pathophysiology of histological changes in early pregnancy loss. *Placenta*. 26(2-3), 114–123 (2005).
111. Horii M, Touma O, Bui T, Parast MM. Modeling human trophoblast, the placental epithelium at the maternal fetal interface. *Reproduction*. 160(1), R1–R11 (2020).
112. Endler M, Saltvedt S, Cnattingius S, Stephansson O, Wikström A-K. Retained placenta is associated with pre-eclampsia, stillbirth, giving birth to a small-for-gestational-age infant, and spontaneous preterm birth: a national register-based study. *BJOG*. 121(12), 1462–1470 (2014).
113. Derricott H, Jones RL, Heazell AEP. Investigating the association of villitis of unknown etiology with stillbirth and fetal growth restriction - a systematic review. *Placenta*. 34(10), 856–862 (2013).
114. Khong TY, Liddell HS, Robertson WB. Defective haemochorial placentation as a cause of miscarriage: a preliminary study. *Br J Obstet Gynaecol*. 94(7), 649–655 (1987).
115. Hustin J, Jauniaux E, Schaaps JP. Histological study of the materno-embryonic interface in spontaneous abortion. *Placenta*. 11(6), 477–486 (1990).
116. Roberts RM, Green JA, Schulz LC. The evolution of the placenta. *Reproduction*. 152(5), R179–89 (2016).
117. Georgiades P, Ferguson-Smith AC, Burton GJ. Comparative developmental anatomy of the murine and human definitive placentae. *Placenta*. 23(1), 3–19 (2002).
118. Carter AM, Enders AC. The evolution of epitheliochorial placentation. *Annual Review of Animal Biosciences*. 1(1), 443–467 (2013).
119. Soncin F, Khater M, To C, *et al.* Comparative analysis of mouse and human placentae across gestation reveals species-specific regulators of placental development. *Development*. 145(2), dev156273–26 (2018).

120. Rossant J, Cross JC. Placental development: lessons from mouse mutants. *Nature Reviews Genetics*. 2(7), 538–548 (2001).
121. Perez-Garcia V, Fineberg E, Wilson R, *et al.* Placentation defects are highly prevalent in embryonic lethal mouse mutants. *Nature*. 555(7697), 463–468 (2018).
122. Maston GA, Ruvolo M. Chorionic gonadotropin has a recent origin within primates and an evolutionary history of selection. *Mol. Biol. Evol.* 19(3), 320–335 (2002).
123. Boyson JE, Iwanaga KK, Golos TG, Watkins DI. Identification of the rhesus monkey HLA-G ortholog. Mamu-G is a pseudogene. *J Immunol*. 157(12), 5428–5437 (1996).
124. Esnault C, Cornelis G, Heidmann O, Heidmann T. Differential evolutionary fate of an ancestral primate endogenous retrovirus envelope gene, the EnvV syncytin, captured for a function in placentation. *PLoS Genet*. 9(3), e1003400 (2013).
125. Brinkman-Van der Linden ECM, Hurtado-Ziola N, Hayakawa T, *et al.* Human-specific expression of Siglec-6 in the placenta. *Glycobiology*. 17(9), 922–931 (2007).
126. Krugner-Higby L, Luck M, Hartley D, Crispen HM, Lubach GR, Coe CL. High-risk pregnancy in rhesus monkeys (Macaca mulatta): A case of ectopic, abdominal pregnancy with birth of a live, term infant, and a case of gestational diabetes complicated by pre-eclampsia. *J. Med. Primatol.* 38(4), 252–256 (2009).
127. Palmer AE, London WT, Sly DL, Rice JM. Spontaneous preeclamptic toxemia of pregnancy in the patas monkey (Erythrocebus patas). *Lab. Anim. Sci.* 29(1), 102–106 (1979).
128. Stout C, Lemmon WB. Glomerular capillary endothelial swelling in a pregnant chimpanzee. *Am J Obstet Gynecol*. 105(2), 212–215 (1969).
129. Carter AM. Animal Models of Human Placentation - A Review. *Placenta*. 28(SUPPL.), S41–S47 (2007).
130. Abbas Y, Turco MY, Burton GJ, Moffett A. Investigation of human trophoblast invasion in vitro. *Hum. Reprod. Update*. 26(4), 501–513 (2020).
131. Hall CS, James TE, Goodyer C, Branchaud C, Guyda H, Giroud CJ. Short term culture of human midterm and term placenta: parameters of hormonogenesis. *Steroids*. 30(4), 569–580 (1977).
132. Stromberg K, Azizkhan JC, Speeg KV. Isolation of functional human trophoblast cells and their partial characterization in primary cell culture. *In Vitro*. 14(7), 631–638 (1978).
133. Mayhew TM. Turnover of human villous trophoblast in normal pregnancy: what do we know and what do we need to know? *Placenta*. 35(4), 229–240 (2014).
134. Caniggia I, Taylor CV, Ritchie JWK, Lye SJ, Letarte M. Endoglin regulates trophoblast differentiation along the invasive pathway in human placental villous explants. *Endocrinology*. 138(11), 4977–4988 (1997).
135. James JL, Stone PR, Chamley LW. The effects of oxygen concentration and gestational age on extravillous trophoblast outgrowth in a human first trimester villous explant model. *Human Reproduction*. 21(10), 2699–2705 (2006).
136. HELLMAN LM, HARRIS BA, ANDREWS MC. Studies of the metabolism of the human placenta; oxygen consumption and anaerobic glyolysis in relation to aging and severe toxemia. *Bull Johns Hopkins Hosp*. 87(3), 203–214 (1950).
137. VILLEE CA. The metabolism of human placenta in vitro. *J Biol Chem*. 205(1), 113–123 (1953).
138. TREMBLAY PC, SYBULSKI S, MAUGHAN GB. ROLE OF THE PLACENTA IN FETAL MALNUTRITION. *Am J Obstet Gynecol*. 91, 597–605 (1965).
139. Fox H. Effect of hypoxia on trophoblast in organ culture. A morphologic and autoradiographic study. *Am J Obstet Gynecol*. 107(7), 1058–1064 (1970).
140. Graham CH, Hawley TS, Hawley RG, *et al.* Establishment and characterization of first trimester human trophoblast cells with extended lifespan. *Exp Cell Res*. 206(2), 204–211 (1993).

141. Straszewski-Chavez SL, Abrahams VM, Alvero AB, *et al.* The isolation and characterization of a novel telomerase immortalized first trimester trophoblast cell line, Swan 71. *Placenta*. 30(11), 939–948 (2009).
142. Cerneus DP, van der Ende A. Apical and basolateral transferrin receptors in polarized BeWo cells recycle through separate endosomes. *The Journal of cell biology*. 114(6), 1149–1158 (1991).
143. Pattillo RA, Gey GO. The establishment of a cell line of human hormone-synthesizing trophoblastic cells in vitro. *Cancer Res*. 28(7), 1231–1236 (1968).
144. Pattillo RA, Ruckert ACF, Hussa RO, Bernstein R, Delfs E. The JAr cell line -- continuous human multihormone production and controls. *In Vitro*. 6, 398–399 (1971).
145. Kohler PO, Bridson WE, Hammond JM, Weintraub B, Kirschner MA, Van Thiel DH. Clonal lines of human choriocarcinoma cells in culture. *Eur J Endocrinol*. 153(1_Suppl), 137–153 (1971).
146. Wice B, Menton D, Geuze H, Schwartz AL. Modulators of cyclic AMP metabolism induce syncytiotrophoblast formation in vitro. *Exp Cell Res*. 186(2), 306–316 (1990).
147. Chou JY. Effects of retinoic acid on differentiation of choriocarcinoma cells in vitro. *J Clin Endocrinol Metab*. 54(6), 1174–1180 (1982).
148. Kato Y, Braunstein GD. Retinoic acid stimulates placental hormone secretion by choriocarcinoma cell lines in vitro. *Endocrinology*. 128(1), 401–407 (1991).
149. Sun T, Zhao Y, Mangelsdorf DJ, Simpson ER. Characterization of a region upstream of exon I.1 of the human CYP19 (aromatase) gene that mediates regulation by retinoids in human choriocarcinoma cells. *Endocrinology*. 139(4), 1684–1691 (1998).
150. Tremblay J, Hardy DB, Pereira LE, Yang K. Retinoic acid stimulates the expression of 11beta-hydroxysteroid dehydrogenase type 2 in human choriocarcinoma JEG-3 cells. *Biol Reprod*. 60(3), 541–545 (1999).
151. Sasaki S, Katayama PK, Roesler M, Pattillo RA, Mattingly RF, Ohkawa K. Cytogenetic analysis of choriocarcinoma cell lines. *Nihon Sanka Fujinka Gakkai Zasshi*. 34(12), 2253–2256 (1982).
152. Bilban M, Tauber S, Haslinger P, *et al.* Trophoblast invasion: assessment of cellular models using gene expression signatures. *Placenta*. 31(11), 989–996 (2010).
153. Apps R, Sharkey A, Gardner L, *et al.* Genome-wide expression profile of first trimester villous and extravillous human trophoblast cells. *Placenta.* 32(1), 33–43 (2011).
154. Xu R-H, Chen X, Li DS, *et al.* BMP4 initiates human embryonic stem cell differentiation to trophoblast. *Nature Biotechnology*. 20(12), 1261–1264 (2002).
155. Amita M, Adachi K, Alexenko AP, *et al.* Complete and unidirectional conversion of human embryonic stem cells to trophoblast by BMP4. *Proc. Natl. Acad. Sci. U.S.A.* 110(13), E1212–21 (2013).
156. Horii M, Li Y, Wakeland AK, *et al.* Human pluripotent stem cells as a model of trophoblast differentiation in both normal development and disease. *Proc. Natl. Acad. Sci. U.S.A.* 113(27), E3882–91 (2016).
157. Lee CQE, Gardner L, Turco M, *et al.* What Is Trophoblast? A Combination of Criteria Define Human First-Trimester Trophoblast. *Stem Cell Rep*. 6(2), 257–272 (2016).
158. Krendl C, Shaposhnikov D, Rishko V, *et al.* GATA2/3-TFAP2A/C transcription factor network couples human pluripotent stem cell differentiation to trophectoderm with repression of pluripotency. *Proc. Natl. Acad. Sci. U.S.A.* 114(45), E9579–E9588 (2017).
159. Jain A, Ezashi T, Roberts RM, Tuteja G. Deciphering transcriptional regulation in human embryonic stem cells specified towards a trophoblast fate. *Sci Rep*. 7(1), 17257–12 (2017).
160. van der Laan LJ, Lockey C, Griffeth BC, *et al.* Infection by porcine endogenous retrovirus after islet xenotransplantation in SCID mice. *Nature*. 407(6800), 90–94 (2000).

161. Kobayashi H, Sakurai T, Imai M, *et al.* Contribution of intragenic DNA methylation in mouse gametic DNA methylomes to establish oocyte-specific heritable marks. *PLoS Genet*. 8(1), e1002440 (2012).
162. Wang L, Zhang J, Duan J, *et al.* Programming and inheritance of parental DNA methylomes in mammals. *Cell*. 157(4), 979–991 (2014).
163. Guo H, Zhu P, Yan L, *et al.* The DNA methylation landscape of human early embryos. *Nature Publishing Group*. 511(7511), 606–610 (2016).
164. Lee HJ, Hore TA, Reik W. Reprogramming the methylome: erasing memory and creating diversity. *Cell Stem Cell*. 14(6), 710–719 (2014).
165. Okae H, Chiba H, Hiura H, *et al.* Genome-wide analysis of DNA methylation dynamics during early human development. *PLoS Genet*. 10(12), e1004868 (2014).
166. Walsh CP, Chaillet JR, Bestor TH. Transcription of IAP endogenous retroviruses is constrained by cytosine methylation. *Nature genetics*. 20(2), 116–117 (1998).
167. Tristem M. Identification and characterization of novel human endogenous retrovirus families by phylogenetic screening of the human genome mapping project database. *J Virol*. 74(8), 3715–3730 (2000).
168. Bénit L, Dessen P, Heidmann T. Identification, phylogeny, and evolution of retroviral elements based on their envelope genes. *J Virol*. 75(23), 11709–11719 (2001).
169. Fuchs NV, Loewer S, Daley GQ, Izsvák Z, Löwer J, Löwer R. Human endogenous retrovirus K (HML-2) RNA and protein expression is a marker for human embryonic and induced pluripotent stem cells. *Retrovirology*. 10(1), 115 (2013).
170. Wang J, Xie G, Singh M, *et al.* Primate-specific endogenous retrovirus-driven transcription defines naive-like stem cells. *Nature*. 516(7531), 405–409 (2014).
171. Thomas JH, Schneider S. Coevolution of retroelements and tandem zinc finger genes. *Genome Res*. 21(11), 1800–1812 (2011).
172. Manghera M, Douville RN. Endogenous retrovirus-K promoter: a landing strip for inflammatory transcription factors? *Retrovirology*. 10(1), 16 (2013).
173. Leung D, Du T, Wagner U, *et al.* Regulation of DNA methylation turnover at LTR retrotransposons and imprinted loci by the histone methyltransferase Setdb1. *Proc. Natl. Acad. Sci. U.S.A.* 111(18), 6690–6695 (2014).
174. Liu S, Brind'Amour J, Karimi MM, *et al.* Setdb1 is required for germline development and silencing of H3K9me3-marked endogenous retroviruses in primordial germ cells. *Genes and Development*. 28(18), 2041–2055 (2014).
175. Schlesinger S, Goff SP. Retroviral Transcriptional Regulation and Embryonic Stem Cells: War and Peace. *Molecular and Cellular Biology*. 35(5), 770–777 (2015).
176. Wolf G, Yang P, Füchtbauer AC, *et al.* The KRAB zinc finger protein ZFP809 is required to initiate epigenetic silencing of endogenous retroviruses. *Genes and Development*. 29(5), 538–554 (2015).
177. Thompson PJ, Macfarlan TS, Lorincz MC. Long Terminal Repeats: From Parasitic Elements to Building Blocks of the Transcriptional Regulatory Repertoire. *Mol. Cell*. 62(5), 766–776 (2016).
178. Theunissen TW, Friedli M, He Y, *et al.* Molecular Criteria for Defining the Naive Human Pluripotent State. *Cell Stem Cell*. 19(4), 502–515 (2016).
179. Friedli M, Trono D. The developmental control of transposable elements and the evolution of higher species. *Annu. Rev. Cell Dev. Biol.* 31, 429–451 (2015).
180. Fort A, Hashimoto K, Yamada D, *et al.* Deep transcriptome profiling of mammalian stem cells supports a regulatory role for retrotransposons in pluripotency maintenance. *Nature genetics*. 46(6), 558–566 (2014).
181. Macfarlan TS, Gifford WD, Driscoll S, *et al.* Embryonic stem cell potency fluctuates with endogenous retrovirus activity. *Nature*. 487(7405), 57–63 (2012).

182. Ling J, Pi W, Bollag R, *et al.* The solitary long terminal repeats of ERV-9 endogenous retrovirus are conserved during primate evolution and possess enhancer activities in embryonic and hematopoietic cells. *J Virol*. 76(5), 2410–2423 (2002).
183. Beyer U, Moll-Rocek J, Moll UM, Dobbelstein M. Endogenous retrovirus drives hitherto unknown proapoptotic p63 isoforms in the male germ line of humans and great apes. *Proc. Natl. Acad. Sci. U.S.A.* 108(9), 3624–3629 (2011).
184. Liu M, Eiden MV. Role of human endogenous retroviral long terminal repeats (LTRs) in maintaining the integrity of the human germ line. 3(6), 901–905 (2011).
185. Ehrlich M, Gama-Sosa MA, Huang LH, *et al.* Amount and distribution of 5-methylcytosine in human DNA from different types of tissues of cells. *Nucleic Acids Res*. 10(8), 2709–2721 (1982).
186. Fuke C, Shimabukuro M, Petronis A, *et al.* Age related changes in 5-methylcytosine content in human peripheral leukocytes and placentas: an HPLC-based study. *Ann Hum Genet*. 68(Pt 3), 196–204 (2004).
187. Cotton AM, Avila L, Penaherrera MS, Affleck JG, Robinson WP, Brown CJ. Inactive X chromosome-specific reduction in placental DNA methylation. *Human molecular genetics*. 18(19), 3544–3552 (2009).
188. Popp C, Dean W, Feng S, *et al.* Genome-wide erasure of DNA methylation in mouse primordial germ cells is affected by AID deficiency. *Nature*. 463(7284), 1101–1105 (2010).
189. Hon GC, Rajagopal N, Shen Y, *et al.* Epigenetic memory at embryonic enhancers identified in DNA methylation maps from adult mouse tissues. *Nature genetics*. 45(10), 1198–1206 (2013).
190. Schroeder DI, Jayashankar K, Douglas KC, *et al.* Early Developmental and Evolutionary Origins of Gene Body DNA Methylation Patterns in Mammalian Placentas. *PLoS Genet*. 11(8), 1–20 (2015).
191. Yi J-M, Kim H-S. Molecular Phylogenetic Analysis of the Human Endogenous Retrovirus E (HERV-E) Family in Human Tissues and Human Cancers. *Genes Genet Syst*. 82(1), 89–98 (2007).
192. Boyd MT, Bax CMR, Bax BE, Bloxam DL, Weiss RA. The Human Endogenous Retrovirus ERV-3 Is Upregulated in Differentiating Placental Trophoblast Cells. *Virology*. 196(2), 905–909 (1993).
193. Sugimoto J, Sugimoto M, Bernstein H, Jinno Y, Schust D. A novel human endogenous retroviral protein inhibits cell-cell fusion. 3(1), 641–9 (2013).
194. Blond J-L, Lavillette D, Cheynet V, *et al.* An envelope glycoprotein of the human endogenous retrovirus HERV-W is expressed in the human placenta and fuses cells expressing the type D mammalian retrovirus receptor. *J Virol*. 74(7), 3321–3329 (2000).
195. Blaise S, de Parseval N, Bénit L, Heidmann T. Genomewide screening for fusogenic human endogenous retrovirus envelopes identifies syncytin 2, a gene conserved on primate evolution. *Proc. Natl. Acad. Sci. U.S.A.* 100(22), 13013–13018 (2003).
196. Mi S, Lee X, Li X, *et al.* Syncytin is a captive retroviral envelope protein involved in human placental morphogenesis. *Nature*. 403(6771), 785–789 (2000).
197. Blaise S, de Parseval N, Heidmann T. Functional characterization of two newly identified human endogenous retrovirus coding envelope genes. *Retrovirology*. 2 (2005).
198. Dunk CE, Roggensack AM, Cox B, *et al.* A distinct microvascular endothelial gene expression profile in severe IUGR placentas. *Placenta*. 33(4), 285–293 (2012).
199. Matouskova M, Blazkova J, Pajer P, Pavlicek A, Hejnar J. CpG methylation suppresses transcriptional activity of human syncytin-1 in non-placental tissues. *Exp Cell Res*. 312(7), 1011–1020 (2006).

200. Gimenez J, Montgiraud C, Oriol G, *et al.* Comparative Methylation of ERVWE1/Syncytin-1 and Other Human Endogenous Retrovirus LTRs in Placenta Tissues. *DNA Res.* 16(4), 195–211 (2009).
201. Li Y, Moretto-Zita M, Leon-Garcia S, Parast MM. p63 inhibits extravillous trophoblast migration and maintains cells in a cytotrophoblast stem cell-like state. *The American journal of pathology*. 184(12), 3332–3343 (2014).
202. Zhuang X-W, Li J, Brost BC, *et al.* Decreased expression and altered methylation of syncytin-1 gene in human placentas associated with preeclampsia. *Curr Pharm Des*. 20(11), 1796–1802 (2014).
203. Cheng Y-H, Handwerger S. A placenta-specific enhancer of the human syncytin gene. *Biol Reprod*. 73(3), 500–509 (2005).
204. Cheng Y-H, Richardson BD, Hubert MA, Handwerger S. Isolation and characterization of the human syncytin gene promoter. *Biol Reprod*. 70(3), 694–701 (2004).
205. Yu C, Shen K, Lin M, *et al.* GCMa regulates the syncytin-mediated trophoblastic fusion. *Journal of Biological Chemistry*. 277(51), 50062–50068 (2002).
206. Chang C-W, Chang G-D, Chen H. A novel cyclic AMP/Epac1/CaMKI signaling cascade promotes GCM1 desumoylation and placental cell fusion. *Molecular and Cellular Biology*. 31(18), 3820–3831 (2011).
207. Prudhomme S, Oriol G, Mallet F. A retroviral promoter and a cellular enhancer define a bipartite element which controls env ERVWE1 placental expression. *J Virol*. 78(22), 12157–12168 (2004).
208. Cáceres M, NISC Comparative Sequencing Program, Thomas JW. The gene of retroviral origin Syncytin 1 is specific to hominoids and is inactive in Old World monkeys. *J. Hered.* 97(2), 100–106 (2006).
209. Imakawa K, Nakagawa S, Miyazawa T. Baton pass hypothesis: successive incorporation of unconserved endogenous retroviral genes for placentation during mammalian evolution. *Genes Cells*. 20(10), 771–788 (2015).
210. Dupressoir A, Marceau G, Vernochet C, *et al.* Syncytin-A and syncytin-B, two fusogenic placenta-specific murine envelope genes of retroviral origin conserved in Muridae. *Proc. Natl. Acad. Sci. U.S.A.* 102(3), 725–730 (2005).
211. Heidmann O, Vernochet C, Dupressoir A, Heidmann T. Identification of an endogenous retroviral envelope gene with fusogenic activity and placenta-specific expression in the rabbit: a new “syncytin” in a third order of mammals. *Retrovirology*. 6(1), 107 (2009).
212. Cornelis G, Heidmann O, Bernard-Stoecklin S, *et al.* Ancestral capture of syncytin-Car1, a fusogenic endogenous retroviral envelope gene involved in placentation and conserved in Carnivora. *Proc. Natl. Acad. Sci. U.S.A.* 109(7), E432–41 (2012).
213. Redelsperger F, Cornelis G, Vernochet C, *et al.* Capture of syncytin-Mar1, a fusogenic endogenous retroviral envelope gene involved in placentation in the Rodentia squirrel-related clade. *J Virol*. 88(14), 7915–7928 (2014).
214. Cornelis G, Vernochet C, Malicorne S, *et al.* Retroviral envelope syncytin capture in an ancestrally diverged mammalian clade for placentation in the primitive Afrotherian tenrecs. *Proc. Natl. Acad. Sci. U.S.A.* 111(41), E4332–E4341 (2014).
215. Cornelis G, Heidmann O, Degrelle SA, *et al.* Captured retroviral envelope syncytin gene associated with the unique placental structure of higher ruminants. *Proc. Natl. Acad. Sci. U.S.A.* 110(9), E828–37 (2013).
216. Cornelis G, Vernochet C, Carradec Q, *et al.* Retroviral envelope gene captures and syncytin exaptation for placentation in marsupials. *Proc. Natl. Acad. Sci. U.S.A.* 112(5), E487–96 (2015).
217. Mangeney M, Renard M, Schlecht-Louf G, *et al.* Placental syncytins: Genetic disjunction between the fusogenic and immunosuppressive activity of retroviral envelope proteins. *Proc. Natl. Acad. Sci. U.S.A.* 104(51), 20534–20539 (2007).

218. Subramanian RP, Wildschutte JH, Russo C, Coffin JM. Identification, characterization, and comparative genomic distribution of the HERV-K (HML-2) group of human endogenous retroviruses. *Retrovirology*. 8(1), 1–22 (2011).
219. Katoh I, Kurata S-I. Association of Endogenous Retroviruses and Long Terminal Repeats with Human Disorders. *Frontiers in Oncology*. 3 (2013).
220. Golan M, Hizi A, Resau JH, *et al.* Human endogenous retrovirus (HERV-K) reverse transcriptase as a breast cancer prognostic marker. *Neoplasia*. 10(6), 521–533 (2008).
221. Wang-Johanning F, Radvanyi L, Rycaj K, *et al.* Human endogenous retrovirus K triggers an antigen-specific immune response in breast cancer patients. *Cancer Res*. 68(14), 5869–5877 (2008).
222. Salmons B, Lawson JS, Günzburg WH. Recent developments linking retroviruses to human breast cancer: infectious agent, enemy within or both? *Journal of General Virology*. 95(12), 2589–2593 (2014).
223. Buscher K, Trefzer U, Hofmann M, Sterry W, Kurth R, Denner J. Expression of human endogenous retrovirus K in melanomas and melanoma cell lines. *Cancer Res*. 65(10), 4172–4180 (2005).
224. Schmitt K, Reichrath J, Roesch A, Meese E, Mayer J. Transcriptional profiling of human endogenous retrovirus group HERV-K(HML-2) loci in melanoma. *Genome Biol Evol*. 5(2), 307–328 (2013).
225. Lamprecht B, Walter K, Kreher S, *et al.* Derepression of an endogenous long terminal repeat activates the CSF1R proto-oncogene in human lymphoma. *Nat Med*. 16(5), 571–579 (2010).
226. Douville RN, Nath A. Human endogenous retroviruses and the nervous system. *Handb Clin Neurol*. 123, 465–485 (2014).
227. Douville R, Liu J, Rothstein J, Nath A. Identification of active loci of a human endogenous retrovirus in neurons of patients with amyotrophic lateral sclerosis. *Ann Neurol*. 69(1), 141–151 (2011).
228. Li W, Lee M-H, Henderson L, *et al.* Human endogenous retrovirus-K contributes to motor neuron disease. *Sci Transl Med*. 7(307), 307ra153–307ra153 (2015).
229. Oluwole SOA, Yao Y, Conradi S, Kristensson K, Karlsson H. Elevated levels of transcripts encoding a human retroviral envelope protein (syncytin) in muscles from patients with motor neuron disease. *Amyotroph Lateral Scler*. 8(2), 67–72 (2007).
230. Alfahad T, Nath A. Retroviruses and amyotrophic lateral sclerosis. *Antiviral Res.* 99(2), 180–187 (2013).
231. Christensen T. Human endogenous retroviruses in neurologic disease. *APMIS*. 124(1-2), 116–126 (2016).
232. Perron H, Germi R, Bernard C, *et al.* Human endogenous retrovirus type W envelope expression in blood and brain cells provides new insights into multiple sclerosis disease. *Mult Scler*. 18(12), 1721–1736 (2012).
233. Karlsson H, Bachmann S, Schröder J, McArthur J, Torrey EF, Yolken RH. Retroviral RNA identified in the cerebrospinal fluids and brains of individuals with schizophrenia. *Proc. Natl. Acad. Sci. U.S.A.* 98(8), 4634–4639 (2001).
234. Huang W-J, Liu Z-C, Wei W, Wang G-H, Wu J-G, Zhu F. Human endogenous retroviral pol RNA and protein detected and identified in the blood of individuals with schizophrenia. *Schizophrenia Research*. 83(2-3), 193–199 (2006).
235. Huang W, Li S, Hu Y, *et al.* Implication of the env gene of the human endogenous retrovirus W family in the expression of BDNF and DRD3 and development of recent-onset schizophrenia. *Schizophr Bull*. 37(5), 988–1000 (2011).
236. Perron H, Hamdani N, Faucard R, *et al.* Molecular characteristics of Human Endogenous Retrovirus type-W in schizophrenia and bipolar disorder. *Transl Psychiatry*. 2(12), e201 (2012).

237. Hegyi H. GABBR1 has a HERV-W LTR in its regulatory region--a possible implication for schizophrenia. *Biol. Direct*. 8, 5–5 (2013).
238. Suntsova M, Gogvadze EV, Salozhin S, *et al.* Human-specific endogenous retroviral insert serves as an enhancer for the schizophrenia-linked gene PRODH. *Proc. Natl. Acad. Sci. U.S.A.* 110(48), 19472–19477 (2013).
239. Malfavon-Borja R, Feschotte C. Fighting Fire with Fire: Endogenous Retrovirus Envelopes as Restriction Factors. *J Virol*. 89(8), 4047–4050 (2015).
240. Chuong EB, Elde NC, Feschotte C. Regulatory evolution of innate immunity through co-option of endogenous retroviruses. *Science (New York, N.Y.)*. 351(6277), 1083–1087 (2016).
241. Chiappinelli KB, Strissel PL, Desrichard A, *et al.* Inhibiting DNA Methylation Causes an Interferon Response in Cancer via dsRNA Including Endogenous Retroviruses. *Cell*. 162(5), 974–986 (2015).
242. Buzdin A, Ustyugova S, Khodosevich K, *et al.* Human-specific subfamilies of HERV-K (HML-2) long terminal repeats: three master genes were active simultaneously during branching of hominoid lineages. *Genomics*. 81(2), 149–156 (2003).
243. Mager DL, Medstrand P. Retroviral Repeat Sequences. John Wiley & Sons, Ltd, Chichester.
244. Reus K, Mayer J, Sauter M, Scherer D, Muller-Lantzsch N, Meese E. Genomic organization of the human endogenous retrovirus HERV-K(HML-2.HOM) (ERVK6) on chromosome 7. *Genomics*. 72(3), 314–320 (2001).
245. Steinhuber S, Brack M, Hunsmann G, Schwelberger H, Dierich MP, Vogetseder W. Distribution of human endogenous retrovirus HERV-K genomes in humans and different primates. *Human genetics* [Internet]. 96(2), 188–192 (1995). Available from: https://link.springer.com/article/10.1007/BF00207377.
246. Kliger Y, Aharoni A, Rapaport D, Jones P, Blumenthal R, Shai Y. Fusion peptides derived from the HIV type 1 glycoprotein 41 associate within phospholipid membranes and inhibit cell-cell Fusion. Structure-function study. *J Biol Chem*. 272(21), 13496–13505 (1997).
247. Oostendorp RA, Meijer CJ, Scheper RJ. Immunosuppression by retroviral-envelope-related proteins, and their role in non-retroviral human disease. *Crit Rev Oncol Hematol*. 14(3), 189–206 (1993).
248. Robinson LR, Whelan SPJ. Infectious Entry Pathway Mediated by the Human Endogenous Retrovirus K Envelope Protein. *J Virol*. 90(7), 3640–3649 (2016).
249. Contreras-Galindo R, Kaplan MH, Dube D, *et al.* Human Endogenous Retrovirus Type K (HERV-K) Particles Package and Transmit HERV-K–Related Sequences. *J Virol*. 89(14), 7187–7201 (2015).
250. Kramer P, Lausch V, Volkwein A, Hanke K, Hohn O, Bannert N. The human endogenous retrovirus K(HML-2) has a broad envelope-mediated cellular tropism and is prone to inhibition at a post-entry, pre-integration step. *Virology*. 487, 121–128 (2016).
251. Morozov VA, Thi V, Denner J. The Transmembrane Protein of the Human Endogenous Retrovirus - K (HERV-K) Modulates Cytokine Release and Gene Expression. *Plos One*. 8(8), e70399 (2013).
252. Rosenkrantz JL, Gaffney JE, Roberts VH, Carbone L, Chavez SL. Transcriptomic analysis of primate placentas and novel rhesus trophoblast cell lines informs investigations of human placentation. 26, 501.
253. Apps R, Murphy SP, Fernando R, Gardner L, Ahad T, Moffett A. Human leucocyte antigen (HLA) expression of primary trophoblast cells and placental cell lines, determined using single antigen beads to characterize allotype specificities of anti-HLA antibodies. *Immunology*. 127(1), 26–39 (2009).
254. Abou-Kheir W, Barrak J, Hadadeh O, Daoud G. HTR-8/SVneo cell line contains a mixed population of cells. *Placenta*. 50, 1–7 (2017).

255. Reiter JL, Drendel HM, Chakraborty S, Schellinger MM, Lee M-J, Mor G. Cytogenetic features of human trophoblast cell lines SWAN-71 and 3A-subE. *Placenta*. 52, 17–20 (2017).
256. Malassine A, Frendo JL, Evain-Brion D. A comparison of placental development and endocrine functions between the human and mouse model. *Hum. Reprod. Update*. 9(6), 531–539 (2003).
257. Soncin F, Natale D, Parast MM. Signaling pathways in mouse and human trophoblast differentiation: A comparative review. *Cell Mol Life Sci*. 72(7), 1291–1302 (2015).
258. Dunn-Fletcher CE, Muglia LM, Pavlicev M, *et al.* Anthropoid primate-specific retroviral element THE1B controls expression of CRH in placenta and alters gestation length. *PLoS Biol*. 16(9), e2006337–21 (2018).
259. Green BB, Houseman EA, Johnson KC, *et al.* Hydroxymethylation is uniquely distributed within term placenta, and is associated with gene expression. *FASEB J*. 30(8), 2874–2884 (2016).
260. Pavlicev M, Wagner GP, Chavan AR, *et al.* Single-cell transcriptomics of the human placenta: Inferring the cell communication network of the maternal-fetal interface. *Genome Res*. 27(3), 349–361 (2017).
261. Sun M-A, Wolf G, Wang Y, *et al.* Deciphering the evolution of the transcriptional and regulatory landscape in human placenta. 76, 3.
262. Uhlén M, Fagerberg L, Hallström BM, *et al.* Tissue-based map of the human proteome. *Science (New York, N.Y.)*. 347(6220), 1260419 (2015).
263. Golos TG, Durning M, Fisher JM, Fowler PD. Cloning of four growth hormone/chorionic somatomammotropin-related complementary deoxyribonucleic acids differentially expressed during pregnancy in the rhesus monkey placenta. *Endocrinology*. 133(4), 1744–1752 (1993).
264. González Alvarez R, Revol de Mendoza A, Esquivel Escobedo D, *et al.* Growth hormone locus expands and diverges after the separation of New and Old World Monkeys. *Gene*. 380(1), 38–45 (2006).
265. Papper Z, Jameson NM, Romero R, *et al.* Ancient origin of placental expression in the growth hormone genes of anthropoid primates. *Proc. Natl. Acad. Sci. U.S.A.* 106(40), 17083–17088 (2009).
266. Hutter S, Knabl J, Andergassen U, *et al.* Placental Expression Patterns of Galectin-1, Galectin-2, Galectin-3 and Galectin-13 in Cases of Intrauterine Growth Restriction (IUGR). *Int J Mol Med*. 17(4), 523 (2016).
267. Knuth A, Liu L, Nielsen H, Merril D, Torry DS, Arroyo JA. Placenta growth factor induces invasion and activates p70 during rapamycin treatment in trophoblast cells. *Am J Reprod Immunol*. 73(4), 330–340 (2015).
268. Athanassiades A, Lala PK. Role of placenta growth factor (PIGF) in human extravillous trophoblast proliferation, migration and invasiveness. *Placenta*. 19(7), 465–473 (1998).
269. Enquobahrie DA, Hevner K, Qiu C, Abetew DF, Sorensen TK, Williams MA. Differential Expression of HrtA1 and ADAM12 in Placentas from Preeclamptic and Normotensive Pregnancies. *Reprod Syst Sex Disord*. 1(3), 1000110 (2012).
270. Ishibashi O, Ohkuchi A, Ali MM, *et al.* Hydroxysteroid (17-β) dehydrogenase 1 is dysregulated by miR-210 and miR-518c that are aberrantly expressed in preeclamptic placentas: a novel marker for predicting preeclampsia. *Hypertension*. 59(2), 265–273 (2012).
271. Kapustin RV, Drobintseva AO, Alekseenkova EN, *et al.* Placental protein expression of kisspeptin-1 (KISS1) and the kisspeptin-1 receptor (KISS1R) in pregnancy complicated by diabetes mellitus or preeclampsia. *Arch. Gynecol. Obstet.* 301(2), 437–445 (2020).
272. Sekizawa A, Purwosunu Y, Yoshimura S, *et al.* PP13 mRNA expression in trophoblasts from preeclamptic placentas. *Reprod Sci*. 16(4), 408–413 (2009).

273. Nishizawa H, Pryor-Koishi K, Suzuki M, *et al.* Increased levels of pregnancy-associated plasma protein-A2 in the serum of pre-eclamptic patients. *Mol. Hum. Reprod.* 14(10), 595–602 (2008).
274. Kaartokallio T, Cervera A, Kyllönen A, *et al.* Gene expression profiling of pre-eclamptic placentae by RNA sequencing. 5(1), 14107–16 (2015).
275. Knerr I, Beinder E, Rascher W. Syncytin, a novel human endogenous retroviral gene in human placenta: Evidence for its dysregulation in preeclampsia and HELLP syndrome. *Am J Obstet Gynecol*. 186(2), 210–213 (2002).
276. Eidem HR, Rinker DC, Ackerman WE, *et al.* Comparing human and macaque placental transcriptomes to disentangle preterm birth pathology from gestational age effects. *Placenta*. 41, 74–82 (2016).
277. Liu Y, Fan X, Wang R, *et al.* Single-cell RNA-seq reveals the diversity of trophoblast subtypes and patterns of differentiation in the human placenta. *Cell Res*. 28(8), 819–832 (2018).
278. Douglas GC, King BF. Isolation and morphologic differentiation in vitro of villous cytotrophoblast cells from rhesus monkey placenta. *In Vitro Cell Dev Biol*. 26(8), 754–758 (1990).
279. Golos TG, Handrow RR, Durning M, Fisher JM, Rilling JK. Regulation of chorionic gonadotropin-α and chorionic somatomammotropin messenger ribonucleic acid expression by 8-bromo-adenosine 3“, 5-”monophosphate and dexamethasone in cultured rhesus monkey syncytiotrophoblasts. *Endocrinology*. 131(1), 89–100 (1992).
280. Golos TG, Bondarenko GI, Breburda EE, Dambaeva SV, Durning M, Slukvin II. Immune and trophoblast cells at the rhesus monkey maternal-fetal interface. *Methods Mol. Med.* 122, 93–108 (2006).
281. Kumar P, Thirkill TL, Ji J, Monte LH, Douglas GC. Differential Effects of Sodium Butyrate and Lithium Chloride on Rhesus Monkey Trophoblast Differentiation. *Plos One*. 10(8), e0135089 (2015).
282. Aboagye-Mathiesen G, Laugesen J, Zdravkovic M, Ebbesen P. Isolation and characterization of human placental trophoblast subpopulations from first-trimester chorionic villi. *Clin. Diagn. Lab. Immunol.* 3(1), 14–22 (1996).
283. King A, Thomas L, Bischof P. Cell culture models of trophoblast II: Trophoblast cell lines - A workshop report. S113–S119 (2000).
284. Daughtry BL, Rosenkrantz JL, Lazar NH, *et al.* Single-cell sequencing of primate preimplantation embryos reveals chromosome elimination via cellular fragmentation and blastomere exclusion. *Genome Res*. 29(3), 367–382 (2019).
285. Wang Y-L, Qiu W, Feng H-C, *et al.* Immortalization of normal human cytotrophoblast cells by reconstitution of telomeric reverse transcriptase activity. *MHR: Basic science of reproductive medicine*. 12(7), 451–460 (2006).
286. da Silva Francisco Junior R, Santos Ferreira dos C, Santos e Silva JC, *et al.* Pervasive Inter-Individual Variation in Allele-Specific Expression in Monozygotic Twins. *Front Genet*. 10, 1178 (2019).
287. Micci L, Ryan ES, Fromentin R, *et al.* Interleukin-21 combined with ART reduces inflammation and viral reservoir in SIV-infected macaques. *J Clin Invest*. 125(12), 4497–4513 (2015).
288. Yabe S, Alexenko AP, Amita M, *et al.* Comparison of syncytiotrophoblast generated from human embryonic stem cells and from term placentas. *Proc. Natl. Acad. Sci. U.S.A.* 113(19), E2598–607 (2016).
289. Azar C, Valentine M, Trausch-Azar J, Druley T, Nelson DM, Schwartz AL. RNA-Seq identifies genes whose proteins are transformative in the differentiation of cytotrophoblast to syncytiotrophoblast, in human primary villous and BeWo trophoblasts. 8(1), 5142–12 (2018).

290. Zhang X, Pavlicev M, Jones HN, Muglia LJ. Eutherian-Specific Gene TRIML2 Attenuates Inflammation in the Evolution of Placentation. *Mol. Biol. Evol.* 37(2), 507–523 (2020).
291. Yang C-T, Song J, Bu X, *et al.* Herpes simplex virus type-1 infection upregulates cellular promoters and telomerase activity in both tumor and nontumor human cells. *Gene Ther*. 10(17), 1494–1502 (2003).
292. Okae H, Toh H, Sato T, *et al.* Derivation of Human Trophoblast Stem Cells. *Stem Cell*. 22(1), 50–63.e6 (2018).
293. De Oliveira T, Abiatari I, Raulefs S, *et al.* Syndecan-2 promotes perineural invasion and cooperates with K-ras to induce an invasive pancreatic cancer cell phenotype. *Mol Cancer*. 11(1), 19–10 (2012).
294. Liu W, Li M, Chen X, *et al.* MicroRNA-373 promotes migration and invasion in human esophageal squamous cell carcinoma by inhibiting TIMP3 expression. *Am J Cancer Res*. 6(1), 1–14 (2016).
295. Zhang H, Qi M, Li S, *et al.* microRNA-9 targets matrix metalloproteinase 14 to inhibit invasion, metastasis, and angiogenesis of neuroblastoma cells. *Mol Cancer Ther*. 11(7), 1454–1466 (2012).
296. Eckert MA, Santiago-Medina M, Lwin TM, Kim J, Courtneidge SA, Yang J. ADAM12 induction by Twist1 promotes tumor invasion and metastasis via regulation of invadopodia and focal adhesions. *J Cell Sci*. 130(12), 2036–2048 (2017).
297. Rosario GX, Konno T, Soares MJ. Maternal hypoxia activates endovascular trophoblast cell invasion. *Developmental Biology*. 314(2), 362–375 (2008).
298. Zhu J, Wang K, Li T, *et al.* Hypoxia-induced TET1 facilitates trophoblast cell migration and invasion through HIF1α signaling pathway. *Sci Rep*. 7(1), 8077–11 (2017).
299. Coulter CL, Han VK. Expression of insulin-like growth factor-II and IGF-binding protein-1 mRNAs in term rhesus monkey placenta: comparison with human placenta. *Horm Res*. 45(3-5), 167–171 (1996).
300. Thul PJ, Åkesson L, Wiking M, *et al.* A subcellular map of the human proteome. *Science (New York, N.Y.)*. 356(6340), eaal3321 (2017).
301. Hamilton GS, Lysiak JJ, Han VK, Lala PK. Autocrine-paracrine regulation of human trophoblast invasiveness by insulin-like growth factor (IGF)-II and IGF-binding protein (IGFBP)-1. *Exp Cell Res*. 244(1), 147–156 (1998).
302. McKinnon T, Chakraborty C, Gleeson LM, Chidiac P, Lala PK. Stimulation of human extravillous trophoblast migration by IGF-II is mediated by IGF type 2 receptor involving inhibitory G protein(s) and phosphorylation of MAPK. *J Clin Endocrinol Metab*. 86(8), 3665–3674 (2001).
303. Mossman HW. Vertebrate Fetal Membranes. Palgrave.
304. Cross JC, Simmons DG, Watson ED. Chorioallantoic morphogenesis and formation of the placental villous tree. 84–93 (2003).
305. Carter AM, Enders AC. Comparative aspects of trophoblast development and placentation. *Reprod Biol Endocrin*. 2(1), 46 (2004).
306. Rogers J, Gibbs RA. Comparative primate genomics: Emerging patterns of genome content and dynamics. *Nature Reviews Genetics*. 15(5), 347–359 (2014).
307. Pijnenborg R, Vercruysse L, Carter AM. Deep trophoblast invasion and spiral artery remodelling in the placental bed of the chimpanzee. *Placenta*. 32(5), 400–408 (2011).
308. Rosenberg KR, Trevathan WR. An anthropological perspective on the evolutionary context of preeclampsia in humans. *J. Reprod. Immunol.* 76(1-2), 91–97 (2007).
309. Rodriguez A, Tuuli MG, Odibo AO. First-, Second-, and Third-Trimester Screening for Preeclampsia and Intrauterine Growth Restriction. *Clin Lab Med*. 36(2), 331–351 (2016).
310. Hou Z-C, Sterner KN, Romero R, *et al.* Elephant transcriptome provides insights into the evolution of eutherian placentation. *Genome Biol Evol*. 4(5), 713–725 (2012).

311. Armstrong DL, McGowen MR, Weckle A, *et al.* The core transcriptome of mammalian placentas and the divergence of expression with placental shape. *Placenta*. 57, 71–78 (2017).
312. Than NG, Romero R, Goodman M, *et al.* A primate subfamily of galectins expressed at the maternal-fetal interface that promote immune cell death. *Proc. Natl. Acad. Sci. U.S.A.* 106(24), 9731–9736 (2009).
313. Sammar M, Drobnjak T, Mandala M, Gizurarson S, Huppertz B, Meiri H. Galectin 13 (PP13) Facilitates Remodeling and Structural Stabilization of Maternal Vessels during Pregnancy. *Int J Mol Med*. 20(13), 3192 (2019).
314. Than NG, Abdul Rahman O, Magenheim R, *et al.* Placental protein 13 (galectin-13) has decreased placental expression but increased shedding and maternal serum concentrations in patients presenting with preterm pre-eclampsia and HELLP syndrome. *Virchows Arch*. 453(4), 387–400 (2008).
315. Toouli CD, Huschtscha LI, Neumann AA, *et al.* Comparison of human mammary epithelial cells immortalized by simian virus 40 T-Antigen or by the telomerase catalytic subunit. *Oncogene*. 21(1), 128–139 (2002).
316. Vento-Tormo R, Efremova M, Botting RA, *et al.* Single-cell reconstruction of the early maternal-fetal interface in humans. *Nature*. 563(7731), 347–353 (2018).
317. Zerbino DR, Achuthan P, Akanni W, *et al.* Ensembl 2018. *Nucleic Acids Res*. 46(D1), D754–D761 (2017).
318. Kinsella RJ, Kähäri A, Haider S, *et al.* Ensembl BioMarts: a hub for data retrieval across taxonomic space. *Database*. 2011(0), bar030–bar030 (2011).
319. Bolger AM, Lohse M, Usadel B. Trimmomatic: a flexible trimmer for Illumina sequence data. *Bioinformatics*. 30(15), 2114–2120 (2014).
320. Langmead B, Wilks C, Antonescu V, Charles R. Scaling read aligners to hundreds of threads on general-purpose processors. *Bioinformatics*. 35(3), 421–432 (2019).
321. Li H, Handsaker B, Wysoker A, *et al.* The Sequence Alignment/Map format and SAMtools. *Bioinformatics*. 25(16), 2078–2079 (2009).
322. Liao Y, Smyth GK, Shi W. featureCounts: an efficient general purpose program for assigning sequence reads to genomic features. *Bioinformatics*. 30(7), 923–930 (2014).
323. Love MI, Huber W, Anders S. Moderated estimation of fold change and dispersion for RNA-seq data with DESeq2. *Genome Biol*. 15(12), 550 (2014).
324. Raudvere U, Kolberg L, Kuzmin I, *et al.* g:Profiler: a web server for functional enrichment analysis and conversions of gene lists (2019 update). *Nucleic Acids Res*. 47(W1), W191–W198 (2019).
325. Pletscher-Frankild S, Pallejà A, Tsafou K, Binder JX, Jensen LJ. DISEASES: text mining and data integration of disease-gene associations. *Methods*. 74, 83–89 (2015).
326. Kuleshov MV, Jones MR, Rouillard AD, *et al.* Enrichr: a comprehensive gene set enrichment analysis web server 2016 update. *Nucleic Acids Res*. 44(W1), W90–7 (2016).
327. Abrahams VM, Bole-Aldo P, Kim YM, *et al.* Divergent trophoblast responses to bacterial products mediated by TLRs. *J Immunol*. 173(7), 4286–4296 (2004).
328. Straszewski-Chavez SL, Abrahams VM, Funai EF, Mor G. X-linked inhibitor of apoptosis (XIAP) confers human trophoblast cell resistance to Fas-mediated apoptosis. *MHR: Basic science of reproductive medicine*. 10(1), 33–41 (2004).
329. Garvin T, Aboukhalil R, Kendall J, *et al.* Interactive analysis and assessment of single-cell copy-number variations. *Nat Methods*. 12(11), 1058–1060 (2015).
330. Li B, Dewey CN. RSEM: accurate transcript quantification from RNA-Seq data with or without a reference genome. *BMC bioinformatics*. 12(1), 323–16 (2011).
331. Necsulea A, Soumillon M, Warnefors M, *et al.* The evolution of lncRNA repertoires and expression patterns in tetrapods. *Nature*. 505(7485), 635–640 (2014).

332. Lander ES, Linton LM, Birren B, *et al.* Initial sequencing and analysis of the human genome. *Nature*. 409(6822), 860–921 (2001).
333. Vargiu L, Rodriguez-Tome P, Sperber GO, *et al.* Classification and characterization of human endogenous retroviruses; mosaic forms are common. *Retrovirology*. 1–29 (2016).
334. Boeke JD, Stoye JP. Retrotransposons, Endogenous Retroviruses, and the Evolution of Retroelements. In: Retroviruses. *Cold Spring Harbor Laboratory Press*. (1997).
335. Blond J-L, Besème F, Duret L, *et al.* Molecular characterization and placental expression of HERV-W, a new human endogenous retrovirus family. *J Virol*. 73(2), 1175–1185 (1999).
336. Mallet F, Bouton O, Prudhomme S, *et al.* The endogenous retroviral locus ERVWE1 is a bona fide gene involved in hominoid placental physiology. *Proc. Natl. Acad. Sci. U.S.A.* 101(6), 1731–1736 (2004).
337. Mamedov I, Lebedev Y, Hunsmann G, Khusnutdinova E, Sverdlov E. A rare event of insertion polymorphism of a HERV-K LTR in the human genome. *Genomics*. 84(3), 596–599 (2004).
338. Chen FC, Li WH. Genomic divergences between humans and other hominoids and the effective population size of the common ancestor of humans and chimpanzees. *Am. J. Hum. Genet*. 68(2), 444–456 (2001).
339. Phipps EA, Thadhani R, Benzing T, Karumanchi SA. Pre-eclampsia: pathogenesis, novel diagnostics and therapies. *Nat Rev Nephrol*. 15(5), 275–289 (2019).
340. Romero R, Dey SK, Fisher SJ. Preterm labor: one syndrome, many causes. *Science (New York, N.Y.)*. 345(6198), 760–765 (2014).
341. Brukman NG, Uygur B, Podbilewicz B, Chernomordik LV. How cells fuse. *The Journal of cell biology*. 218(5), 1436–1451 (2019).
342. Dewannieux M, Harper F, Richaud A, *et al.* Identification of an infectious progenitor for the multiple-copy HERV-K human endogenous retroelements. *Genome Res*. 16(12), 1548–1556 (2006).
343. Flockerzi A, Ruggieri A, Frank O, *et al.* Expression patterns of transcribed human endogenous retrovirus HERV-K(HML-2) loci in human tissues and the need for a HERV Transcriptome Project. *BMC genomics*. 9(1), 354–17 (2008).
344. Thomas G. Furin at the cutting edge: from protein traffic to embryogenesis and disease. *Nature Reviews Molecular Cell Biology*. 3(10), 753–766 (2002).
345. Lim R, Barker G, Riley C, Lappas M. Apelin is decreased with human preterm and term labor and regulates prolabor mediators in human primary amnion cells. *Reprod Sci*. 20(8), 957–967 (2013).
346. Heil F, Hemmi H, Hochrein H, *et al.* Species-specific recognition of single-stranded RNA via toll-like receptor 7 and 8. *Science (New York, N.Y.)*. 303(5663), 1526–1529 (2004).
347. Yu P, Lübben W, Slomka H, *et al.* Nucleic Acid-Sensing Toll-like Receptors Are Essential for the Control of Endogenous Retrovirus Viremia and ERV-Induced Tumors. *Immunity*. 37(5), 867–879 (2012).
348. Rabson AB, Graves BJ, Graves. Synthesis and Processing of Viral RNA. In: *Retroviruses*. Cold Spring Harbor Laboratory Press, Cold Spring Harbor (NY) (1997).
349. Katz RA, Kotler M, Skalka AM. cis-acting intron mutations that affect the efficiency of avian retroviral RNA splicing: implication for mechanisms of control. *J Virol*. 62(8), 2686–2695 (1988).
350. Katz RA, Skalka AM. Control of retroviral RNA splicing through maintenance of suboptimal processing signals. *Molecular and Cellular Biology*. 10(2), 696–704 (1990).
351. Petropoulos C. Retroviral Taxonomy, Protein Structures, Sequences, and Genetic Maps. In: *Retroviruses*. Cold Spring Harbor Laboratory Press, Cold Spring Harbor (NY) (1997).
352. White JM. Membrane fusion. *Science*. 258(5084), 917–924 (1992).

353. Schütze S, Potthoff K, Machleidt T, Berkovic D, Wiegmann K, Krönke M. TNF activates NF-kappa B by phosphatidylcholine-specific phospholipase C-induced “acidic” sphingomyelin breakdown. *Cell*. 71(5), 765–776 (1992).
354. Matsusaka T, Fujikawa K, Nishio Y, *et al.* Transcription factors NF-IL6 and NF-kappa B synergistically activate transcription of the inflammatory cytokines, interleukin 6 and interleukin 8. *Proc Natl Acad Sci USA*. 90(21), 10193–10197 (1993).
355. Mayer-Barber KD, Yan B. Clash of the Cytokine Titans: counter-regulation of interleukin-1 and type I interferon-mediated inflammatory responses. *Cell Mol Immunol*. 14(1), 22–35 (2017).
356. Whitehead KA, Dahlman JE, Langer RS, Anderson DG. Silencing or stimulation? siRNA delivery and the immune system. *Annu Rev Chem Biomol Eng*. 2(1), 77–96 (2011).
357. Ahmed ST, Ivashkiv LB. Inhibition of IL-6 and IL-10 signaling and Stat activation by inflammatory and stress pathways. *J Immunol*. 165(9), 5227–5237 (2000).
358. Tilg H, Dinarello CA, Mier JW. IL-6 and APPs: anti-inflammatory and immunosuppressive mediators. *Immunol Today*. 18(9), 428–432 (1997).
359. Opal SM, DePalo VA. Anti-inflammatory cytokines. *Chest*. 117(4), 1162–1172 (2000).
360. Chen C-P, Chen L-F, Yang S-R, *et al.* Functional characterization of the human placental fusogenic membrane protein syncytin 2. *Biol Reprod*. 79(5), 815–823 (2008).
361. Langbein M, Strick R, Strissel PL, *et al.* Impaired cytotrophoblast cell-cell fusion is associated with reduced Syncytin and increased apoptosis in patients with placental dysfunction. *Mol. Reprod. Dev*. 75(1), 175–183 (2008).
362. Ruebner M, Strissel PL, Ekici AB, *et al.* Reduced syncytin-1 expression levels in placental syndromes correlates with epigenetic hypermethylation of the ERVW-1 promoter region. *Plos One*. 8(2), e56145–10 (2013).
363. Vargas A, Zhou S, Ethier-Chiasson M, *et al.* Syncytin proteins incorporated in placenta exosomes are important for cell uptake and show variation in abundance in serum exosomes from patients with preeclampsia. *FASEB J*. 28(8), 3703–3719 (2014).
364. Roland CS, Hu J, Ren C-E, *et al.* Morphological changes of placental syncytium and their implications for the pathogenesis of preeclampsia. *Cell Mol Life Sci*. 73(2), 365–376 (2015).
365. Vincendeau M, Gottesdorfer I, Schreml JMH, *et al.* Modulation of human endogenous retrovirus (HERV) transcription during persistent and de novo HIV-1 infection. *Retrovirology*. 12(1), 814 (2015).
366. Simon M, Haltmeier M, Papakonstantinou G, Werner T, Hehlmann R, Leib-Mösch C. Transcription of HERV-K-related LTRs in human placenta and leukemic cells. (1994).
367. Ono M, Yasunaga T, Miyata T, Ushikubo H. Nucleotide sequence of human endogenous retrovirus genome related to the mouse mammary tumor virus genome. *J Virol*. 60(2), 589–598 (1986).
368. Löwer R, Tönjes RR, Korbmacher C, Kurth R, Lower J. Identification of a Rev-related protein by analysis of spliced transcripts of the human endogenous retroviruses HTDV/HERV-K. *J Virol*. 69(1), 141–149 (1995).
369. Etkind PR, Lumb K, Du J, Racevskis J. Type 1 HERV-K genome is spliced into subgenomic transcripts in the human breast tumor cell line T47D. *Virology*. 234(2), 304–308 (1997).
370. Hung M, Patel P, Davis S, Green SR. Importance of ribosomal frameshifting for human immunodeficiency virus type 1 particle assembly and replication. *J Virol*. 72(6), 4819–4824 (1998).
371. Stone ML, Chiappinelli KB, Li H, *et al.* Epigenetic therapy activates type I interferon signaling in murine ovarian cancer to reduce immunosuppression and tumor burden. *Proc. Natl. Acad. Sci. U.S.A.* 114(51), E10981–E10990 (2017).

372. Haffner MC, Taheri D, Luidy-Imada E, *et al.* Hypomethylation, endogenous retrovirus expression, and interferon signaling in testicular germ cell tumors. *Proc. Natl. Acad. Sci. U.S.A.* 115(37), E8580–E8582 (2018).
373. Cappelletti M, Presicce P, Lawson MJ, *et al.* Type I interferons regulate susceptibility to inflammation-induced preterm birth. *JCI Insight*. 2(5), e91288 (2017).
374. Mangeney M, de Parseval N, Thomas G, Heidmann T. The full-length envelope of an HERV-H human endogenous retrovirus has immunosuppressive properties. *Journal of General Virology*. 82(10), 2515–2518 (2001).
375. Denner J. The transmembrane proteins contribute to immunodeficiencies induced by HIV-1 and other retroviruses. *AIDS*. 28(8), 1081–1090 (2014).
376. Montesion M, Bhardwaj N, Williams ZH, Kuperwasser C, Coffin JM. Mechanisms of HERV-K (HML-2) Transcription during Human Mammary Epithelial Cell Transformation. *J Virol*. 92(1), 709 (2018).
377. Burger O, Pick E, Zwickel J, *et al.* Placental protein 13 (PP-13): effects on cultured trophoblasts, and its detection in human body fluids in normal and pathological pregnancies. *Placenta*. 25(7), 608–622 (2004).